DOKUZ EYLÜL UNIVERSITY
GRADUATE SCHOOL OF NATURAL AND APPLIED SCIENCES

THERMOPHYSICAL PROPERTIES OF POLYMER COMPOSITES REINFORCED WITH CONDUCTIVE FILLERS

by
Tuba EVGİN

January, 2014
İZMİR

THERMOPHYSICAL PROPERTIES OF POLYMER COMPOSITES REINFORCED WITH CONDUCTIVE FILLERS

A Thesis Submitted to the
Graduate School of Natural and Applied Sciences of Dokuz Eylül University
In Partial Fulfillment of the Requirements for the Degree of Master of Science
in Mechanical Engineering, Energy Program

by
Tuba EVGİN

January, 2014
İZMİR

M.Sc THESIS EXAMINATION RESULT FORM

We have read the thesis entitled **"THERMOPHYSICAL PROPERTIES OF POLYMER COMPOSITES REINFORCED WITH CONDUCTIVE FILLERS"** completed by **TUBA EVGİN** under supervision of **PROF. DR. İSMAİL HAKKI TAVMAN** and we certify that in our opinion it is fully adequate, in scope and in quality, as a thesis for the degree of Master of Science.

Prof. Dr. İsmail Hakkı TAVMAN

Supervisor

Assist. Prof. Dr. Alpaslan TURGUT

(Jury Member)

Assist. Prof. Dr. Mehmet SARIKANAT

(Jury Member)

Prof.Dr. Ayşe OKUR

Director

Graduate School of Natural and Applied Sciences

ACKNOWLEDGMENTS

Firstly, I would like to thank my supervisor Prof. Dr. İsmail Hakkı Tavman for his support, contributions and guidance during all study.

I would like to express my thanks to Assist. Prof. Alpaslan Turgut for his support, valuable advises, imcomparable helps through all thesis.

I wish to thank Assist. Prof. Kutlay Sever and Assist. Prof. Ziya Haktan Karadeniz for their help and providing instrument for thermal conductivity measurements.

Finally, I am very much thankful to my family and friends for their loving support, understanding and encouragement which made all this possible.

This research was supported by the Science Support of the Project No. 2013.KB. FEN.013 of Dokuz Eylül University.

Tuba EVGİN

THERMOPHYSICAL PROPERTIES OF POLYMER COMPOSITES REINFORCED WITH CONDUCTIVE FILLERS

ABSTRACT

In this study, thermal conductivity of aluminium particles reinforced high density polyethylene composites has been examined experimentally, numerically and theoretically. High density polyethylene-aluminium composite materials have been produced by using mold compression process in various (1, 2, 4, 6, 8, 10, 12, 15, 18, 21, 25, 30 percent) volumetric concentrations of aluminium.

Thermal conductivity of polymer composites has been measured by C-Therm thermal analyzer depending on the modified transient plane source technique. Thermal conductivity of high density polyethylene-aluminium composite materials increases by increasing volume fraction of aluminium particles.

Numerical study is carried out as functions of concentrations, arrangements and geometries of filler materials in two and three dimensional by ANSYS 14.0 based on finite element analysis software. For two dimensional analyses, shapes of filler are selected as cylinder and square prism, shape of matrix is chosen square prism. For there dimensional analysis, shape of matrix is selected as cube and filler materials' shapes are simulated sphere and cube. Effect of changing amount of fillers in the matrix is examined that the fillers number in the matrix is assumed to be as 1, 2, 4, 8 and 16. As shape of aluminium particles are assumed to be spherical, sphere filler models are found to be in good correlation with experimental values.

Experimental measured thermal conductivity values have been compared with theoretically calculated ones. Maxwell's, Hamilton & Crosser's, Meredith & Tobias's, Lord Rayleigh's, Agari & Uno's, Lewis & Nielsen's theoretical models are found to be closer to experimental values.

Keywords: Thermal conductivity, polymer composites, theoretical thermal conductivity model, ANSYS

İLETKEN KATKI MALZEMELERİ İLE TAKVİYE EDİLMİŞ POLİMER KOMPOZİTLERİN TERMOFİZİKSEL

ÖZ

Bu çalışmada, alüminyum tanecikler ile takviye edilmiş yüksek yoğunluklu polietilen kompozitlerin ısıl iletkenlik değeri deneysel, sayısal ve teorik olarak incelenmiştir. Yüksek yoğunluklu polietilen-alüminyum kompozitler farklı alüminyum hacimsel konsantrasyon (1, 2, 4, 6, 8, 10, 12, 15, 18, 21, 25 ve 30 yüzde) değerlerinde kalıp sıkıştırma yöntemi kullanılarak üretilmiştir.

Polimer kompozitlerin ısıl iletkenliği "modified transient plane source" tekniğine dayalı C-Therm thermal analyzer cihazı ile belirlenmiştir. Alüminyum taneciklerin hacimsel konsantrasyonu artışıyla, yüksek yoğunluklu polietilen kompozitlerin ısıl iletkenlik değeri artmaktadır.

Sayısal çalışma dolgu maddesinin konsantrasyonunun, dizilişinin ve geometrisinin fonksiyonu olarak sonlu eleman analiz yöntemine dayanan ANSYS 14. 0 yazılımıyla 2 ve 3 boyutda gerçekleştirilmiştir. İki boyutlu analizler için, dolgu maddesi şekli silindir ve kare prizma, matris malzeme şekli kare prizma olarak seçilmiştir. Üç boyutlu analizler için, dolgu maddesi şekli küre ve küp, matris malzeme şekli küp olarak seçilmiştir. Matris içindeki dolgu maddesi sayısının değişiminin etkisi, dolgu maddesinin sayısı 1, 2, 4, 8 ve 16 olarak varsılarak incelenmiştir. Alüminyum taneciklerin şekli küre varsayıldığı için, küre dolgu modeli deneysel verilerle iyi ilişki göstermektedir.

Deneysel ölçülen ısıl iletkenlik değerleri teorik modellerle hesaplanan ısıl iletkenlik değerleri ile karşılaştırılmıştır. Maxwell, Hamilton ve Crosser, Meredith ve Tobias, Lord Rayleigh, Agari ve Uno, Lewis ve Nielsen teorik modellerin sonuçları deneysel sonuçlara yakın değerlerde elde edilmiştir.

Anahtar Kelimeler: Isıl iletkenlik, polimer kompozitler, teorik ısıl iletkenlik modelleri, ANSYS

CONTENTS

Page

LIST OF FIGURES

Page

LIST OF TABLES

Page

CHAPTER ONE
INTRODUCTION

1.1 Introduction

A composite material includes two or more constituent materials with importantly various chemical and physical properties, they macroscopic combined to produce a material of which characteristics properties vary from individual constituents. Composites can be classified into three categories; polymer, metal and ceramic composites. Polymer composite is main topic of this study (Bal, 2009; Durmaz, 2004)

Polymer composites reinforced with metallic particles are used in helicopters, ships, aircraft, space craft, submarines, equipments of chemical processing, electronic packaging, automobiles, medical prosthesis, microelectronic devices, civil infrastructure and sporting goods etc (Bal, 2009; Boudenne, Ibos, Fois, Majeste & Gehin, 2005; Chikhi, Agoudjil, Haddadi & Boudenne, 2011; Mamunya, Davydenko, Pissis & Lebedev, 2002; Tong, Mauritz & Bannister, 2002)

Metals, metallic alloy, carbon black, carbon nanotube (CNT), carbon nanofiber, graphite and expanded graphite, graphene have been used as filler materials to produce polymer composites reinforced with conductive materials (Tavman & Turgut, 2012)

Filler materials have significant role in polymer composites' production. The adhesion between components of composite materials is the most significant point for production of composites. Some additives are added in matrix material to develop construction of the bond between the filler and matrix materials. Besides, filler materials are coated to develop the adhesion. In addition, filler materials strongly effect on many properties of polymer composites. Thermal, mechanical, electrical and optical properties of polymeric materials have been developed by fillers. Cost saving, improved or other value-added properties are gotten by using fillers (Bal, 2009; Luyt, Molefi & Krump, 2006).

In new system designs, physical properties of composites materials have won more importance. The reasons of raising interest for polymer composites are electrical and thermal properties of polymer composites are close to metallic filler materials and the other physical properties are maintained for plastics. Moreover, composites are high specific strength and stiffness, light-weight, notable corrosion and fatigue resistance when composites are compared to metals and metallic alloys. For many applications of materials, thermal properties of composites are needed. Determining the thermal conductivity of composite materials is very important for many industrial applications to simulate the heat transfer ability of composite materials. The thermal conductivity of materials is needed to define the optimum conditions along materials process and heat transfer of materials during applications. If their thermal conductivity aren't known, distribution of temperature in composite materials isn't determined. Some relationships are offered to determine composite materials' effective thermal conductivity. Many empirical, semiempirical, theoretical and numerical models were improved to predict the effective conductivity value depend on the dispersion, the each component characteristics and and shape of the fillers. The thermal properties of polymer composites are developed based on several factors as thermal conductivity of filler and matrix materials, shape, size and concentration of filler materials, type of processing, filler and matrix interaction and filler materials interaction each other. Thermal conductivity is present lower and upper boundary values by greater part of theoretical models. But, many of them fail to predict thermal conductivity for medium (15-30%) and high (>30) filler concentration (Boundenne et al., 2005; Chikhi et. al., 2011; Jouni, Boudenne, Boiteux, Massardier, Garnier & Serghei, 2013; Kumlutaş, Tavman & Çoban, 2003; Luyt, et. al., 2006; Mamunya et. al., 2002; Tong et. al., 2002).

The structure and composition of composites have important effects on the thermal conductivity of composites. And this hasn't been shown in a single model yet. In addition, greater part of theoretical models fail to estimate the thermal conductivity for high concentration of filler materials and the ratio of thermal conductivity of matrix and fillers is higher than 200. The weaknesses of the

theoretical models occurred when thinking thermal conductivity of three dimensional (3-D) combinations which have random distribution by various materials shapes. Many theoretical models suffer from non-physical assumptions and/or the empirical parameters included. Numerical modelling creates another method to investigate complicated systems. Numerical methods, for example finite element method, are used to examine thermal conductivity of composite as a function of differences in type, size, shape and concentration of fillers. (Aadmi, Karkri, Ibos & Hammouti, 2013; Chikhi et. al., 2011)

In this study, thermal conductivity of polymer composites reinforced with conductive materials was investigated experimentally, numerically and theoretically. High density polyethylene (HDPE) was selected as matrix material and aluminium (Al) was chosen as a filler material. Composite materials were prepared by mold compression method. Experimantal thermal conductivities of HDPE/Al composites were measured by C-Therm thermal analyzer. Experimental data was compared to numerical and theoretical results. Numerical analyses were carried by using ANSYS 14.0. Numerical models were examined to determine factors affect on thermal conductivity of HDPE/Al composites. The factors considered as shape, concentration and arrangement of filler materials.

CHAPTER TWO
LITERATURE REVIEW

2.1 Literature Review

Polymer composites reinforced with conductive materials are used for many of application, industry and engineering fields such as electronic packaging, aircraft etc. The determining of the thermal conductivity of polymer composites materials is very significant in application and design of composites. Because, the thermal conductivity of materials is needed to define the optimum conditions along materials process and heat transfer of materials during applications. So, many of study has been carried out on thermal conductivity of polymer composites in recent years.

Jouni et. al. (2013) studied on thermal conductivity of HDPE/Silver (Ag) composites. HDPE was used as a matrix material and silver particles of which average diameter was 100 nm was used as filler materials. HDPE/Ag composites were produced with melt mixing method by using corotating twin-screw mini extruder for 15 min at 100 rpm mixing speed, at 170 ºC. The dimension of samples was 0.5×0.5×0.8 mm. Range of Ag contents in HDPE/Ag composites was from 0 to 22 vol %. Thermal conductivity of composites was measured with experimental equipment that made a design for low thermal conductivity (0.1-5 W/mK) and shape of sample was square prism (15×15 mm) and thickness in range of 0.1-10 mm. This device operated according to hot-guarded plate method. At high concentration of fillers, the thermal conductivity of composites give high values. For all concentrations of filler, the theoretical models fail to estimate the experimental values. They found that raising in thermal conductivity by raising volume fraction of Ag. Thermal conductivity of composites at 22 vol % of Ag content increased approximately 4.5 times compared to pure HDPE. In this study, thermal conductivity was also investigated by theoretical models, such as parallel, series, Lichtenecker, Hashin & Shtrikman, Bruggeman models. The thermal condcutivity of HDPE was measured as 0.47 W/mK and Ag thermal conductivity was determined as 430 W/mK. The values of Series and Hashin & Shtrikman models were below experimental data.

In addidition, parallel model values were above experimental data. Lichtenecker, Bruggeman models gave closed results with experimental data.

New 3-D method based on 3-D FEM models was developed to determine effective thermal conductivity for two phase composites as a function of arrangement of materials. Volume fraction, distribution, shape of particles and resistance of thermal contact, ratio of thermal conductivity of matrix and filler were considered. The numerical study was carried out by COMSOL coupled with a pattern generation algorithm developed under Matlab and 3D-representative volume element (3D-RVE) was used to simulate structure of composites. The shapes of filler materials were considered as cylindrical, ellipsoidal and spherical and filler materials were distributed randomly for volume concentration changed from 0 to 0.4. The results of numerical study contrast to results of theoretical models and experimental results existed in literature. As expected, the thermal conductivity increases nonlinearly. Composites with ellipsoidal particles had higher thermal conductivity than that of composites with cylindrical and spherical particles. The results of composites with cylindrical particles were closed to results of composites with spherical particles. They noticed that if fillers geometry aspect ratio increases thermal conductivity of composites materials will increase. Numerical and experimental thermal conductivity was investigated for three cells elementary, such as simple cubic (SC), body centered cubic (BCC) and face centered cubic (FCC) as a function of concentration of filler, ratio of matrix to filler thermal conductivity and Kapitza resistance of the contact inclusion/matrix. At low resistance of thermal contact, heat transfer among filler and matrix was affected dominantly by concentration of filler. At high resistance of thermal contact, thermal contact resistance had more significant effect on effective thermal conductivity than filler concentration. The results of numerical analysis were closed to results of Hasselman & Johnson model. When filler concentration increased, the difference between numerical results and Hasselman & Johnson model's results increased. Numerical thermal conductivity values were lower than those found from Hasselman and Johnson model. The numerical results were compared with experimental data for HDPE/Sn in literature. It was found that numerical analysis gave near results to experimental data (Aadmi et. al, 2013)

Tavman & Turgut (2012), investigated thermal diffusivity of ethylene-vinyl acetate (EVA)/ nano sized expanded graphite (EG) and standard, micro sized graphite (UG) by flash technique. Volume fraction of graphite particles in composite materials were up to 29.3 % and composite materials were gotten ready by melt-mixing process in Brabender Plasticorder. Size of EG and UG particles were respectively 5 to 6 μ, 20 to 25 μ and aspect ratio of most of the particles were between 20 and 250. The four samples with dimensions of 10mm×10mm×4 mm were processed and five measurements were conducted at room temperature for each sample. Thermal diffusivity of EVA/EG composites raised more quickly than EVA/UG composites. In the maximum volumetric concentration (29.3 %), the maximum thermal diffusivity values were 8.23 $x10^{-7}$ m^2/s for EVA/EG and 6.14$x10^{-7}$ m^2/s for EVA/UG and the thermal diffusivity of pure EVA was measured as the value of 1.74 $x10^{-7}$ m^2/s.

Chauhan, Singhvi & Singh (2012) carried out a study about geometry effect on thermal conductivity of polymer composites. The shape of filler particles was less taken noticed in previous models. The new thermal conductivity model was developed based on equal law of the specific equivalent thermal conductivity and minimal thermal resistance law for hexagonal, spherical and elliptical of filler shapes. The results of new developed model were compared with theoretical models and experimental values in literature for polypropylene (PP)/Al, PP/Copper(Cu), phenol-aldehyde/aluminum oxide and phenol-aldehyde/graphite for various volume fraction of filler (0-0.5). Used theoretical models were Maxwell, Russel and Hamilton & Crosser models. Thermal conductivities of Russel and Maxwell models were below the experimental data during whole range of volume fraction of fillers. Whereas, for aldehyde/aluminum oxide and phenol-aldehyde/graphite, Hamilton Crosser model estimated upper thermal conductivity values than experimental data. They found that their new thermal conductivity model for various shapes of filler got better correlation with experimental data than other models. The thermal conductivity increased by increasing filler concentration. The thermal conductivity of fillers was importantly bigger than that of matrix. Effective thermal conductivity raised nonlinearly as a function of filler concentration. At below Ø< 0.3, thermal

conductivity determined by using development models for hexagonal, spherical and elliptical of filler shapes, with other models gave closed results with each other. After this volume concentration, thermal conductivity went up rapidly.

Other researchers determinated experimental thermal conductivity of HDPE/AL (200 μm) by using guarded hot-plate apparatus (Chifor, Tekiner &Orban, 2011). Increasing volume fraction of Al in composites, increasing its thermal conductivity. The aluminum particles were placed in interlamellar spaces, in close contact with the lamellar surfaces. Because of high thermal conductivity of aluminum, aluminum particles get higher temperature fastly than covering matrix. Hence, the thermal conductivity of composite materials raised depending on amount of Al concentration in HDPE.

Chikhi et. al. (2011), studied on thermal conductivities of ethylene vinyl acetate (EVA)/ barium titanate ($BaTiO_3$) and polypropylene (PP)/ Copper (Cu) numerically and experimentally. The average particles diameter of $BaTiO_3$ and Cu are 105 μm and 234 μm, respectively. The numerical analyses were carried out by COMSOL 3.5 depending on finite element method as a function of concentrations and structure of filler materials. For numerical analysis, circle in matrix models were used to model composites microstructure in 2D and the experimental results were compared with numerical and theoretical results. It was noticed that thermal conductivity of composites increased nonlinearly by increasing concentration of filler materials. This increase was foreseeable because thermal conductivity of filler materials was higher than that of matrix. For Ø<20 %, numerical results, experimental data and all theoretical models results were near to each other. Because particles were distributed homogeneously in matrix and they didn't get in touch with each other. After above this concentration, the particles occurred the conductive chains and this caused large increase in thermal conductivity. For EVA/$BaTiO_3$ composites, the results of numerical analysis are closer to Bruggeman models results. For Ø>20 % the numerical models fail to estimate experimental data. This reason is that numerical analysis didn't take notice of interfacial thermal barrier resistance and this resistance had strong effect on thermal conductivity. For volume fraction of filler materials is

the same, the thermal conductivity of composite with bigger particles had higher than that of composite with smaller particles. For EVA/$BaTiO_3$ and PP/Cu, decreasing thermal conductivity, as increasing particle size for Ø<20 %.

Tavman, Aydogdu, Kök, Turgut & Ezan (2011) studied on thermal conductivity and heat capacity of HDPE/expanded graphite (EG) composites. Two types of EG were used that is to say expanded graphite with 50 μm (EG50) and expanded graphite with 5 μm (EG5) in diameter. Thermal conductivity of composites increased with increasing graphite concentration of composite materials. Thermal conductivity of pure HDPE was measured in range of 40 ºC and 100 ºC. Increasing temperature, decreasing thermal conductivity of composites. While thermal conductivity of pure HDPE was 0.442 W/mK at 46 ºC, thermal conductivity of HDPE/EG5 and HDPE/EG50 (7 % wieght) were respectively 0.468 W/mK and 0.938 W/mK in the same temperature. It is showed that thermal conductivity of composites included larger size graphite particle was higher than thermal conductivity of composites included smaller size graphite particle. The reason was that the higher aspect ratio of filler cause to higher values of thermal conductivity. Heat capacity of pure HDPE and HDPE/EG composites increase by increasing temperature. Heat capacity values of HDPE/EG composites weren't detected significant difference because of particle size of expanded graphite particle. Heat capacity of HDPE/EG for both particle size decreased by increasing graphite concentration.

Das (2011) examined thermal conductivity of Al filled epoxy polymer composites experimentally and numerically. Experimental thermal conductivity of composites was measured by using Unitherm Model 2022 based on Guarded heat flow meter test method. Numerical analysis were carried out by ANSYS software in 3-D. Used model was three dimension sphere filler in cube matrix to model composites materials' microstructure as a function of filler concentration (0.4 %, 1.4 %, 3.34 % volume fraction of Al contents). The average size of Al was 100-200 μm. The composites were prepared by hand-lay-up method in 9 mm diameter and 120 mm length dimension. As seen in results, thermal conductivity of composites developed as a function of volume fraction of Al contents. Composite materials with filled of

3.34 % vol. of Al, the thermal conductivity was higher about 1.1 times than pure epoxy.

Linear low-density polyethylene (LLDPE) composite with aluminum nitride (AIN) as filler materials was produced in different volume fraction of AIN (0-40 %) in heat press molding. Thermal conductivity of LLDPE/AIN composite materials increased by increasing volume fraction of AIN in LLDPE matrix. At low volume fraction, AIN particles distributed randomly in LLDPE matrix and contact each other weakly. So, thermal conductivity of LLDPE/AIN composite materials increased little. When volume fraction of AIN particles raised, particles started to touch each other and to create partial conductive path or network, this developed heat conductance. Thermal conductivity of LLDPE/AIN composite material was determined 1.25- 1.39 W/mK for 40 vol % AIN. This value was about five times more than thermal conductivity of pure LLDPE (Zhou, 2011a).

Zhou (2011b) investigated thermal conductivity of Al particle filled LLDPE composites which were prepared by melt mixing and hot pressing. Various Al particles were used as filler materials. One of them was spherical Al powders whose average particle size of 7 μm and 20 μm. The other Al powder had mean thickness in 1 μm and in length in 10 μm. Surface treatment of Al particles were made by silane coupler. The thermal conductivity of composites for various filler contents (0-45 % volume fraction) were calculated from thermal diffusivity values, determined by Netzsch system at room temperature in air and high temperature in argon. The samples were prepared in circle disc form (d=20 mm, t= 1mm) for measurement of thermal diffusivity. It was founded that the thermal conductivity of LLDPE/Al composites went up with raise in filler volume fraction because of high thermal conductivity of Al particles. At low volume fraction of Al particles, they distributed uniformly in matrix materials and have poor connect with each other, so they showed a small thermal conductivity increase. Al particles were covered by Polymer matrix and they can not touch each other. The thermal conductivity was low because of high resistance of interfacial thermal contact between the matrix materials and filler materials. At high volume fraction, particles started to contact with each other and

the form of particles was more compact packing structure or clusters in matrix. This caused to develop thermal conductivity due to reduce resistance of interfacial thermal contact resistance. The shape of Al particles had effect on thermal conductivity of LLDPE/Al composites. Spherical Al particle reinforced polymer composites showed lower thermal conductivity the flaky particle reinforced polymer composites. For example, thermal conductivity of flaky Al particle filled LLDPE at 34 vol % was nearly the same with spherical Al with mean particle sizes of 7 μm and 20 μ filled LLDPE composites.

Çolak (2011) studied on thermal conductivity of HDPE/graphite, graphite powder was 400 nm and volume fractions of graphite were 2, 3, 4, 5, 6, 7, 10, and 16 % in nanocomposites. The study was carried out experimentally and theoretically. Experimental thermal conductivity of nanocomposites was determined by Hot-disk Method. It was found that thermal conductivity of HDPE/graphite went up nonlinearly by raising volume fraction of graphite. Geometric mean, series, Cheng & Vachon, Russell, Maxwell, Lewis & Nielsen (A=1.5, Øm=0.637) and Lewis & Nielsen (A=3, Øm=0.637) models were used as theoretical models. In whole concentration, these models underestimate experimental data. Only, Russell method results were the best correlation with experimental results until 6 % of volume fraction of graphite.

Luyt et. al. (2006) study on thermal conductivity of polymers composites. They used low density polyethylene (LDPE) and linear low-density polyethylene (LLDPE) as matrix materials and copper (Cu) paritcles of which average particle sizes were <38 μm as fillers. LDPE/Cu and LLDPE/Cu composites were produced by melt mixing method for various Cu contents (0-24 % vol.). Dispensation of copper particles was homogenous at both matrix materials. At higher Cu contents, cluster formation of copper occurred, copper's percolation paths formulation in the matrix obtained. Thermal conductivity of composites was determined by using multipurpose apparatus (ISOMET). When thermal conductivity of composites compared with that of the pure PE, thermal conductivity of pure PE has lower than that of composites. Thermal conductivity of LLDPE/Cu and LDPE/Cu composites increased linearly by

increasing Cu content in matrix. As seen examined results, for all volume fraction of Cu, the thermal conductivity of LDPE/Cu composites were lower than that of LLDPE/Cu composites. The reason of this, generated more conductive paths as results of higher particles agglomeration. Because polymer materials covered to Cu particles and amorphous content was less in LLDPE, Cu particles may more aggregate in LLDPE matrix. A value of 18.7 vol % copper was found as percolation concentration for LDPE and LLDPE polymers.

Boudenne et. al. (2005) carried out a study on thermal and electrical properties of polypropylene (PP)/ copper (Cu) composites with mixing pellets method. Electrical conductivity, thermal conductivity, effusivity, diffusivity and specific heat of PP/Cu composites were determined for two different diameter of Cu particles. The samples were prepared at 100×100 mm square plates and 3 mm thickness by compression molding. The greatest heat transfer ability was seen for the composites reinforced with smaller particles. Thermal conductivity increased nonlinearly by increasing volume fraction of filler materials. The composites reinforced with smaller particles gave higher thermal conductivity than that of composites reinforced with higher particles. For higher concentrations of filler, this difference between two composites was more important. The Agari's model predicted thermal conductivity of composites well for all concentrations of filler. Coefficients of Agari's model as C_1 and C_2 were calculated. It was seen that particles size didn't affect on C_1 coefficient of Agari model, but C_2 was strongly affected by fillers size. The value of C_2 was bigger for larger fillers than smaller fillers.

Durmaz (2004) studied on thermal conductivity of composites reinforced with particle and fiber fillers numerically and theoretically as a function of concentration, geometries and arrangements of filler and ratio of k_f/k_m. Numerical analysis was carried out as 2-D and 3-D. Infinitely long square prism and cylinder were used as a shape of fiber fillers in 2-D. Cube and sphere were used as a shape of particle filler in 3-D. Concentration of filler materials were selected 5 %, 15 %, 30 %, 50 % and 75 % for fiber and 5 %, 25% and 45 % for particle. The ratios of k_f/k_m were chosen as 10, 100,1000 and 10000. The arrangements were made as 1, 2, 4, 8 and 16 piece for

fibers and 1, 8 and 27 pieces for particles. Numerical results were compared with theoretical results. Springer & Tsai's and Hamilton & Crosser's models were close to 2-D analysis. Results of Lewis & Nielsen, Hamilton & Crosser, Russell and Meredith & Tobias' models were near to 3-D analysis. Difference of arrangement forms had more effect on thermal conductivity in 2-D models than in 3-D. Spinger & Tsai and Hamilton & Crosser's model showed near results to numerical results for 2-D models. Levis & Nielsen, Meredith & Tobias, Russell and Hamilton & Crosser's models had close results with numerical analysis results for 3-D models.

Weidenfeller, Höfer & Schillingc (2003) carried out a study about thermal properties of polymer composites reinforced with oxide and metal particles. Matrix material was used as polypropylene (PP) and filler materials were selected as glass fibers, talc, magnetite, copper, barite and strontium ferrite. Polymer composites with different filler materials were produced by injection molding process in various volume fractions (up to 50 %). The some properties of these composites such as thermal diffusivity, density and specific heat capacity were determined and thermal conductivities were calculated with these properties. Thermal conductivity of polymer composites increased by increasing filler concentration in matrix. For example, thermal conductivity of PP/ talc composite was determined as 2.5 W/mK in 30 vol % filler concentration, which as thermal conductivity of pure PP was determined as 0.27 W/mK.

Kumlutas et. al (2003) studied on the thermal conductivity HDPE/ aluminum composites numerically as a function of filler volume fraction. The thermal conductivity of composites were measured by hot-wire method. Numerical analyses were studied in two-dimensional models. The numerical results were compared with the theoretical models and experimental results. Up to 10 % volume fraction, experimental, numerical and all theoretical models' results were approximated. Above 10% volume fraction, the experimental thermal conductivity increased exponentially, the numerical results were closed to experimental results, but all theoretical models failed to forecast thermal conductivity. Up to 10 % volume fraction of Al, Cheng & Vachon, Russell models results were closed to experimental

results. Above 10 % volume fraction of Al, all using theoretical models gave lower values than experimental values. The numerical results were higher than experimental results.

Sofian, Rusu, R. Neagu & E. Neagu (2001) studied on thermal properties of metal - such as copper, zinc, iron and bronze- powder filled HDPE in 0-24 % of filler volume fraction. In this study, determined thermal properties were thermal conductivity, thermal diffusivity and specific heat. In low volume fraction of filler materials (0-16 %), theoretical thermal conductivity models had good correlation with experimental results. Because, filler materials had homogenous distribution in matrix and weren't interaction with one another. At higher volume fraction of filler materials, filler materials tended to create conductive chains and agglomerates. As a result of this, thermal conductivity of composites increased rapidly.

Girgin & Kılavuz (2001) carried out a numerical and theoretical study about composites reinforced with fiber and particular fillers. Numerical study was conducted in 2-D and 3-D as a function of volume fraction of filler and various ratio of k_f/k_m by ANSYS 5.4. Numerical results were compared with results of theoretical models and numerical results of D. Veyret et. al. in literature. Shape of fiber filler was selected as cylinder and square prism and shape of particle filler was selected as sphere and cube. The ratio of k_f/k_m selected as 1, 10, 100, 1000, 1000 and filler concentrations were 13.5 %, 44 %, 52% for 2-D analysis and 4 %, 27 %, 44 % for 3-D analysis. Used theoretical models were as Chawla, Springer & Tsai, Rayleigh, parallel, geometric mean, Levis & Nielsen, Cheng & Vachon. 2-D analysis in this study gave closed results with 2-D analysis by D. Veyret. For high ratio of k_f/k_m, all theoretical models, expect geometric mean and parallel model, and numerical study continued almost the content results. According to these results, thermal conductivity of composite materials changed not depending on thermal conductivity of filler materials, depending on shape and concentration of filler materials. For low concentration of filler, obtained results were nearly equal to D. Veyret results, but the difference between results of this study and D. Veyret increased, as increasing filler concentration. The reason was that ANSYS computer program was different in this

study and D. Veyret study. Also, for composites with particle filler, numerical study was made as using two different filler materials. In this study, the maximum volume fraction of filler materials was 37 % for aluminium and 18 % for tin in HDPE matrix. Obtained results were compared with theoretical models and it was found that results of Maxwell model were in complainced with these results.

Thermal conductivity of HDPE composites reinforced with tin particles were investigated experimentally, numerically and theoretically for various volume fraction (0-16 vol %) of tin by Tavman (1998). Shape of samples was rectangular (100 mm length, 50 mm width, 17 mm thickness) and polymer composites were produced by mold compression method. Experimental thermal conductivity of HDPE/tin composites was measured by Shotherm QTM device depend on hot wire method for various temperature (0-70 °C). Used theoretical models were as Maxwell, Agari & Uno, Nielsen and Baschirow & Selenew models for comparing with experimental thermal conductivity values. The thermal conductivity of HDPE (0.532 W/mK) used as matrix are 120 times lower than that of tin (64 W/mK) particles used as filler. Increasing temperature, decreasing thermal conductivity. Experimental thermal conductivities of HDPE/tin composites raise slowly by raising volume fraction of tin until approximetaly 10 % vol. In this region, experimental values were good agreement with results of Maxwell and Nielsen (A=1.5, $Ø_m$=0.647) models. At above 10 % vol., the tin particles occur agglomerates form and conductive chains in heat flow direction, this reason is that thermal conductivity of polymer composites increased rapidly. Shape of tin particles was approximately spherical. Tin particles were aggregates form and the particle shapes cannot be maintained at high volume fraction. So, Lewis & Nielsen model (A=3, $Ø_m$=0.647), showing random distribution and irregular particles shape, were closed to experimental values. At above 10 % volume fraction of tin, Cheng & Vachon model can predict experimental values. For all volume contents of tin particles, Agari & Uno models gave closed results to experimental values, because coefficients of Agari & Uno model were found from experimental values. Baschirow & Selenew model was under experimental values and results of Russell model were above experimental values for all volume contents of tin particles.

Thermal conductivity of HDPE composites reinforced with copper particles was investigated experimentally and obtained results were compared with existing theoretical models by Tavman (1997). Thermal conductivity of polymer composites was measured by using modified hot wire method for up to 10 vol %. Thermal conductivity of HDPE/Cu composite samples was measured by Shotherm QTM thermal conductivity device depending on modified hot wire method. Maxwell, Cheng & Vachon, Lewis & Nielsen (A=1.5, A=3 and $Ø_m$=0.637) theoretical models were used. For theoretical comparisons, the Lewis & Nielsen model gave the closest results with experimental values for below 8 % vol. Because this model takes notice of particles shapes and packing type. The Maxwell model didn't estimate experimental results after 6 % volume fraction of Cu. For all volume fraction of Cu, predicted thermal conductivities of Cheng & Vachon model are higher than that of experimental.

CHAPTER THREE
MATERIALS & METHOD

3.1 Materials & Methods

A high density polyethylene (HDPE) in powder shape, which is produced in Petkim Petrokimya Holding A.Ş., is used as matrix material. Its commercial name is Petilen I 668 (UV), density of HDPE is range of 966-970 kg/m^3 at 23ºC and melt flow rate of HDPE 4.4-6.5g/10 min (at190ºC, 2.16 kg). HDPE is thermosetting polymer and its colour is white. Molecular chains of HDPE are relatively straight and nearly aligned. Impact and tensile strength of HPDE is high and it is indissoluble in organic solvents and it is proof against most chemicals.

The aluminum in form of fine powder, whose shape is approximately spherical and size is about 80 nm. Colour of Al particles are silvery white. The density and thermal conductivity of aluminum are respectively 2.7 g/cm^3 and 204 W/mK. Components of structural are produced from aluminium. Aluminium's alloys have very significant role in building, transportation and aerospace industry.

HDPE/Al composite materials are produced in various volumetric concentrations (1, 2, 4, 6, 8, 10, 12, 15, 18, 21, 25 and 30 %). Composite materials are prepared by using mold compression process. Firstly, in Brabender Plasticorder W30 internal mixer, HDPE and aluminum powders are mixed. The process conditions of mixing is 180°C and total mixing time of 10 min, the capacity of mixing chamber is 30 ml. The rotors are turned at 35 rpm for 15 minutes at 180°C. This powder mixture is melted in a mold under pressure (40 kPA) at 180°C for 1 minute and solidified by air cooling.

Figure 3.1 General view Brabender Plasticorder W30/The mixing chamber and the rotors after the mixing process of the composite (Çolak, 2011).

3.2 Thermal Conductivity Measurement Method & Device

The thermal conductivity of HDPE/Al composites was measured by using C-Therm Thermal Conductivity Analyzer (TCi) in Katip Çelebi University. This equipment is based on the modified transient plane source technique. The TCi system includes a sensor, computer software and control electronics.

Figure 3.2 C-Therm thermal conductivity analyzer

As seen in Figure 3.2, the sensor contains a central heater, shape of this heater is spiral and guard ring covers this heater. The guard ring produces heat besides spiral heater. So, likeness one dimensional heat flow from sensor to samples below test get in touch with sensor.

Figure 3.3 C-Therm sensor

The difference between this configuration and the traditional hot-wire or transient plane source method is that the central heater and guard ring are supported on a backing material, which provides mechanical support, electrical insulation, and thermal insulation which enable a one-sided interfacial measurement and greatly enhance flexibility. The external sensor is studied from -50 to +200 ◦C and so that solids, liquids, powders and pastes can be measured (C-Therm, 2013; Harris and Sorensen, 2007; Ouellette, & Harris, 2010).

The sample is analyzed by directly stayed in touch with the heat sensor for definite time length (0.8 s). It uses a one-sided, interfacial, heat reflectance sensor that applies a momentary, constant heat source to the sample. A known current is used to sensor's heating element supplied a small quality of heat. The heat supplied results that temperature of interface between sample and sensor generally increases less than 2 ºC. This event causes a difference in the sensor element's voltage drop. The rate of raise in sensor voltage is utilized to identify thermophysical properties of sample. The voltage change is shown in Figure 3.4, voltage raise can be related to thermal conductivity through a calibration by reference materials known thermal conductivity. The unknown materials' thermal conductivity can be determined from calibration. The thermal conductivity of sample is inversely proportional to voltage-time graph's slope. These properties are inversely proportional to the rate of increased in sensor voltage. Obtained results are shown on computer in real time. C-Therm thermal analyzer directly measures effusivity and determines thermal

conductivity from this measurement (C-Therm, 2013; Harris and Sorensen, 2007; Ouellette, & Harris, 2010).

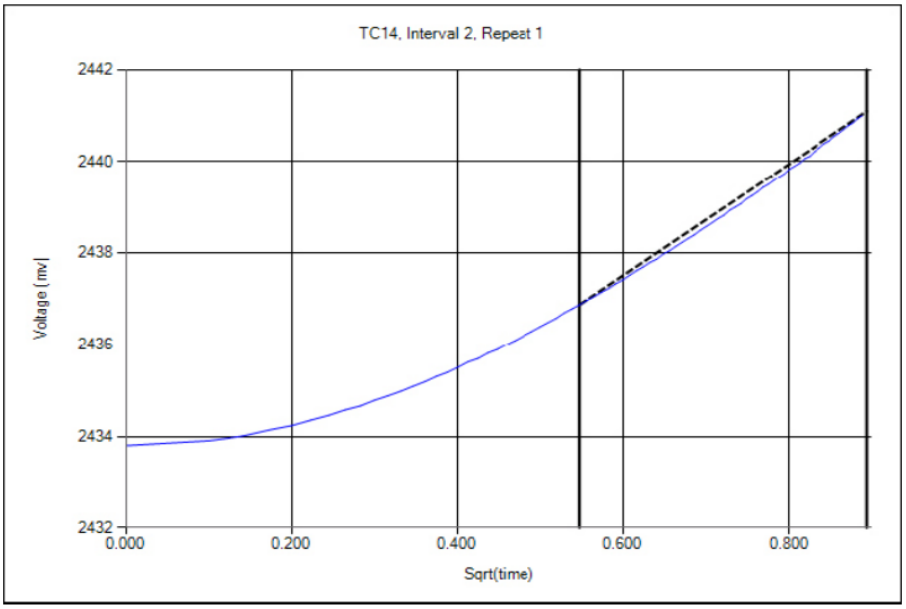

Figure 3.4 Plot of change in voltage

Thermal conductivity of samples is determined depending on effusivity measurement. Effusivity contains thermal conductivity (k), density (ρ) and heat capacity (Cp). Two various materials may own the same effusivity, if these (ρ, Cp) material is different, k is various. So, at all time, a sample measured by this method that calibration group closest to type of sample materials. If you obtain optimum thermal conductivity values, you enter right properties (ρCp) of your samples.

The TCi sensor owns solid surface is designed for fluids testing. As solids are measured, contact agent is necessary, because some contact resistances importantly effect on results occurs if the measurement procedure doesn't apply. The quality of contact and therefore the heat transfer depends on many parameters such as type of material, surface quality and wettability. Water is the best contact agent because water has low viscosity, comparatively high thermal conductivity (~0.6 W/mK), is easy to use and clean. These using temperatures are from 5 ºC to 70 ºC (C-Therm, 2013).

Experimental Set-up;

The TCi program is started. Pyrex is used as reference materials to control calibration of device. Water is used as contact agent to ensure accurate contact between samples and sensor. Three drops of water are dropped over the sensor. The material is put in a way that permits heat transfer between material and sensor. A 500 g weight is placed on materials to permit it to add to the sensor at suitable pressure. Click diagnostic tools in TCi program to control temperature difference between sensor and material. This temperature difference should be less than 5 ºC for correct measurements. Measurements are carried out at different points of sample. And the thermal conductivity of sample is determined by taking average of these measurements.

CHAPTER FOUR
NUMERICAL ANALYSIS

4.1 Finite Element Method

Turner et. al. (1956) introduced the finite element analysis (FEA). FEA is a strong computation technique for approach solutions for difference of real world engineering problems possessing complex domains depending on common boundary conditions. FEA has been a fundamentel step in physical phenomenon modeling or design in different engineering disciplines. A physical phenomenon mostly happens in solid, liquid or gas including some field variables. The field variables change from point to point. So, having an infinite number of solutions in the domain. The fundamental of FEA depends on the decomposition of the domain into a finite number of subdomains (elements) for which the systematic approximate solution is modelled by applying the variation or weighted residual methods. FEA reduces the problem into a finite number of unknowns by dividing the domain into elements and by expressing the unknown field variable in terms of the assumed approximating functions within each element. Functions, which are called interpolation functions, are determined in values of field variables at particular points, called as nodes. Nodes are generally placed along the element boundaries and nodes attach adjacent elements. The facility to discretize the irregular domains by finite elements creates the method a valuable and useful analysis tool for the solution of boundary, eigenvalue and initial problems increasing in various engineering disciplines. So, the FEA is used as numerical procedure which can be utilized for large engineering problems type, such as heat transfer, fluid flow, stress analysis. For numerical solution of mechanical problems including structural analysis (both linear and nonlinear), acoustic and electromagnetic problems, static/dynamic, fluid problems, heat transfer, ANSYS is general purpose finite element modeling package program (Mishra, Mohapatra, Satapathy & Patnaik, 2011; Prahan, 2013).

4.2 Modelling & Analysis

Thermal analyses of composites are carried out in two and three dimension by ANSYS 14.0 software. The aim of thermal analysis is to determinate the heat flux and temperatures on each nodes created by ANSYS 14.0 for numerical solution in 2D and 3D. Thus, numerical thermal conductivity of composites is determined by using obtained solutions. In this chapter, how to create and analysis two and three dimensional models by ANSYS are described.

Simulating composite materials microstructure with unit cells assumption has been made commonly in previous studies which were about calculating composite materials thermal conductivity (Durmaz, 2004).

For 2-D models, each unit cell includes square site simulating the matrix material and rectangular or circular area representing as filler particles. The dimensions of square of matrix are fixed and have been taken unity. Cube shaped as matrix site and spheres, cubes representing as filler particles for 3-D models. The dimensions of cube of matrix are fixed and have been taken unity.

Thermal analysis of 2-D and 3-D models was carried out by using Steady-State Thermal Analysis in ANSYS Workbench 14.0. For numerical analysis, it has been assumed that:

- ✓ The composites are thought to be macroscopically uniform
- ✓ The filler and matrix are considered to be isotropic and homogeneous.
- ✓ Resistance of thermal contact between filler and matrix is negligible.
- ✓ Voids are not seen in composites

During analysis, HDPE has been used as matrix materials, Al particles have been used as fillers. Isotropic thermal conductivity of HDPE and Al has been given in Table 4.1. Different volume fractions of Al in HDPE matrix (Ø= 1%, 2%, 4%, 6%, 8%, 10%, 12%, 15%, 18%, 21%, 25% and 30%) have been selected to examine how

volume fraction effects on thermal conductivity of composites. In addition, amount of fillers has been changed by holding the same volume fraction, so as to observe changes between temperature distributions and heat fluxes and to research the effect on thermal conductivity. First, it has been supposed that 1 piece filler is in matrix material, and then 2, 4, 8 and 16 pieces fillers have been carried out in matrix materials.

Table 4.1 Thermal conductivity of materials

Materials	Thermal conductivity (W/mK)
HDPE	0.614
Al	204

4.2.1 Two Dimensional Models Development & Analysis

The heat fluxes and temperature distribution of HDPE/Al composites have been investigated in two dimensions (2-D). Heat fluxes obtained from numerical analyses have been used to determine the thermal conductivity of HDPE/Al composites.

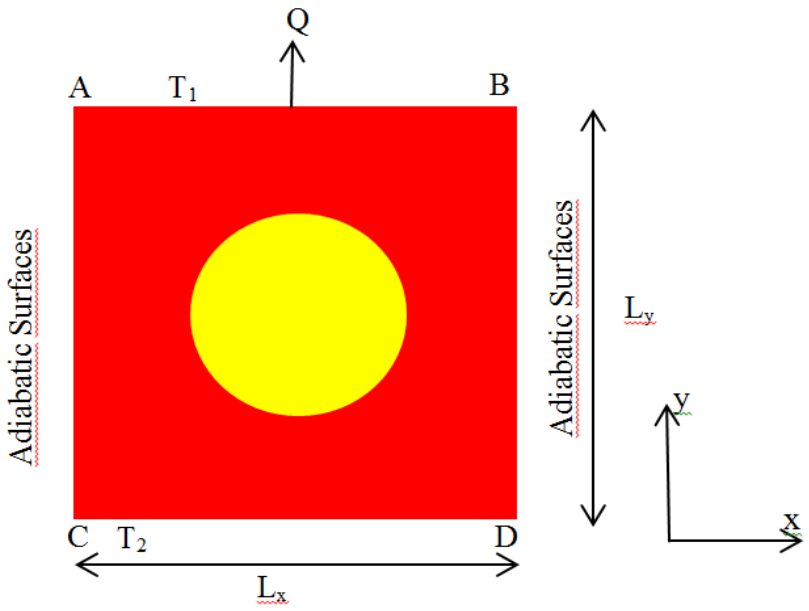

Figure 4.1 2-D geometry used in assumptions

Geometry has been applied in 2-D models is given in Figure 4.1. The temperatures on both upper (AB) and lower (CD) have been named as T_1 and T_2, respectively. Direction of heat flow (Q) has been displayed and L_x and L_y show lengths of surfaces.

To carry out the analysis possible and simple, making some assumptions: The AB (upper) and DC (lower) surfaces are perpendicular to the heat flow and these surfaces were presumed to be isothermal. The other surfaces, (AC) and (BD), are parallel to heat flow. So, these surfaces are supposed to be adiabatic. It is thought that the fillers aren't kept in touch with each other and they homogeneously dispersed into matrix material.

Generated mesh for Ø=30 % cylinder filler models were given in Figure 4.2.

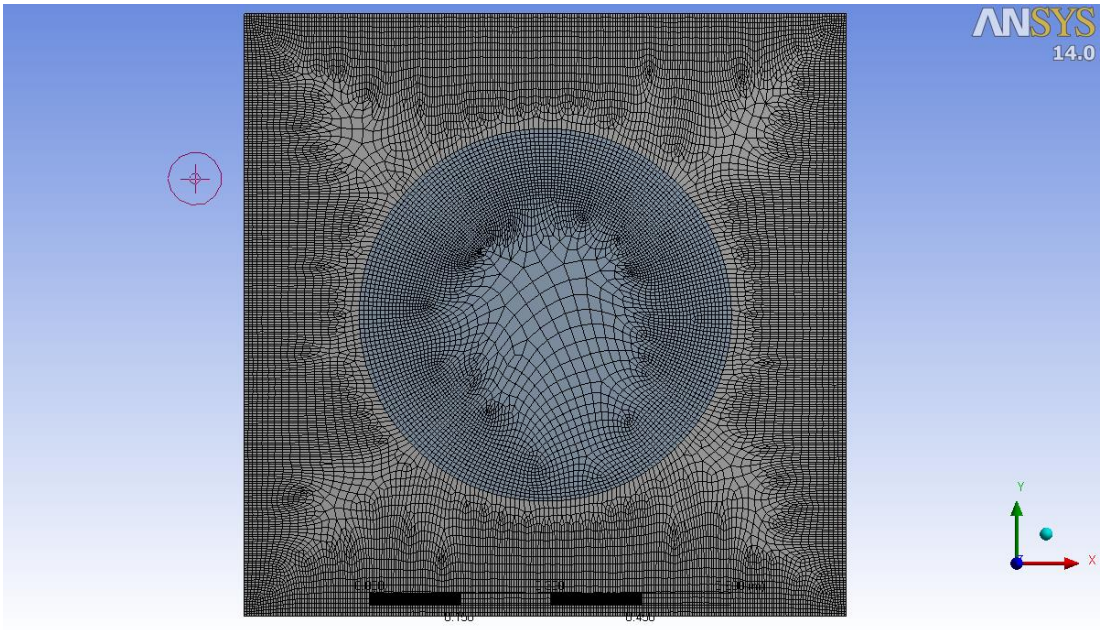

Figure 4.2 Meshed 2-D cylinder filler models for Ø=30 %

After the generation of mesh, the boundary conditions have been entered to software. The boundary surfaces (AB and CD)' temperatures have been given as T_1= 293 °K, T_2=303 °K and hold constant during the analysis. Finally, the desired solutions have been achieved. For Ø=30 % and 1 piece cylinder fillers, the heat

fluxes and temperature distribution of HDPE/Al composites obtained are shown in Figure 4.3 and Figure 4.4.

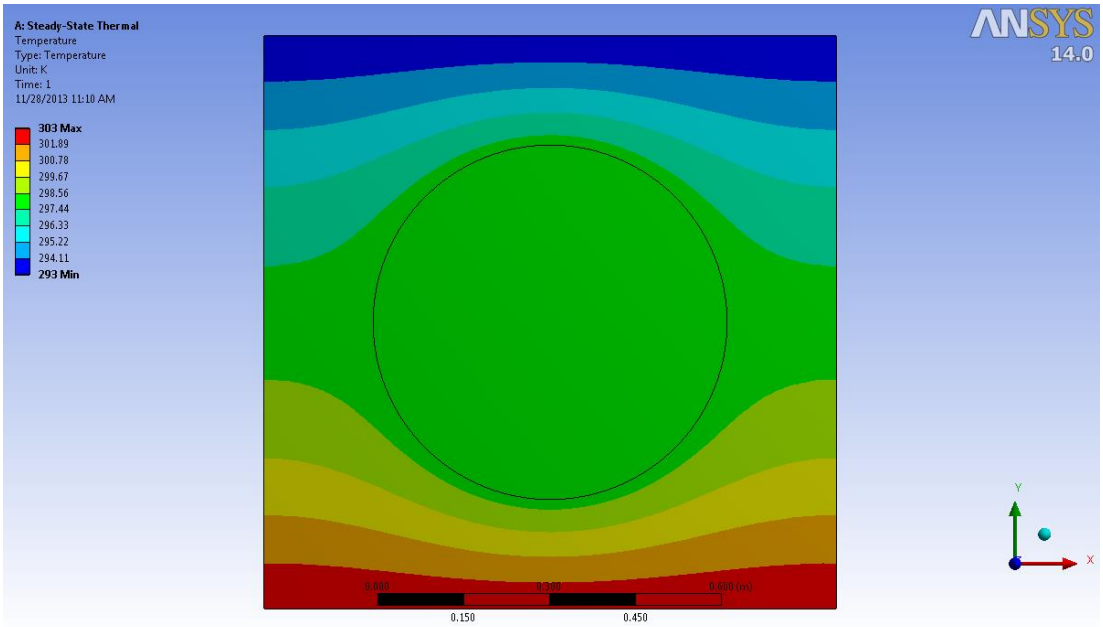

Figure 4.3 Temperature distribution of 1 piece circle filler model for Ø=30 %

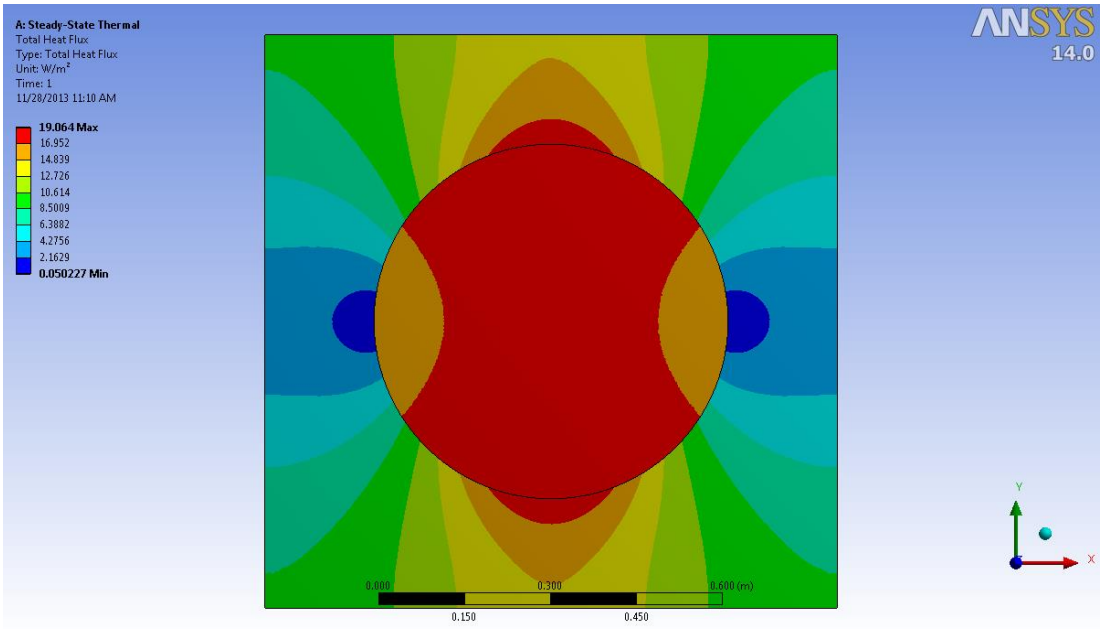

Figure 4.4 Total heat flux of 1 piece circle filler model for Ø=30 %

The same analysis steps have been carried out for square filler models. The generated mesh of square filler model was shown in Figure 4.5.

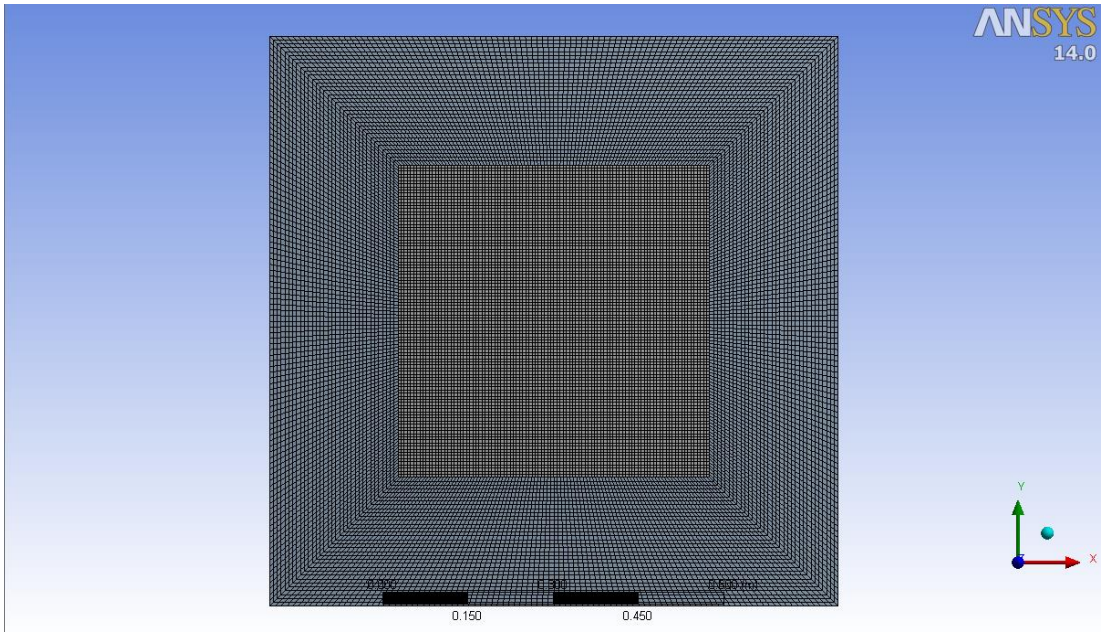

Figure 4.5 Meshed 2-D square filler models for Ø=30 %

Obtained solution for square filler models have been given in Figure 4.6 and Figure 4.7.

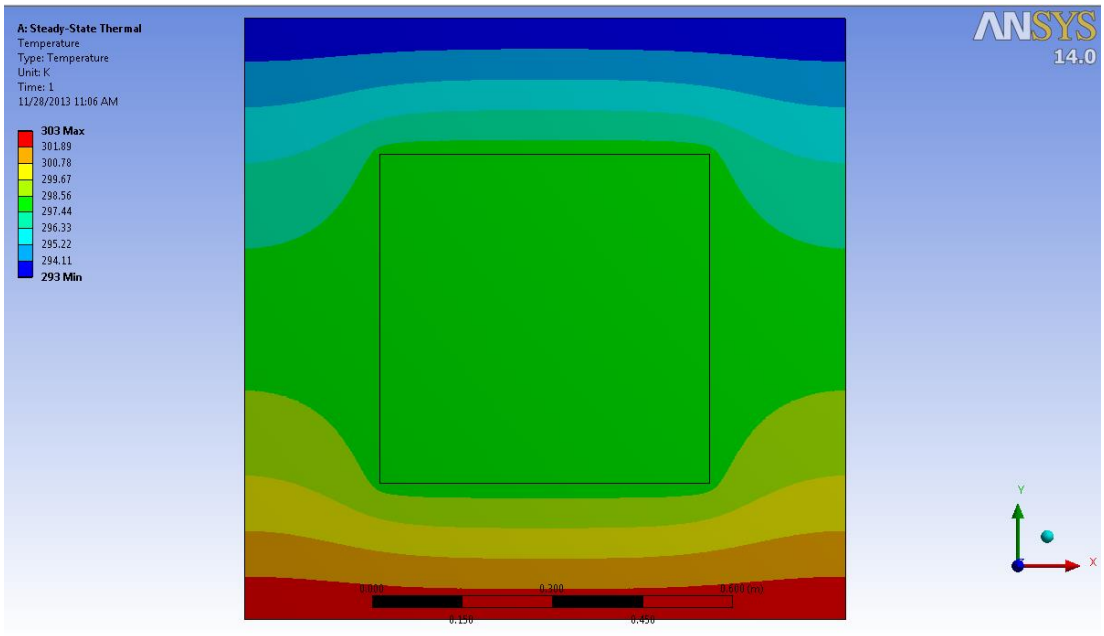

Figure 4.6 Temperature distribution of 1 piece square filler model for Ø=30 %

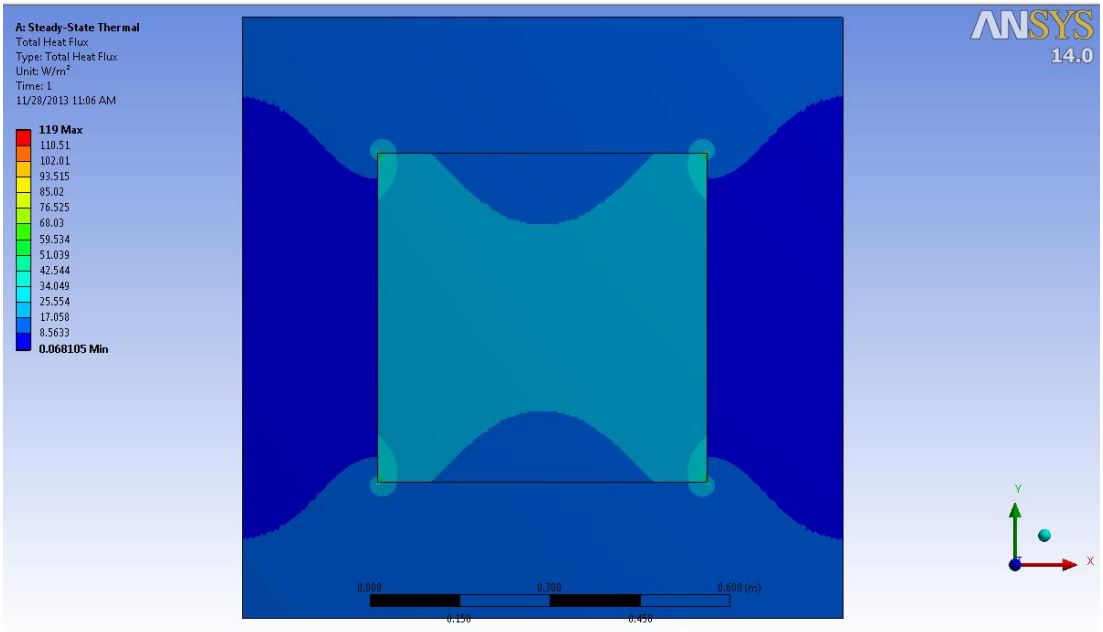

Figure 4.7 Total heat flux of 1 piece square filler model for Ø=30 %

Founded the other solution of 2-D models were detailed in results and all figures and tables of results were given in Appendix D and Appendix F for various volume fraction.

4.2.2 Calculation of Thermal Conductivity for 2-D

Temperature distributions and heat fluxes of 2-D models have been obtained by using ANSYS 14.0. Some assumptions are made to perfom analysis. These assumptions:

- Upper and lower surfaces of models have been perpendicular to heat flow and isothermal.
- Surfaces which are parallel to heat flow are assumed to be adiabatic.
- Filler particles don’t touch each other.
- Temperatures of lower and upper surfaces have been holding constant along analysis.

Equation of heat flow is solved for steady state with using ANSYS 14.0 and heat fluxes have been obtained. And thermal conductivity has been calculated by using obtained heat fluxes. As seen in Figure 4.8, two sides have been assumed to be adiabatic; other two sides have been given T_1 and T_2 temperatures as boundary conditions in models. The changes of heat flux of upper surfaces through x direction have been shown in Figure 5.8. In this figure, the area below curve is equal to quantity of total heat passing along upper surface (AB). As utilizing some integration methods, this area can be determined.

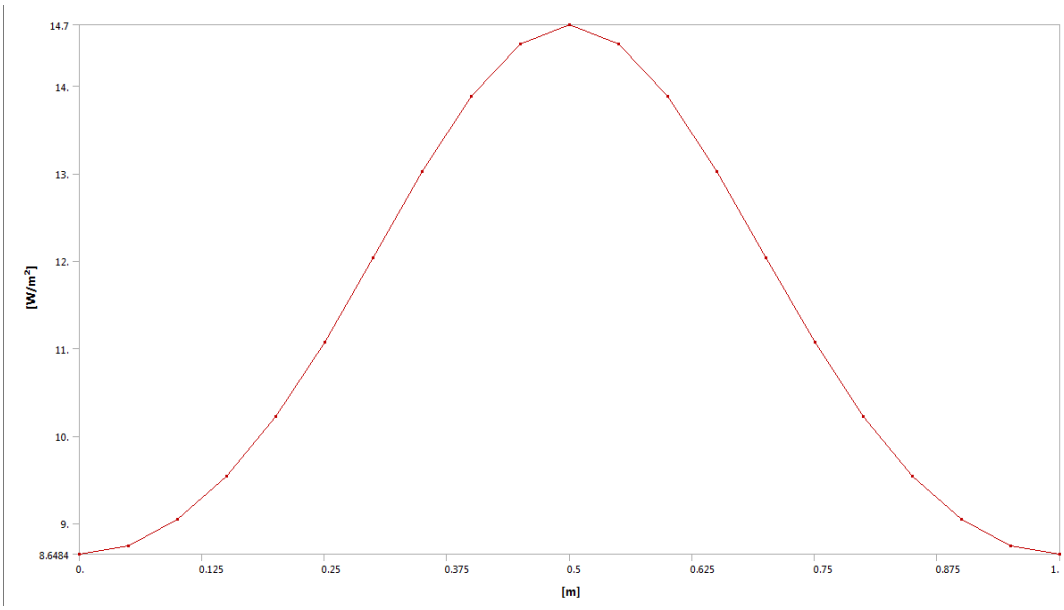

Figure 5.8 Changes of heat flow (q_y) through AB surface in x-direction

Geometry in Figure 4.1. and following equations have been used to calculate thermal conductivity:

$$k_e \frac{\Delta T}{L_y} = \frac{1}{L_x} \sum_i k_i x_i \left(\frac{\partial T_i}{\partial y} \right) \tag{4.1}$$

Where;

$$\sum_i x_i = L_x \text{ and } k_i = \begin{cases} k_f & \textit{if inside of filler material} \\ k_m & \textit{ifinside of matrix material} \end{cases}$$

In Equation (4.1), "$\sum_{i} k_i x_i \left(\frac{\partial T_i}{\partial y} \right)$" is equal to the area below the curve. The Equation (4.1) transform to Equation (4.2):

$$\sum_{i} k_i x_i \left(\frac{\partial T_i}{\partial y} \right) = \int_{x} q_x dx = Q \tag{4.2}$$

Substuting Equation (4.2) into Equation (4.2)

$$k_e \frac{\Delta T}{L_y} = Q \frac{1}{L_x} \tag{4.3}$$

L_x=L_y=1 m and ΔT=10 ˚ K have been used in analyses.

Consequently, The equation (4.3) returns to equation (4.4):

$$k_e = \frac{Q}{\Delta T} \tag{4.4}$$

In this equation, only amount of total heat passing through upper surfaces are unknown. The Simpson method has been used to determine the total quantity of heats obtained from the numerical analyses in ANSYS 14.0. According to Simpson Method;

$$\int_{a}^{b} f(x)dx = \frac{h}{3}\left(f_0 + 4f_1 + 2f_2 + ... + 2f_{2m-2} + 4f_{2m-1} + f_{2m} \right) \tag{4.5}$$

Where;

$$h = \frac{(b-a)}{2m}; \quad f_i = f(x_i)$$

4.2.3 Three Dimensional Models Development & Analysis

The heat fluxes and temperature distributions of 3-D models have been investigated. Obtained heat fluxes form analyses have been used to determine the thermal conductivity of HDPE/Al composites numerically, just as 2-D models.

Geometry designed for 3-D models has been illustrated in Figure 4.9 Temperature of ABCD (lower) surface has been defined as T_1 and EFGH (upper) surface temperature has been defined as T_2. Direction of heat flow is showed and cubic matrix dimensions are developed as L_x, L_y and L_z.

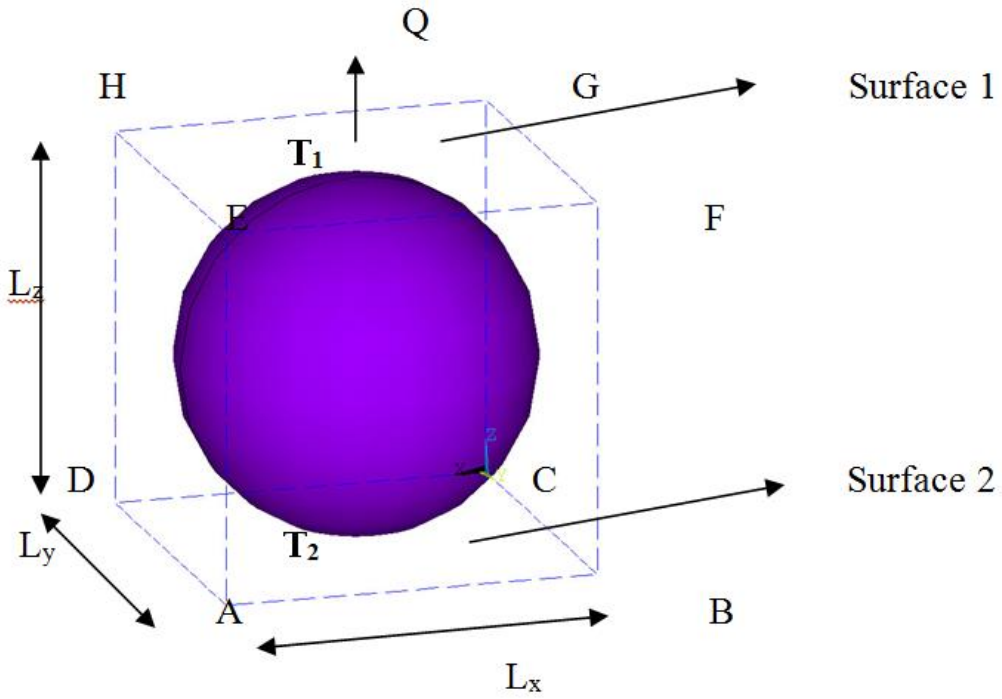

Figure 4.9 Geometry in 3-D models

Heat flow is perpendicular to EFGH and ABCD surfaces, so these surfaces are presumed to be isothermal. The other surfaces (ADEH, BCGF, CDHG and ABEF) are parallel to heat flow; therefore, they are accepted to be adiabatic. It is thought that the fillers are not kept in touch with each other and they homogeneously dispersed into matrix material.

Generated mesh for Ø=30 % sphere filler models were given in Figure 4. 10

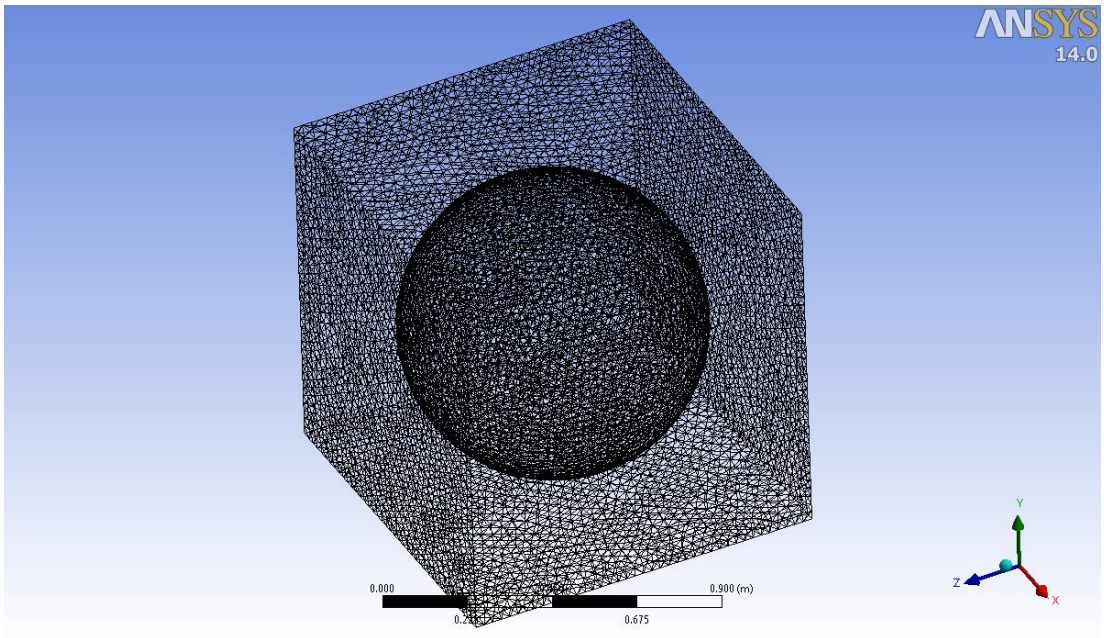

Figure 4.10 Mesh of sphere filler 3-D models for Ø=30 %

Then, the boundary conditions of analysis have been defined. Temperature of EFGH and ABCD surfaces have been set as T_1= 293 °K and T_2=303 °K respectively and constant during analysis. But, temperatures of interior region and adiabatic boundaries aren't known. These temperatures can be determined by ANSYS package. After completed the analysis, obtained heat fluxes and temperature for 1 piece sphere filler models and Ø=30 % have been in the following Figure 4.11 and Figure 4. 12.

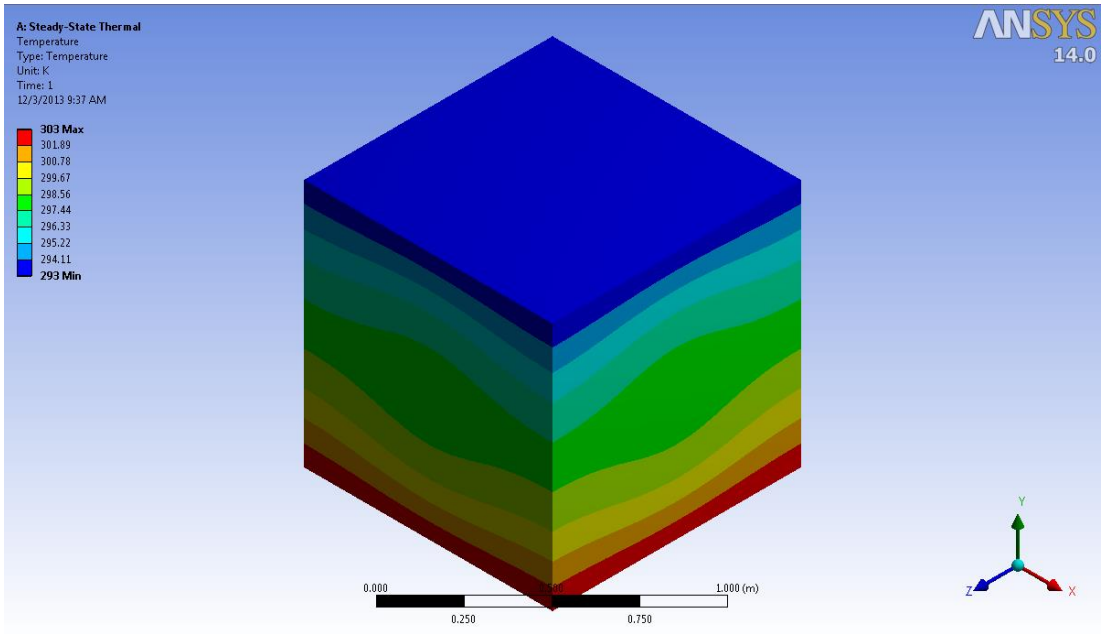

Figure 4.11 Temperature distribution of 1 piece sphere filler models for Ø=30 %.

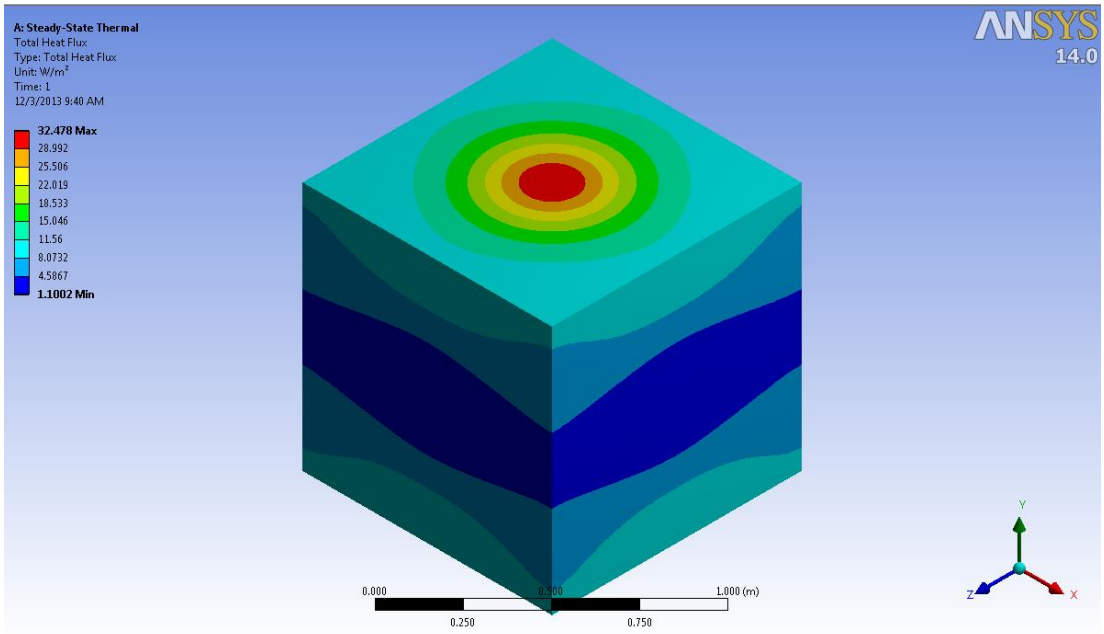

Figure 4.12 Total heat flux of 1 piece sphere filler models for Ø=30 %.

The same procedure has been carried out for cube filler models. Generated mesh for 1 piece cube filler model was shown in Figure 4.13.

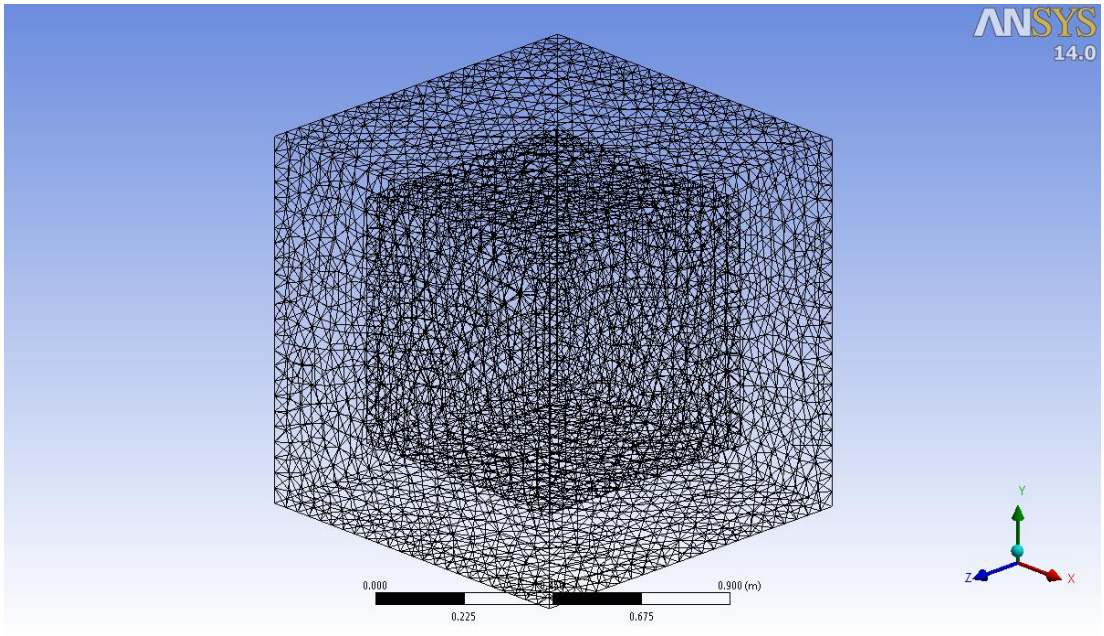

Figure 4.13 Mesh of 1 piece cube filler model for Ø=30 %.

Obtained temperature distribution and heat fluxes of 1 piece cube filler model for Ø=30 % have been shown in Figure 4.14 and Figure 4.15.

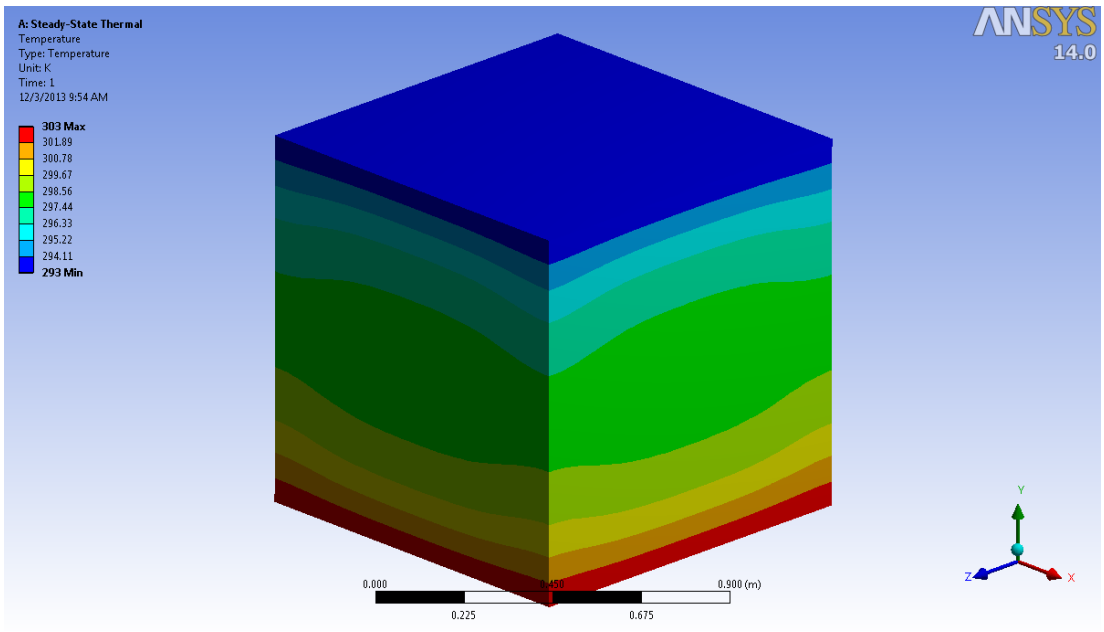

Figure 4.14 Temperature distribution of 1 piece cube filler models for Ø=30 %.

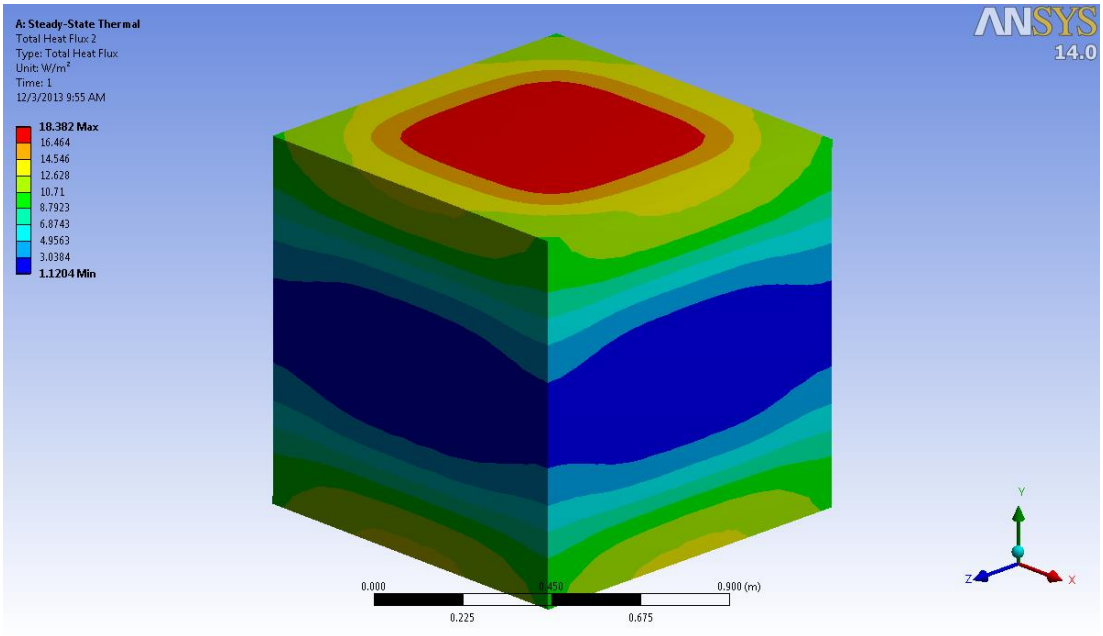

Figure 4.15 Total heat flux of 1 piece cube filler models for Ø=30 %.

The other solutions of sphere and cube models for various volume fraction have been given in Appendix E and Appendix F. And the results of analyses have discussed in Results & Discussion section.

4.2.4 Calculation of Thermal Conductivity for 3-D

Temperature distributions and heat fluxes of 3-D models have been obtained by using ANSYS 14.0 for sphere filler in cube matrix and cube filler in cube matrix. Some assumptions are made to perform analysis. These assumptions:

- Upper and lower surfaces of models have been perpendicular to heat flow and isothermal.
- Surfaces which are parallel to heat flow are assumed to be adiabatic.
- Filler particles don’t touch each other.
- Temperatures of lower and upper surfaces have been holding constant along analysis.

Equation of heat flow is solved for steady state with using ANSYS 14.0 and heat fluxes have been obtained. And thermal conductivity has been calculated by using

obtained heat fluxes. As seen in Figure 4.9, two surfaces have been assumed to be adiabatic; other two surfaces have been given T_1 and T_2 temperatures as boundary conditions in models.

Geometry in Figure 4.9 and following equations have been used to calculate thermal conductivity:

$$k_e \frac{\Delta T}{L_z} = \frac{1}{S} \sum_i \sum_j k_{ij} x_i y_j \left(\frac{\partial T_{ij}}{\partial z} \right) \tag{4.7}$$

Where;

$$s_{ij} = x_i y_j, \quad \sum_i \sum_j s_{ij} = S \text{ and } k_i = \begin{cases} k_f & \textit{if inside of filler material} \\ k_m & \textit{ifinside of matrix material} \end{cases}$$

The following equations have been achieved by benefit from Equations (4.7) and obtained graph of changes of heat flux along z direction.

$$\sum_i \sum_j k_{ij} \left(\frac{\partial T_{ij}}{\partial z} \right) = q_z \tag{4.8}$$

Consequently, a general used Equation (4.7) has taken form of following equations.

$$k_e \frac{\Delta T}{L_z} = q_z \tag{4.9}$$

L_z=1 m and ΔT=10 ˚ K have been used in analyses.

After solutions have been made by ANSYS 14.0 and heat fluxes of each point has been found. The upper surface is divided into ten equal longitudinal and transverse edges. In this equation, only amount of total heat passing through edges are unknown. The Simpson method has been used to integrate heat fluxes in z direction

for these edges. And k of these edges has been calculated by equation (4.9). Thermal conductivity of HDPE/Al composites has been determined by taking average of k of these edges.

CHAPTER FIVE
THEORETICAL AND EMPIRICAL THERMAL CONDUCTIVITY MODELS

5.1 Thermal Conductivity Theory

One of the essential and important properties of solids is their skills to conduct heat. This charcteristic is generally quantified in point of coefficient of thermal conductivity (Shinde & Goela, 2006). “The thermal conductivity of a material can be defined as a rate at which heat is transferred by conduction through a given unit area of a given material, when the temperature gradient is normal to the cross sectional area” (Mutruni, 2006, p. 5).

Fourier proposed thermal conductivity theory in 1822. Fourier developed equation which is called Fourier’s law for the local heat flux is proportional to negative local temperature gradient, homogeneous solid. For one dimension steady state heat transfer, the equation is as follows (Durmaz, 2006; Mutruni, 2006):

$$q = -kA\frac{dT}{dx} \tag{5.1}$$

Where;

q= Heat flow (W/m)
k= Thermal conductivity (W/m^2K)
A= Cross section area (m^2)
dT/dx= Temperature gradient

Negative sign in equation shows the reduction of temperature occurs from hot side to cooler side. The amount of k is constant and is called as coefficient of thermal conductivity. The thermal conductivity measurement includes temperature difference and heat flux measurement. For cross section area, it is constant and trough L, this equation return to following equation:

$$-q\frac{L}{Ak}=\int_{T_1}^{T_2}dT \tag{5.2}$$

where T_1 and T_2 are the temperatures at any two points along the heat flow.

5.2 Theoretical and Empirical Thermal Conductivity Models

The thermal conductivity of a material is affected by various significant factors. The thermal conductivity of filler and matrix, polymer crystalline, filler size, concentration, shape, mixing degree, orientation, bonding between the filler and matrix are some of these factors. Thermal conductivity is a bulk property and is analogous to viscosity, tensile modulus, and shear modulus. The numerical relationship among the composite and the pure polymer is given by following equation (Weber, 2001):

$$\frac{k_c}{k_p}=\frac{\eta_c}{\eta_p}=\frac{E_c}{E_p}=\frac{G_c}{G_p} \tag{5.3}$$

In equation (3.3), k is thermal conductivity, p is pure polymer, c is composite, η is viscosity, E is elastic modulus, and G is shear modulus.

Inverse mixture rule and standard mixture rule formed basis of thermal conductivity models (Tekçe, 2004).

- ✓ Standart mixture rule :

$$K=\sum_{i=1}^{n}\theta_i K_i \tag{5.4}$$

- ✓ Inverse mixture rule :

$$K = \sum_{i=1}^{n} \frac{\theta_i}{K_i} \tag{5.5}$$

Where K is thermal conductivity of composite, n is the number of constituents of composites, i is the index variable for constituents of composite, K_i is thermal conductivity of i^{th} constituent.

Mixture rule predict the thermal conductivity of composite in direction of filler. Mixtures rule is weighted average of thermal conductivity of matrix and filler. For unidirectional composite with continuous fibers, the thermal conductivity is predicted by rule of mixtures. The inverse mixture rule (series model) is utilized to predict unidirectional composite with continuous fibers' thermal conductivity in the direction is at 90 degrees to fillers (Tekçe, 2004).

When two component composites are investigated, the simplest approaches would be that materials ordered in either series or parallel with respect to heat flow. While series arrangement gives the lowest thermal conductivity value, the parallel arrangement gives uppest thermal conductivity values (Kumlutaş et. al. 2003).

A great number of theoretical and empirical models have been recommended to estimate thermal conductivity coefficient of polymer composites.

In equation, k_m is matrix material thermal conductivity coefficient (continuous phase) (W/mK), k_f is filler material thermal conductivity coefficient (discontinuous phase) (W/mK), Φ is volume fraction of filler material (%).

Among these models, series, parallel and geometric mean models are taken notice for the simplest cases. These models are followed by (Kumlutaş & Tavman, 2003):

✓ Series Model:

$$k_e = \frac{k_f k_m}{k_m \theta + k_f (1-\theta)} \tag{5.6}$$

✓ Parallel Model:

$$k_e = k_f \theta + k_m (1-\theta) \tag{5.7}$$

✓ Geometric Mean Model:

$$k_e = k_f^{\theta} + k_m^{(1-\theta)} \tag{5.8}$$

Cheng & Vacon accepted that filler materials are discontunuous phase which has parabolic distribution. And a study was started depending on Tsao's possibility model. Results of studies, Cheng & Vachon improved a model for spherical particles and fiber filled composites. In two phase composite materials, Tsao constants were evaluated, a expression depending on volumetric fraction of filler materials in closed-form was obtained. This model is given by (Cheng & Vachon, 1970):

✓ Cheng &Vacon Theoretic Model:

if $k_m > k_f$

$$\frac{1}{k_e} = \frac{2}{\sqrt{C(k_f - k_m)\left[k_m + B(k_f - k_m)\right]}} \tan^{-1} \frac{B}{2} \sqrt{\frac{C(k_f - k_m)}{k_m + B(k_f - k_m)}} + \frac{1-B}{k_m} \tag{5.9}$$

if $k_f > k_m$

$$\frac{1}{k_e} = \frac{2}{\sqrt{C(k_f - k_m)\left[k_m + B(k_f - k_m)\right]}} \ln \frac{\sqrt{k_m + B(k_f - k_m)} + \frac{B}{2}\sqrt{C(k_f - k_m)}}{\sqrt{k_m + B(k_f - k_m)} - \frac{B}{2}\sqrt{C(k_f - k_m)}} + \frac{1-B}{k_m} \tag{5.10}$$

where

$$B = \sqrt{\frac{3\theta}{2}} \quad \text{and} \quad C = -4\sqrt{\frac{2}{3\theta}}$$

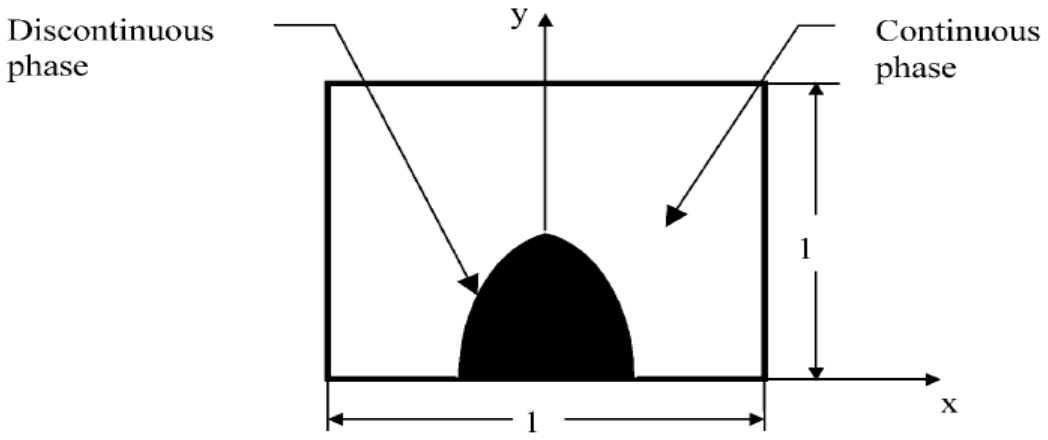

Figure 5.1 Discontinuous phase parabolic distribution for Cheng and Vachon model (Kumlutaş et. al., 2003)

Lewis & Nielsen used an elastic moduli analogy. Lewis & Neilsen arranged the Haplin-Tsai equations so as to contain geometrical particle shape and orientation of packing in two phase system. Obtained form equations (Lewis & Nielsen, 1970; Nielsen, 1970):

- ✓ Lewis and Nielsen Semi-Theoretical Model:

$$k_e = k_m\left[\frac{1+AB\theta}{1-B\theta\Psi}\right] \tag{5.11}$$

Where

$$B = \frac{k_f/k_m - 1}{k_f/k_m + A} \quad \text{and} \quad \Psi = 1+\left(\frac{1-\theta_m}{\theta_m^2}\right)$$

A and $Ø_m$ depend on shape and orientation of filler materials. $Ø_m$ is maximum packing fraction of the filler materials. This means the correct volume of partial partition to the volume look like taking up when packed to their maximum dimension. The values of A and $Ø_m$ for many geometric shapes and orientation are given in Table 5.1 and Table 5.2 (Lewis & Nielsen, 1970; Nielsen, 1970).

Table 5.1 Value of *A* for various systems (Lewis & Nielsen, 1970; Nielsen, 1970).

Type of filler material phase	**Direction of heat flow**	***A***
Cubes	Any	2.00
Spheres	Any	1.50
Aggregates of Spheres	Any	3.00
Randomly oriented rods		
Aspect ratio=2	Any	1.58
Aspect ratio=4	Any	2.08
Aspect ratio=6	Any	2.80
Aspect ratio=10	Any	4.93
Aspect ratio=15	Any	8.38
Uniaxial oriented fibers	Perpendicular to fibers	2L/D(Length, D:Diameter)
Uniaxial oriented fibers	Parallel to fibers	0.50

Table 5.2 Value of $Ø_m$ for various systems (Lewis & Nielsen, 1970; Nielsen, 1970).

Shape of particle	**Type of packing**	$Ø_m$
Spheres	Hexagonal close	0.7405
Spheres	Face centered cubic	0.7405
Spheres	Body centered cubic	0.6000
Spheres	Simple cubic	0.5240
Spheres	Random close	0.6370
Rods or fibers	Uniaxial hexagonal close	0.9070
Rods or fibers	Uniaxial simple cubic	0.7850
Rods or fibers	Uniaxial random	0.8200
Rods or fibers	Three dimensional random	0.5200

Maxwell is one of the first researchers studied on heterogeneous materials thermal conductivity. Using potential theory, Maxwell derived an expression for conductivity of randomly dispersed and non-interaction homogeneous spheres in homogeneous medium. Maxwell model is not used in many systems because this model is derived for non-interacting spheres. This expression is followed by (Maxwell, 1954):

- ✓ Maxwell Theoretical Model :

$$k_e = k_m \frac{k_f + 2k_m + 2\theta(k_f - k_m)}{k_f + 2k_m - \theta(k_f - k_m)} \tag{5.12}$$

Agari & Uno model depends on generalization of series and parallel models and correlates with skill of fillers to make conductive chains of particle with thermal conductivity (Agari & Uno, 1986):

- ✓ Agari and Uno Model :

$$k_e = k_f^{\theta C_2} (C_1 k_m)^{(1-\theta)} \tag{5.13}$$

C_1 and C_2, which depend on type of matrix and filler material, are constant. C_1 is value of particle effect on the polymer secondary structure. C_2 measures the ease of the particles to form conductive chains, the more easily particles are gathered to form conductive chains, the more thermal conductivity of particles contributes to change thermal conductivity of composite, C_2 becomes closer to 1. Values of C_1 and C_2 are given in Table 5.3 (Agari & Uno, 1986; Kumlutaş and Tavman, 2003).

Coefficients of C_1 and C_2 are determined by using linear regression method. The logarithm of experimental thermal conductivity is plotted against to volume fraction of filler particles. And linear regression equation is obtained from this graph is used to calculate coefficients of Agari & Uno model. So, Agari & Uno model give closed values with experimental values. But the disadvantage of this model is that experimental results are required to determine C_1 and C_2 coefficients or table of C_1 and C_2 values must be available for each filler and matrix materials. In addition, Lin et. al. found that C_2 is based on used unit (Agari & Uno, 1986; Tavman, 1998).

Table 5.3 C_1 and C_2 constant (Kumlutaş & Tavman, 2003)

Matrix Material	Filler Material	C_1	C_2
Polyethylene	Graphite	0.898	0.882
Polyethylene	Copper	1.073	0.888
Polyethylene	Al_2O_3	0.859	0.902
Polyamide	Graphite	1.017	0.922
polystyrene	Graphite	1.024	0.892

Lord Rayleigh took into account thermal interaction between particles, and developed Maxwell's solution. The equation for a cubic array was given (Rayleigh, 1892):

- ✓ Lord Rayleigh Model:

$$k_e = k_m \left[\frac{\frac{2k_m + k_f}{k_m - k_f} - 2\theta - 0.525\left(\frac{3k_m - 3k_f}{4k_m + 3k_f}\right)\theta^{\frac{10}{3}}}{\frac{2k_m + k_f}{k_m - k_f} - 2\theta - 0.525\left(\frac{3k_m - 3k_f}{4k_m + 4k_f}\right)\theta^{\frac{10}{3}}} \right] \quad (5.14)$$

If Ø is small enough, the final term may be neglected and equations return to Maxwell's equation.

Meredith & Tobias modified Maxwell's model by thinking infinite count of small fillers addition to a two phase uniform mixture. Meredith & Tobias model is given by (Meredith & Tobias, 1960).

- ✓ Meredith & Tobias Model:

$$k_e = k_m \left[\frac{\frac{2k_m + k_f}{k_m - k_f} - 2\theta + 0.409\left(\frac{6k_m + 3k_f}{4k_m + 3k_f}\right)\theta^{\frac{7}{3}} - 2.133\left(\frac{3k_m - 3k_f}{4k_m + 3k_f}\right)\theta^{\frac{10}{3}}}{\frac{2k_m + k_f}{k_m - k_f} - 2\theta + 0.409\left(\frac{6k_m + 3k_f}{4k_m + 3k_f}\right)\theta^{\frac{7}{3}} - 0.906\left(\frac{3k_m - 3k_f}{4k_m + 4k_f}\right)\theta^{\frac{10}{3}}} \right] \quad (5.15)$$

Hamilton & Crosser defined followed equation for the thermal conductivity of two-component mixture (Hamilton & Crosser, 1962):

- ✓ Hamilton & Crosser Model:

$$k_e = k_m \frac{k_f + (n-1)k_m - (n-1)\theta(k_m - k_f)}{k_f + (n-1)k_m + \theta(k_m - k_f)} \tag{5.16}$$

Where n is an empirical constant (n=3 for spheres).

Russell obtained one of the first models by using the electrical analogy. Assuming that the filler particle is isolated cubes of same size distributed in matrix material and isothermal lines are planes, he obtained a thermal conductivity model for composite by series parallel network (Russell, 1935).

- ✓ Russell Model:

$$k_e = k_m \left[\frac{\theta^{\frac{2}{3}} + \frac{k_m}{k_f}\left(1 - \theta^{\frac{2}{3}}\right)}{\theta^{\frac{2}{3}} - \theta + \frac{k_m}{k_f}\left(1 + \theta - \theta^{\frac{2}{3}}\right)} \right] \tag{5.17}$$

Springer & Tsai supposed a cylindrical model fibers had square distribution in the matrix material and developed a semi-theoretical model. The analogy between unidirectional composite and thermal conductivity problem respond to heat transfer and shear loading. The predicting of the thermal conductivity is on basis of this in the direction normal to the fibers (Springer & Tsai, 1967).

✓ Spinger & Tsai Semi-Theoretical Model:

$$k_e = \left[1 - 2\sqrt{\frac{\theta}{\pi}} - \frac{4}{\sqrt{1-\left(B^2\frac{\theta}{\pi}\right)}}\tan^{-1}\left(\frac{\sqrt{1-\left(B^2\frac{\theta}{\pi}\right)}}{1+B\sqrt{\frac{\theta}{\pi}}}\right)\right] \quad (5.18)$$

Where

$$B = 2\left(\frac{k_m}{k_f} - 1\right)$$

Given equation was developed by Basschirow & Selenew for spherical of particles and two phases which are isotropic (Basschirow & Selenew, 1976).

✓ Basschirow & Selenew Model:

$$k_e = k_m\left[1 - \frac{a^2\pi}{4} + \frac{a\pi p}{2}\left(1 - \frac{p}{a}\ln\left(1+\frac{a}{p}\right)\right)\right] \quad (5.19)$$

Where

$$p = \frac{k_f}{k_m - k_f} \text{ and } a = \left(\frac{6\theta}{\pi}\right)^{1/3}$$

Zehner & Schlünder developed a model depending on heat flow model, which is a one dimension, for conduction along a packed bed of spherical particles; the supposed particles included point connection in heat flow direction (Zehner & Schlünder, 1970).

✓ Zehner & Schlünder Model:

$$k_e = k_f\left[1-(1-\theta)^{0.5}+\frac{2(1-\theta)^{0.5}}{1-KB}\left[\frac{(1-K)B}{(1-KB)^2}\ln\left(\frac{1}{K}B\right)-\frac{B+1}{2}-\frac{B-1}{1-KB}\right]\right] \quad (5.20)$$

Where

$$K=\frac{k_f}{k_m} \text{ and } B=1.25\left(\frac{1-\theta}{\theta}\right)^{\frac{10}{9}}$$

Woodside & Messmer offered a model being a mixture of series and parallel distributions. They used the electrical conductivity analogy of an aggreegate of conductive particles saturated with conducting electrolyte to derive a modified resistor equation to predict the effective thermal conductivity of porous media (Woodside & Messmer, 1961).

✓ Woodside & Messmer Model:

$$k_e=\frac{ak_mk_f}{k_m(1-d)+dk_f}+ck_f \quad (5.21)$$

Where

$$c=\theta-0.03,\ a=1-c \text{ and } d=\frac{1-\theta}{a}$$

The signification for “c” is determined by exercising the experimental result of Stephenson and Woodside for a cubic pack of spheres model at a concentration of 47.6%.

CHAPTER SIX
RESULTS & DISCUSSION

6.1 Experimental Results

The aim of the experimental study is to determine thermal conductivity of HDPE/Al composites as a function of volume fraction and size of Al particles. The HDPE/Al (80 nm) composites were prepared to according to refer in Materials & Method section in 150 mm width, 150 mm length, 1 mm thickness. The values of volume fraction of Al for HDPE/Al (80 nm) composites are 1, 2, 4, 6, 8, 10, 12, 15, 18, 21, 25 and 30 %. But the HDPE/Al (40-80 μm) composites were produced for Tavman (1996). These samples were prepared by using mold compression process. HDPE and Al powders were mixed in tumble mixer for 20 min. Then this mixture was melted pressure in a mold and solidified with air cooling. The process conditions were: molding pressure of 4 MPa, molding temperature of 185 ºC and heating residence time of 20 min for samples prepared. The resulting samples for thermal conductivity measurements were rectangular in shape of 50 mm width, 100 mm length and 17 mm thickness. The values of volume fraction of Al for HDPE/Al (40-80 μm) composites are 1, 2, 3, 4, 5, 6, 8, 10, 12, 14, 17, 29, 24, 28 and 33 %.

Thermal conductivities of both types of composite samples were measured by C-THERM thermal conductivity analyzer. Experimental results of HDPE/Al composites are given in Figure 6.1 for aluminum particle sizes as a function of Al contents in matrix material. As shown in Figure 6.1, thermal conductivity of HDPE/Al composites raises by increasing volume fraction of Al in HDPE matrix. This increase is foreseeable, because thermal conductivity of Al particles is higher than that of HDPE. It is found that size of Al particles hasn't significant effect on thermal conductivity, thermal conductivity of HDPE/Al (80 nm) is close to thermal conductivity of HDPE/Al (40-80 μm).

The thermal conductivity value of pure HDPE is measured as 0.614 W/mK. The thermal conductivity is gone up to mean value of 1.372 W/mK for HDPE composites at 30 vol % of maximum concentration of Al (80 nm). The thermal conductivity of

HDPE/ Al (40-80 µm), is nearly 2.5 times that of pure HDPE, is 1.503 W/mK at 33 vol % of maximum concentration of Al. With addition of 12 % of Al (80 nm) and Al (40-80 µm), the thermal conductivity improves by about 42.48 % and 44.83 % respectively with respect to pure HDPE.

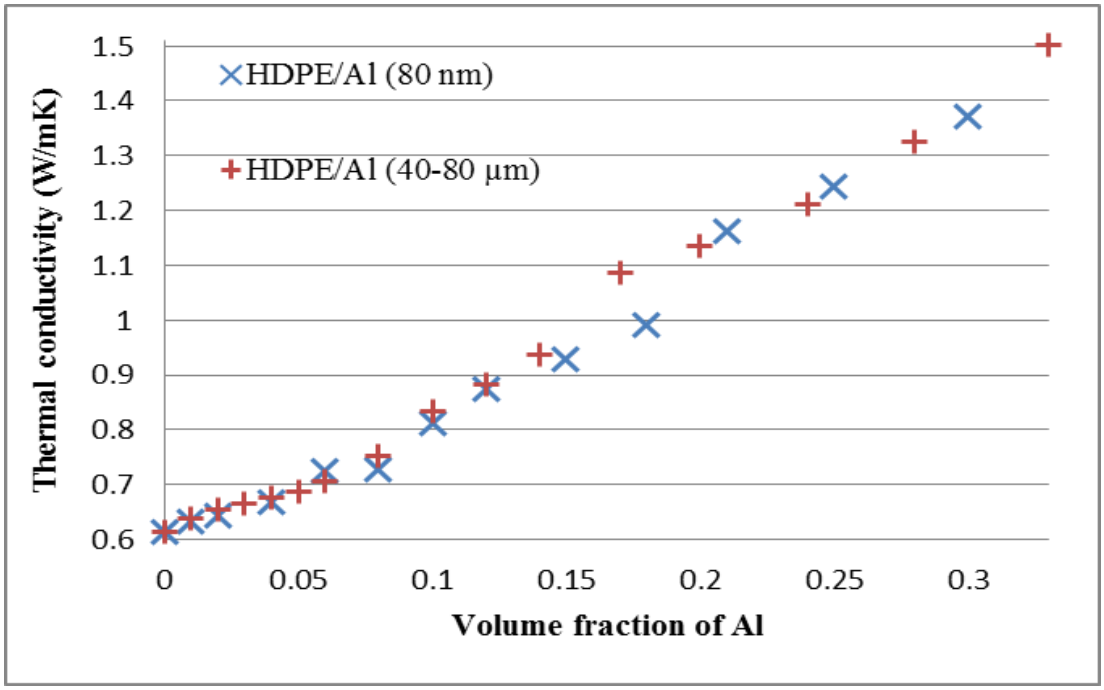

Figure 6.1 Comparison of experimental values for different aluminium filler size

At low volume concentrations of Al (Ø≤6 %), thermal conductivity of composites rises slowly. The reason is that Al particles homogenously disperse in HDPE matrix and cannot get in touch with each other and maintain spherical shape. At high volume concentration of Al, Al particles occur aggregate forms and conductive chains occur along heat flow direction. Thus, thermal conductivity of HDPE/Al composites increases more rapidly.

6.2 2-D Model Analysis Results

Numerical analysis were carried out for various filler shapes (square prism and long cylinder), arrangement (1, 2, 4, 8 and 16 piece of fillers), and volume contents of Al particles (1%, 2%, 4%, 6%, 8%, 10%, 12%, 15%, 18%, 21%, 25% and 30%) in

2-D. Forms of arrangement for using numerical analysis have been given in Appendix B.

Solutions of heat fluxes and temperature distributions have been obtained by ANSYS 14.0. Heat fluxes and temperature distributions of all models have been shown in Appendix D. As increasing concentration of fillers, the maximum heat flux values increase and the more waves occur in thermal isotherm. For square models, the maximum heat flux values occur at edge of fillers. For circle models, especially better noticeable as increasing volume fraction, the maximum heat fluxes are at end points of closest to upper and lower surfaces.

Thermal conductivity of each arrangement forms were calculated by calculation methods explained in previous chapter. Obtained effective thermal conductivity values have been shown in Appendix F, In Figure 6.2 and Figure 6.3, experiment values were compared with different arrangement forms as a function of volume fraction of Al particles in HDPE matrix.

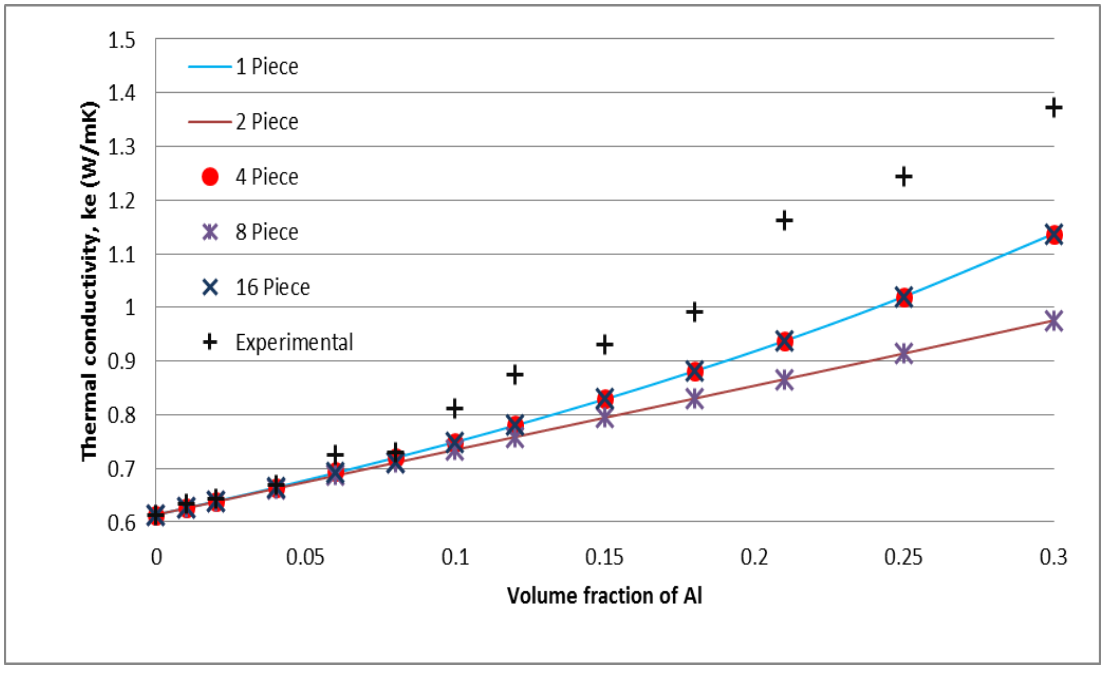

Figure 6.2 Comparison of numerical solution for various piece circle filler models and experimental values for different volume fraction of Al

As seen in Figure 6.2 and Figure 6.3, up to 10 % volume fraction of Al content, good agreement was seen between all arrangements form estimation and experimental data of thermal conductivity. After this concentration, all arrangement forms in 2-D fail to estimate experimental results. This is because making assumption to solve numerical analysis. The Al particles distributed in matrix and don't touch each other. These assumptions are effective at low Al particles contents Ø< 10%. But at above Ø>10%, Al particles occurs conductive chains along direction of heat transfers, this phenomenon causes large rising in thermal conductivity of polymer composites.

In 2-D analyses, the square prism is selected as matrix shape and the circle infinitely long cylinder (circle) or square prism are chosen as filler material for making simulation. Generally 2-D models are used to simulation of composite reinforced with fiber. HDPE/Al composite is a polymer composites reinforced with particulate. So, at especially high concentration, 2-D models fail to estimate the experimental values.

If all piece-circle filler models are compared themselves, results of 2 piece filler model is closed to results of 8 circle filler model. In addition, 1, 4 and 16 piece filler models give closed results each other. Moreover, thermal conductivity of 2 and 8 piece filler models are lower than that of 1, 4 and 16 piece filler models. This reason is that if amount of fillers along heat flow direction (y direction) increases, thermal bridges improve in y direction and heat easily flow along the composite. If arrangement of fillers difference, but the amount of fillers perpendicular to and parallel to heat flow are nearly equal, the thermal conductivity values of this arrangement are too much close.

As seen in Figure 6.4, thermal conductivity of all piece square filler models are higher than thermal conductivity of the same piece circle filler models. Up to 6 vol % of Al, all piece circle and square models agree very well each other. After this value difference between sphere and cube models increases with increase in Al contents. This difference is most likely depending on increase in total heat flux because of shape of fillers.

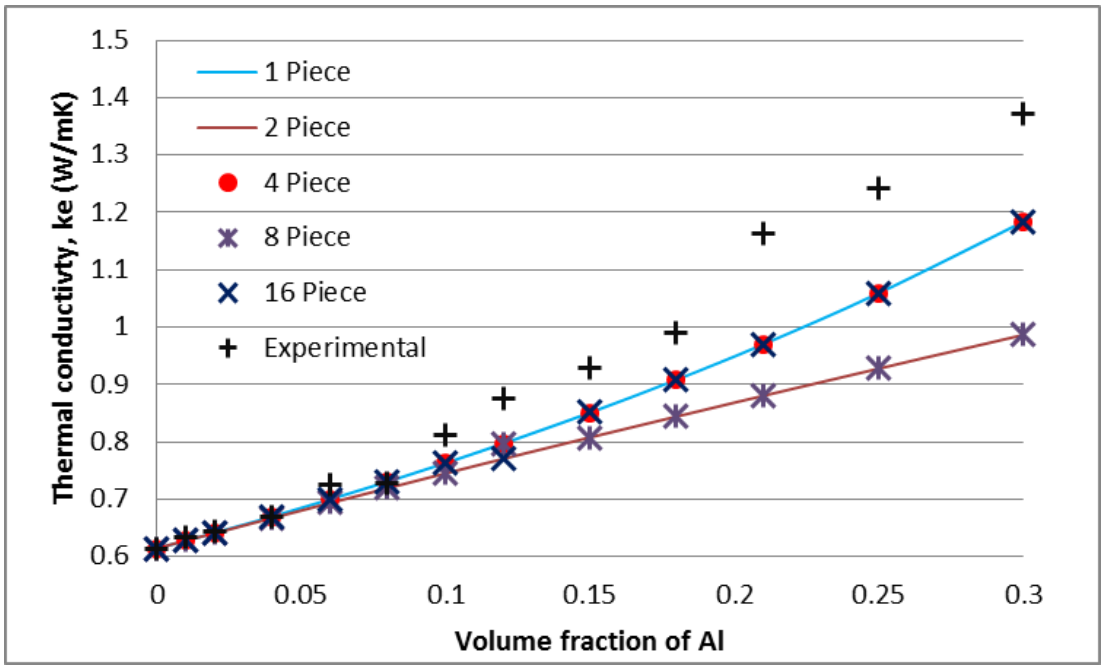

Figure 6.3 Comparision of numerical solution for various piece square filler models and experimental values for different volume fraction of Al

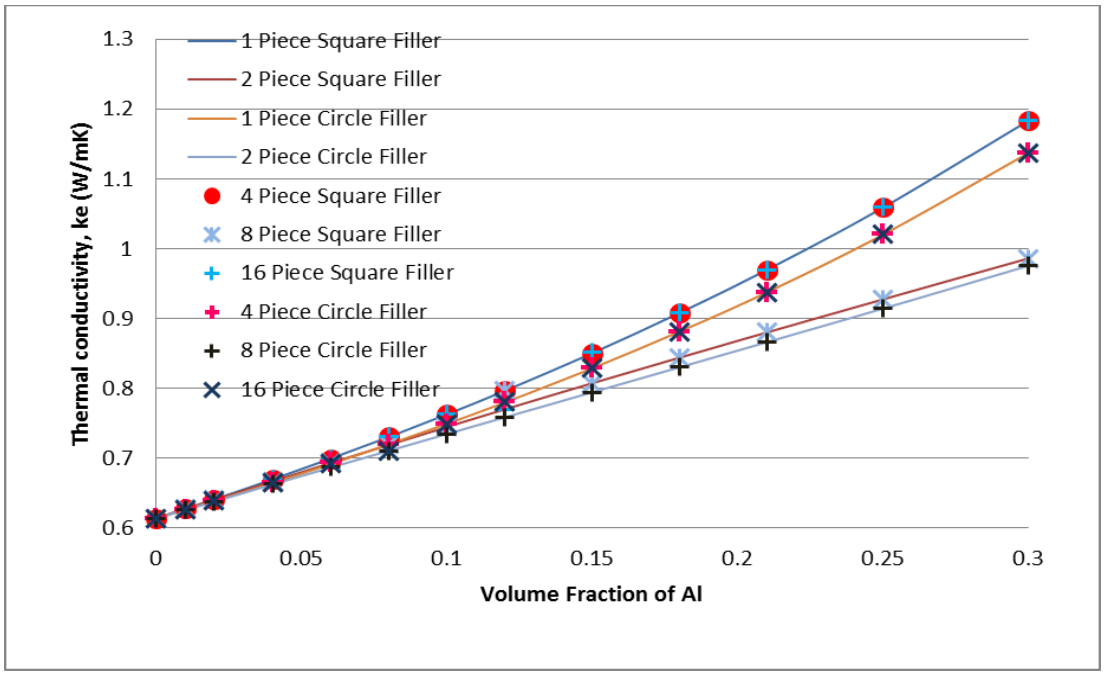

Figure 6.4 Comparision of numerical solution for various piece square and criclefiller models values for different volume fraction of Al

6.3 3-D Model Analysis Results

Numerical analyses were carried out for various filler shapes (sphere and cube), arrangement (1, 2, 4, 8 and 16 piece of fillers), and volume contents of Al particles (1%, 2%, 4%, 6%, 8%, 10%, 12%, 15%, 18%, 21%, 25% and 30%) in 3-D. Forms of arrangement for using numerical analysis have been given in Appendix C.

Solutions of heat fluxes and temperature distributions have been obtained by ANSYS 14.0. Heat fluxes and temperature distributions of all models have been given in Appendix E. As addition of Al particles increases, deflection of thermal isotherm lines increase rapidly. Deflection is seen in the surfaces more near to filler materials. When increasing thermal conductivity, shape of filler materials occur in the surfaces. For 4-piece-filler model, the model which is shown in Appendix B.4. is designed to disperse homogenously and symmetrically. Because of this model, the deflection of isothermal lines is much more than other models. One part of model has filler materials occurred deflection and the other side hasn't occurred and isothermal lines maintained. As seen the Appendix E.2., it is noticed that increasing concentration of Al content, the maximum values of heat fluxes go up. The maximum heat fluxes of sphere filler models are higher than that of cube models. But the maximum heat flux area on surfaces in the cube models is bigger than in sphere filler. At the lower concentration of fillers, the values and area of heat fluxes for sphere and cube models are similarly each other. The amount of total heat fluxes along upper surfaces, so the thermal conductivity values are nearly equal.

In Appendix F, thermal conductivity of each arrangement forms were calculated by calculation methods explained in previous chapter. Obtained effective thermal conductivity values have been shown in Appendix F. In Figure 6.5 and Figure 6.6, experiment values were compared with different arrangement forms as a function of volume fraction of Al particles in HDPE matrix.

Experimental values have been compared with sphere filler arrangements shown in Figure 6.5. At above 12 % volume fraction of Al in HDPE matrix, fillers begun to

get in touch with each other and not to fit inside matrix for 2 and 16 piece sphere fillers. But the same problem occurs for upper 25 % volume fraction of Al in HDPE matrix for 4 piece sphere fillers.

As shape of Al particles are assumed to be spherical, sphere filler models are good correlation with experimental values. At Ø<10 vol %, thermal conductivity of all piece sphere filler models predict experimental results well. 1, 4 and 8 piece sphere filler models have given closed thermal conductivity values with experimental data for all volume contents of Al. In addition, 2 and 16 piece sphere filler models give approximately the same effective thermal conductivity values in whole range of Al content.

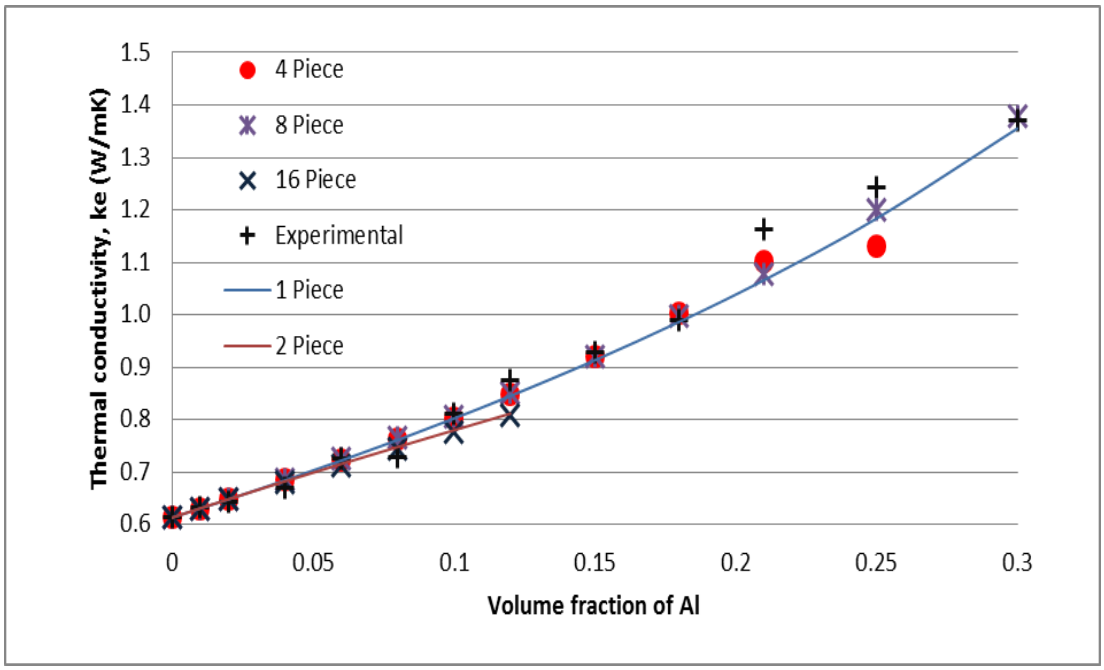

Figure 6.5 Comparision of numerical solution for various piece sphere filler models and experimental values for different volume fraction of Al

As seen in Figure 6.5, at above 21 % volume fraction of Al in HDPE matrix, fillers begun to get in touch with each other and not to fit inside matrix for 2 and 16 piece cube fillers.

Like as sphere filler models, thermal conductivities of 1 and 8 piece cube filler models are nearly the same. In addition, 2 and 16 cube filler models give closed results to each other. After Ø>18 %, thermal conductivities of 4 piece cube filler model are above other piece cube filler models. Until this value of volume fraction, results of 4 piece cube arrangement have not been very much different from 1 and 8 piece cube filler models. Especially, at low volume fraction (Ø≤6 %), results of all cube filler arrangement are closed each other. For 1 and 2 vol % of Al contents, all cube models show nearly equal value to experimental data. But at above this value, 1, 4 and 8 piece cube filler models overestimate experimental data. 2 and 16 piece cube filler models underestimate experimental thermal conductivity in range of 4-10 vol % of Al, the thermal conductivity is higher than experimental data for Ø> 0.1.

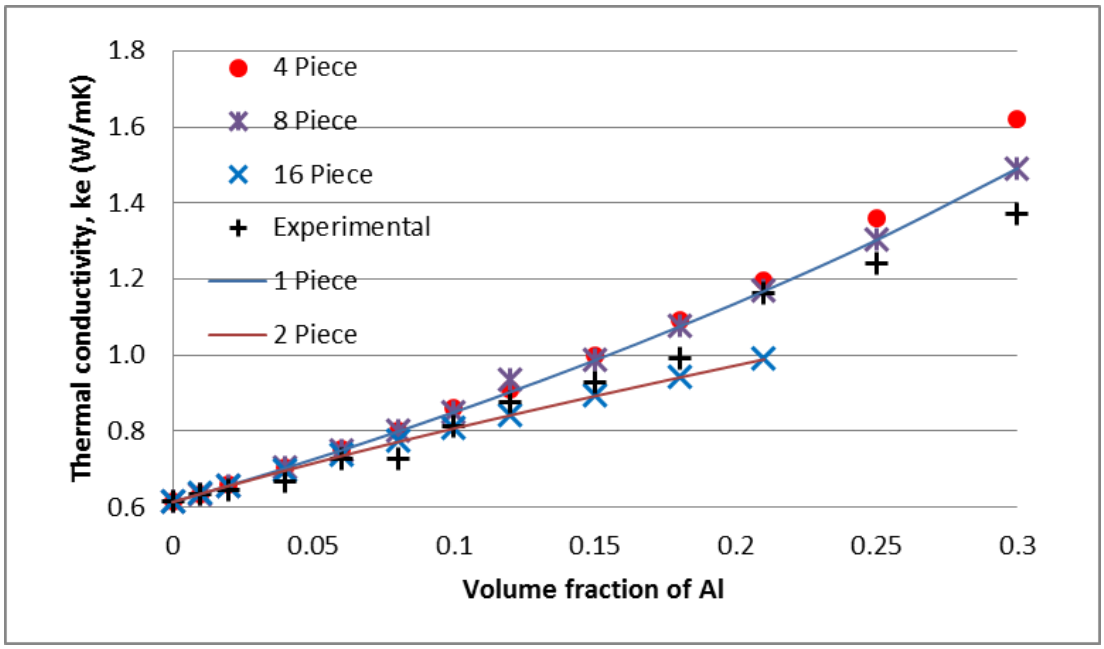

Figure 6.6 Comparision of numerical solution for various piece cube filler models and experimental values for different volume fraction of Al

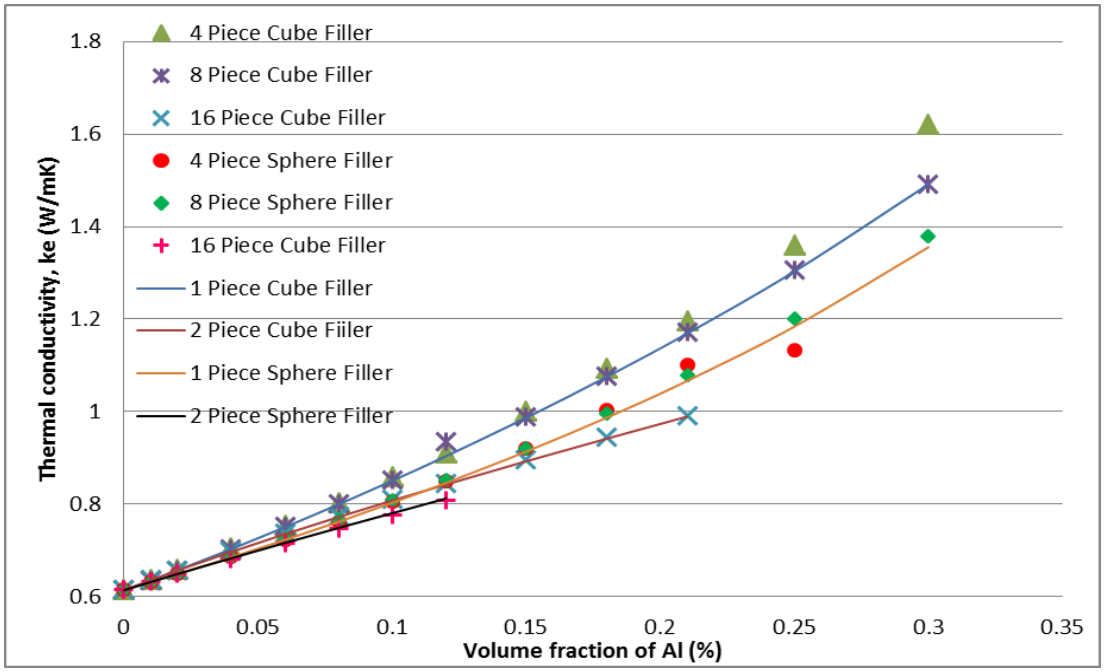

Figure 6.7 Comparision of numerical solution for various piece cube and sphere filler models values for different volume fraction of Al

The cube filler models give bigger thermal conductivity values than sphere filler models. Up to 12 vol % of Al, 1, 4 and 8 sphere filler models are good aggreement with 2 and 16 cube filler models. Beyond 18 % of Al particle content 4 piece cube filler model gives higher thermal conductivity value than the other filler models.

6.4 Theoretical Models Results

Series, Parallel, Geometric Mean, Maxwell, Cheng & Vachon's, Springer & Tsai's Model, Russell, Rayleigh's, Woodsite & Messmer's Theoretical Model, Lewis & Nielsen's Semi-Theoretical Model, Hamilton & Crosser's, Bashirrow & Selenew, Zehner & Schlünder's, Meredith & Tobias and Agari & Uno Model have been used in this study. Results of all theoretical models were given in Appendix G.

Parallel, Zehner & Schlünder's, Woodsite & Messmer's and geometric mean models have given too higher results than experimental results and other theoretical models. If these models plotted versus volume fraction in graph, the other models

results wouldn't be seperated each other. Because of this, these models haven't been shown in Figure 6.8. The other models have been displayed in Figure 6.8.

The geometric mean model fits the thermal conductivity data well at Ø≤6 % in good aggreement with experimental data. But, at Ø>6 %, it overestimates the thermal conductivity. Thermal conductivity obtained by geometric mean model increases exponentially with increasing Al content.

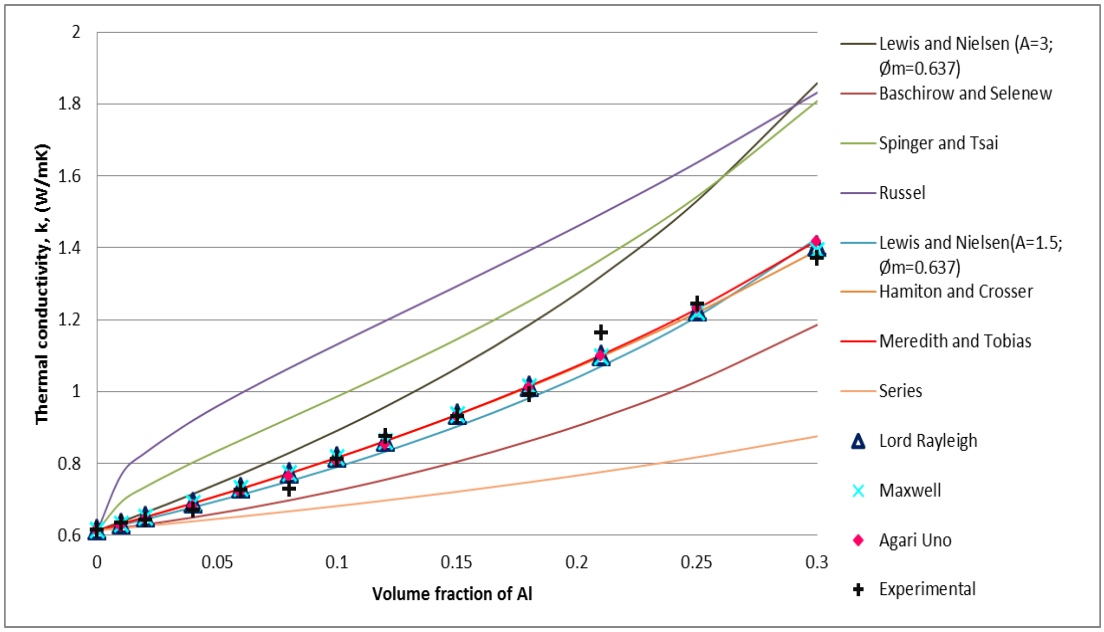

Figure 6.8 Comparision of theoretical models results and experimental values as a function of volume fration of Al

As seen in Appendix G and Figure 6.8, thermal conductivity values are calculated by series models are the lowest and the highest thermal conductivity values are determined by parallel model. Maxwell's, Hamilton & Crosser's, Meredith & Tobias's, Lord Rayleigh's, Agari & Uno's, Lewis & Nielsen's (A=1.5, $Ø_m$=0.637) theoretical models are closer to experimental values. The reasons are that aluminium particles can be assumed to be spherical and Maxwell model was developed for spherical filler which dispersed randomly in matrix and not contact with each other. In addition, Hamilton & Crosser's, Meredith & Tobias's and Lord Rayleigh's models developed from Maxwell's model. For spherical filler shape, Hamilton & Crosser's

theoretical model return to Maxwell model. So, Maxwell's and Hamilton & Crosser's models have been given the same results in this study.

Agari & Uno model are in good agreement with experimental results at all volume content of Al particle. This is because that coefficients of Agari & Uno model are named as C_1 and C_2 are determined by using linear regression equation. This equation obtains from graph of logarithm experimental thermal conductivity values versus volume fraction of Al particles. The main disadvantage of this model is that experimental results are required to calculate C_1 and C_2 coefficients or table including C_1 and C_2 values for filler and matrix materials must be presented.

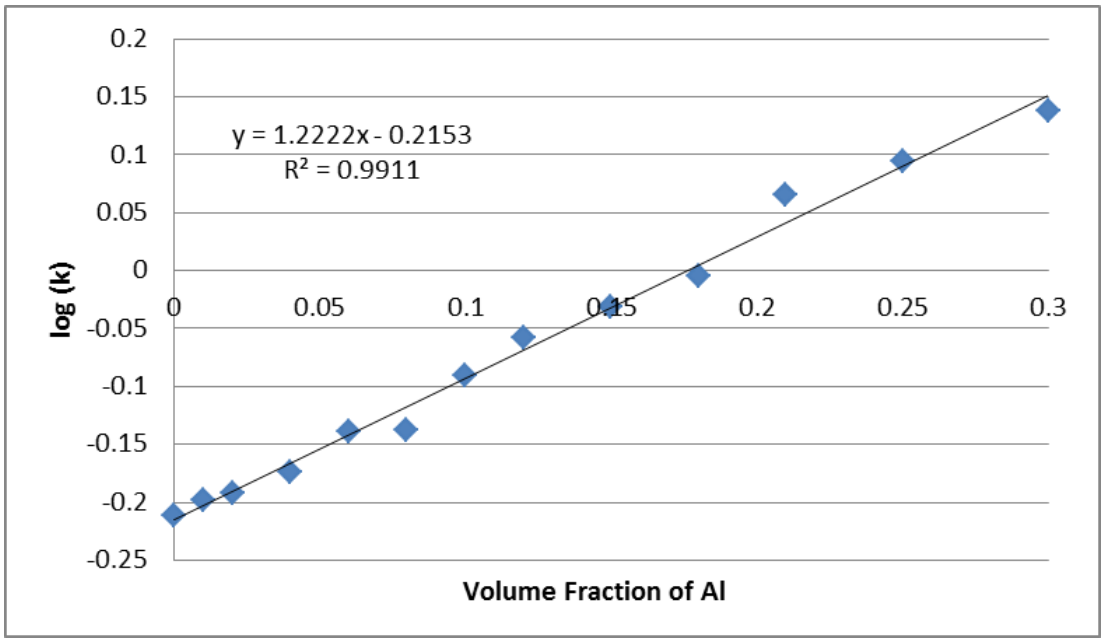

Figure 6.9 Plot of logarthim of experimental values versus volume fraction of Al

This graph is shown in Figure 6.9. It is seen that logarithm of HDPE/Al composites thermal conductivity occurs linear increase as a function of volume fraction of Al particles. In this study, determined coefficients of Agari and Uno model are as C_1= 0.992 and C_2= 0.436 and correlation coefficient of linear regression is 0.991.

Table 6.1 Some previous research about polymer composites reinforced Al particles

Researchers	Year	Materials & Methods	Results
Chauhan, Singhvi, & Singh	2012	• This study about geometry effect on thermal conductivity of polymer composites. • The new thermal conductivity model developed based on equal law of the specific equivalent thermal conductivity and minimal thermal resistance law for hexagonal, spherical and elliptical of filler shapes. • PP/Al, PP/Cu, phenol-aldehyde/aluminum oxide, phenol-aldehyde/graphite • Ø=0-0.5 • Used theoretical models: Maxwell model Russell model Hamilton & Crosser model	• Effective thermal conductivity raised nonlinearly as a function of filler concentration • Thermal conductivities of Russell and Maxwell models were below the experimental data during whole range of volume fraction of fillers. • For aldehyde/aluminum oxide and phenol-aldehyde/graphite, Hamilton Crosser model estimated upper thermal condcutivity values than experimental data. • They found that their new thermal conductivity model for various shapes of filler got better correlation with experimental data than other models. • At below Ø<0.3, thermal conductivity determined by using development models for hexagonal, spherical and elliptical of filler shapes, with other models gave closed results with each other. After this volume concentraion, thermal conductivity went up rapidly.
Chifor, Tekiner, & Orban	2011	• determinated experimental thermal conductivity of HDPE/AL (200 μm) by using guarded hot-plate apparatus • Ø=0.05-0.30 • Agari theoretical model	• Increasing volume fraction of Al in composites, increasing its thermal conductivity. • The aluminum particles were placed in interlamellar spaces, in close contact with the lamellar surfaces. Because of high thermal conductivity of aluminum, aluminum particles get higher temperature fastly matrix. • The model was in good correlation with experimental data.

Table 6.1 Continue

Researchers	Year	Materials & Methods	Results
Das	2011	• Examined thermal conductivity of Al (100-200 μm) filled exopy polymer composites were prepared by hand-lay-up experimentally and numerically • 0.4 %, 1.4 %, 3.34 % volume fraction of Al contents • Experimental thermal conductivity of composites were measured by using Unitherm Model 2022 based on Guarded heat flow meter test method • Numerical analyses were carried out by ANSYS software in 3-D. -sphere filler in cube matrix -	• Thermal conductivity of composites improved as a function of volume fraction of Al contents. • Composite materials with filled of 3.34 % vol. of Al, the thermal conductivity was higher about 1.1 times than pure epoxy. • The numerical results based on FEM were in good agreement with experimental data.
Zhou	2011b	• investigated thermal conductivity of Al particed filled LLDPE composites were prepared by melt mixing and hot pressing • Spherical Al powders whose average particle size of 7 μm and 20 μm. The Al powder had mean thickness in 1 μm and in length in 10 μm • Ø=0-45 % • The thermal conductivity of composites were calculated from thermal diffusivity determined by Netzsch system at room temperature in air and high temperature in argon • Samples (d=20 mm, t= 1mm)	• Raising thermal conductivity of LLDPE/Al composites for all Al particle by increasing volume fraction of Al particles • At low volume fraction, determined a small thermal conductivity increase. • At high volume fraction, thermal conductivity increased rapidly • The Al particles' shape effects on thermal conductivity of LLDPE/Al composites. Spherical Al particle reinforced polymer composites show lower thermal conductivity than the flaky particle reinforced polymer composites.
Kumlutaş	1999	• This study carried out about determining thermal conductivity numerically, experimentally and theoretically • HDPE/Al • Ø=0-33 % • A modified hot-wire technique were used for measurements. • Theoretic Models: Parallel, series, geometric mean, Cheng and Vachon, Lewis and Nielsen, Maxwell and Russell models • The numerical study was carried out by using Laplace's equation depends on finite difference method.	• For Ø<10 %, experimental, theoretical and numerical results were closed each other. • For Ø>10 %, exponentially increased in thermal conductivity of composites. All models underestimated thermal conductivity. but for whole volume fraction of Al range, numerical results were near to experimental data.

Table 6.1 Continue

Researchers	Year	Materials & Methods	Results
Tavman	1996	• Thermal conductivity of HDPE/Al composites were experimentally researched in the range of filler content 0-33% (v/v). • Samples were produced with using the mold compression method. • Thernal conductivity was determined experimentally by using Shotherm QTM thermal conductivity meter based on modified hot wire process. • Theoretical models: Cheng & Vachon, Lewis & Nielsen, Agari & Uno and Maxwell models.	• For Ø=0-12%, the Al particle homogeneously dispersed in HDPE matrix and particle didn't contact with each other. So, many theoretical models gave closed results to experimental data. • For higher than this value, the agglomeration forms and conductive chains occurred, hence thermal conductivity increased rapidly. Only Agari and Uno models didn't fail to estimate thermal conductivity values.

CHAPTER SEVEN
CONCLUSION

7.1 Conclusion

This theoretical, numerical and experimental study on thermal conductivity of Al filled HDPE composites have caused the following conclusions:

- ✓ Addition of Al particles result in development of thermal conductivity of HDPE/Al composites.
- ✓ The thermal conductivity value of pure HDPE is measured as 0.614 W/mK. The thermal conductivity of HDPE/Al (40-80 μm) composite at maximum volume fraction of Al, is nearly 2.5 times that of pure HDPE, is 1.503 W/mK.
- ✓ At low volume concentration of Al (Ø≤6 %), thermal conductivity of composites rises slowly. The reason is that Al particles homogenously disperse in HDPE matrix and cannot get in touch with each other and maintain spherical shape. At high volume concentration of Al, Al particles occur agreemate forms and conductive chains occur along heat flow direction. Thus, thermal conductivity of HDPE/Al composites increases rapidly.
- ✓ In this study, effect of the particle size of Al is not significant on thermal conductivity, thermal conductivity of HDPE/Al (80 nm) is close to thermal conductivity of HDPE/Al (40-80 μm).
- ✓ When concentration of filler materials are went up, voids in polymer composite could not be avoided, by the reason of high sample viscosity. And the voids have negative effect on thermal conductivity. So, the production method of composites is important, should be selected more suitable.
- ✓ Finite element procedure can be successfully applied to find thermal conductivity of polymer composites as a function of volume fraction of filler material.
- ✓ For 2-D models, up to 10 % volume fraction of Al content, results of all arrangement forms in 2-D are closed to experimental values. After this

concentration, all arrangement forms in 2-D fail to estimate experimental results

- ✓ For 3-D models, as shape of Al particles are assumed to be spherical, sphere filler models are good correlation with experimental values. 1, 4 and 8 piece sphere filler models have given closed thermal conductivity values with experimental data for all volume contents of Al. At Ø<10 vol %, thermal conductivity of all piece sphere filler models predict experimental results well.
- ✓ Maxwell's, Hamilton & Crosser's, Meredith & Tobias's, Lord Rayleigh's, Agari & Uno's, Lewis & Nielsen's (A=1.5, $Ø_m$=0.637) theoretical models are closer to experimental values.

Future work;

- ✓ The effect on the thermal conductivity of various production and measurement methods should be determined. So, experimental study should be carried out for these parameters and results should be compared with each other.
- ✓ The various filler or matrix materials will be used to determine thermal conductivity of composites.
- ✓ The experiments were carried out at room temperature. The experiments are performed in various temperature range and temperature effects on thermal conductivity will be established.
- ✓ Numerical and analytical models assist to estimate thermal conductivity of materials without doing any experiments. The thermal conductivity of polymer composite material depends on many parameters, such as size, distribution and geometry of filler, thermal conductivity of filler and matrix, so it isn't really easy to predict accurate thermal conductivity. As using experimental data, new models will be developed based on these parameters for composites.
- ✓ Resistance of interfacial thermal barrier and its effect on thermal conductivity aren't taken account in numerical analysis. The resistance of interfacial

thermal barrier will be determined and the future numerical study may be taken into account to this resistance.

- ✓ The shape of Al is presumed to spherical, whereas in real practice shape of Al is irregular. In addition, even the distribution of Al in HDPE is supposed to be in arranged in manner, it is actually distribute in matrix almost randomly. So, numerical analysis should be carried out for various shapes of filler materials, such as elliptical and for different arrangement, such as random distribution.
- ✓ Convection heat transfer will be taken notice in numerical solution.
- ✓ Various theoretical thermal conductivity models will be used to calculate thermal conductivity.

REFERENCES

Aadmi, M., Karkri, M., Ibos, L., & Hammouti, M., E. (2013). Effective thermal conductivity of random two-phase composites. *Journal of Reinforced Plastics and Composites, 0* (00), 1–12.

Agari, Y. & Uno, T. (1986). Estimation on thermal conductivities of filled polymers. *Journal of Applied Polymer Science, 32*, 5705-5712.

Bal, H. (2009). *Thermal and mechanical properties of continuous fiber reinforced thermoplastics*. Unpublished Master's Thesis, Dokuz Eylül University.

Baschirow, A.B. & Selenew, J.W. (1976). Thermal conductivity of composites. *Plaste Kaut, 23*, 656.

Boudenne, A., Ibos, L., Fois, M., Majeste, J. C. & Gehin, E. (2005). Electrical and thermal behavior of polypropylene filled with copper particles. *Composites: Part A, 36*, 1545–1554.

Chauhan, D., Singhvi, N. & Singh, R. (2012). Effect of geometry of filler particles on the effective thermal conductivity of two-phase systems. *International Journal of Modern Nonlinear Theory and Application, 1*, 40-46.

Cheng, S.C. & Vachon, R.I. (1970). A technique for predicting the thermal conductivity of suspensions, emulsions, and porous materials. *International Journal Heat and Mass Transfer, 13*, 537.

Chifor, V., Tekiner, Z., Turker, M. & Orban, R. (2011). An experimental investigation of properties of polyethylene reinforced with Al powders. *Journal of Zhejiang University-SCINCE A (Applied Physics & Engineering), 12* (8), 583-592.

Chikhi, M., Agoudjil, B., Haddadi, M. & Boudenne, A. (2011). Numerical modelling of the effective thermal conductivity of heterogeneous materials. *Journal of Thermoplastic Composite Materials, 26* (3), 336–345.

Çolak, M. (2011). *A study on thermal conductivity of polymer nanocomposites*. Unpublished Master's Thesis, Dokuz Eylül University.

Das, L. (2011). *Effectıve thermal conductıvıty of epoxy matrıx composıtes fılled wıth alumınıum powder.* Unpublished Bachelor of Technology, Natıonal Instıtute of Technology Rourkela.

Durmaz, S. (2004). *A numerical study on the effective thernal conductivity of composite materials.* Unpublished Master's Thesis, Dokuz Eylül University.

Girgin, E. & Kılavuz, H. R. (2011). *Kompozit malzemelerin termal davranışlarının ansys ile incelenmesi ve ısı iletim katsayısının hesaplanması*. Unpublished Master's Thesis, Dokuz Eylül University.

Hamilton, R. L. & Crosser, O. K. (1962). Thermal conductivity of heterogeneous two-component systems. *Industrial & Engineering Chemistry Fundamentals, 1*(3), 187-191.

Harris, A. & Sorensen, N. (2007) . Thermal conductivity testing of minimal volumes of energetic powders. *Journal of Pyrotechnics, 25,* 49-54.

Kumlutaş, D. (1999). Heat conduction in ısotropic heterogeneous media. *Journal of Engineering Sciences, 5* (2-3) 1025-1032.

Kumlutaş, D. & Tavman, İ.H. (2003). Alüminyum oksit tane katkılı polietilen matriksli kompozitlerin ısı iletim katsayısı. *DEÜ Mühendislik Fakültesi Fen ve Mühendislik Dergisi, 5*(2),19-25.

Kumlutaş, D., Tavman, I. H. & Çoban, M. T. (2003). Thermal conductivity of particle filled polyethylene composite materials. *Composites Science and Technology, 63*, 113–117.

Lewis T., & Nielsen, L. (1970).Dynamic mechanical properties of particulate filled polymers. *Journal of Appied Polymer Science, 14*, 1449.

Luyt, A.S., Molefi, J.A. & Krump, H. (2006) Thermal, mechanical and electrical properties of copper powder filledlow-density and linear low-density polyethylene composites. *Polymer Degradation and Stability*, *91,* 1629-1636.

Mamunya, Ye.P., Davydenko, V.V., Pissis, P. & Lebedev, E.V. (2002). Electrical and thermal conductivity of polymers filled with metal powders. *European Polymer Journal, 38*, 1887–1897.

Maxwell , J.C. (1954). *A treatise on electricity and magnetism*, Dover (3rd Ed.). New York.

Meredith, R.E. & Tobias, C.W. (1960). Resistance to potential flow through a cubical array of spheres. *Journal Applied Physcis, 31*, 1270-1273.

Mishra, D., Mohapatra, L., Satapathy, A. & Patnaik, A. (2011). determination of thermal conductivity of polymer composites filled with solid glass beads. *APM 2011-International Conference on Advancement in Polymeric Materials*, 25th to 27th March, Chennai.

Mutnuri, B. (2006). *Thermal conductivity characterization of composite materials*. Unpublished Master's Thesis, West Virginia University.

Nielsen L. (1970). Generalized equation for the elastic moduli of composite materials. *Journal Applied Physcis, 41*, 4626.

Ouellette, E.A., & Harris, A. (2010). *Thermal conductivity of diamond-loaded glues for the ATLAS particle physics detector*. Retrieved November 20, 2013 from Cornell University Library, http://arxiv.org/abs/1008.0876v2.

Prahan, S. (2013). *Effectıve thermal conductıvıty of epoxy matrıx composıtes fılled wıth red mud powder.* Unpublished Bachelor of Technology, Natıonal Instıtute of Technology Rourkela.

Rayleigh, L. (1892). On the infuence of obstacles arranged in rectangular order upon the properties of a medium. *Philosophical Magazine, 6*, 481-502.

Russell, H.W. (1935). Principles of heat flow in porous ınsulators. *Journal of the American Ceramic Society*, *18*(1), 1-5.

Shinde, S. L. & Geola, J. L. (2006). *High thermal conductivity materials* (1st ed.) New York: Springer Science + Business Media, Inc.

Sofian, N. M., Rusu, M., Neagu, R. & Neagu, E. (2001). Metal powder-filled polyethylenecomposites. V. thermal properties. *Journal of Thermoplastıc Composıte Materıals, 14*, 20-35.

Springer, G. S. & Tsai, S. W. (1967). Thermal conductivities of unidirectional materials. *Journal of Composite Materials, 1*, 166.

Tavman, I. H. (1996). Thermal and mechanical properties of aluminum powder filled high-density polyethylene composites. *Journal of Applied Polymer Science, 62*,2161-2167.

Tavman, I. H. (1997). Thermal and mechanical properties of copper powder filled poly(ethylene) composites. *Powder Technology*, *91*, 63-67.

Tavman, I. H. (1998). Effectıve thermal conductıvıty of ısotropıc polymer composıtes. *International Communications in Heat & Mass Transfer, 25* (5), 723-732.

Tavman, I. H., & Turgut, A. (2012). Applications of thermophysics in science and industry – nanofluids and polymer nanocomposites. *Thermophysical 2012-17th International Meeting of Thermophysical Society*. 31st October - 2th November 2012; Czech Republic, 2012, 223-230.

Tavman, I., Aydogdu, Y., Kök, M., Turgut., A. & Ezan, A. (2011). Measurement of heat capacity and thermal conductivity of HDPE/expanded graphite nanocomposites by differential scanning calorimetry. *Archives of Material Science and Engineering, 50* (1), 56-60.

Tekçe, H. S. (2004). *Evaluation of thermophysical properties of thermal conductive polymer composites*. Unpublished Master's Thesis, Dokuz Eylül University.

Tong, L., Mauritz, A. P. & Bannister, M. K. (2002). *3D Fibre reinforced polymer composites* (1st ed.). Oxford: Elsevier Science.

Weber, E. H. (2001). *Development and modeling of thermally conductive polymer/carbon composites*. Unpublished Doctor of Philosophy, Michigan Technological University.

Weidenfeller, B., Höfer, M. & Schilling, F. R. (2003). Thermal conductivity, thermal diffusivity, and specific heat capacityof particle filled polypropylene. *Composites: Part A, 35*, 423–429.

Woodside, W. & Messmer, J.H. (1961). Thermal conductivity of porous media. I. unconsolidated sand. *Journal of Appied Physics, 12* (9), 1688-1699.

Zehner, P. & Schlunder, E.U. (1970). Thermal conductivity of granular materials at moderate temperatures. *Chemie Ingenieur Technik, 42*, 933-941.

Zhou, W. (2011a). Thermal and dielectric properties of the AIN particle reinforced linear low-density polyethylene composites. *Thermochimica Acta, 512*, 183-188.

Zhou, W. (2011b). Thermal and dielectric properties of the aluminum particle reinforced linear low-density polyethylene composites. *Polymer Engineering and Science*, 917-924.

APPENDICES

Appendix A

Experimental Data

Table A.1. Experimental thermal conductive of HDPE/Al (80 nm) composite for various volume fraction

Volume Fraction of Al	Thermal Conductivity (W/mK)
0.00	0.614
0.01	0.634
0.02	0.643
0.04	0.669
0.06	0.726
0.08	0.728
0.10	0.812
0.12	0.875
0.15	0.930
0.18	0.990
0.21	1.162
0.25	1.243
0.30	1.372

Table A.2. Experimental thermal conductive of HDPE/Al (40-80 μm) composite for various volume fraction

Volume Fraction of Al	Thermal Conductivity (W/mK)
0.00	0.614
0.01	0.638
0.02	0.653
0.03	0.664
0.04	0.675
0.05	0.688
0.06	0.705
0.08	0.752
0.10	0.816
0.12	0.889
0.14	0.964
0.17	1.063
0.20	1.138
0.24	1.217
0.28	1.322
0.33	1.503

Appendix B

2-D ARANGEMENT FORMS USED IN THE THERMAL ANALYSES

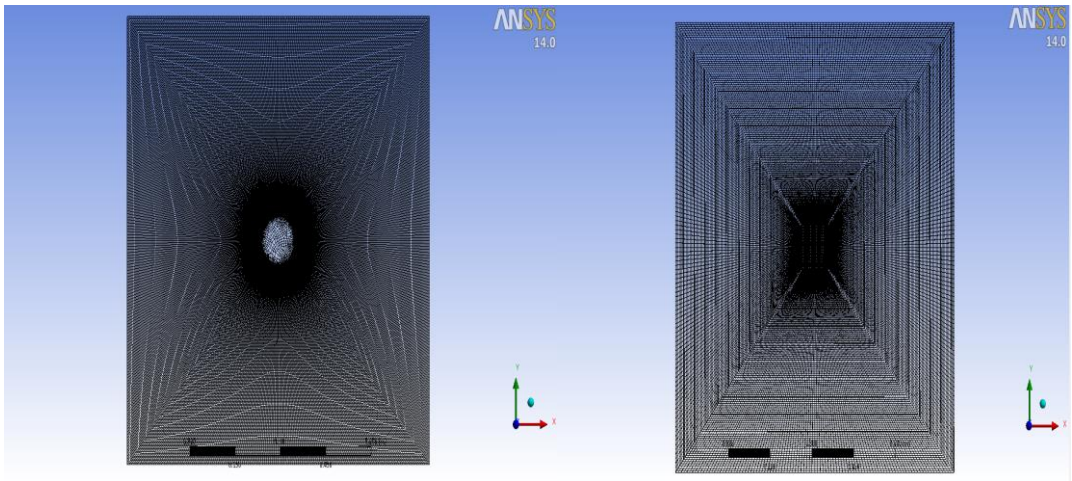

Figure B.1. 2-D models for 1-piece and Ø=1%

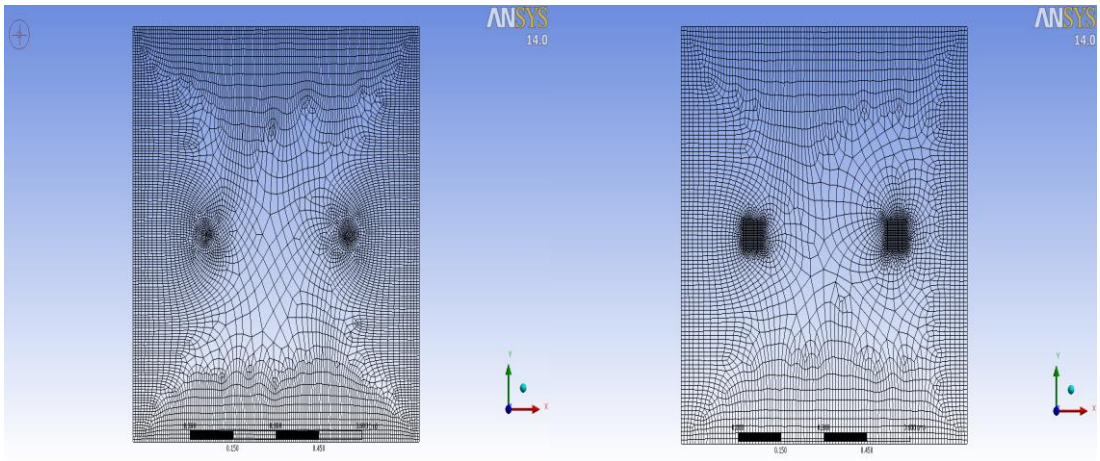

Figure B.2. 2-D models for 2-piece and Ø=1%

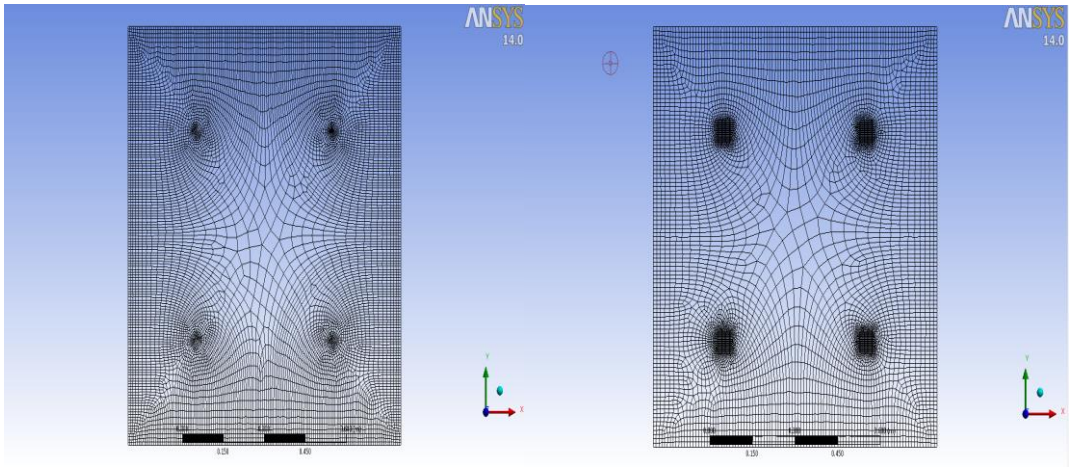

Figure B.3. 2-D models for 4-piece and Ø=1%

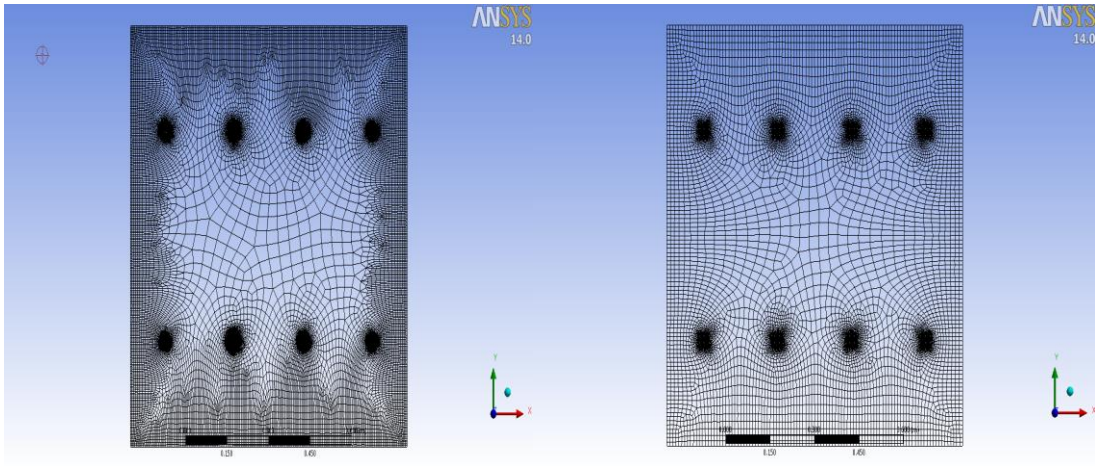

Figure B.4. 2-D models for 8-piece and Ø=1%

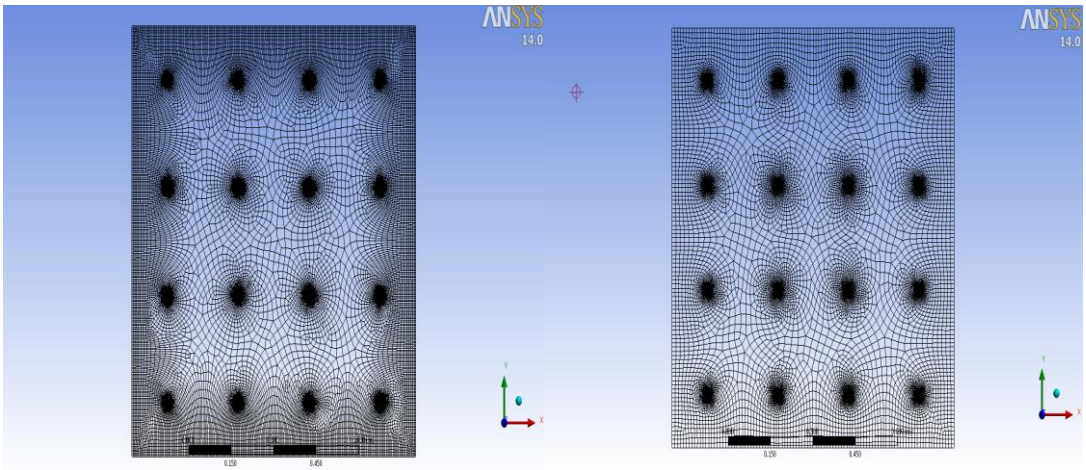

Figure B.5. 2-D models for16-piece and Ø=1%

Appendix C

3-D ARANGEMENT FORMS USED IN THE THERMAL ANALYSES

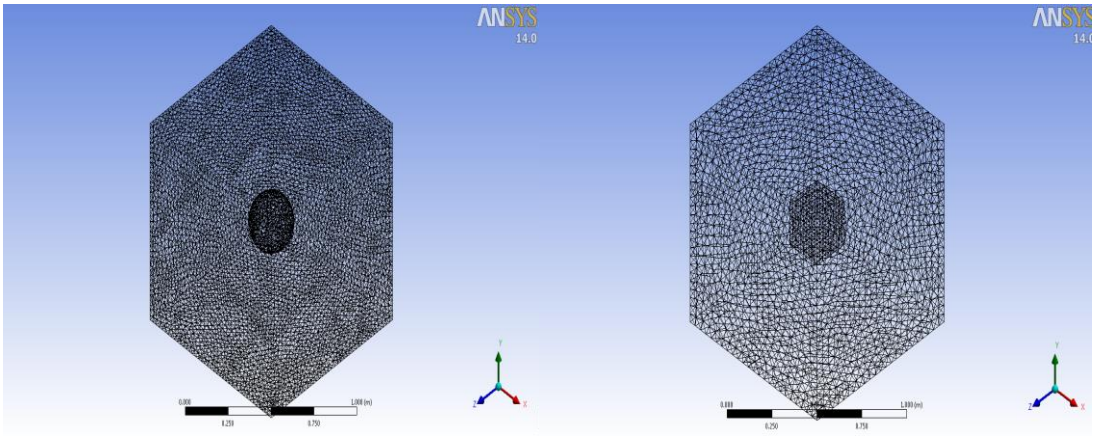

Figure C.1. 3-D models for 1-piece and Ø=1%

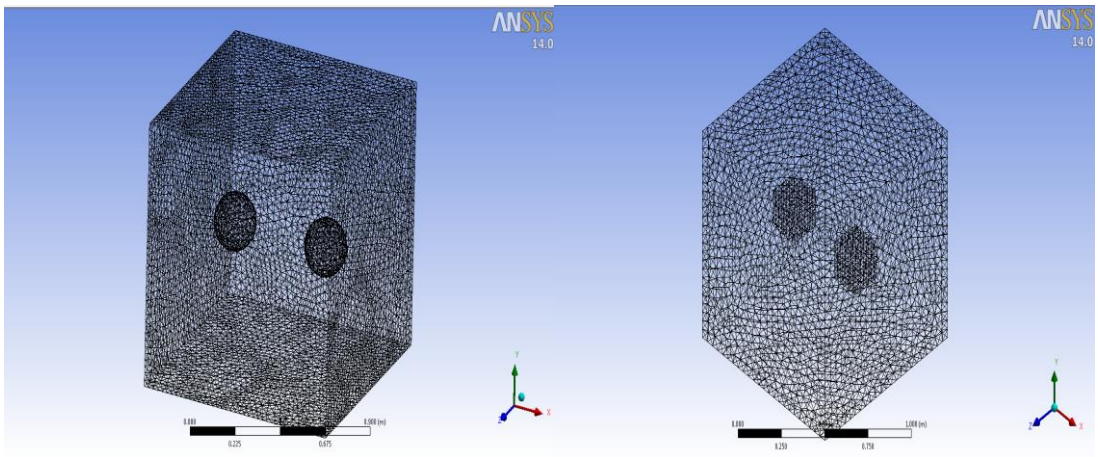

Figure C.2. 3-D models for 2-piece and Ø=1%

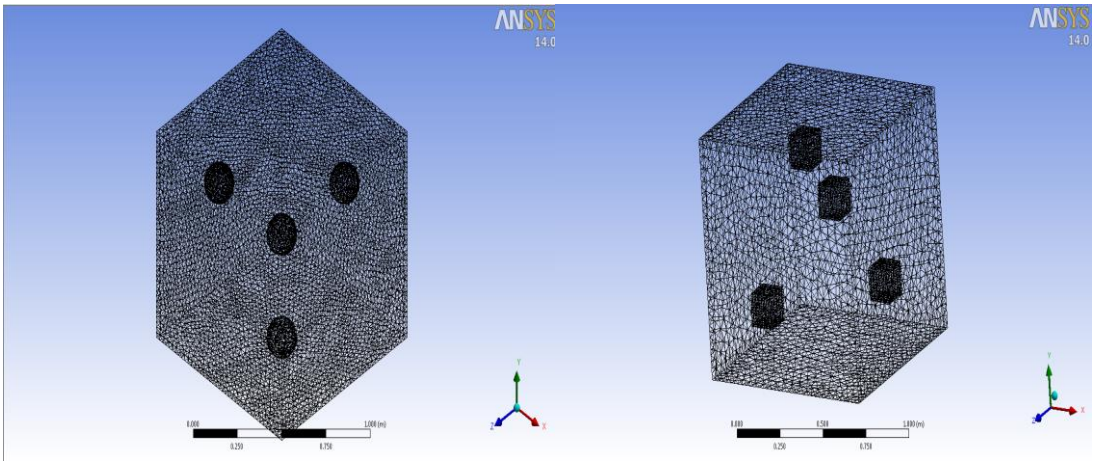

Figure C.3. 3-D models for 4-piece and Ø=1%

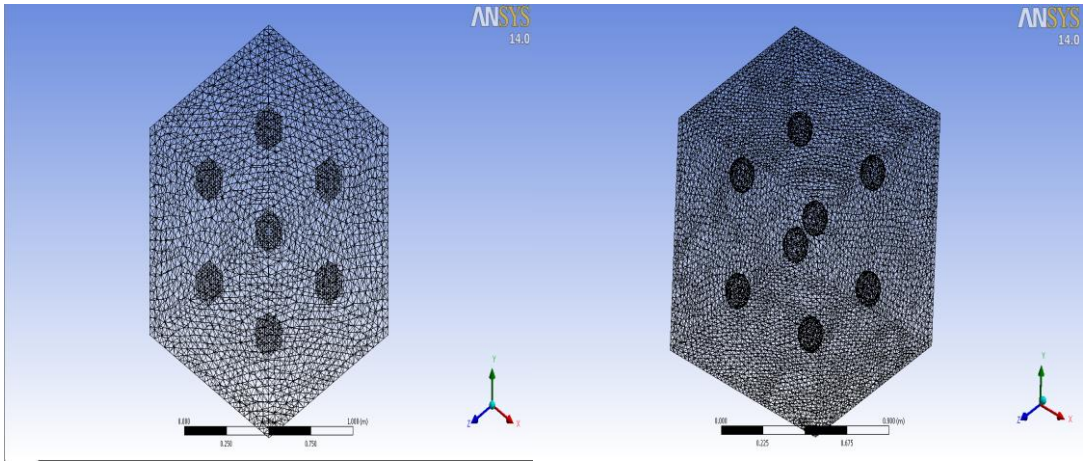

Figure C.4. 3-D models for 8-piece and Ø=1%

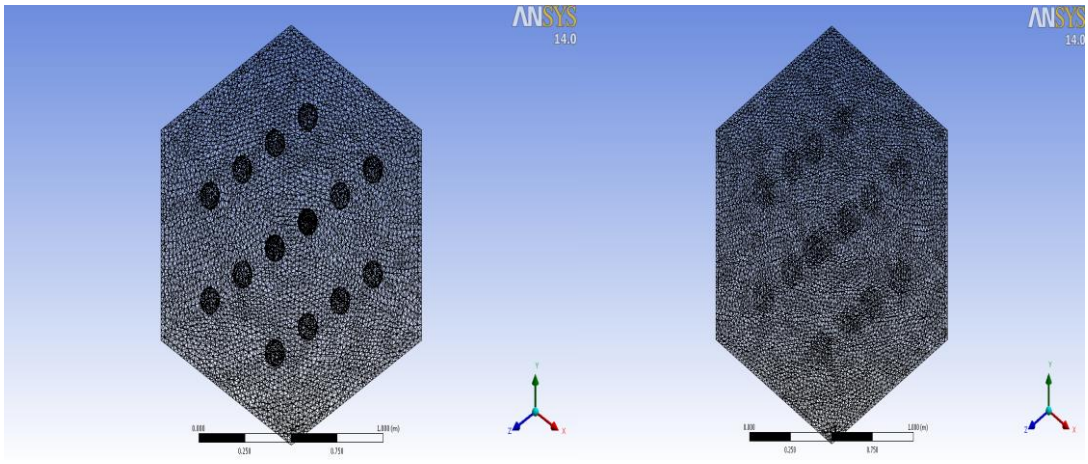

Figure C.5. 3-D models for 16-piece and Ø=1%

Appendix D

2-D THERMAL ANALYSİS

D.1 Temperature Distribution Results

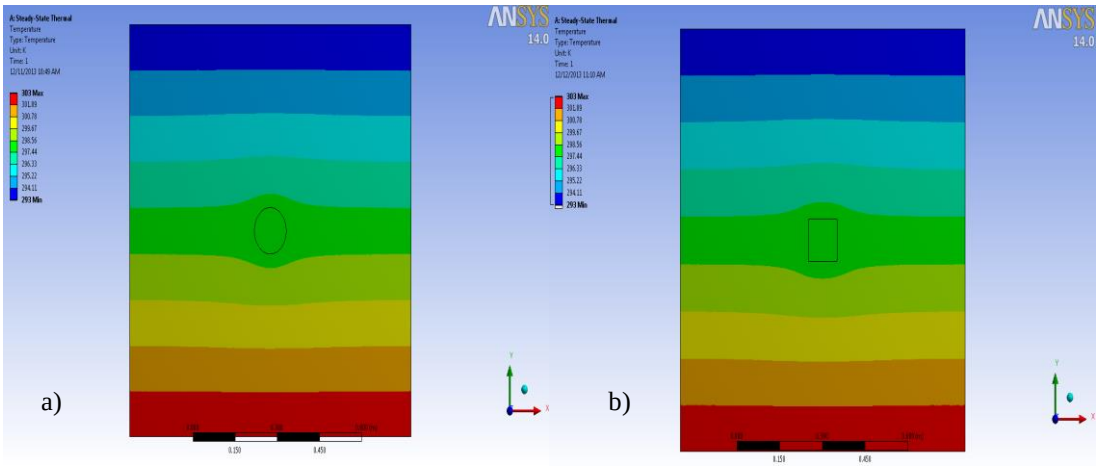

Figure D.1.1. Temperature distribution over 1-piece- a)circle and b) circle-filler model for Ø=1%

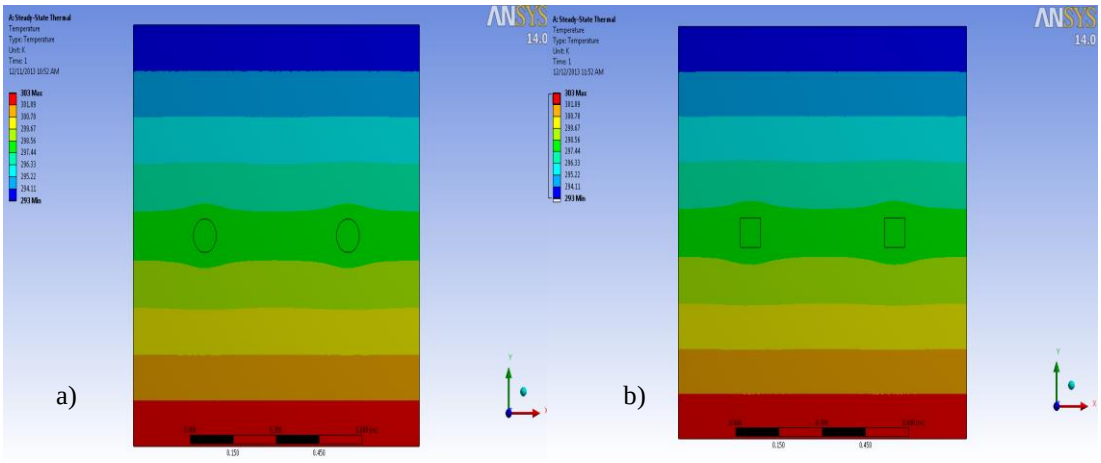

Figure D.1.2. Temperature distribution over 2-piece- a)circle and b) square -filler model for Ø=1%

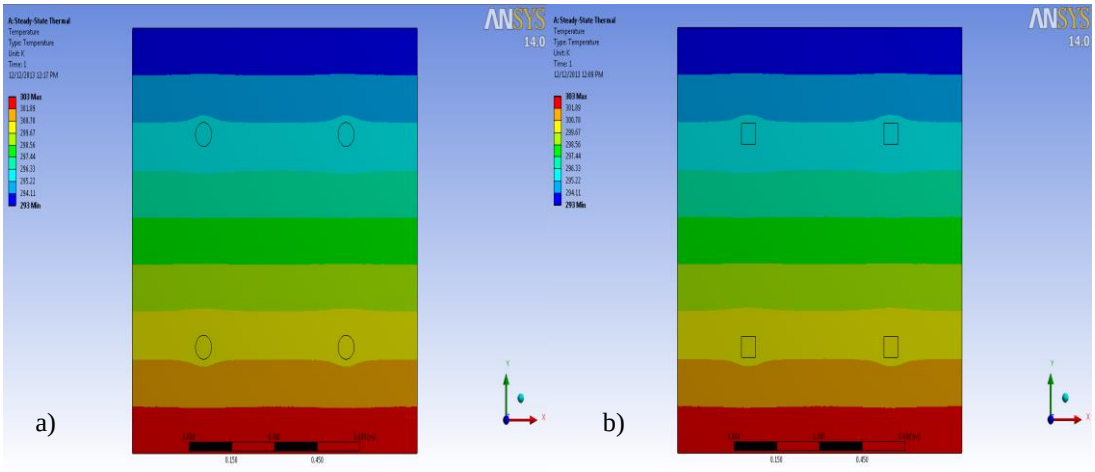

Figure D.1.3. Temperature distribution over 4-piece- a)circle and b) square -filler model for Ø=1%

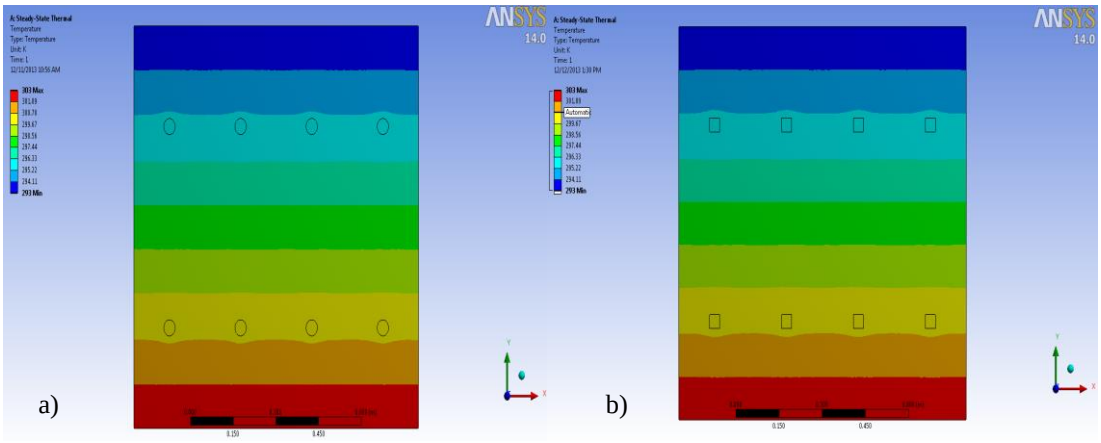

Figure D.1.4. Temperature distribution over 8-piece- a)circle and b) square -filler model for Ø=1%

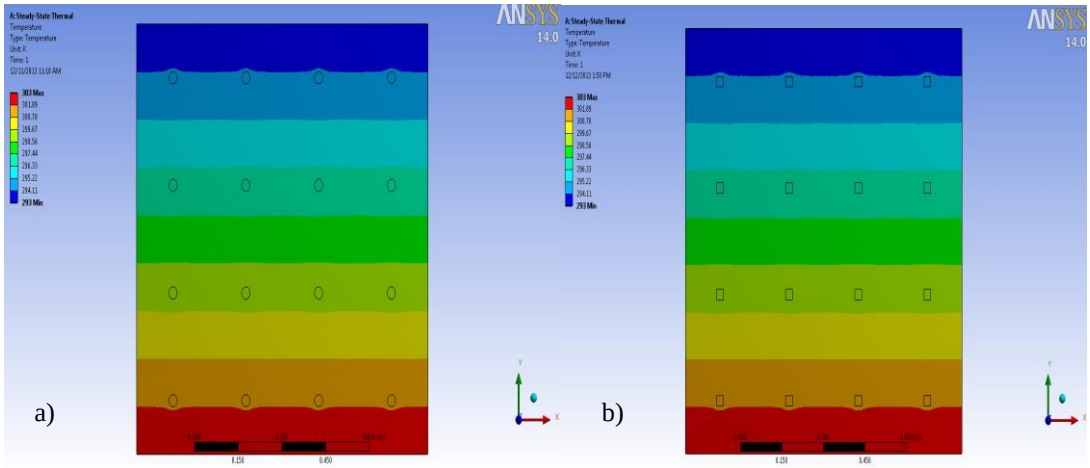

Figure D.1.5. Temperature distribution over 16-piece- a)circle and b) square -filler model for Ø=1%

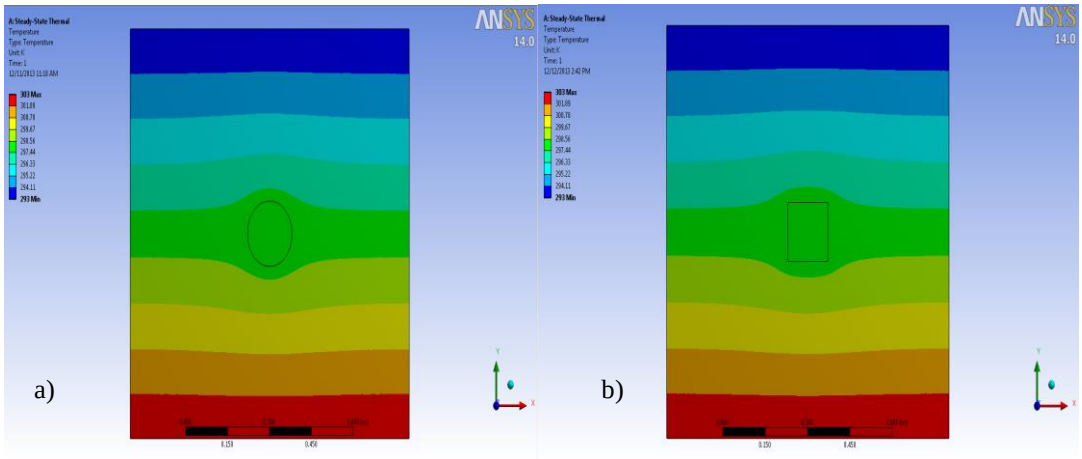

Figure D.1.6. Temperature distribution over 1-piece- a)circle and b) square -filler model for Ø=2%

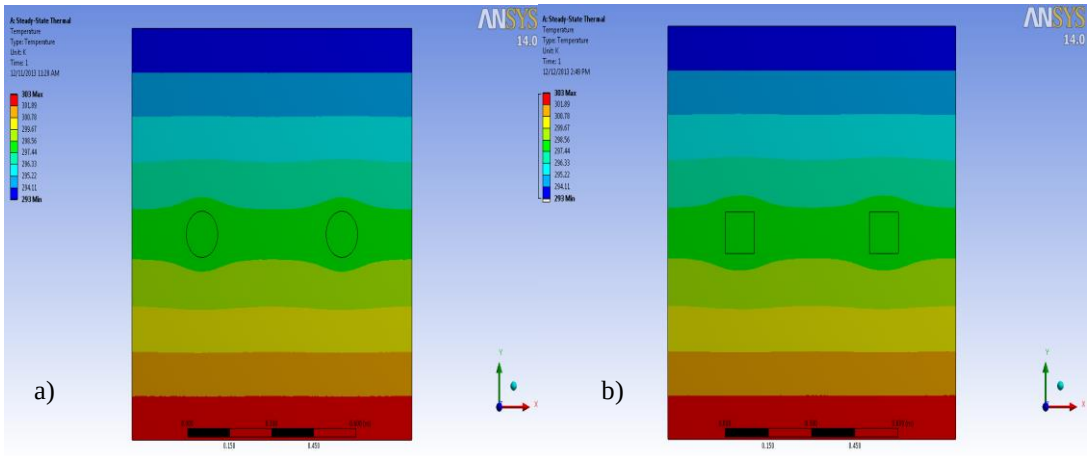

Figure D.1.7. Temperature distribution over 2-piece- a)circle and b) square -filler model for Ø=2%

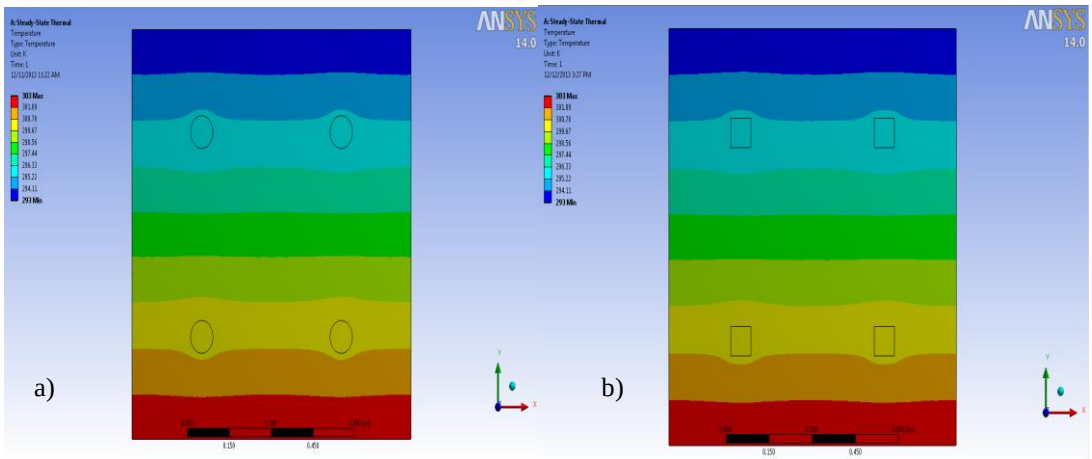

Figure D.1.8. Temperature distribution over 4-piece- a)circle and b) square -filler model for Ø=2%

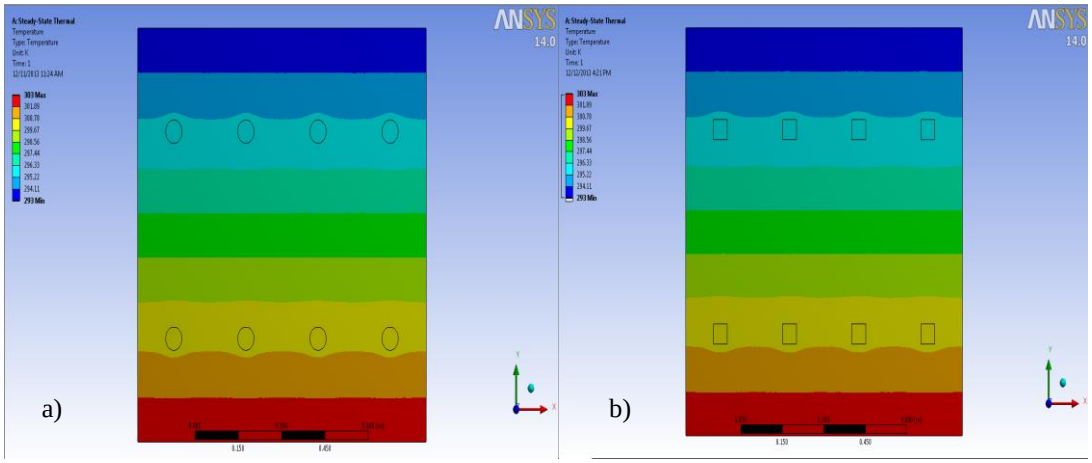

Figure D.1.9. Temperature distribution over 8-piece- a)circle and b) square -filler model for Ø=2%

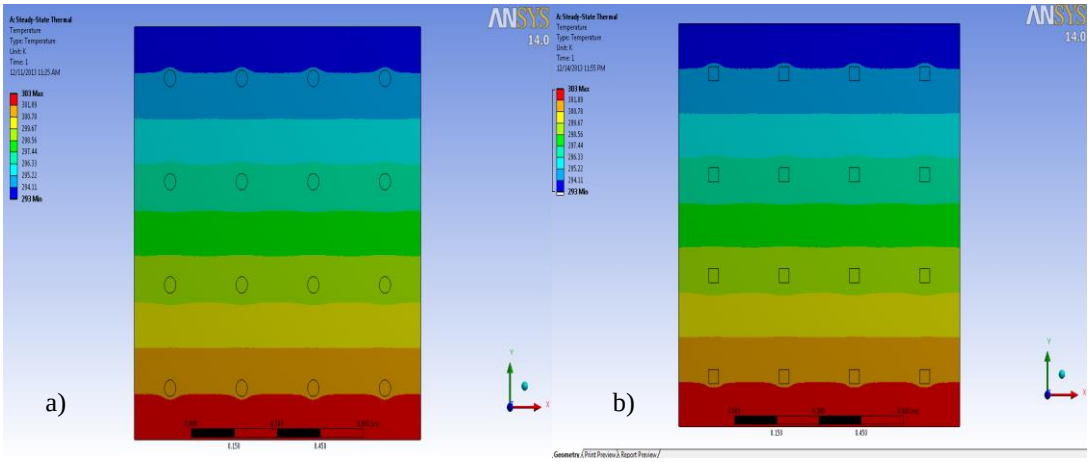

Figure D.1.10. Temperature distribution over 16-piece- a)circle and b) square -filler model for Ø=2%

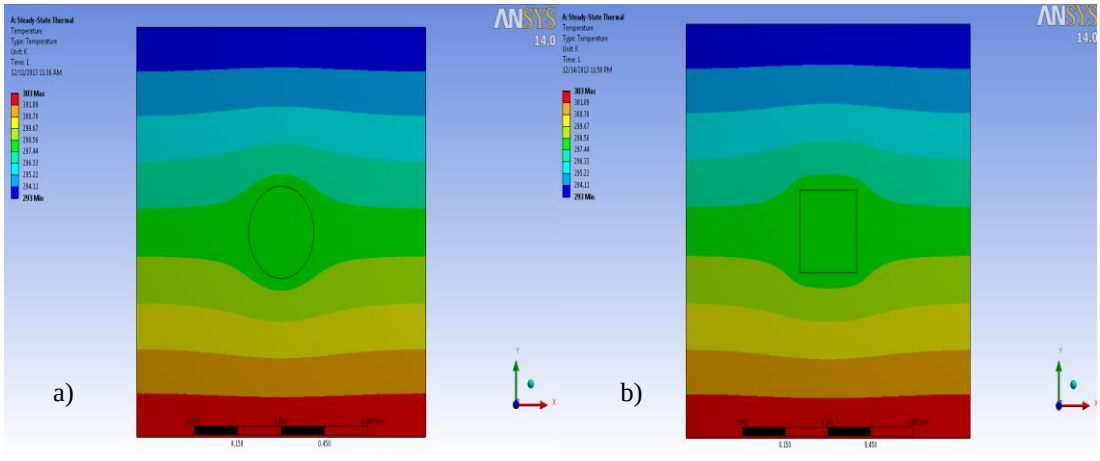

Figure D.1. 11. Temperature distribution over 1-piece- a)circle and b) square -filler model for Ø=4%

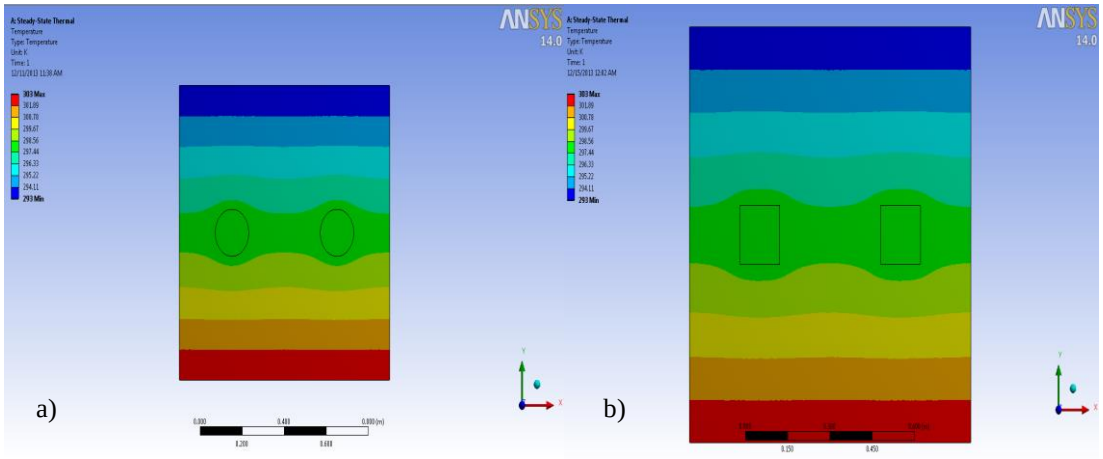

Figure D.1.12. Temperature distribution over 2-piece- a)circle and b) square -filler model for Ø=4%

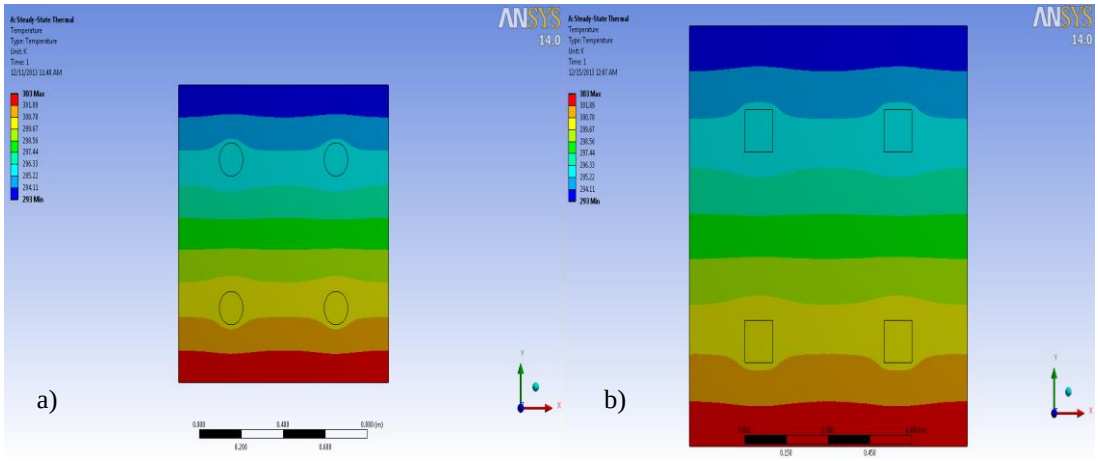

Figure D.1.13. Temperature distribution over 4-piece- a)circle and b) square -filler model for Ø=4%

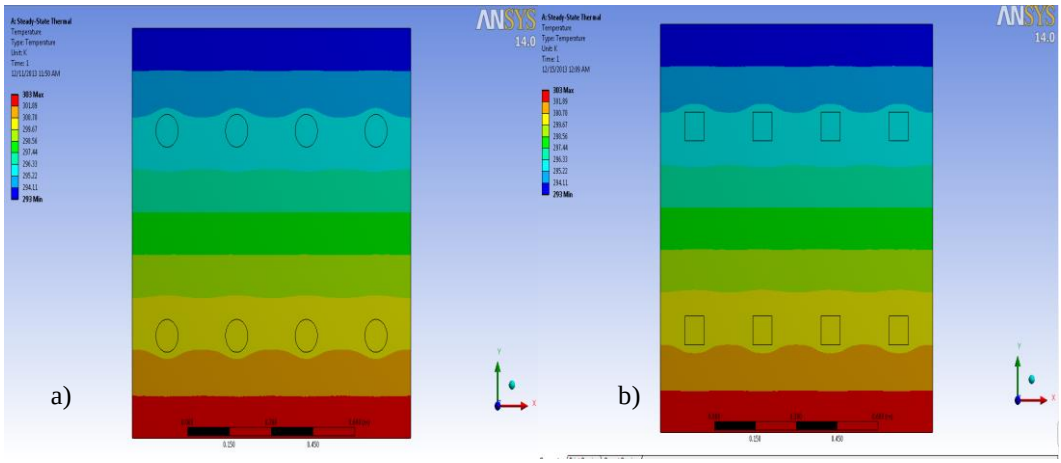

Figure D.1.14. Temperature distribution over 8-piece- a)circle and b) square -filler model for Ø=4%

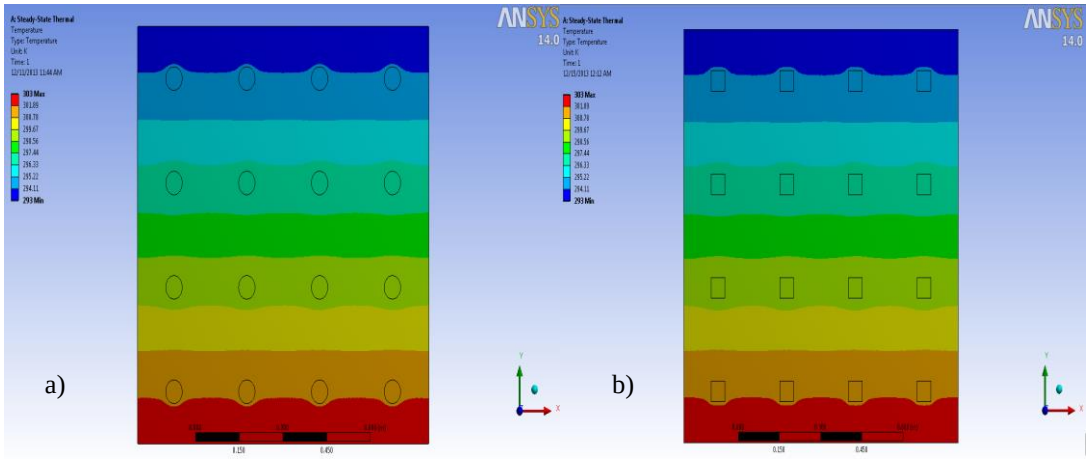

Figure D.1.15. Temperature distribution over 16-piece- a)circle and b) square -filler model for Ø=4%

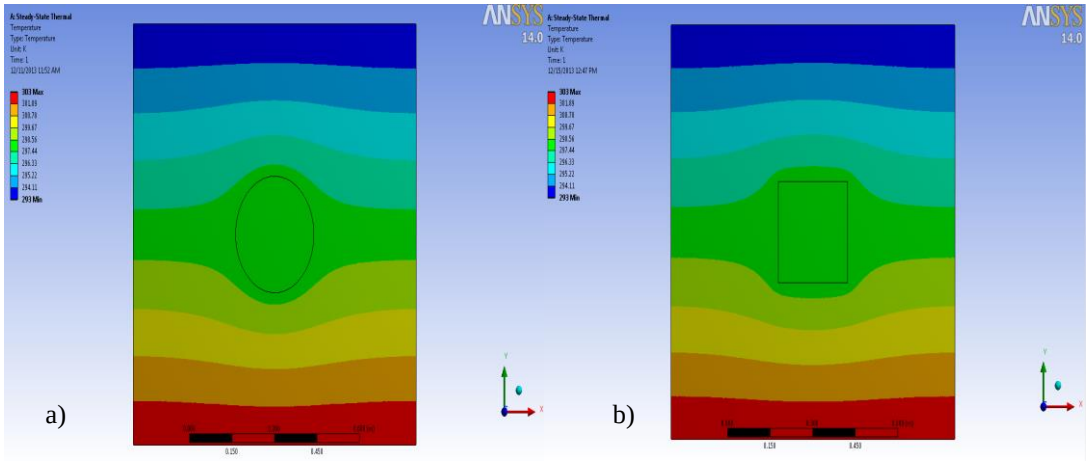

Figure D.1.16. Temperature distribution over 1-piece- a)circle and b) square -filler model for Ø=6%

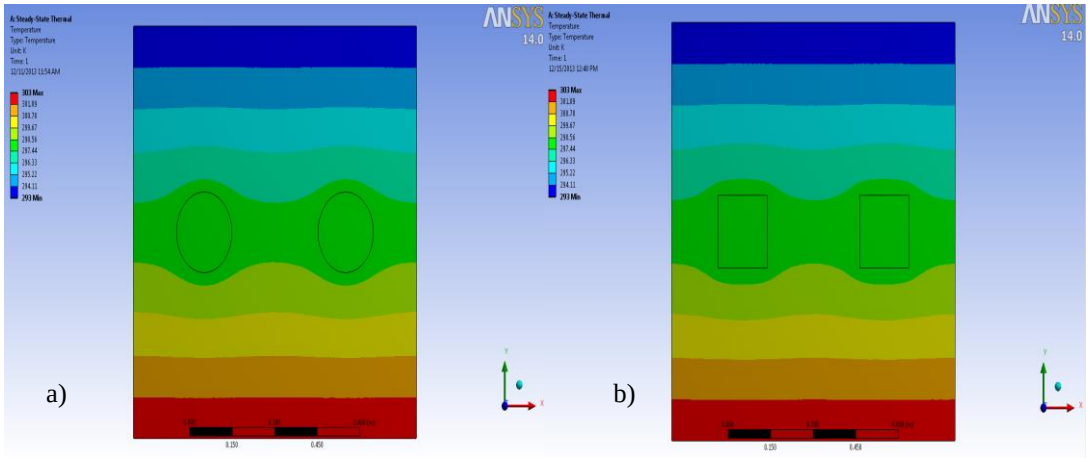

Figure D.1.17. Temperature distribution over 2-piece- a)circle and b) square -filler model for Ø=6%

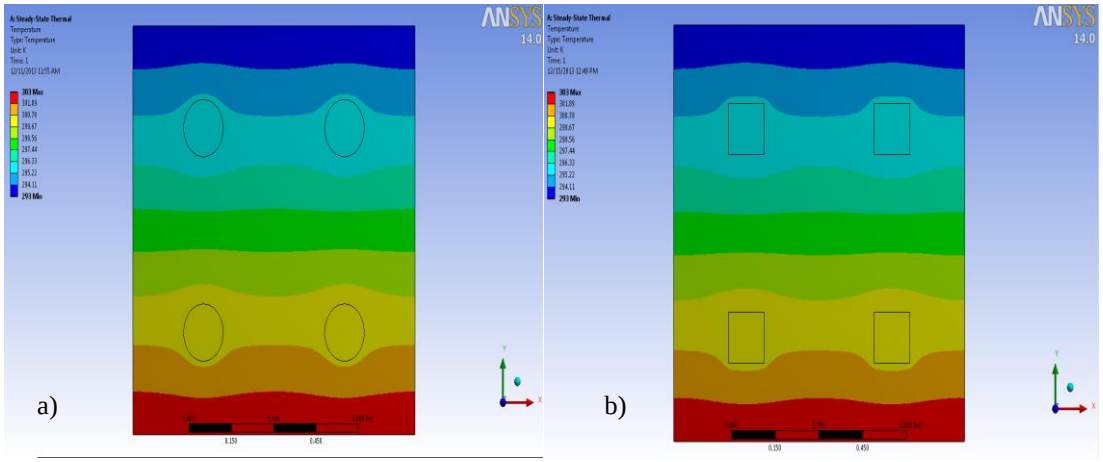

Figure D.1.18 Temperature distribution over 4-piece- a)circle and b) square -filler model for Ø=6%

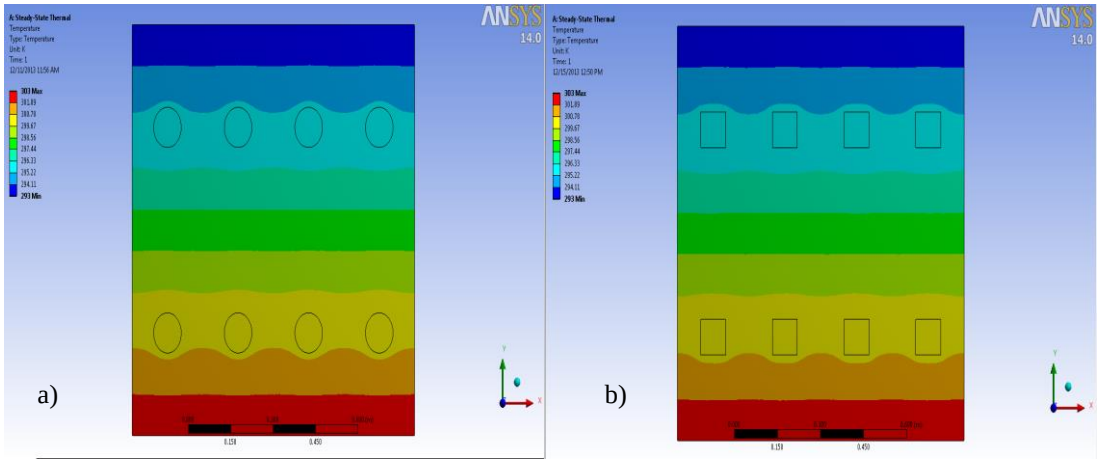

Figure D.1.19. Temperature distribution over 8-piece- a)circle and b) square -filler model for Ø=6%

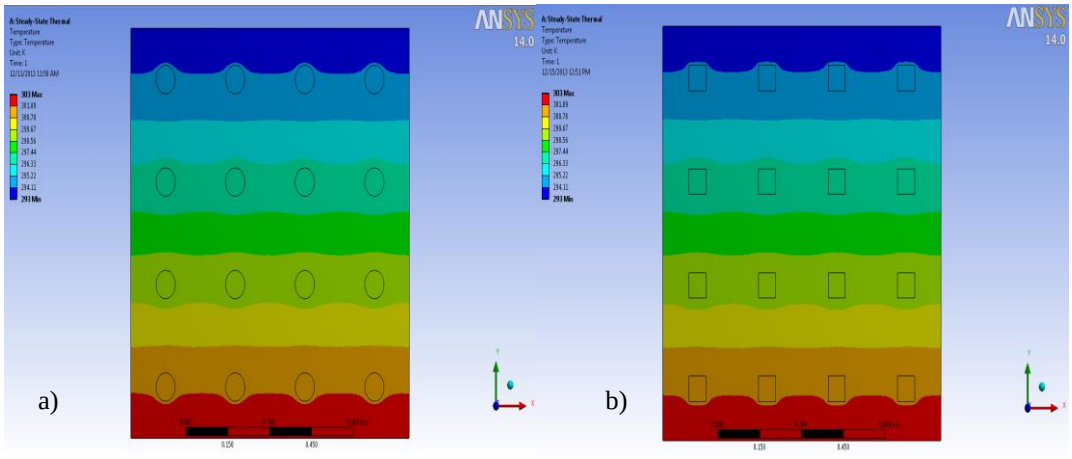

Figure D.1.20. Temperature distribution over 16-piece- a)circle and b) square -filler model for Ø=6%

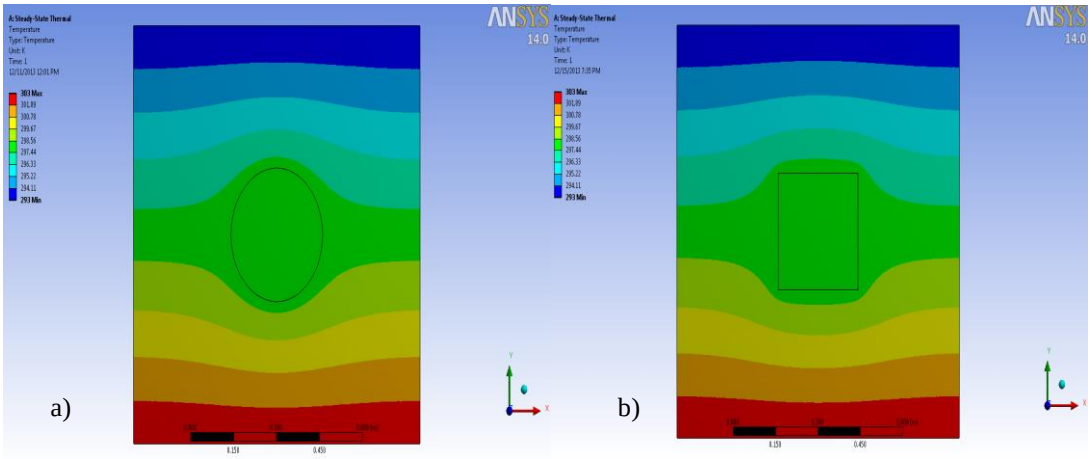

Figure D.1.21. Temperature distribution over 1-piece- a)circle and b) square -filler model for Ø=8%

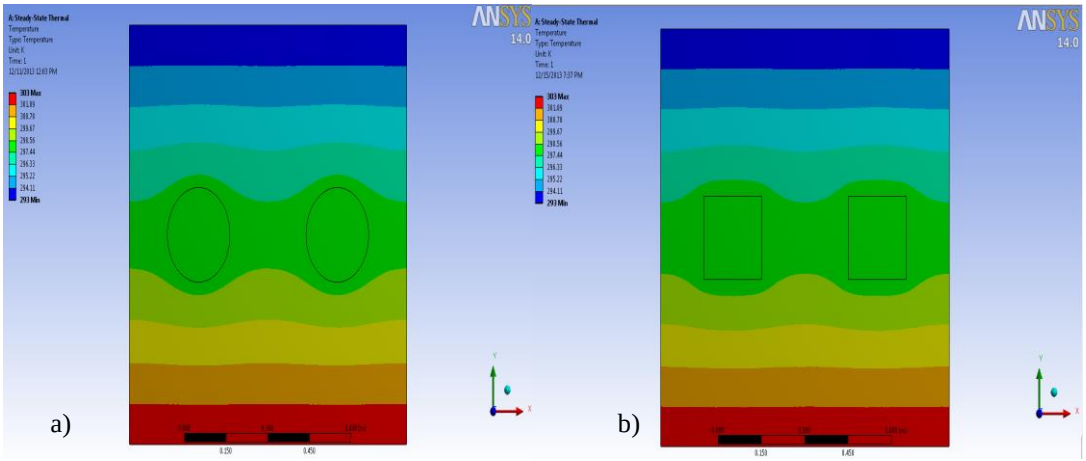

Figure D.1.22. Temperature distribution over 2-piece- a)circle and b) square -filler model for Ø=8%

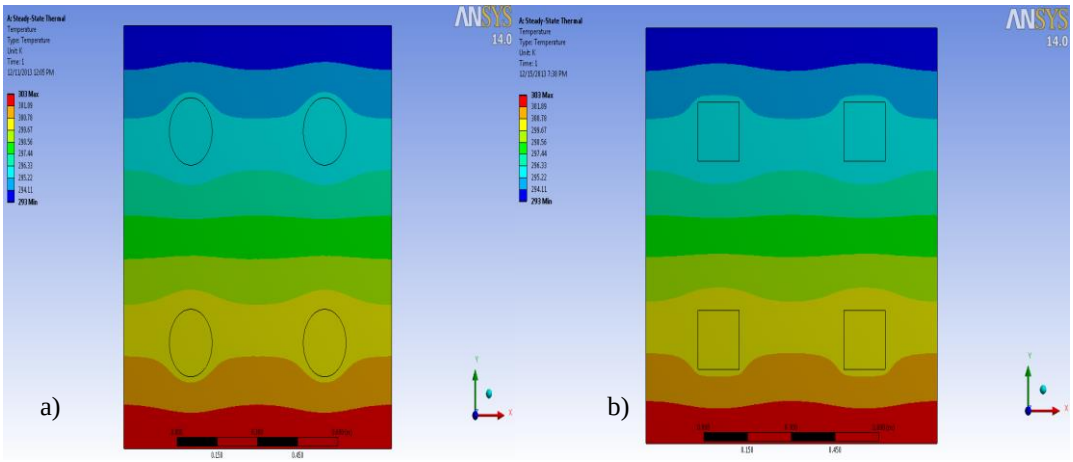

Figure D.1.23. Temperature distribution over 4-piece- a)circle and b) square -filler model for Ø=8%

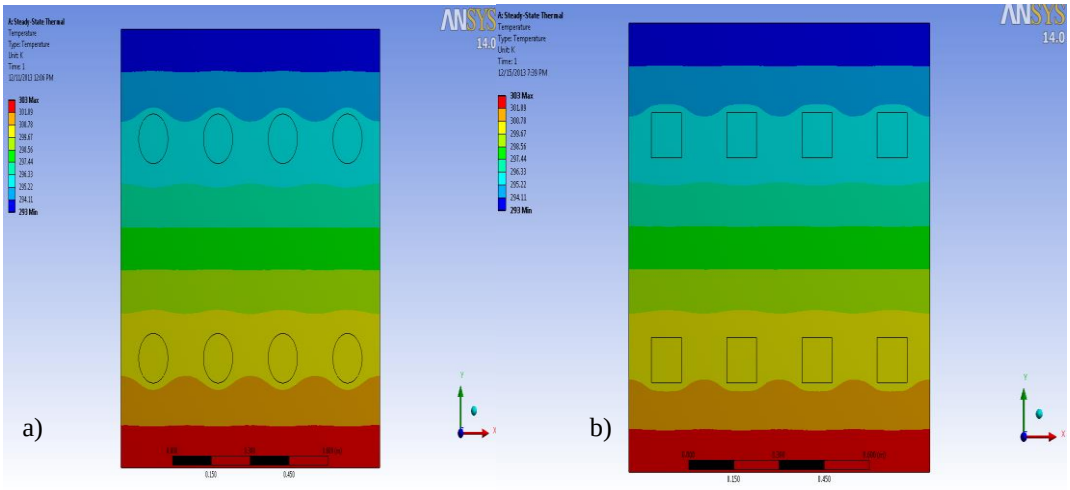

Figure D.1.24. Temperature distribution over 8-piece- a)circle and b) square -filler model for Ø=8%

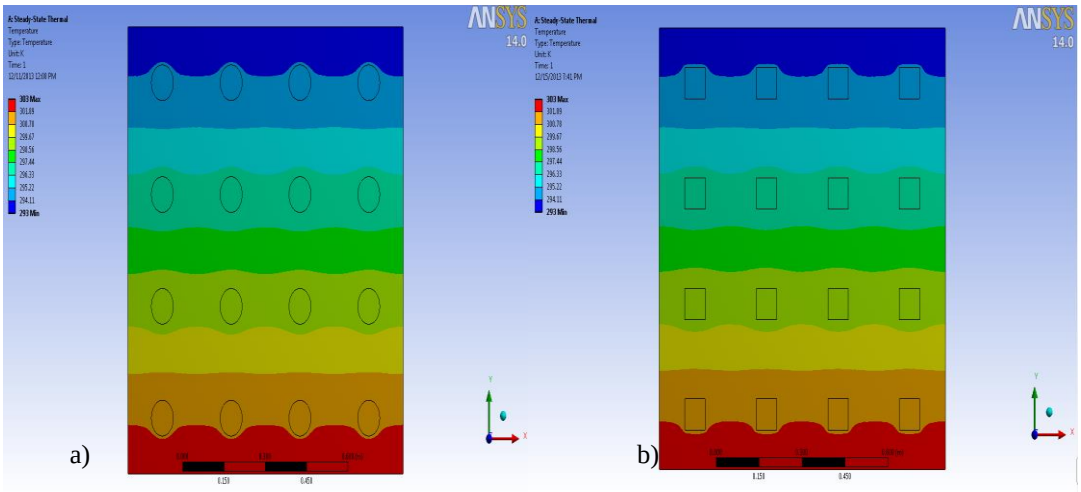

Figure D.1.25. Temperature distribution over 16-piece- a)circle and b) square -filler model for Ø=8%

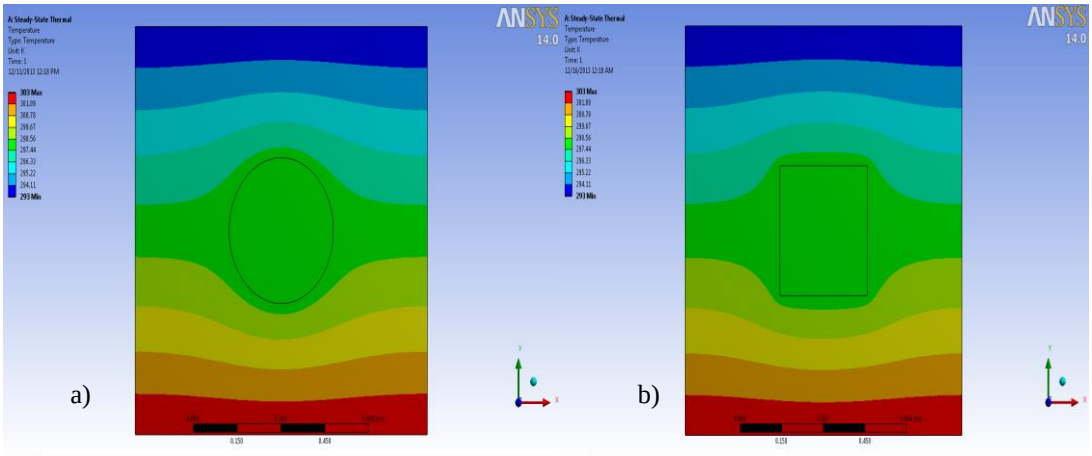

Figure D.1.26. Temperature distribution over 1-piece- a)circle and b) square -filler model for Ø=10%

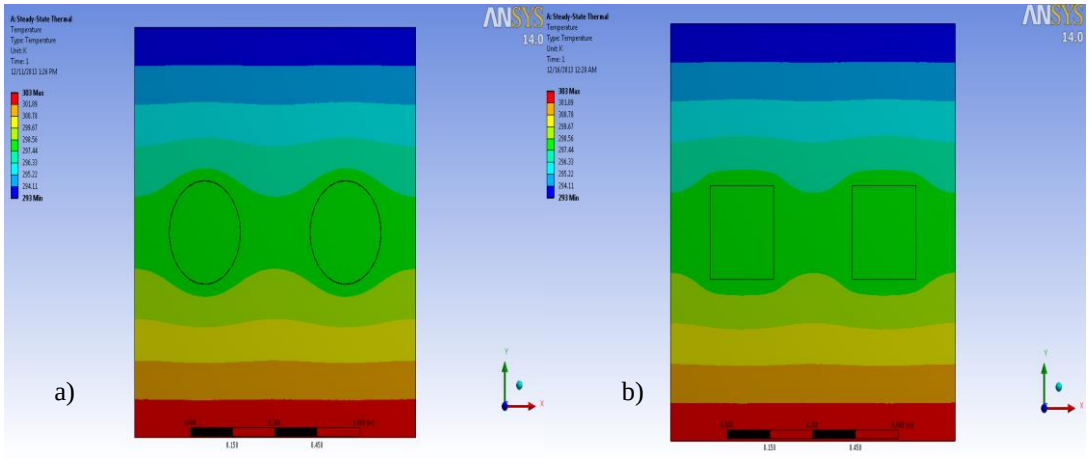

Figure D.1.27. Temperature distribution over 2-piece- a)circle and b) square -filler model for Ø=10%

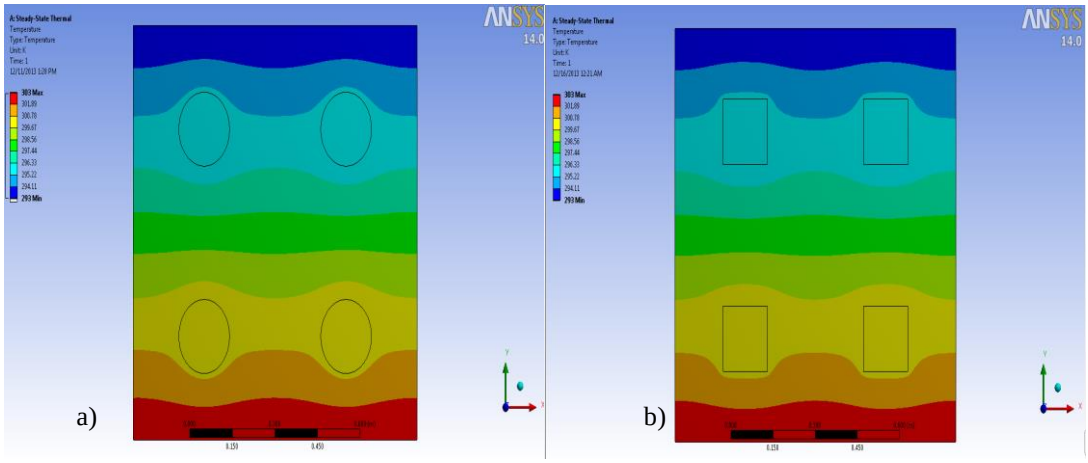

Figure D.1.28. Temperature distribution over 4-piece- a)circle and b) square -filler model for Ø=10%

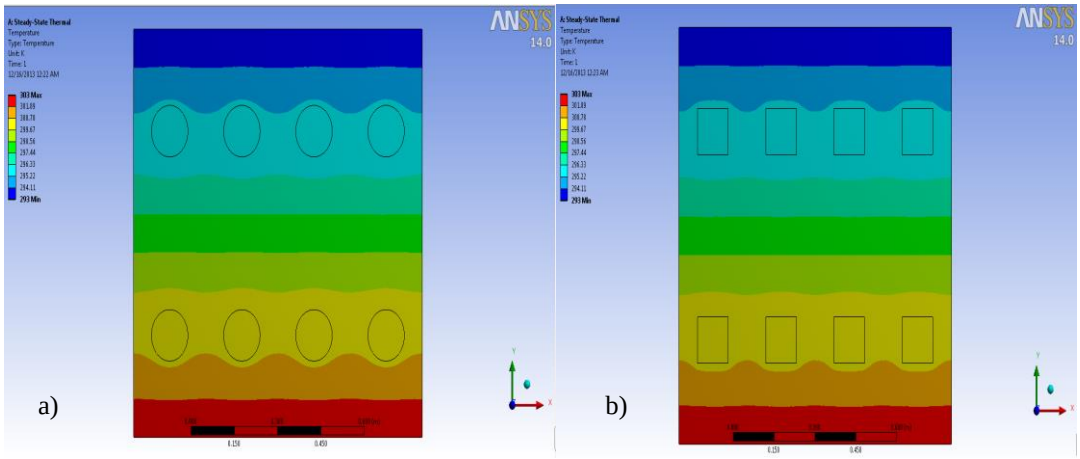

Figure D.1.29. Temperature distribution over 8-piece- a)circle and b) square -filler model for Ø=10%

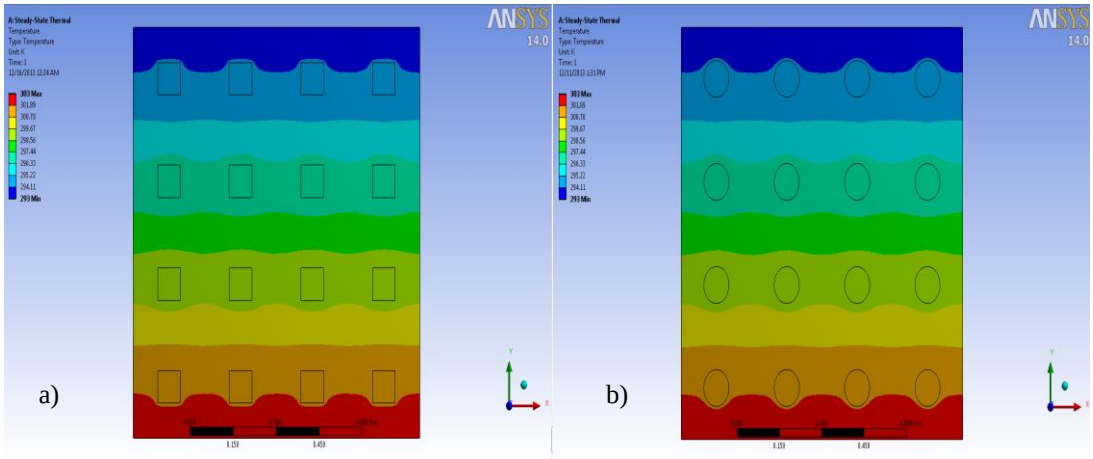

Figure D.1.30. Temperature distribution over 16-piece- a)circle and b) square -filler model for Ø=10%

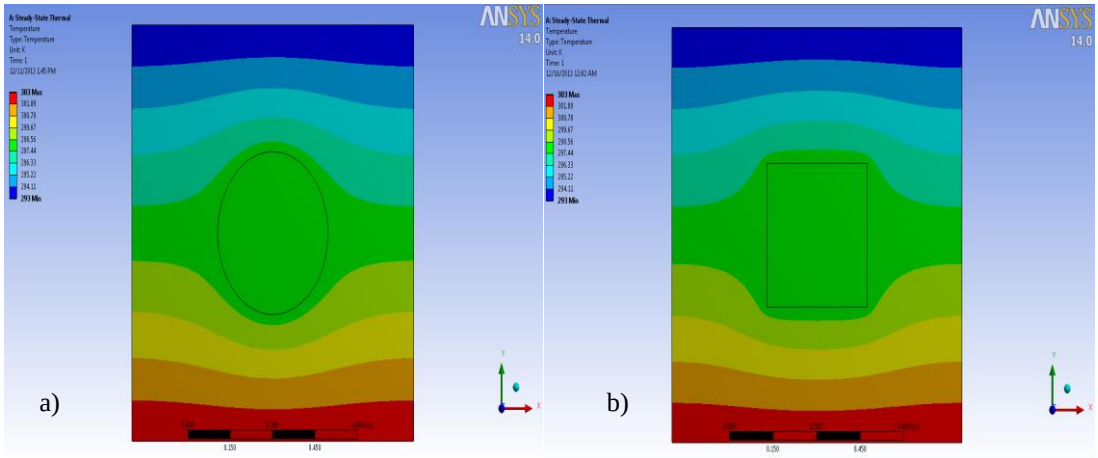

Figure D.1.31. Temperature distribution over 1-piece- a)circle and b) square -filler model for Ø=12%

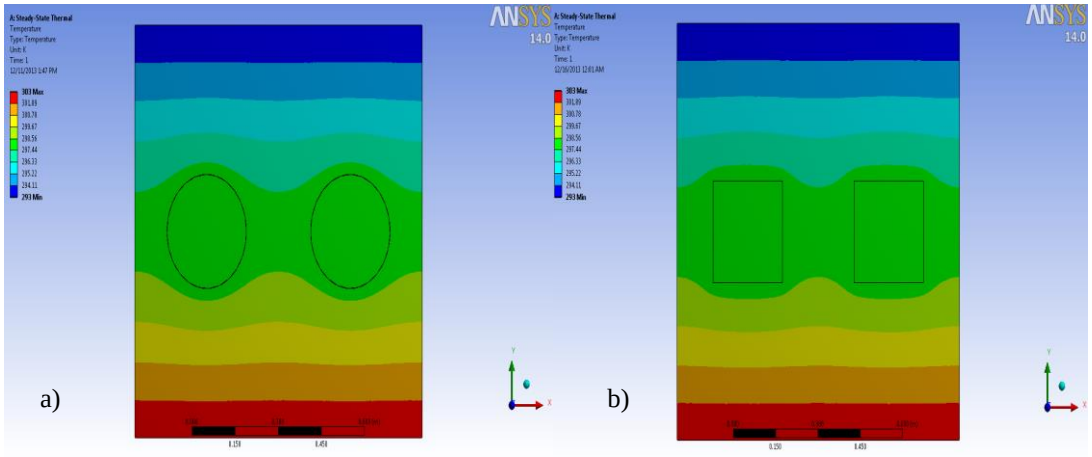

Figure D.1.32. Temperature distribution over 2-piece- a)circle and b) square -filler model for Ø=12%

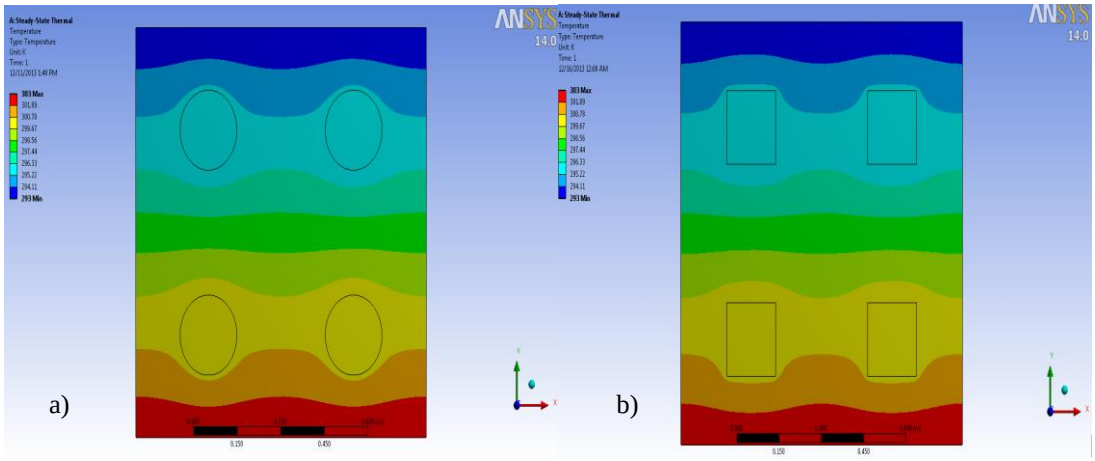

Figure D.1.33. Temperature distribution over 4-piece- a)circle and b) square -filler model for Ø=12%

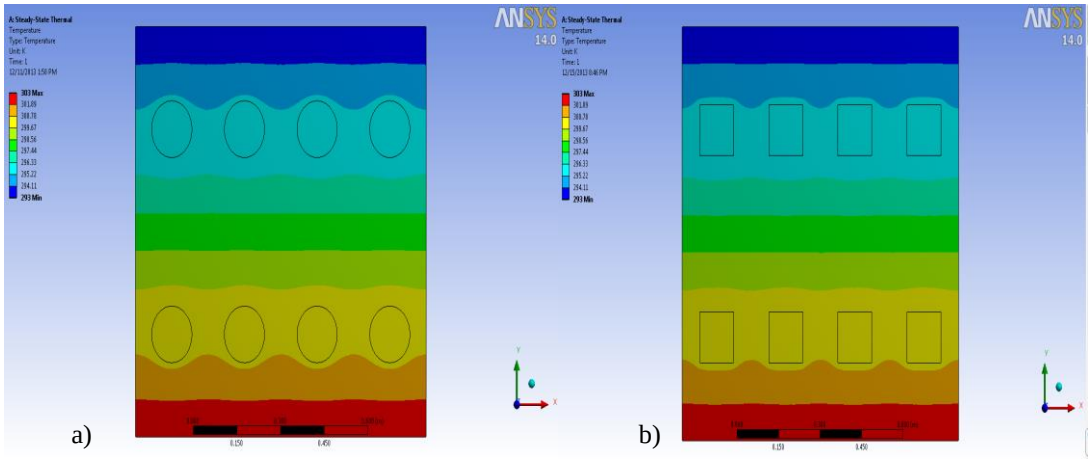

Figure D.1.34. Temperature distribution over 8-piece- a)circle and b) square -filler model for Ø=12%

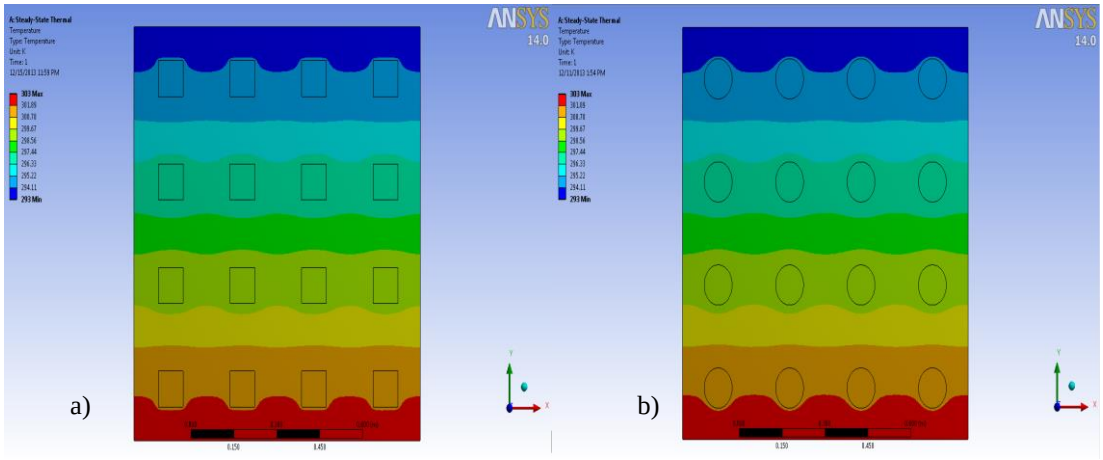

Figure D.1.35. Temperature distribution over 16-piece- a)circle andb) square -filler model for Ø=12%

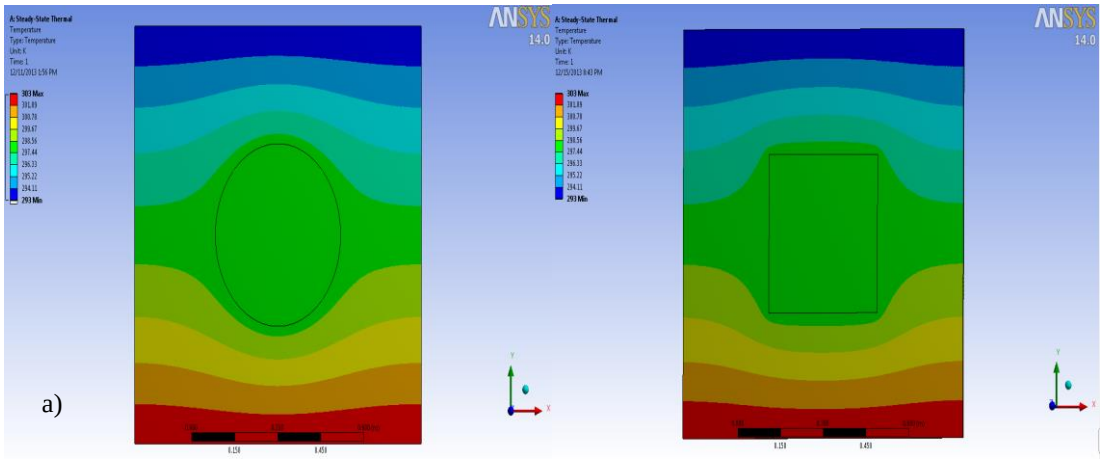

Figure D.1.36. Temperature distribution over 1-piece- a)circle and b) square -filler model for Ø=15%

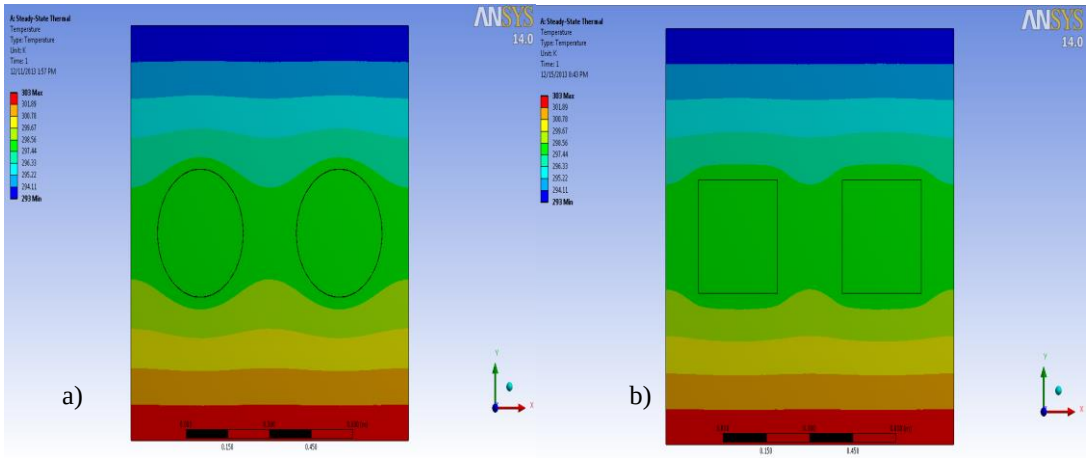

Figure D.1.37. Temperature distribution over 2-piece- a)circle and b) square -filler model for Ø=15%

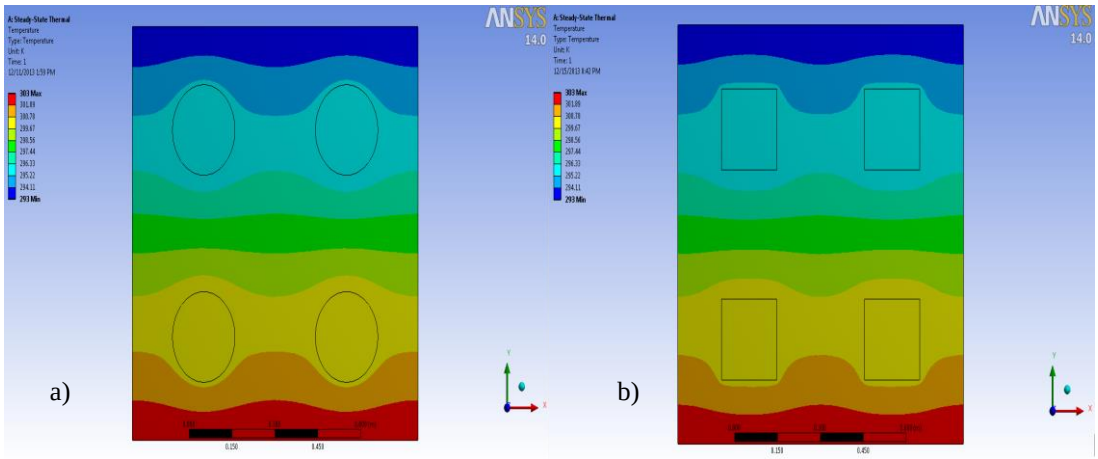

Figure D.1.38. Temperature distribution over 4-piece- a)circle and b) square -filler model for Ø=15%

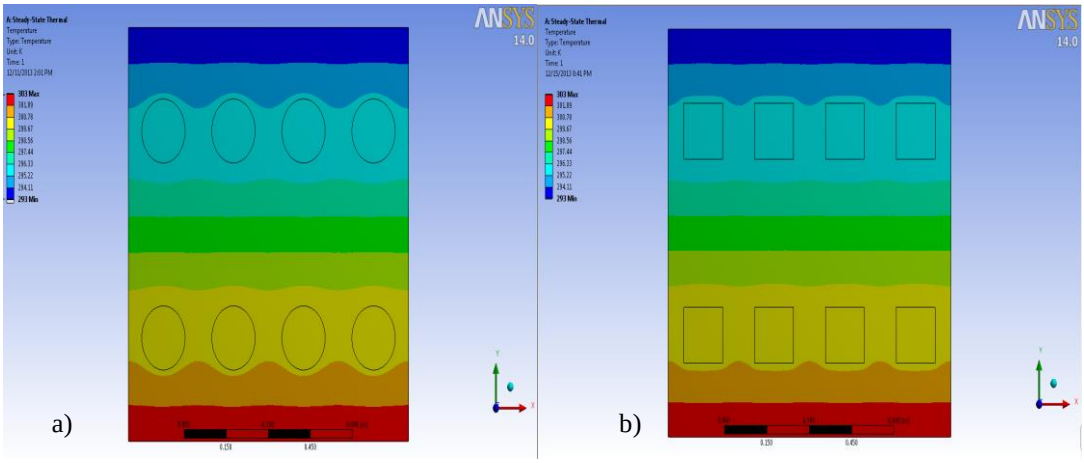

Figure D.1.39. Temperature distribution over 8-piece- a)circle and b) square -filler model for Ø=15%

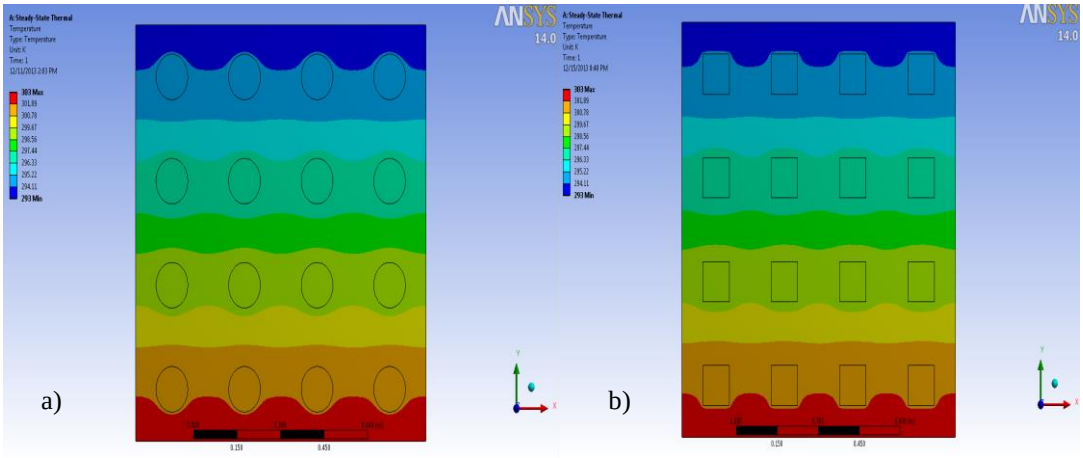

Figure D.1.40 Temperature distribution over 16-piece- a)circle and b) square -filler model for Ø=15%

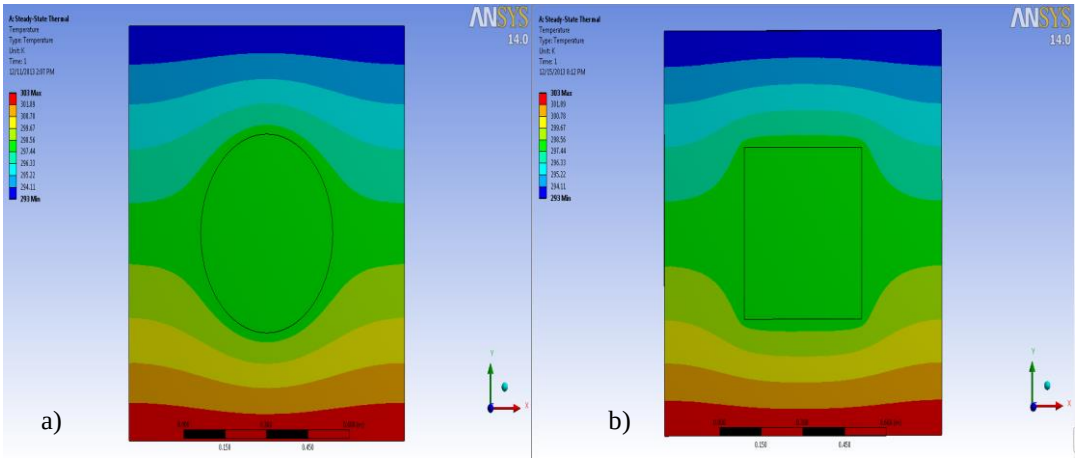

Figure D.1.41. Temperature distribution over 1-piece- a)circle and b) square–filler model for Ø=18%

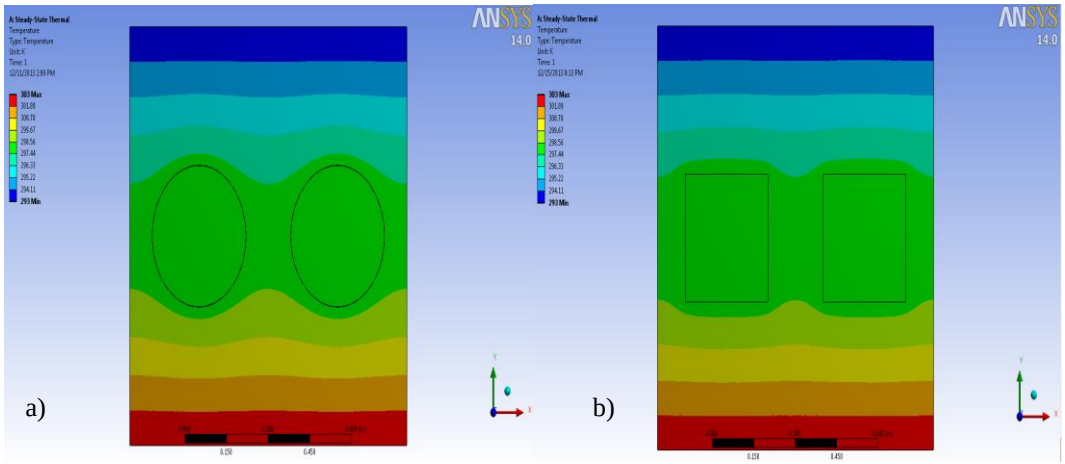

Figure D.1.42. Temperature distribution over 2-piece- a)circle and b) square -filler model for Ø=18%

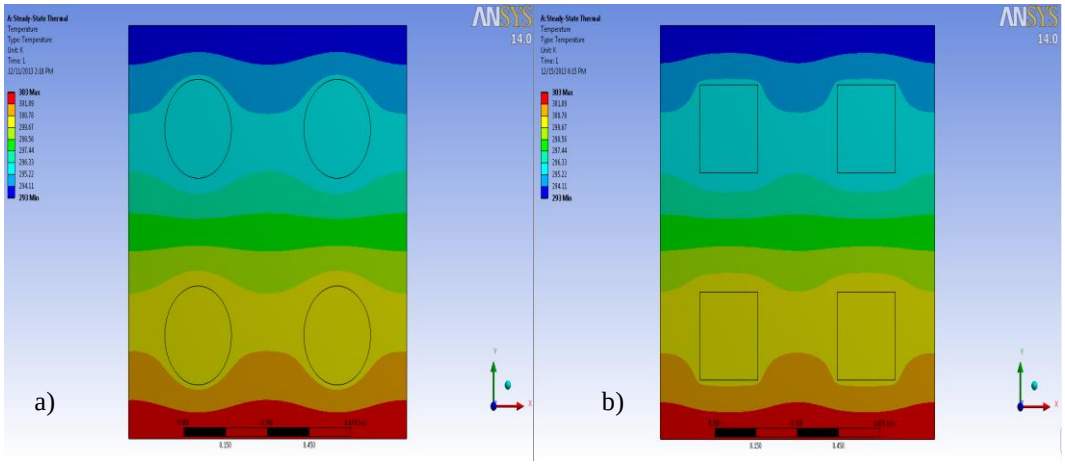

Figure D.1.43. Temperature distribution over 4-piece- a)circle and b) square -filler model for Ø=18%

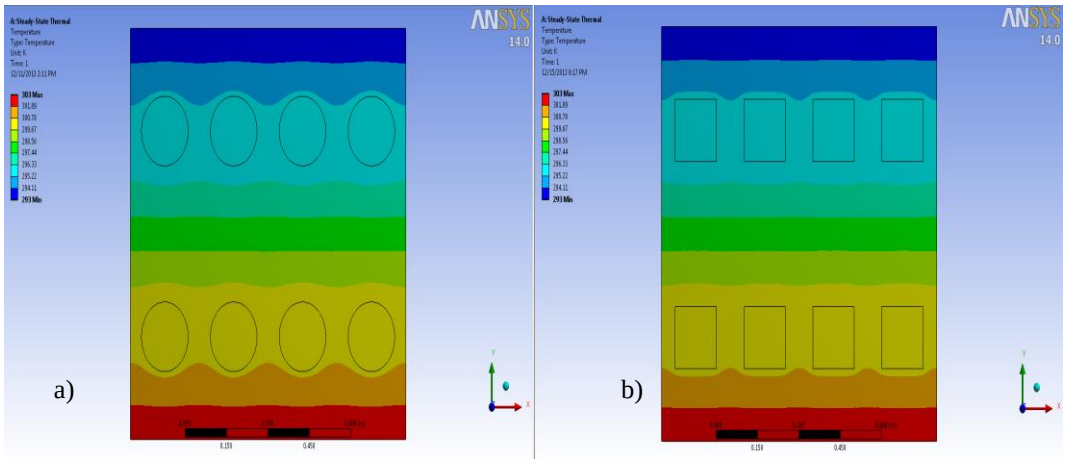

Figure D.1.44. Temperature distribution over 8-piece- a)circle and b) square -filler model for Ø=18%

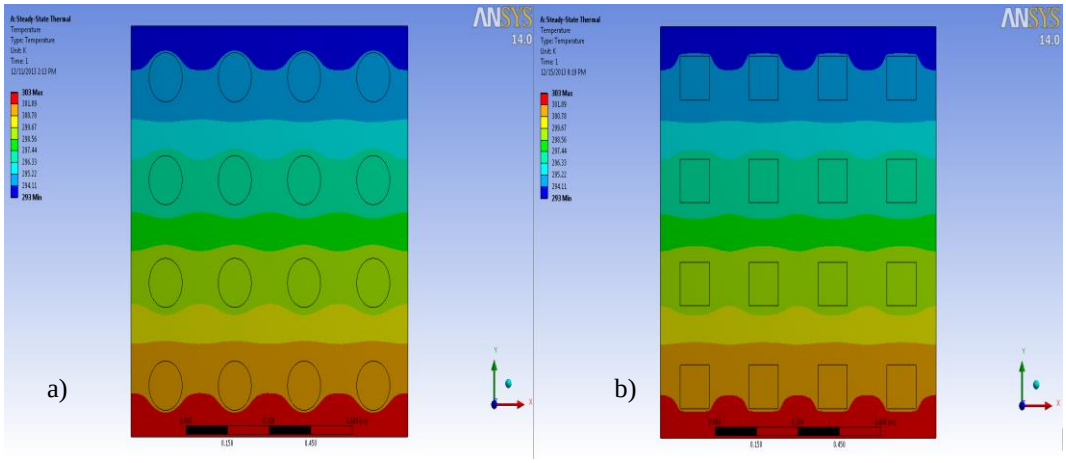

Figure D.1.45. Temperature distribution over 16-piece- a)circle and b) square -filler model for Ø=18%

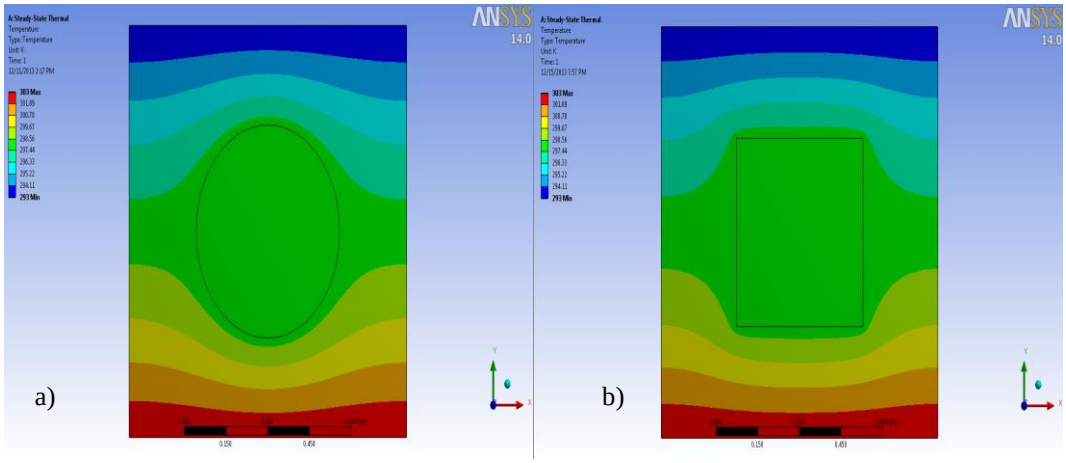

Figure D.1.46. Temperature distribution over 1-piece- a)circle and b) square -filler model for Ø=21%

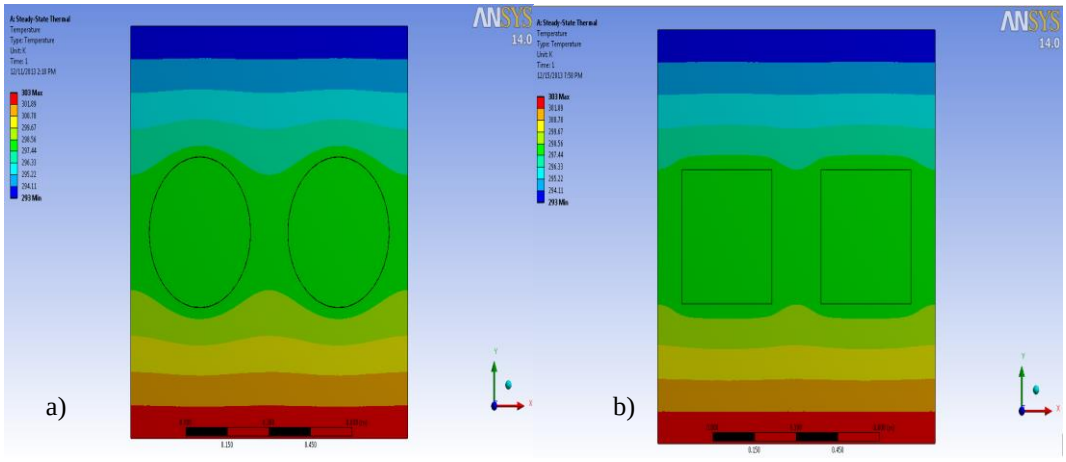

Figure D.1.47. Temperature distribution over 2-piece- a)circle and b) square -filler model for Ø=21%

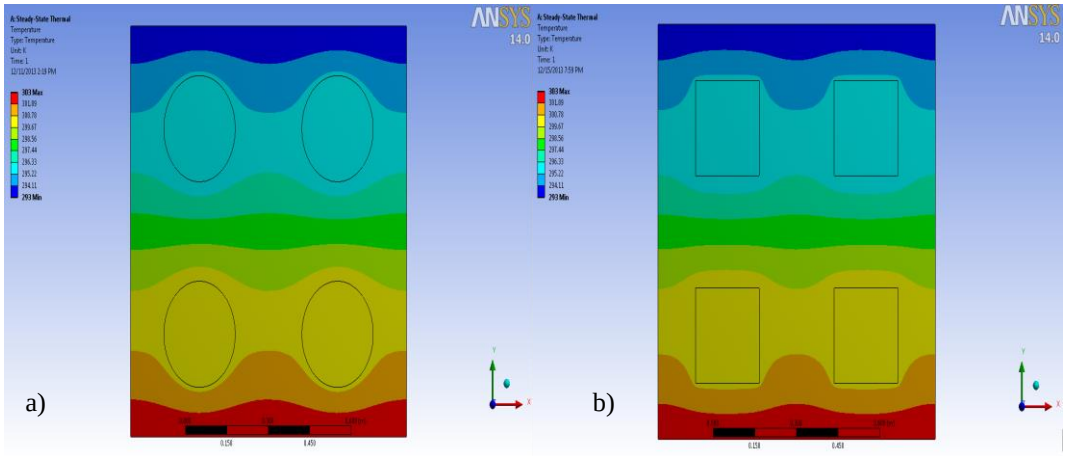

Figure D.1.48. Temperature distribution over 4-piece- a)circle and b) square -filler model for Ø=21%

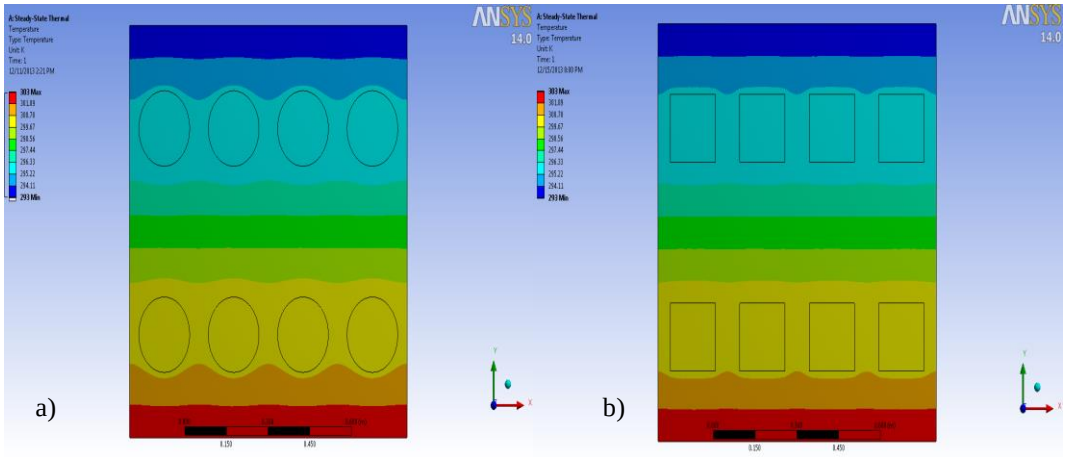

Figure D.1.49. Temperature distribution over 8-piece- a)circle and b) square -filler model for Ø=21%

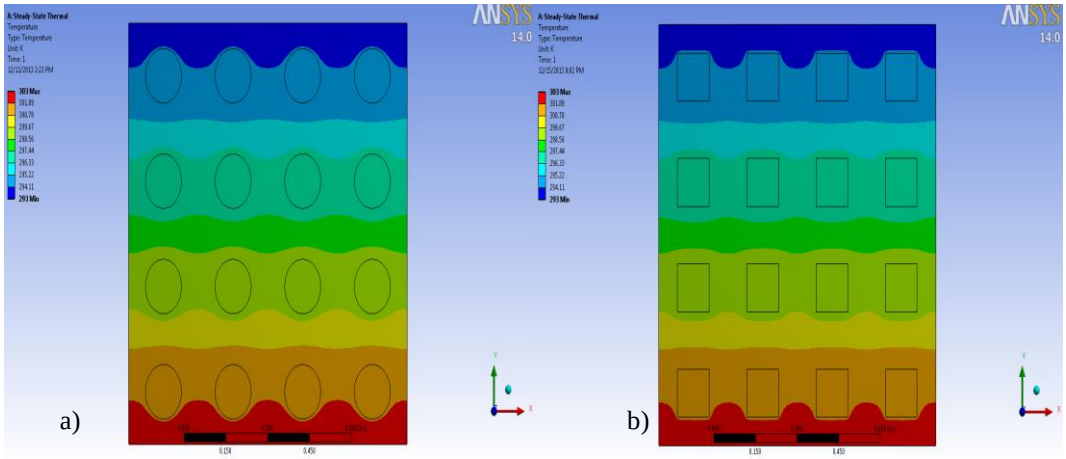

Figure D.1.50. Temperature distribution over 16-piece- a)circle and b) square -filler model for Ø=21%

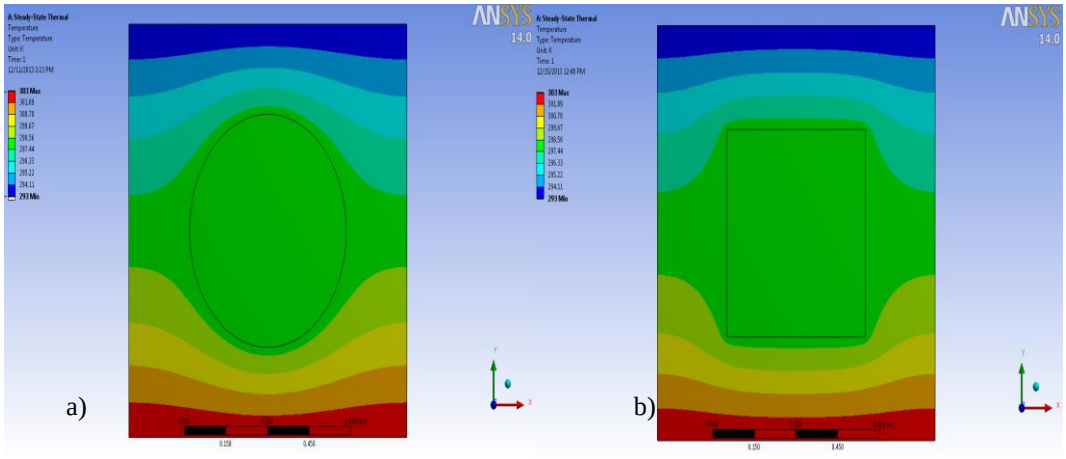

Figure D.1.51. Temperature distribution over 1-piece- a)circle and b) square -filler model for Ø=25%

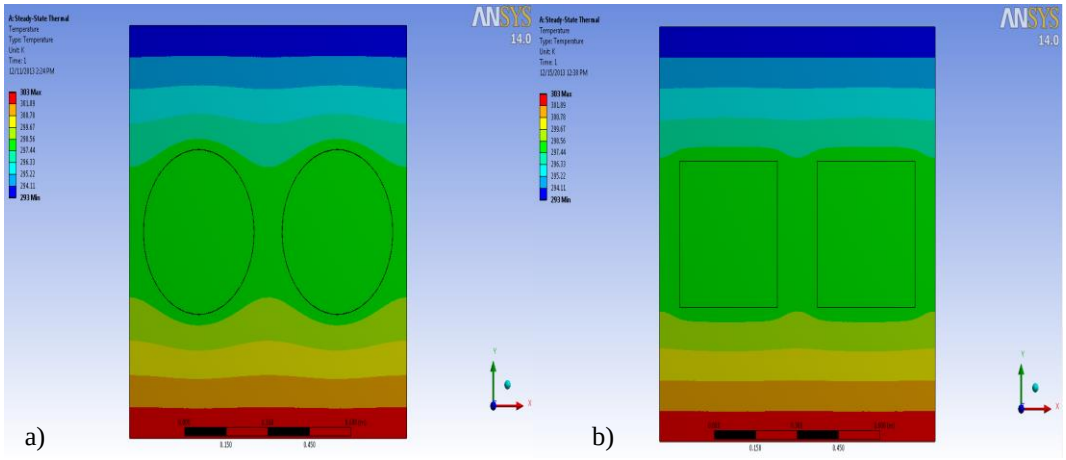

Figure D.1.52. Temperature distribution over 2-piece- a)circle and b) square -filler model for Ø=25%

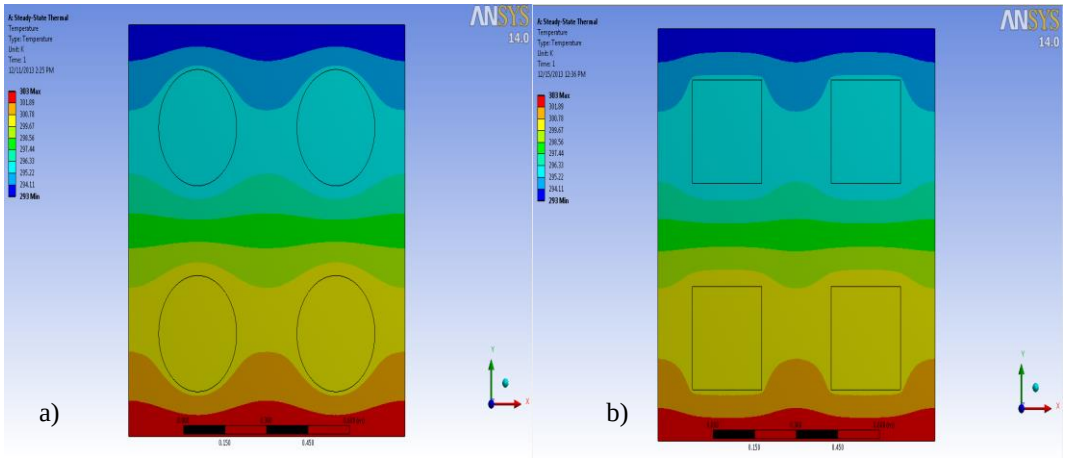

Figure D.1.53. Temperature distribution over 4-piece- a)circle and b) square -filler model for Ø=25%

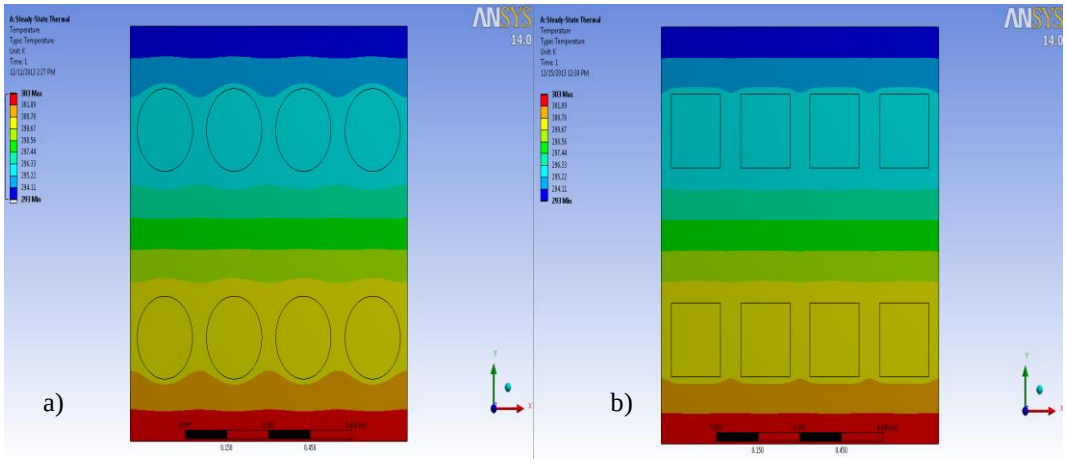

Figure D.1.54. Temperature distribution over 8-piece- a)circle and b) square -filler model for Ø=25%

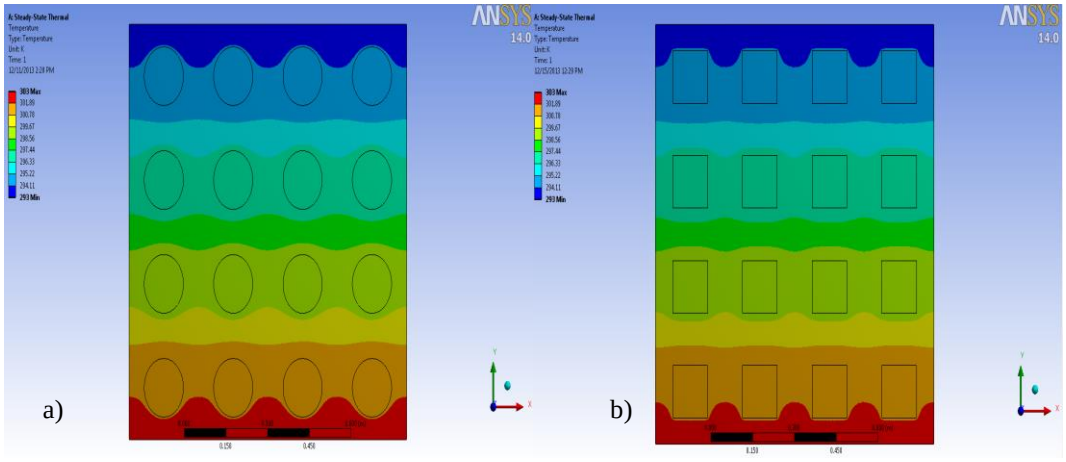

Figure D.1.55. Temperature distribution over 16-piece- a)circle and b) square -filler model for Ø=25%

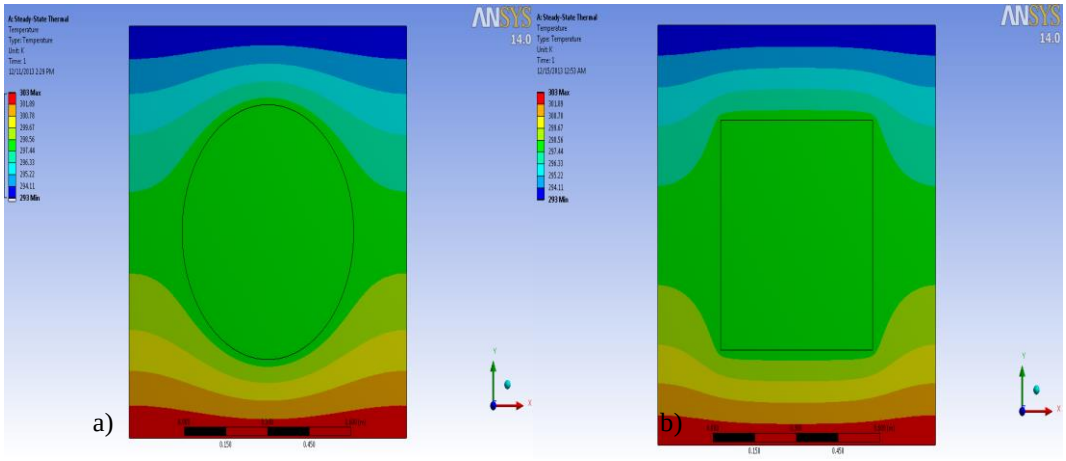

Figure D.1.56. Temperature distribution over 1-piece- a)circle and b) square -filler model for Ø=30%

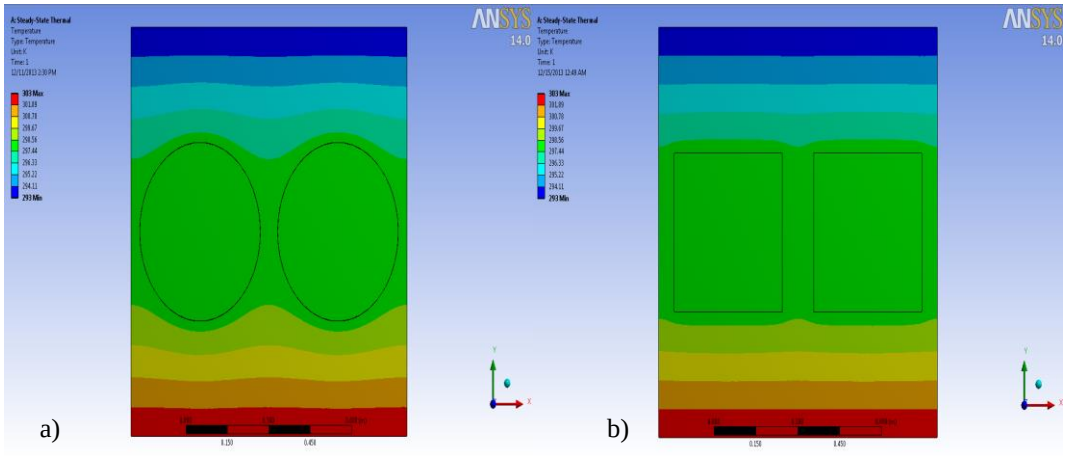

Figure D.1.57. Temperature distribution over 2-piece- a)circle and b) square -filler model for Ø=30%

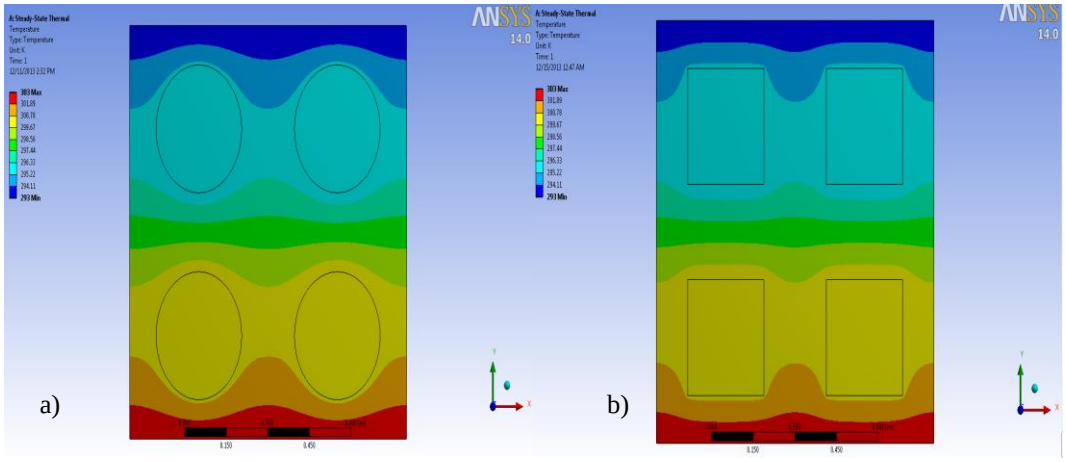

Figure D.1.58. Temperature distribution over 4-piece- a)circle and b) square -filler model for Ø=30%

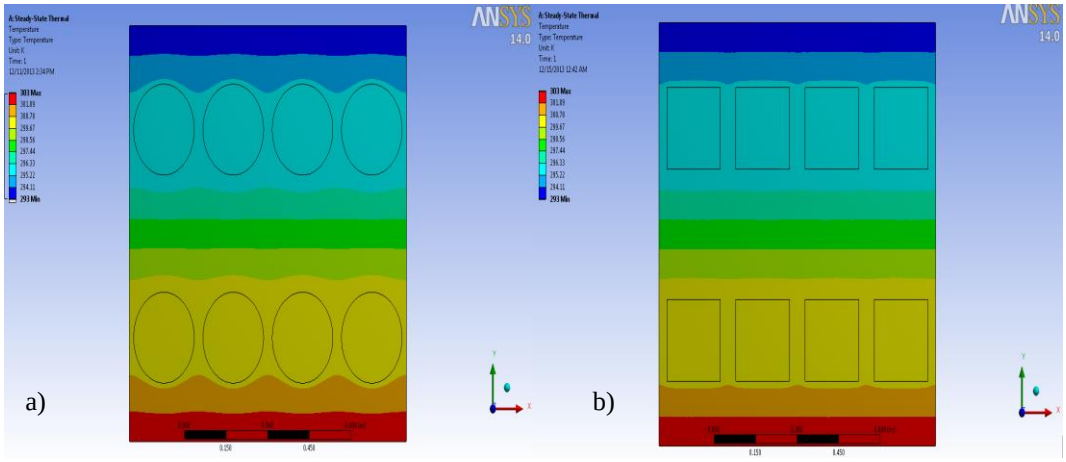

Figure D.1.59. Temperature distribution over 8-piece- a)circle and b) square -filler model for Ø=30%

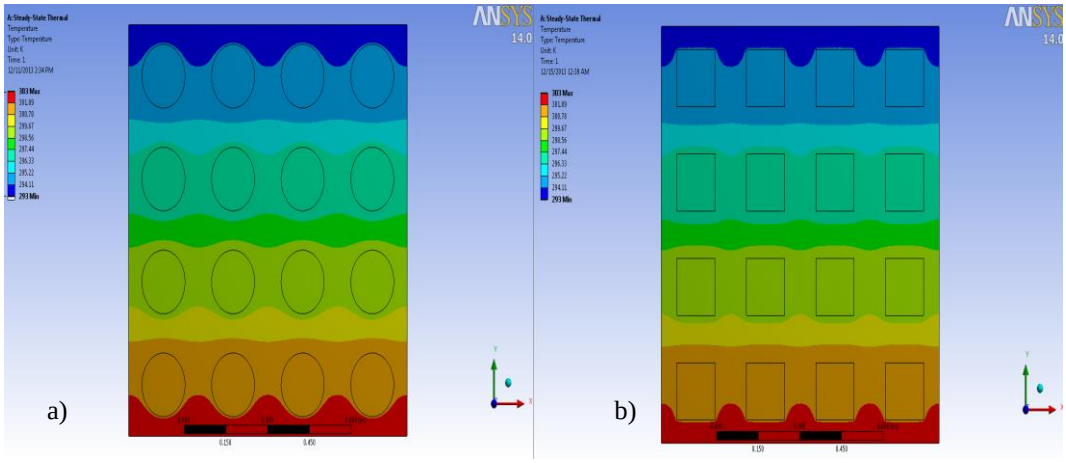

Figure D.1.60. Temperature distribution over 16-piece- a)circle and b) square -filler model for Ø=30%

D.2 Heat Flux Results

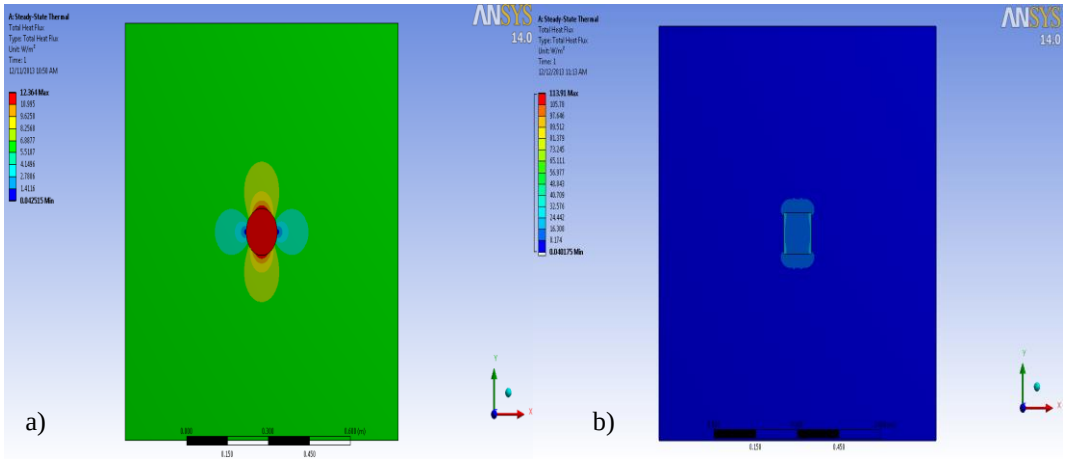

Figure D.2.1. Total heat flux distribution over 1-piece- a)circle and b) square -filler model for Ø=1%

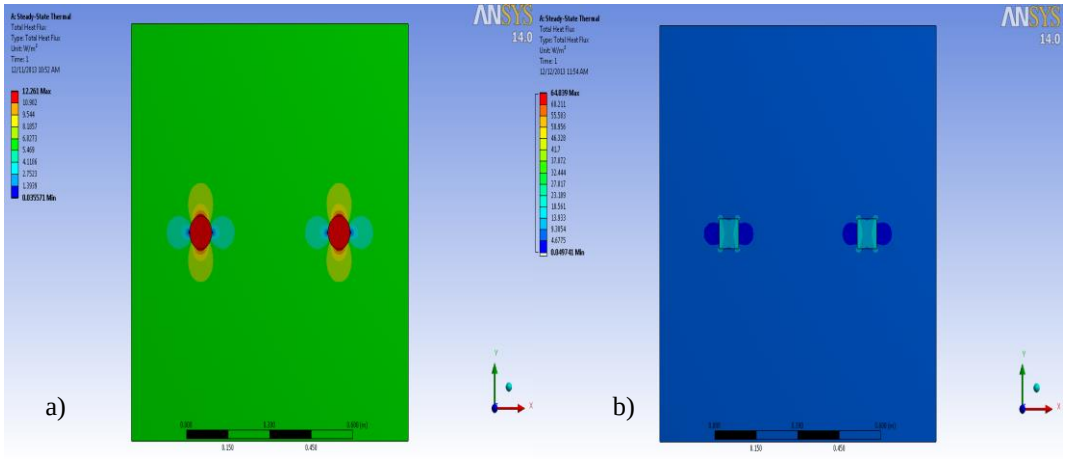

Figure D.2.2. Total heat flux distribution over 2-piece- a)circle and b) square -filler model for Ø=1%

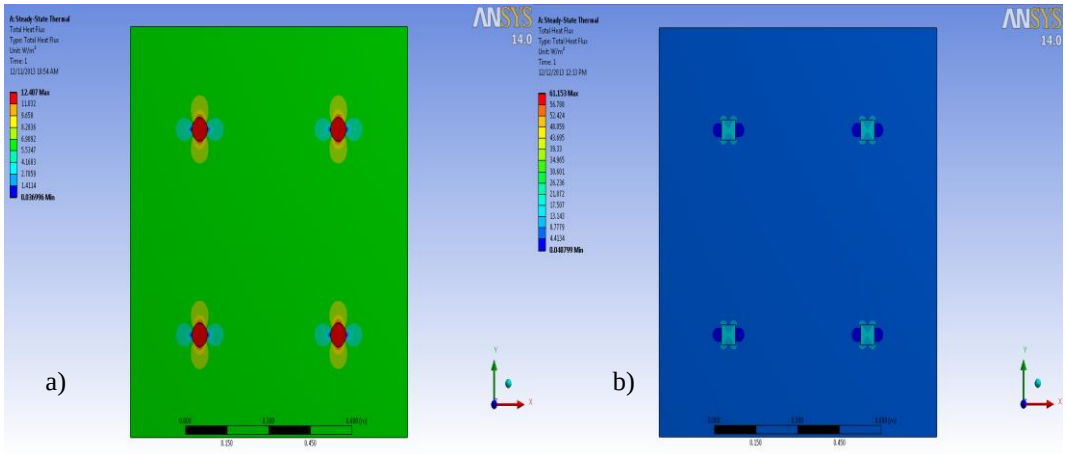

Figure D.2.3. Total heat flux distribution over 4-piece- a)circle and b) square -filler model for Ø=1%

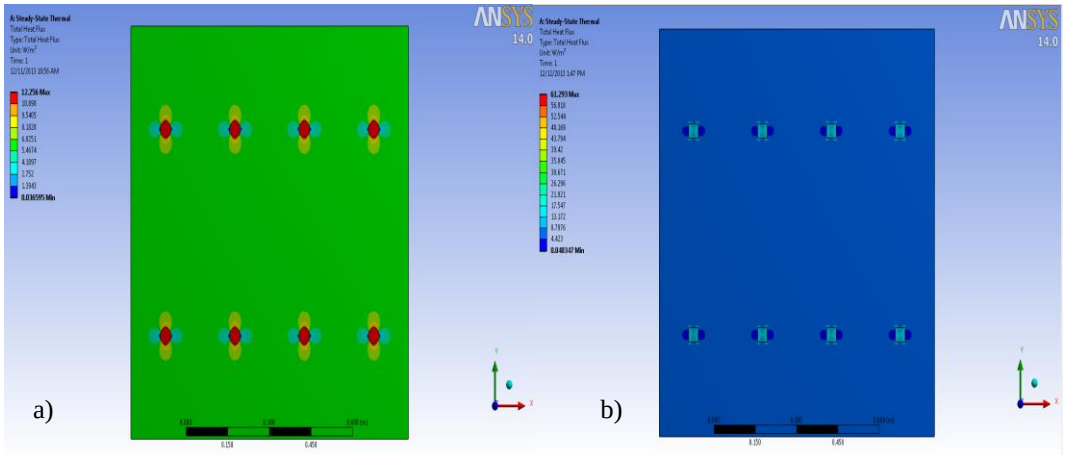

Figure D.2.4. Total heat flux distribution over 8-piece- a)circle and b) square -filler model for Ø=1%

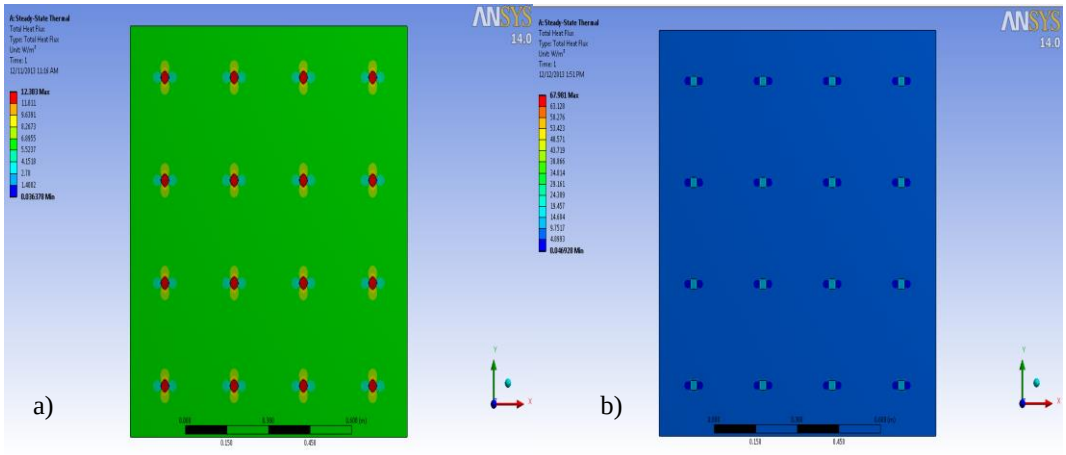

Figure D.2.5. Total heat flux distribution over 16-piece- a)circle and b) square -filler model for Ø=1%

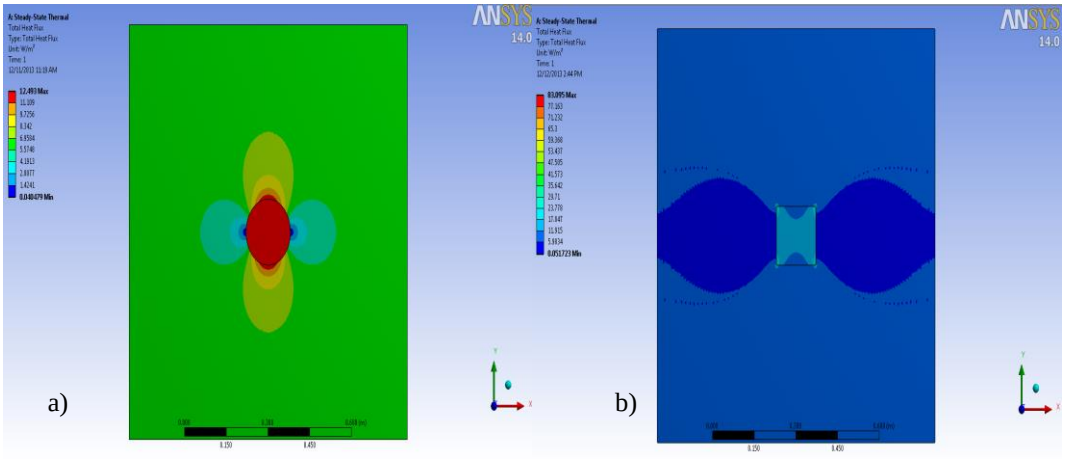

Figure D.2.6. Total heat flux distribution over 1-piece- a)circle and b) square -filler model for Ø=2%

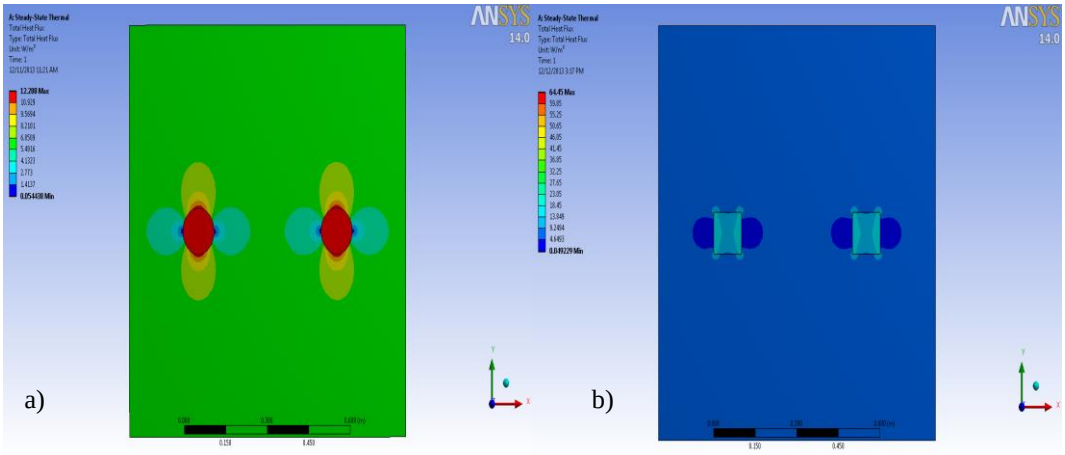

Figure D.2.7. Total heat flux distribution over 2-piece- a)circle and b) square -filler model for Ø=2%

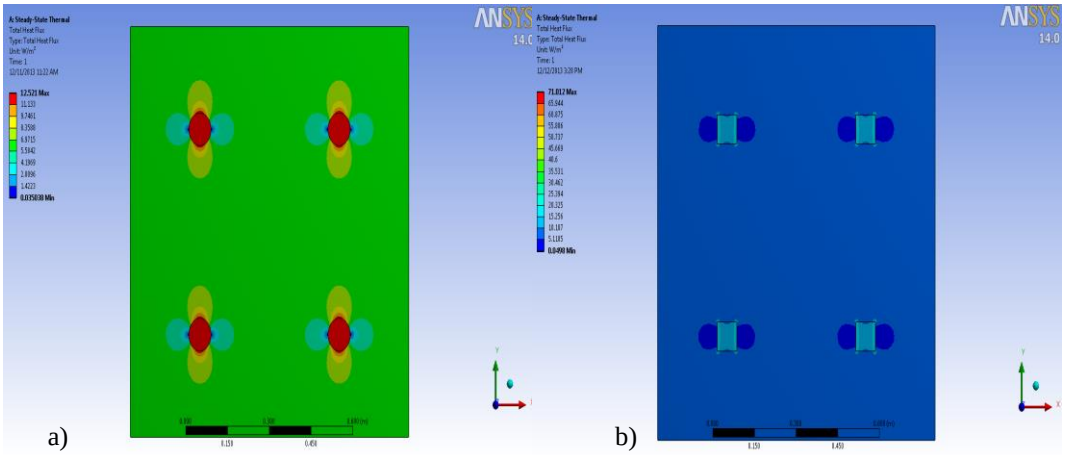

Figure D.2.8. Total heat flux distribution over 4-piece- a)circle and b) square -filler model for Ø=2%

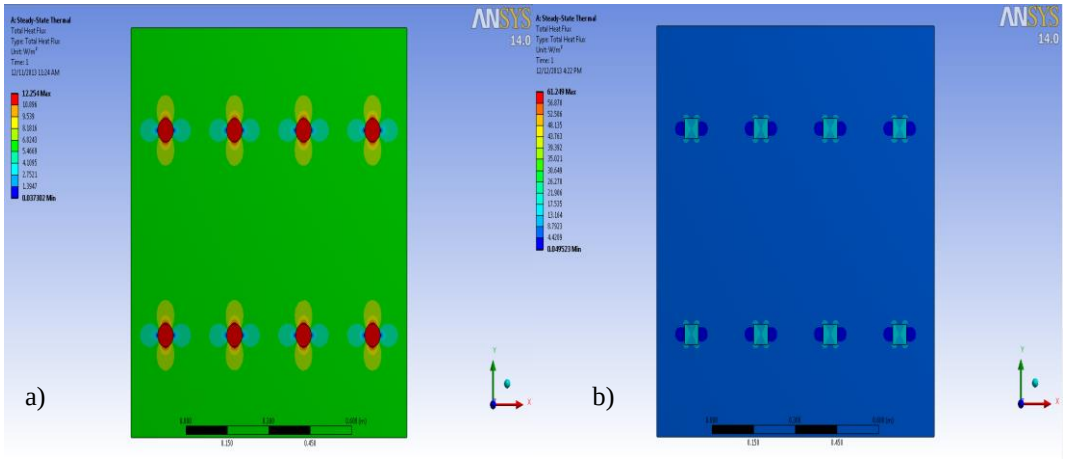

Figure D.2.9. Total heat flux distribution over 8-piece- a)circle and b) square -filler model for Ø=2%

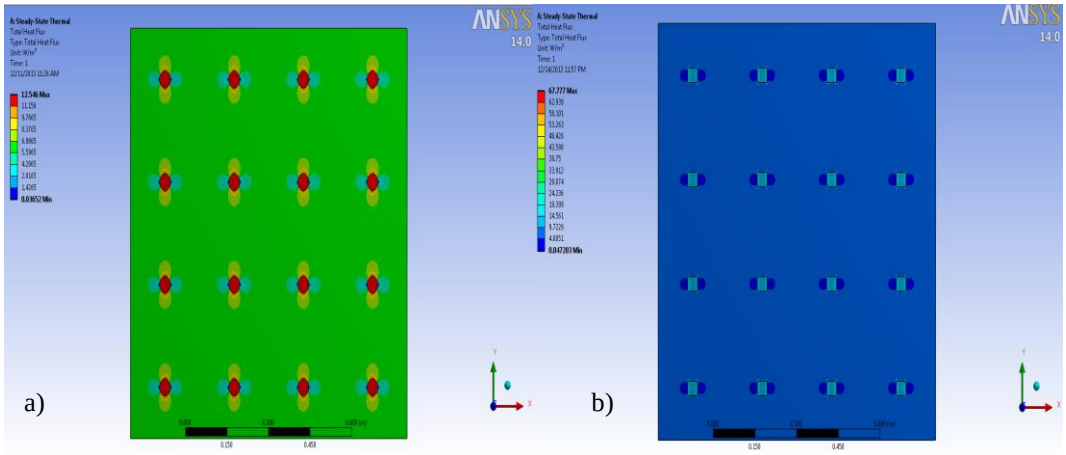

Figure D.2.10. Total heat flux distribution over 16piece- a)circle and b) square -filler model for Ø=2%

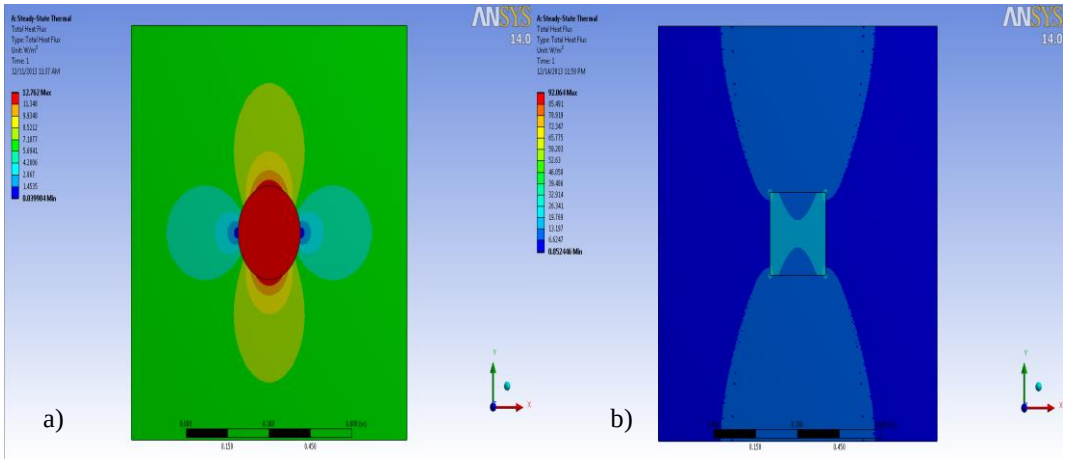

Figure D.2.11. Total heat flux distribution over 1-piece- a)circle and b) square -filler model for Ø=4%

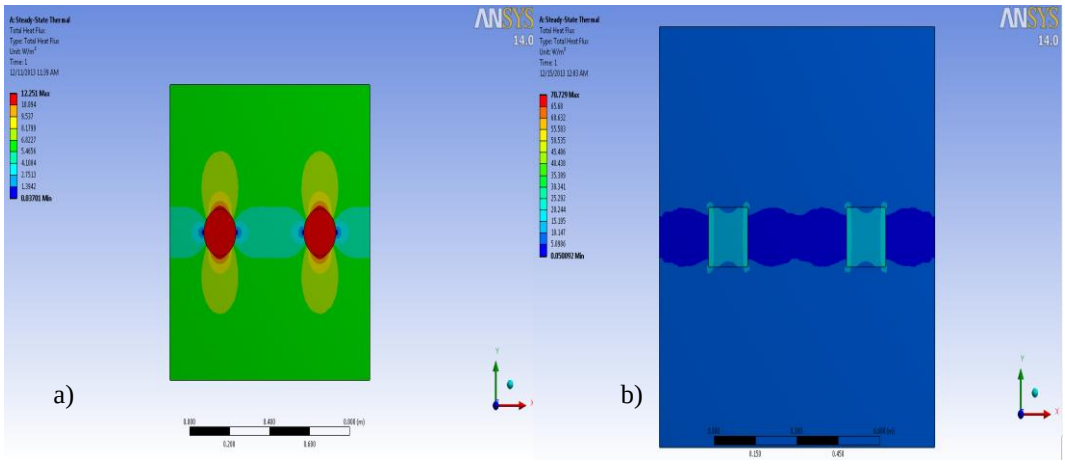

Figure D.2.12. Total heat flux distribution over 2-piece- a)circle and b) square -filler model for Ø=4%

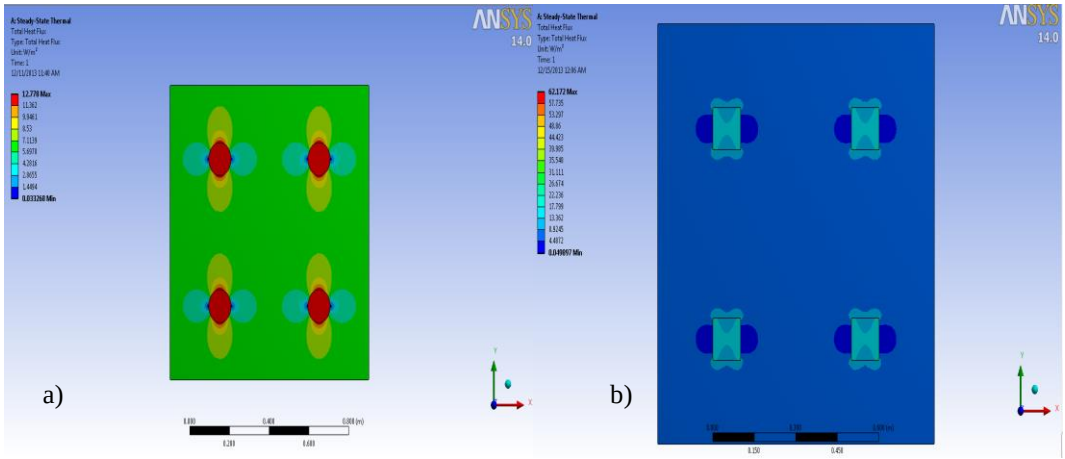

Figure D.2.13. Total heat flux distribution over 4-piece- a)circle and b) square -filler model for Ø=4%

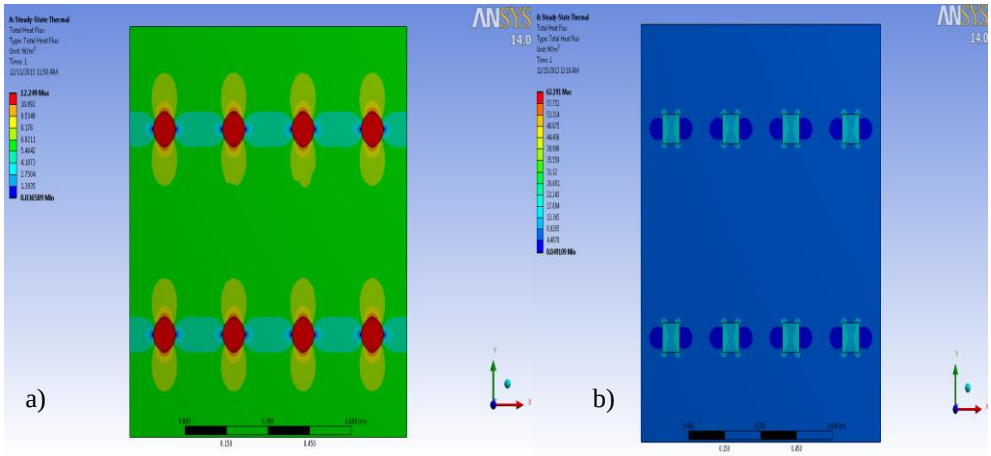

Figure D.2.14. Total heat flux distribution over 8-piece- a)circle and b) square -filler model for Ø=4%

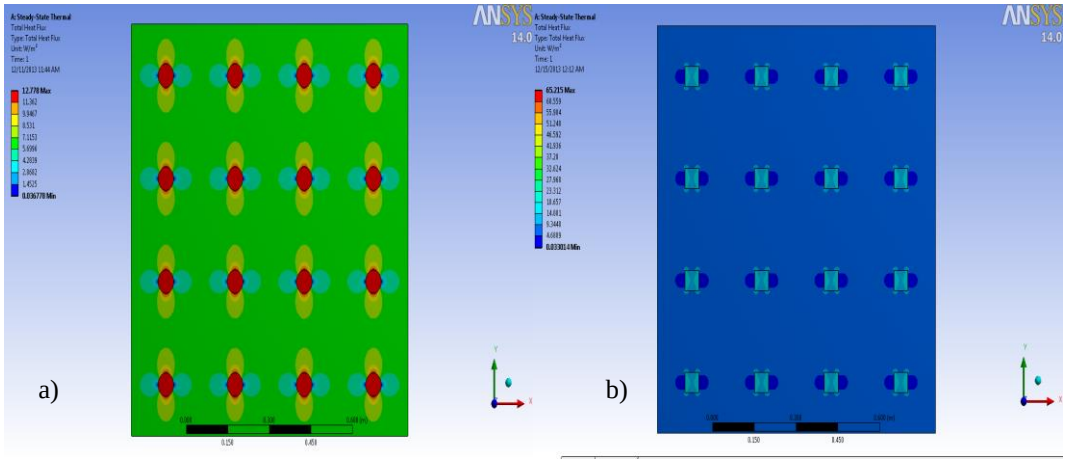

Figure D.2.15. Total heat flux distribution over 16-piece- a)circle and b)square -filler model for Ø=4%

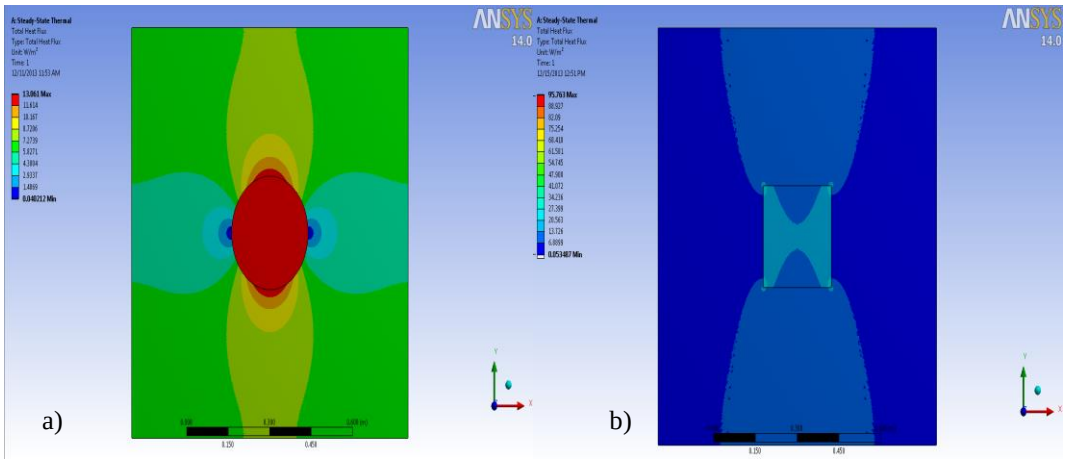

Figure D.2.16. Total heat flux distribution over 1-piece- a)circle and b)square -filler model for Ø=6%

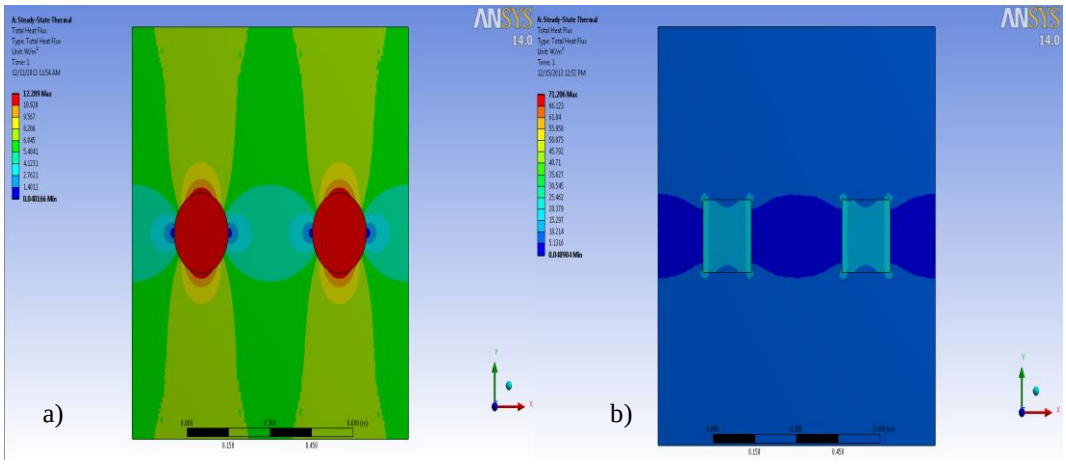

Figure D.2.17. Total heat flux distribution over 2-piece- a)circle and b)square -filler model for Ø=6%

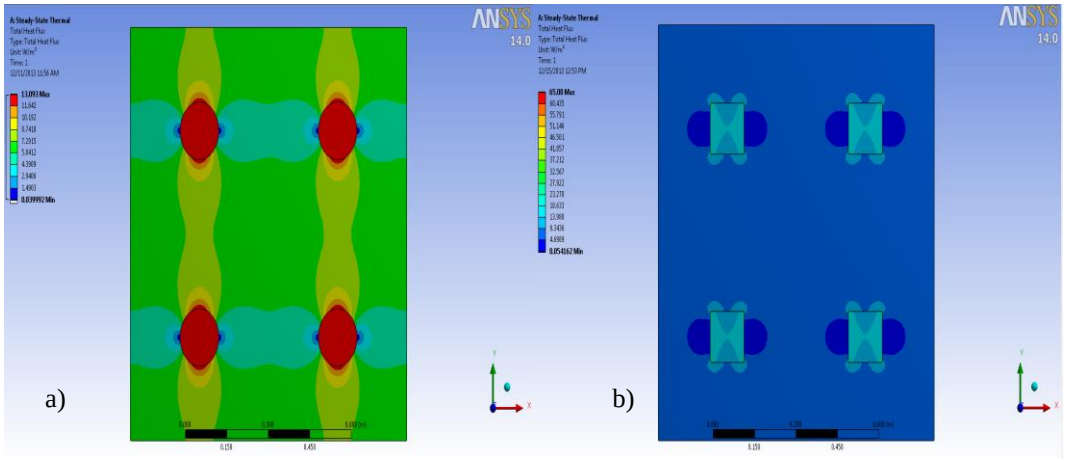

Figure D.2.18. Total heat flux distribution over 4-piece- a)circle and b)square -filler model for Ø=6%

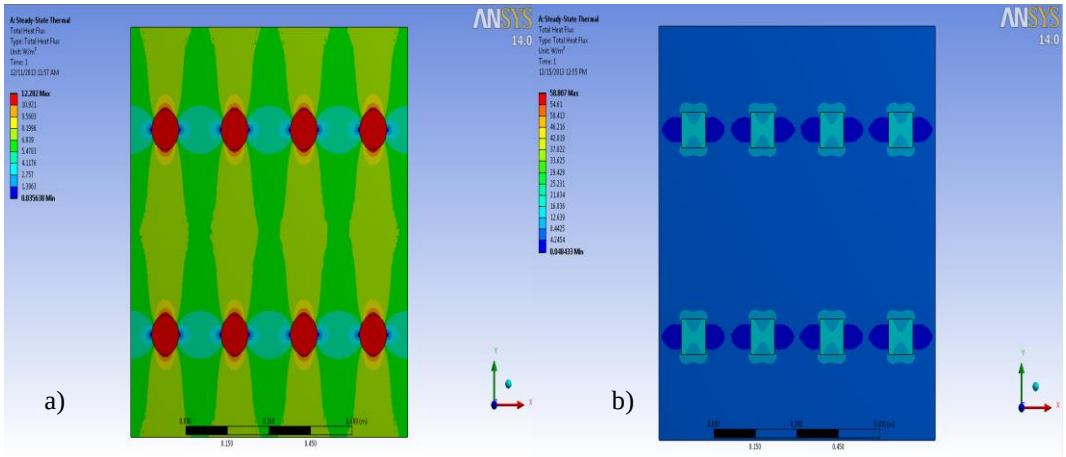

Figure D.2.37. Total heat flux distribution over 8-piece- a)circle and b)square -filler model for Ø=6%

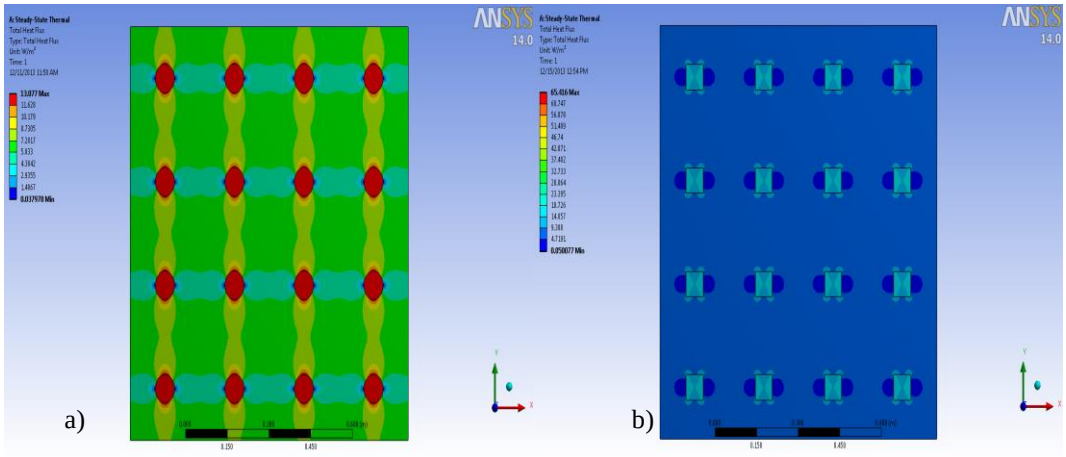

Figure D.2.20. Total heat flux distribution over 16-piece- a)circle and b)square -filler model for Ø=6%

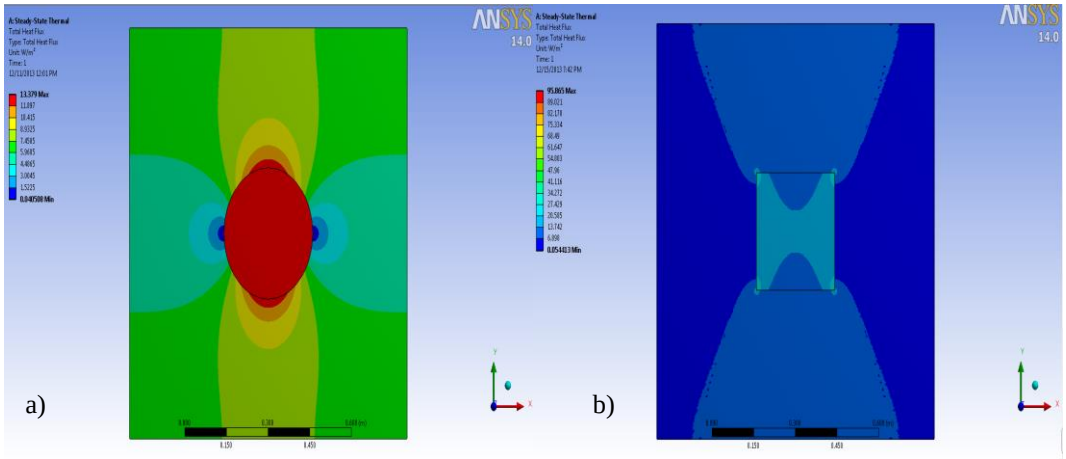

Figure D.2.21. Total heat flux distribution over 1-piece- a)circle and b)square -filler model for Ø=8%

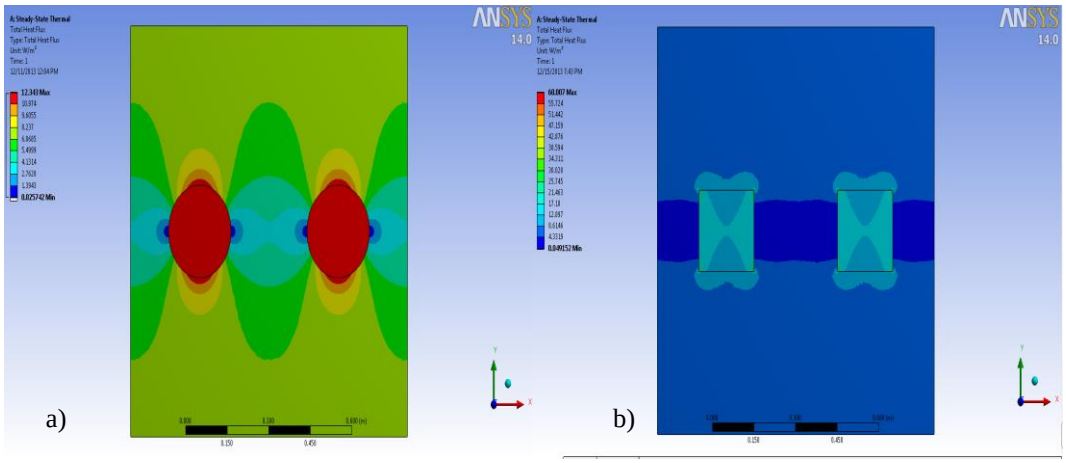

Figure D.2.22. Total heat flux distribution over 2-piece- a)circle and b)square -filler model for Ø=8%

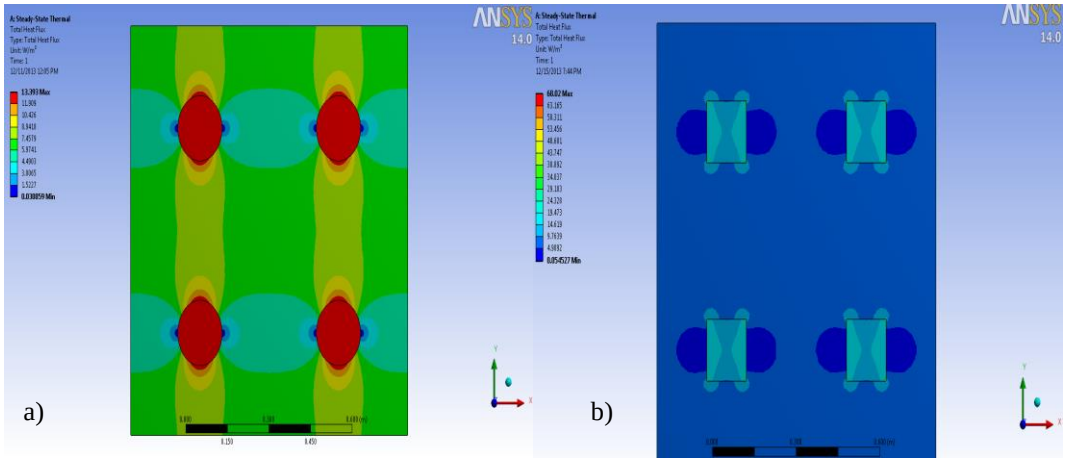

Figure D.2.23. Total heat flux distribution over 4-piece- a)circle and b)square -filler model for Ø=8%

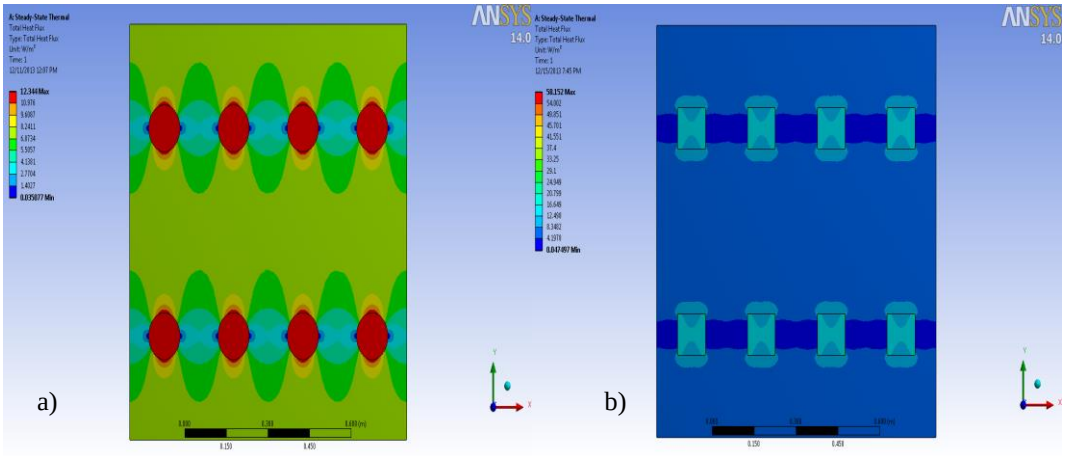

Figure D.2.24. Total heat flux distribution over 8-piece- a)circle and b)square -filler model for Ø=8%

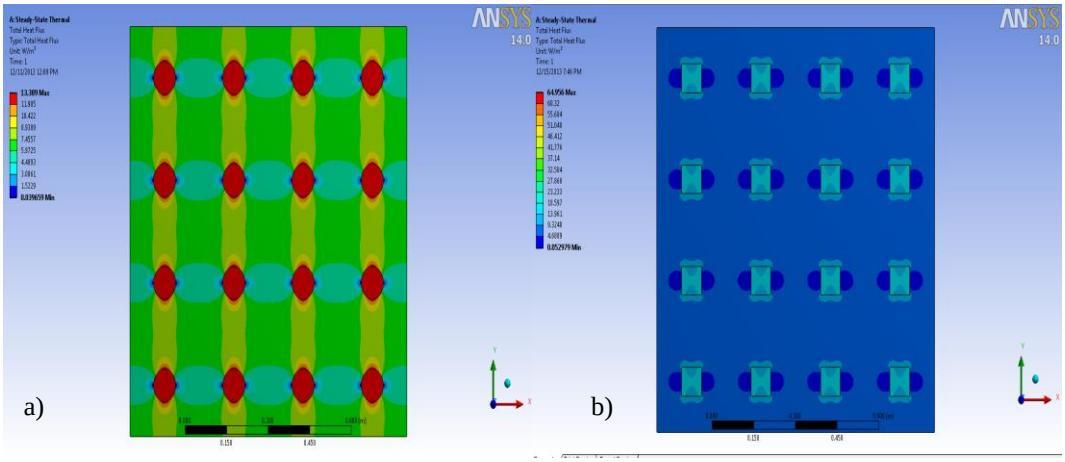

Figure D.2.25. Total heat flux distribution over 16-piece- a)circle and b)square -filler model for Ø=8%

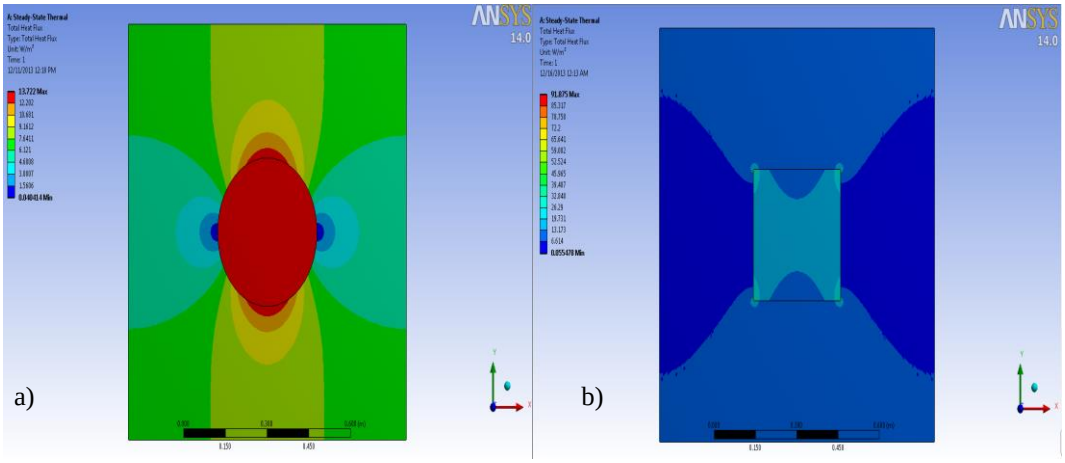

Figure D.2.26. Total heat flux distribution over 1-piece- a)circle and b)square -filler model for Ø=10%

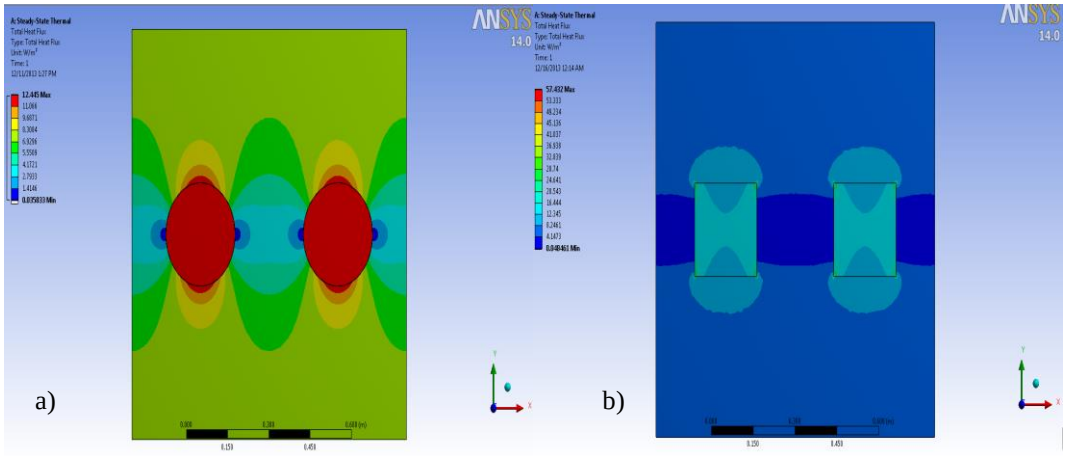

Figure D.2.27. Total heat flux distribution over 2-piece- a)circle and b)square -filler model for Ø=10%

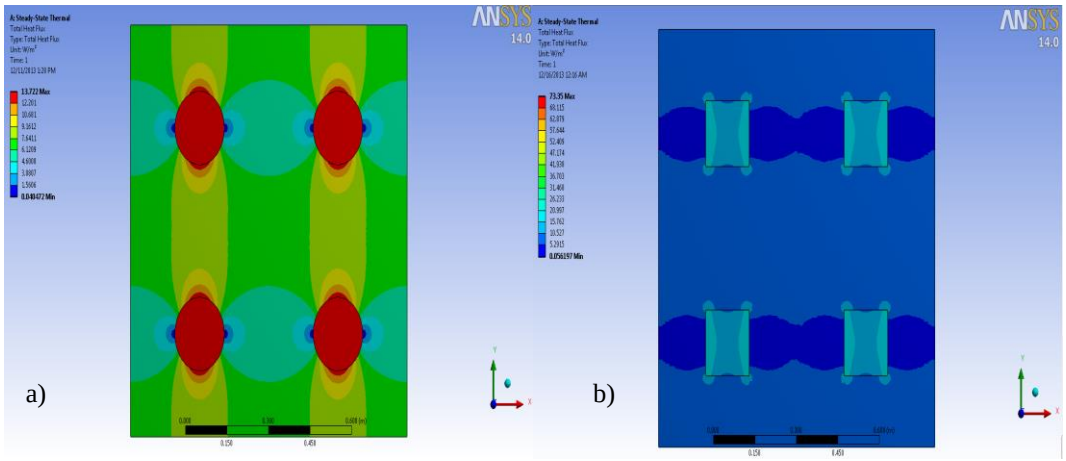

Figure D.2.28. Total heat flux distribution over 4-piece- a)circle and b)square -filler model for Ø=10%

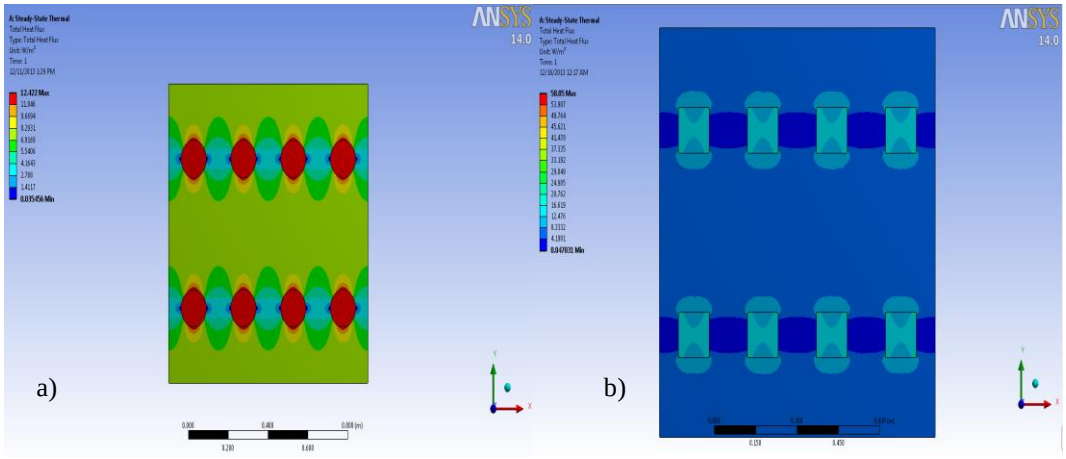

Figure D.2.29. Total heat flux distribution over 8-piece- a)circle and b)square -filler model for Ø=10%

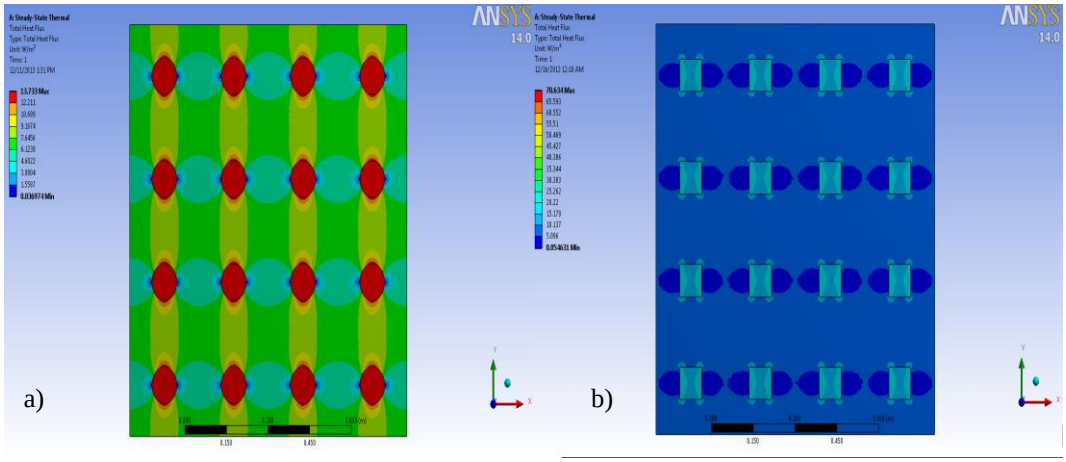

Figure D.2.30.Total heat flux distribution over 16-piece- a)circle andb)square -filler model for Ø=10%

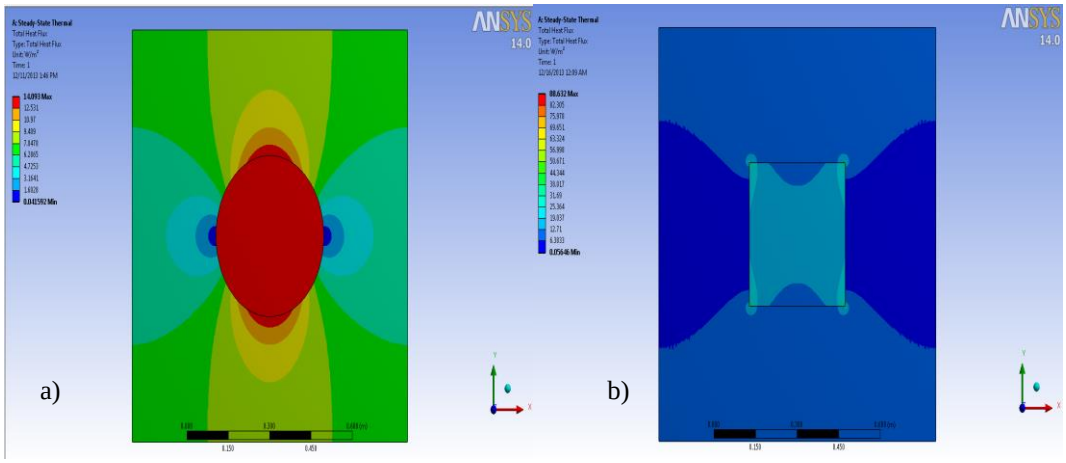

Figure D.2.31. Total heat flux distribution over 1-piece- a)circle and b)square -filler model for Ø=12%

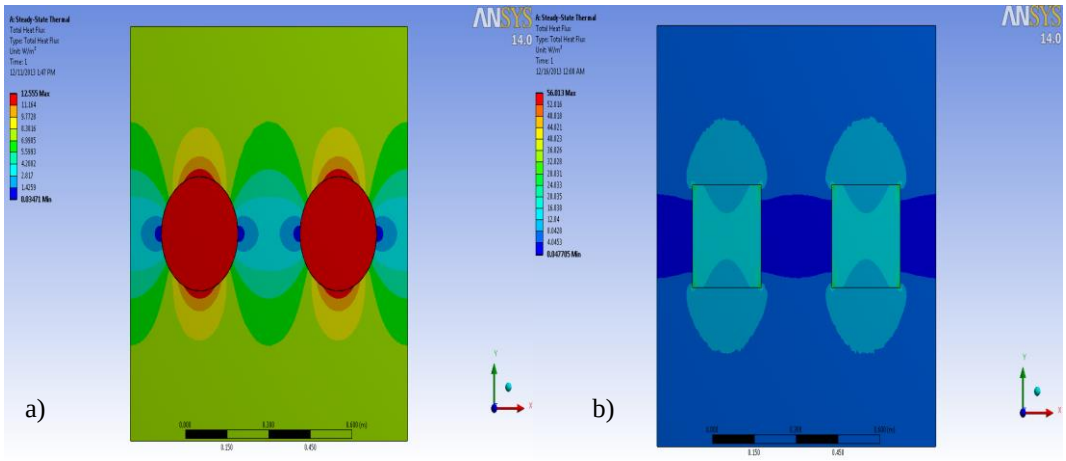

Figure D.2.32. Total heat flux distribution over 2-piece- a)circle and b)square -filler model for Ø=12%

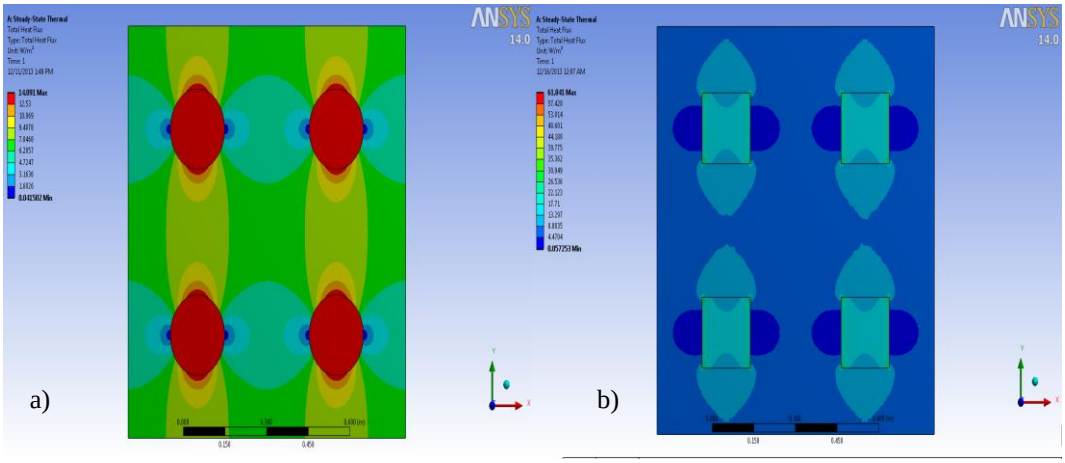

Figure D.2.33. Total heat flux distribution over 4-piece- a)circle and b)square -filler model for Ø=12%

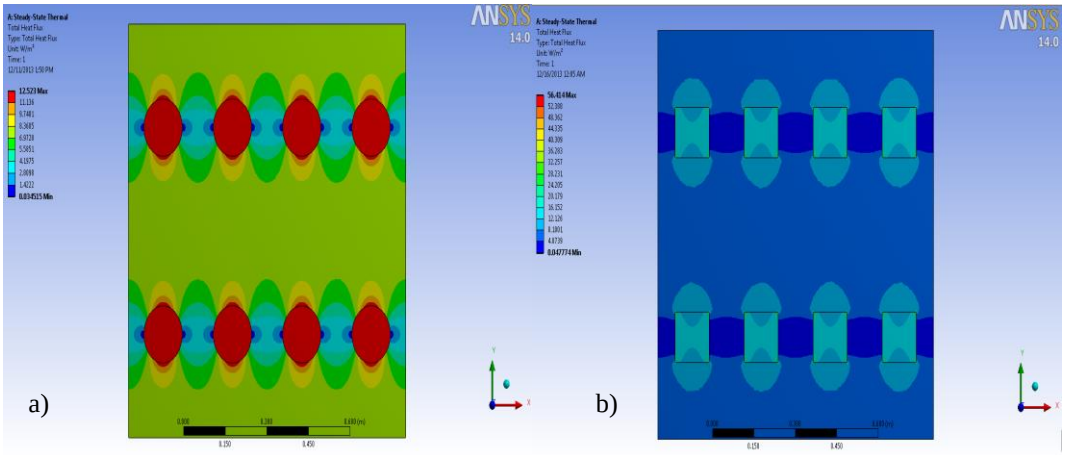

Figure D.2.34. Total heat flux distribution over 8-piece- a)circle and b)square -filler model for Ø=12%

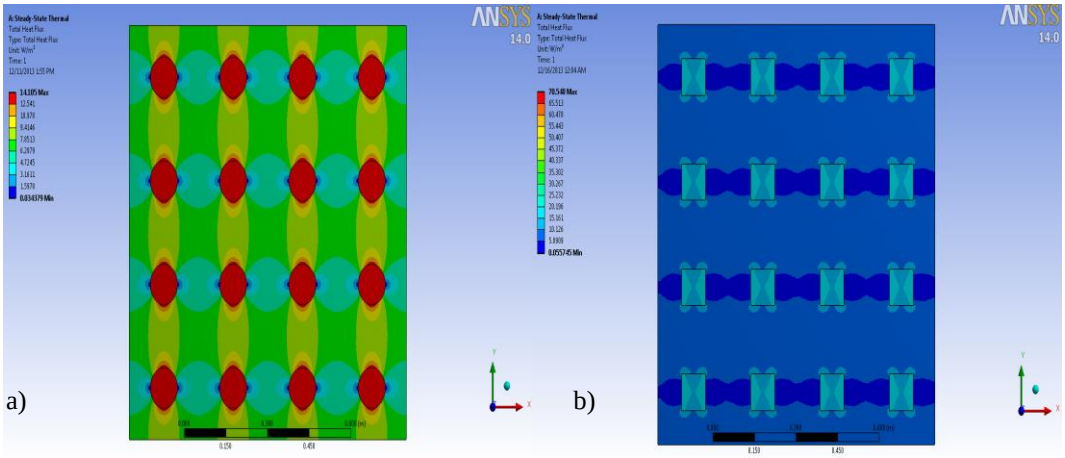

Figure D.2.35. Total heat flux distribution over 16-piece-a)circle and b)square-filler model for Ø=12%

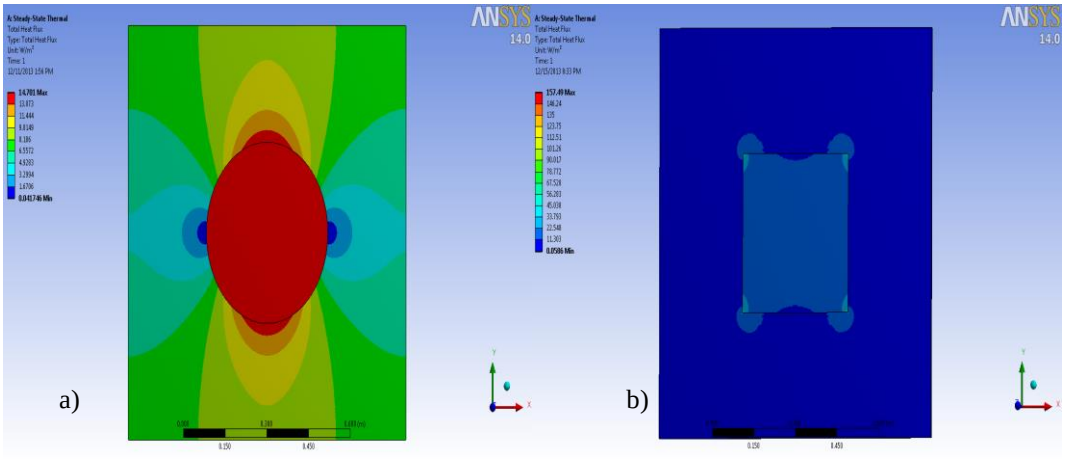

Figure D.2.36. Total heat flux distribution over 1-piece- a)circle and b)square -filler model for Ø=15%

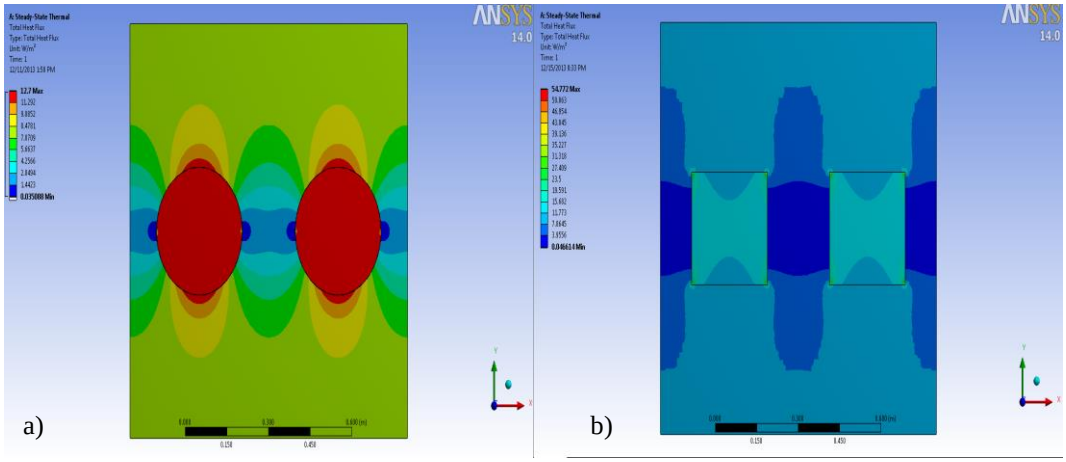

Figure D.2.37. Total heat flux distribution over 2-piece- a)circle and b)square -filler model for Ø=15%

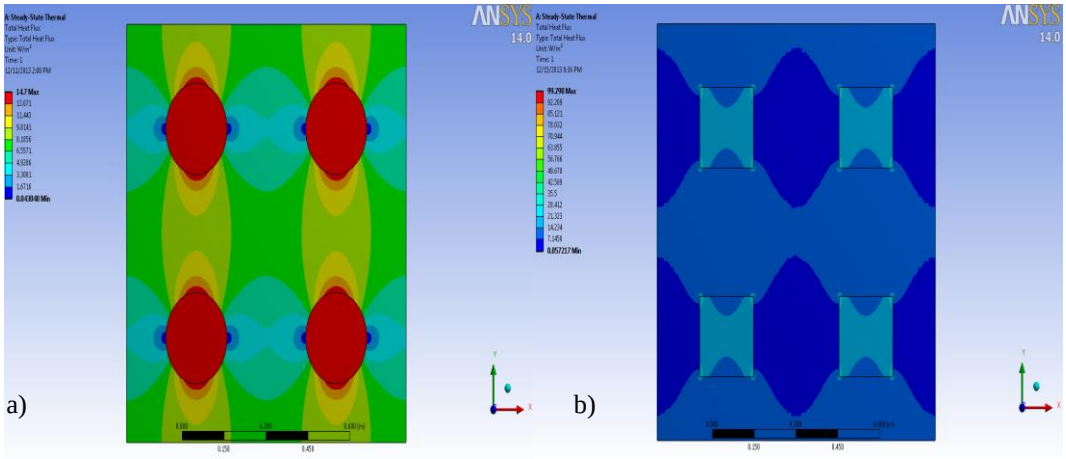

Figure D.2.38. Total heat flux distribution over 4-piece- a)circle and b)square -filler model for Ø=15%

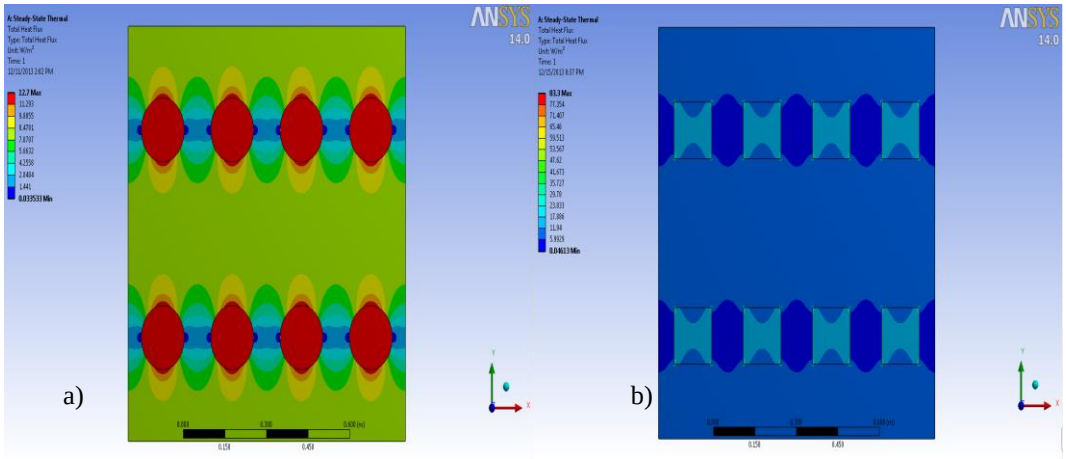

Figure D.2.39. Total heat flux distribution over 8-piece- a)circle and b)square -filler model for Ø=15%

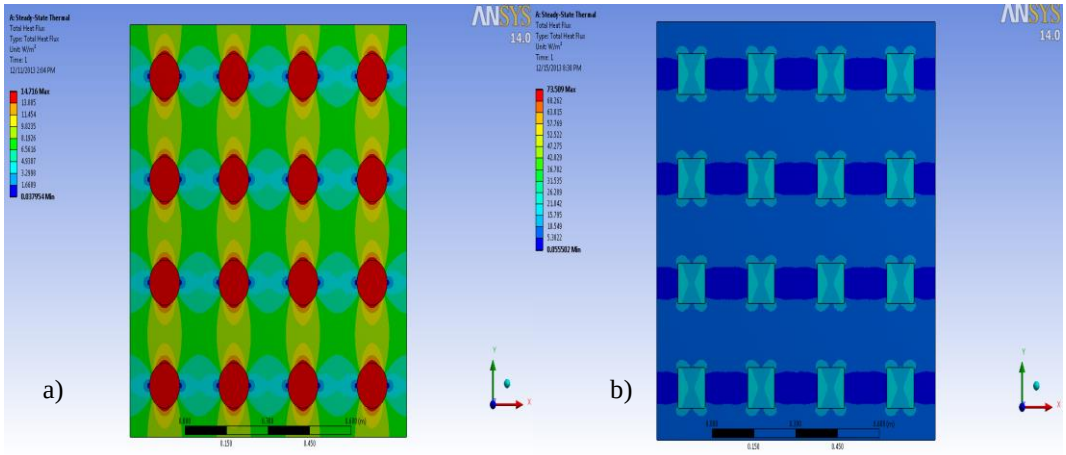

Figure D.2.40. Total heat flux distribution over 16-piece- a)circle andb)square-filler model for Ø=15%

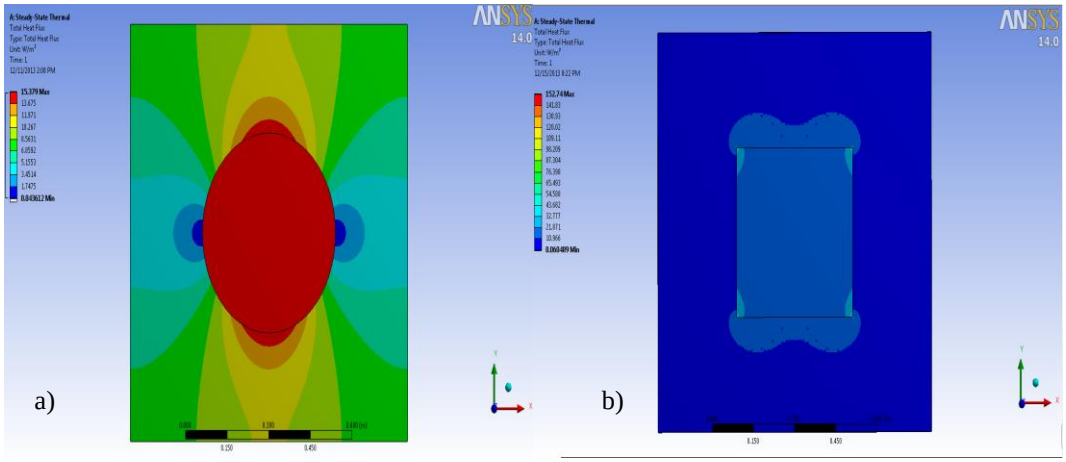

Figure D.2.41. Total heat flux distribution over 1-piece- a)circle and b)square -filler model for Ø=18%

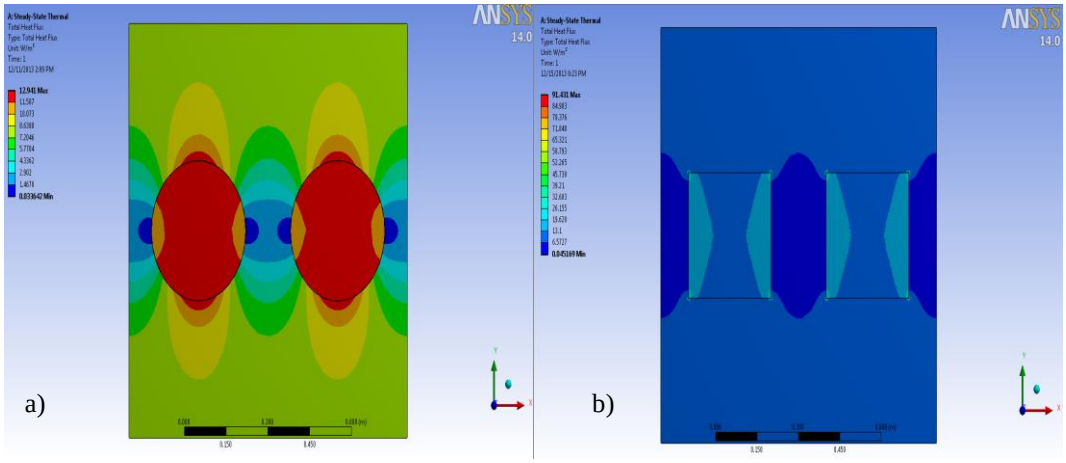

Figure D.2.42. Total heat flux distribution over 2-piece- a)circle and b)square -filler model for Ø=18%

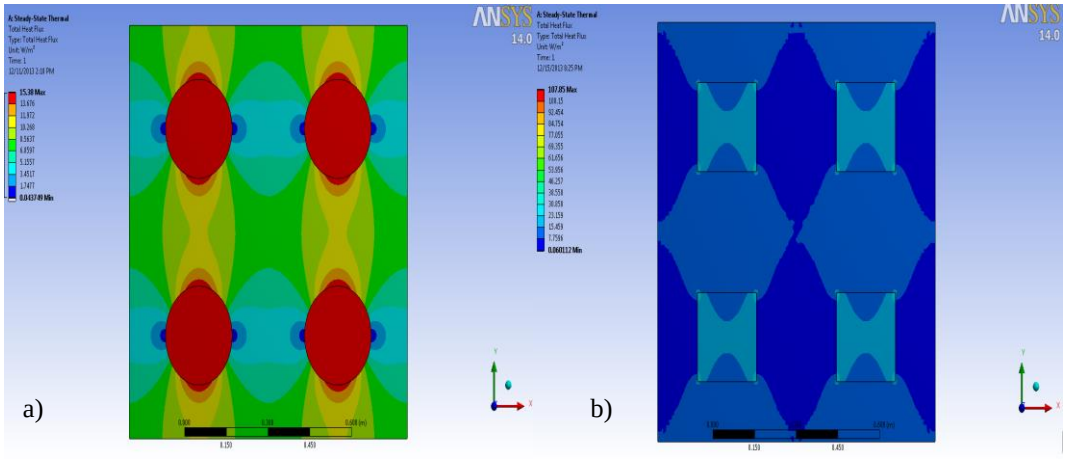

Figure D.2.43. Total heat flux distribution over 4-piece- a)circle and b)square -filler model for Ø=18%

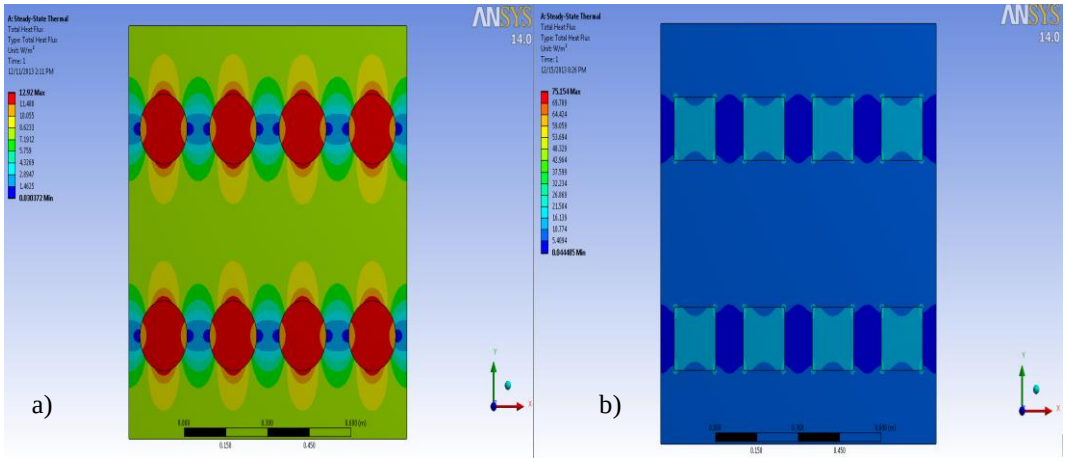

Figure D.2.44.Total heat flux distribution over 8-piece- a)circle and b)square -filler model for Ø=18%

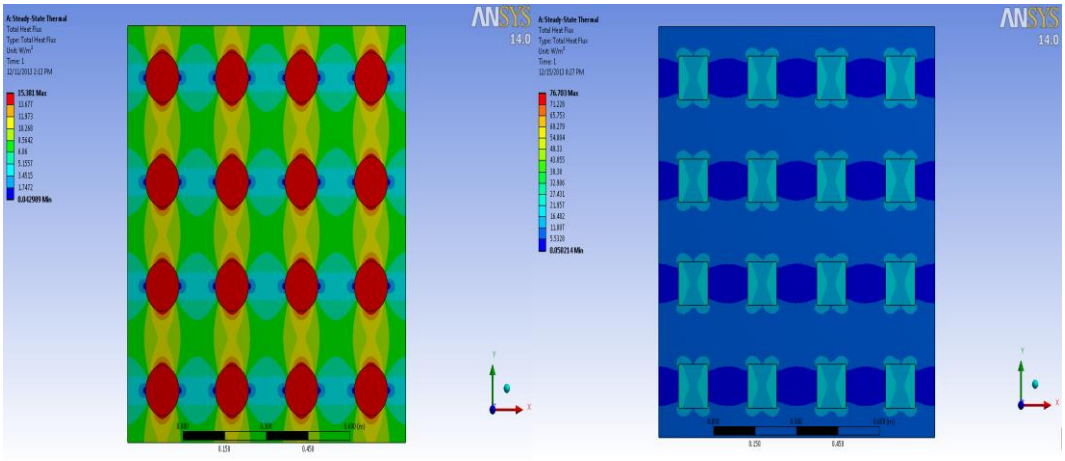

Figure D.2.45. Total heat flux distribution over 16-piece-a)circle andb)square -filler model for Ø=18%

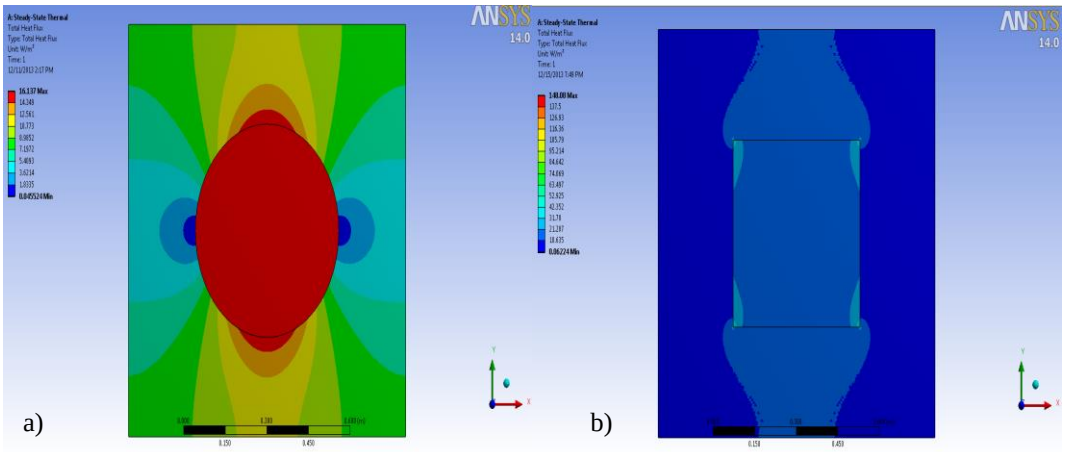

Figure D.2.46. Total heat flux distribution over 1-piece- a)circle and b)square -filler model for Ø=21%

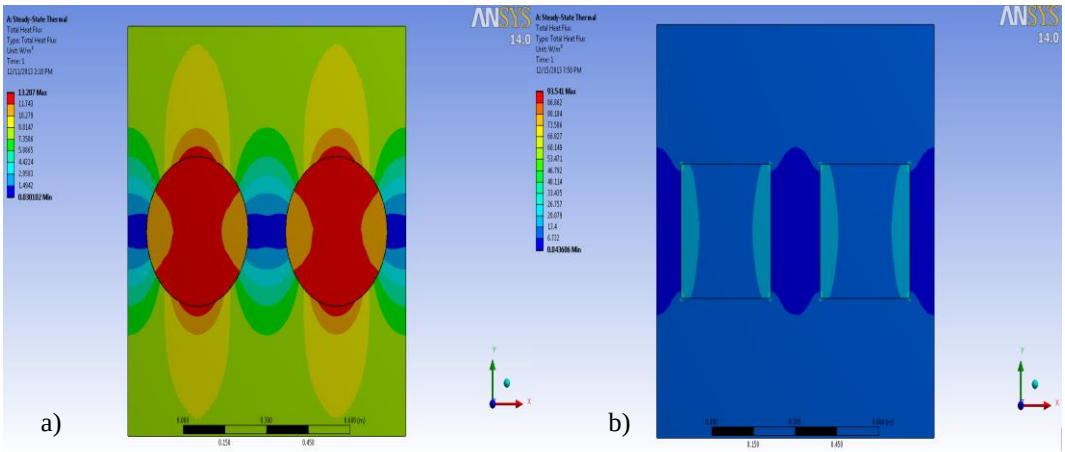

Figure D.2.47. Total heat flux distribution over 2-piece- a)circle and b)square -filler model for Ø=21%

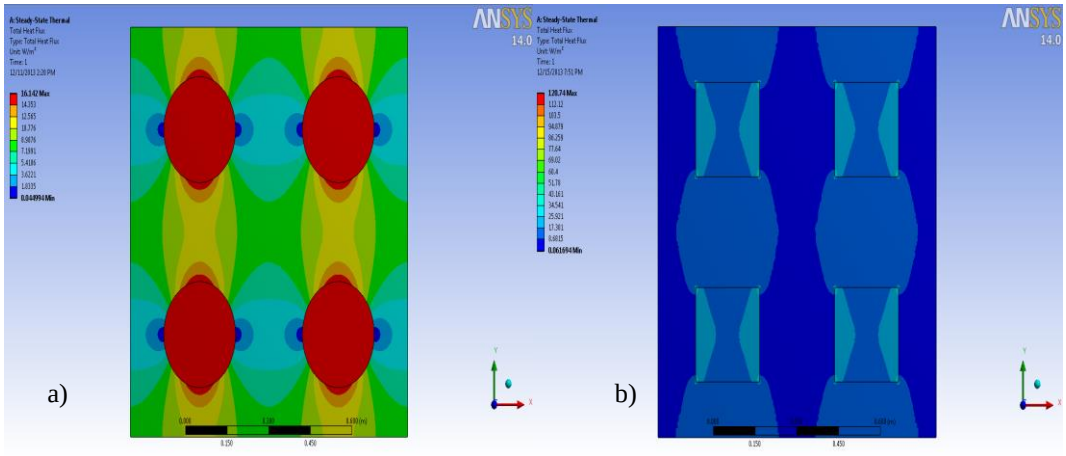

Figure D.2.48. Total heat flux distribution over 4-piece- a)circle and b)square -filler model for Ø=21%

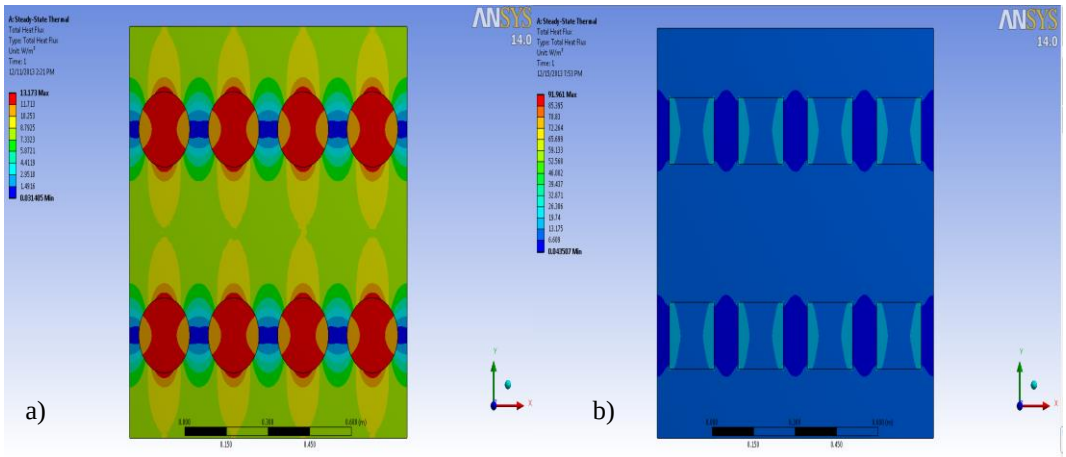

Figure D.2.49. Total heat flux distribution over 8-piece- a)circle and b)square -filler model for Ø=21%

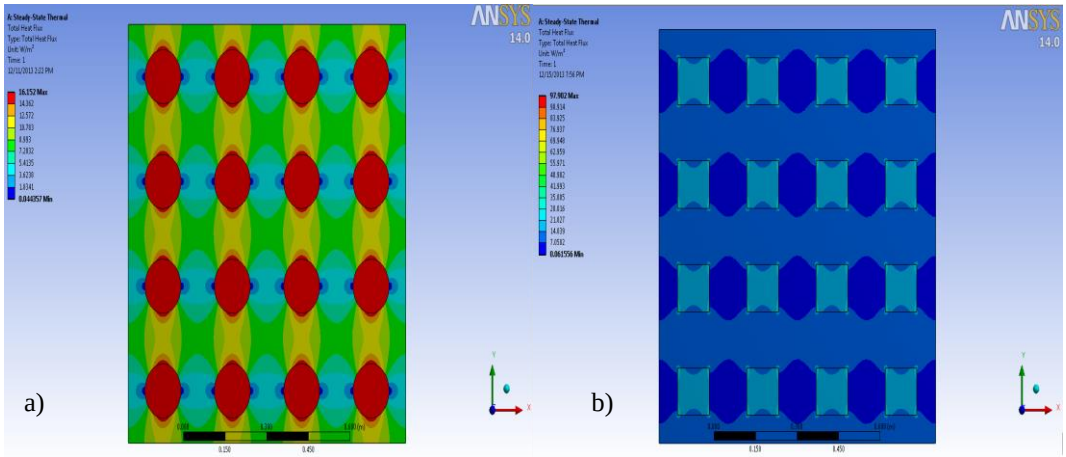

Figure D.2.50.Total heat flux distribution over 16-piece-a)circle and b)square -filler model for Ø=21%

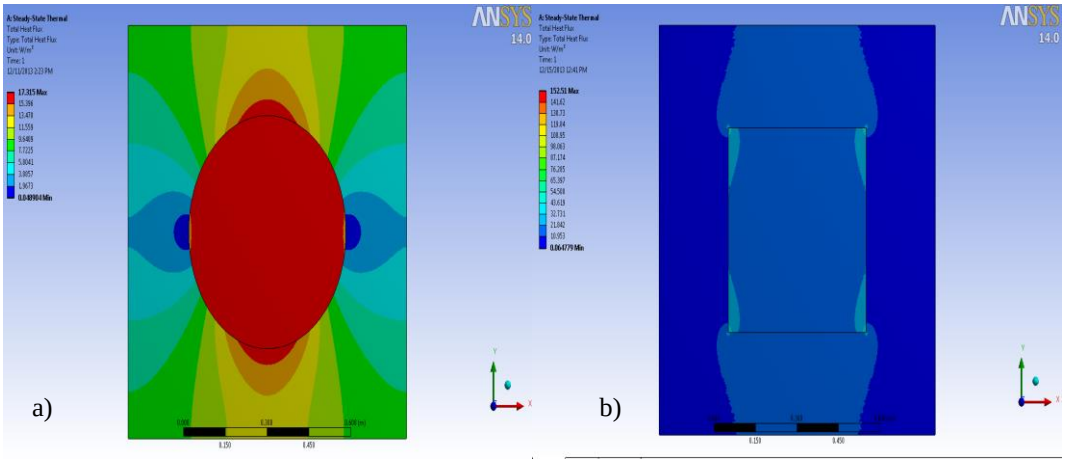

Figure D.2.51. Total heat flux distribution over 1-piece- a)circle and b)square -filler model for Ø=25%

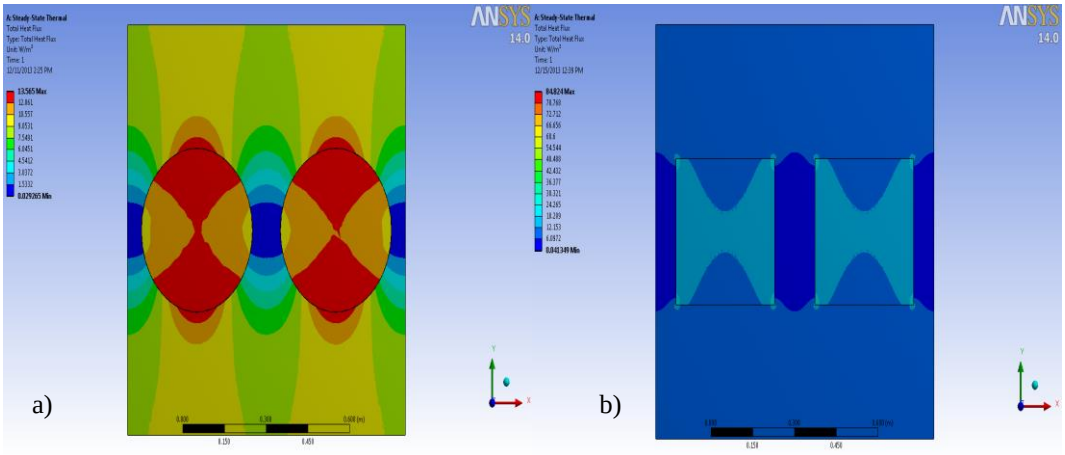

Figure D.2.52. Total heat flux distribution over 2-piece- a)circle and b)square -filler model for Ø=25%

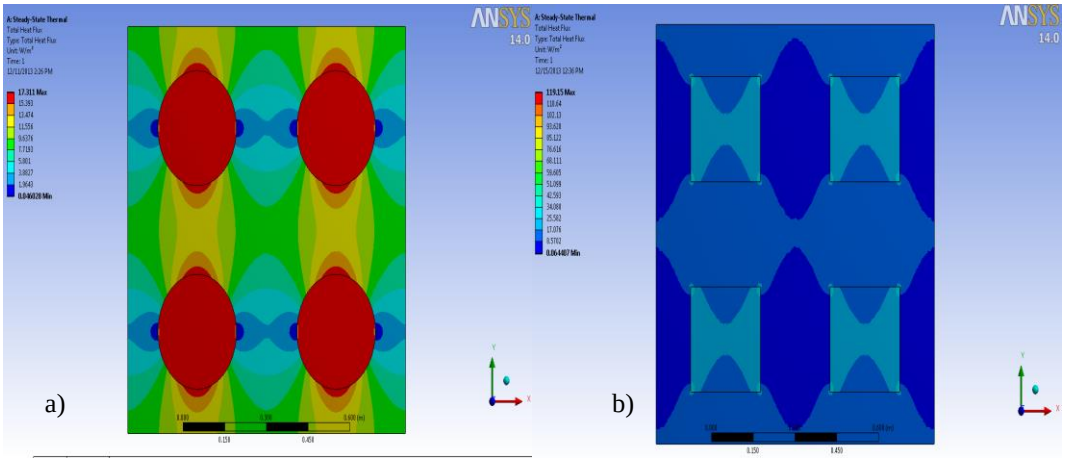

Figure D.2.53. Total heat flux distribution over 4-piece- a)circle and b)square -filler model for Ø=25%

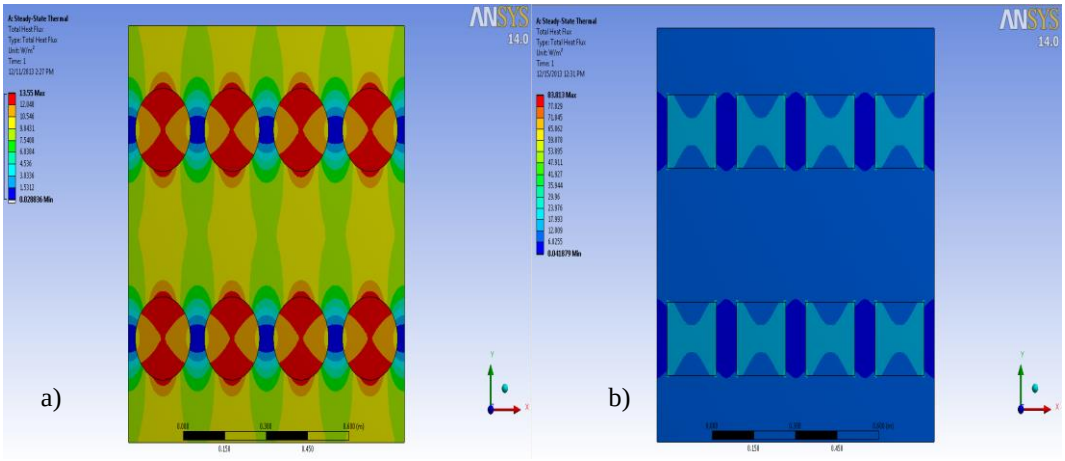

Figure D.2.54. Total heat flux distribution over 8-piece- a)circle and b)square -filler model for Ø=25%

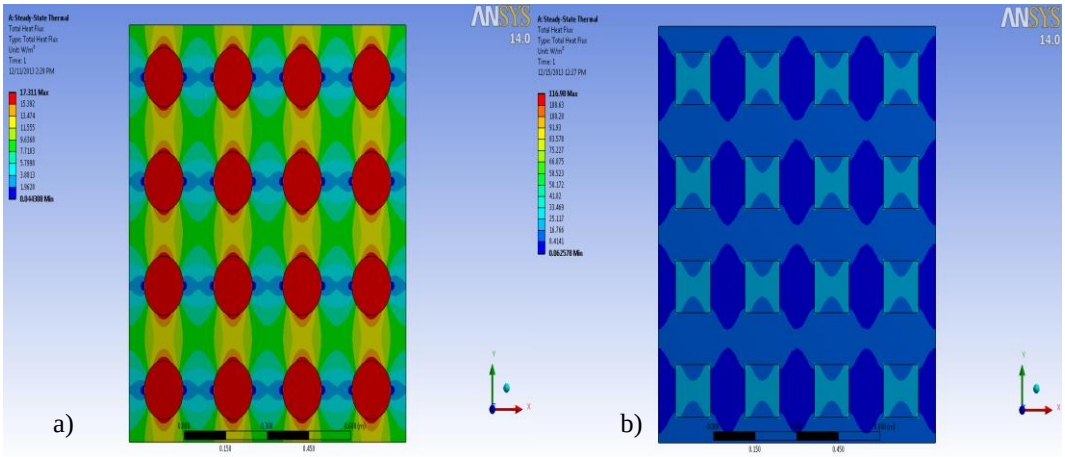

Figure D.2.55.Total heat flux distribution over 16-piece-a)circle and b)square -filler model for Ø=25%

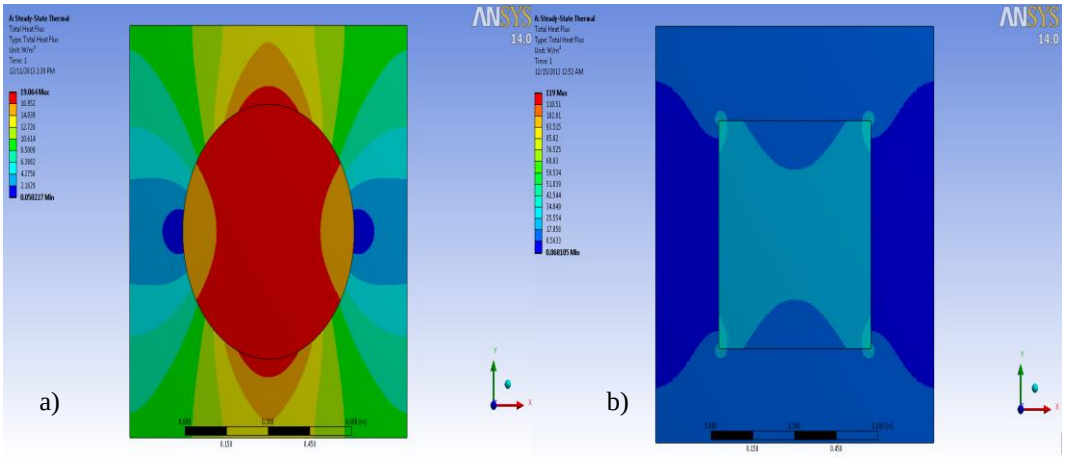

Figure D.2.56. Total heat flux distribution over 1-piece- a)circle and b)square -filler model for Ø=30%

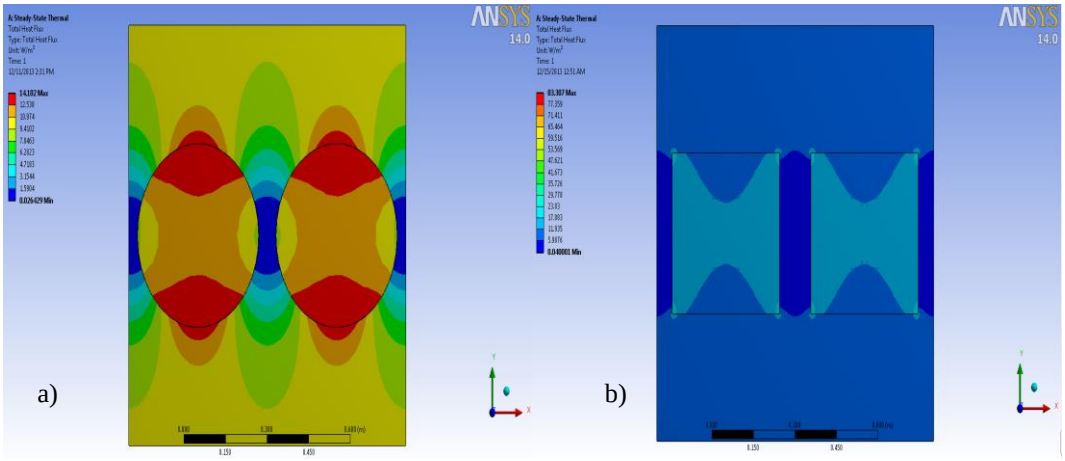

Figure D.2.57. Total heat flux distribution over 2-piece- a)circle and b)square -filler model for Ø=30%

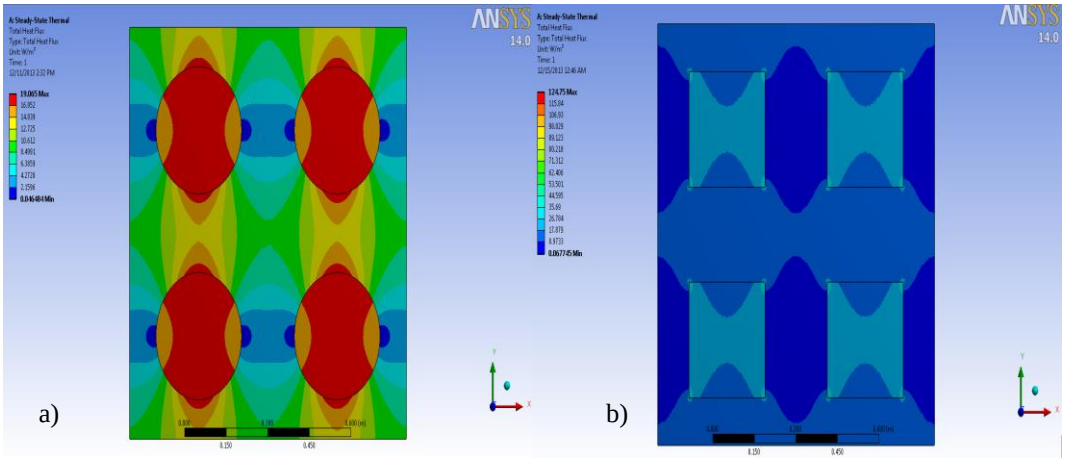

Figure D.2.58. Total heat flux distribution over 4-piece- a)circle and b)square -filler model for Ø=30%

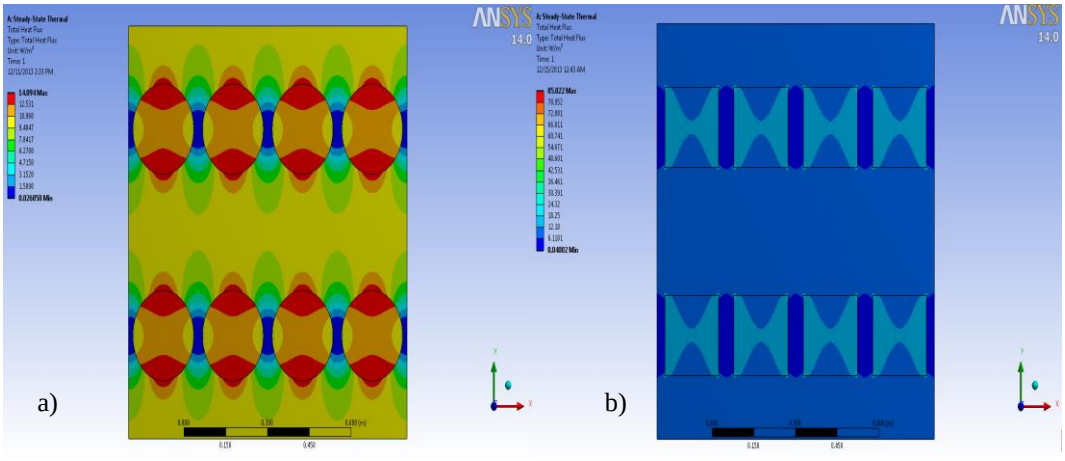

Figure D.2.59. Total heat flux distribution over 8-piece- a)circle and b)square -filler model for Ø=30%

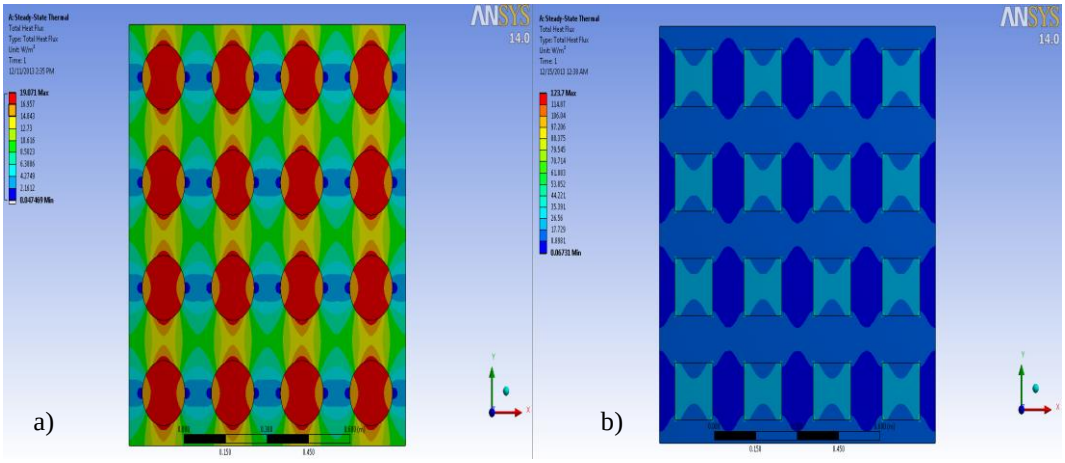

Figure D.2.60.Total heat flux distribution over 16-piece- a)circle and b)square-filler model for Ø=30%

Appendix E

3-D THERMAL ANALYSİS

E.1 Temperature Distribution Results

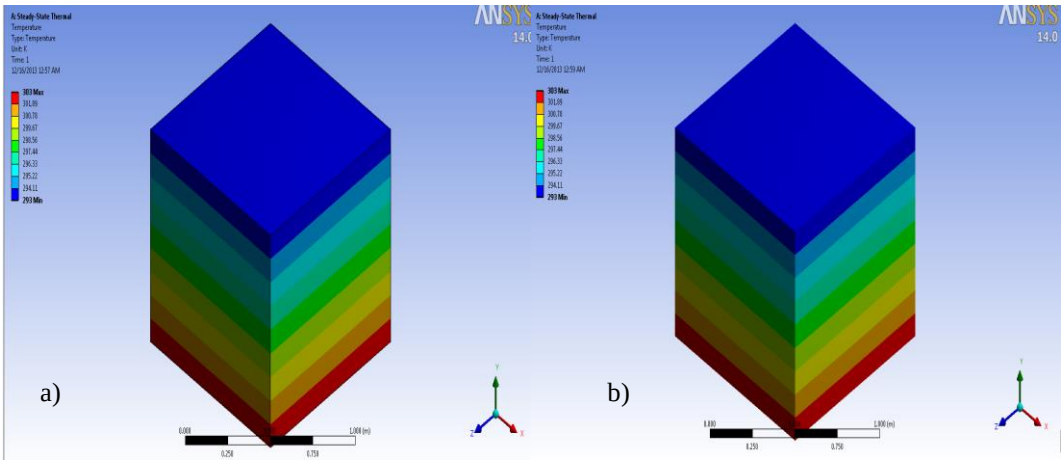

Figure E.1.1. Temperature distribution over 1-piece- a)shpere and b)cube -filler model for Ø=1%

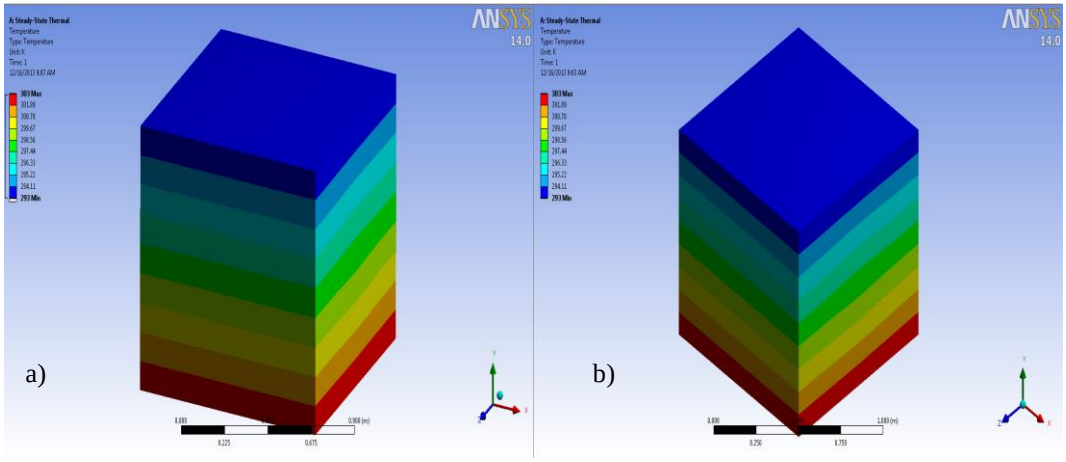

Figure E.1.2. Temperature distribution over 2-piece- a)shpere and b)cube -filler model for Ø=1%

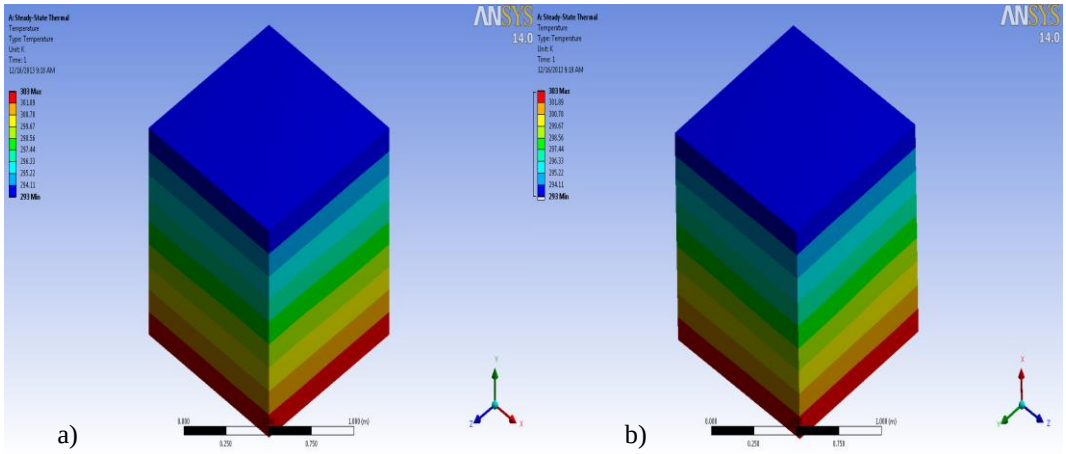

Figure E.1.3. Temperature distribution over 4-piece- a)shpere and b)cube -filler model for Ø=1%

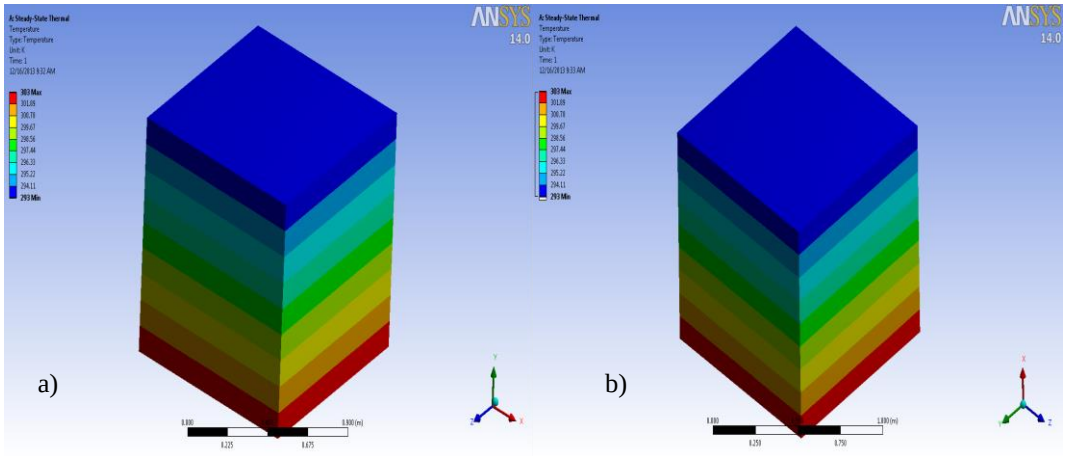

Figure E.1.4. Temperature distribution over 8-piece- a)shpere and b)cube -filler model for Ø=1%

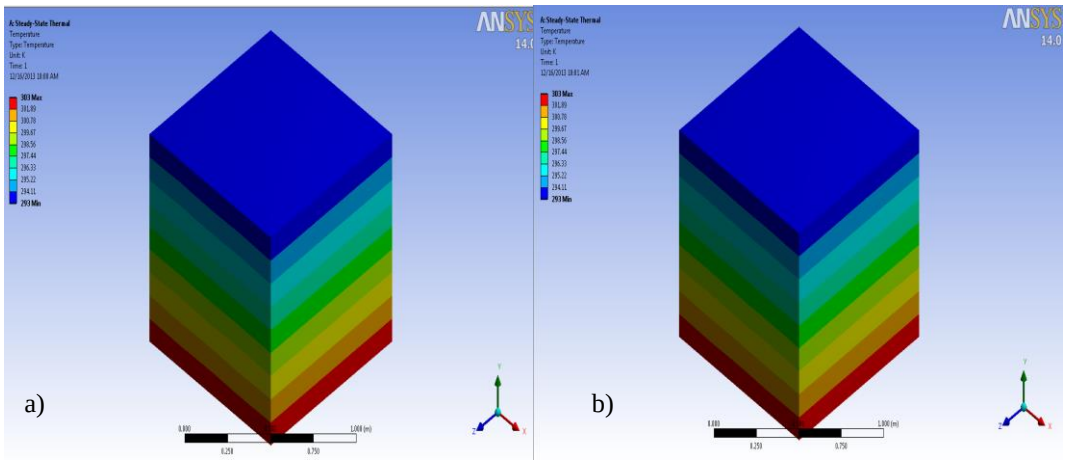

Figure E.1.5. Temperature distribution over 16-piece- a)shpere and b)cube -filler model for Ø=1%

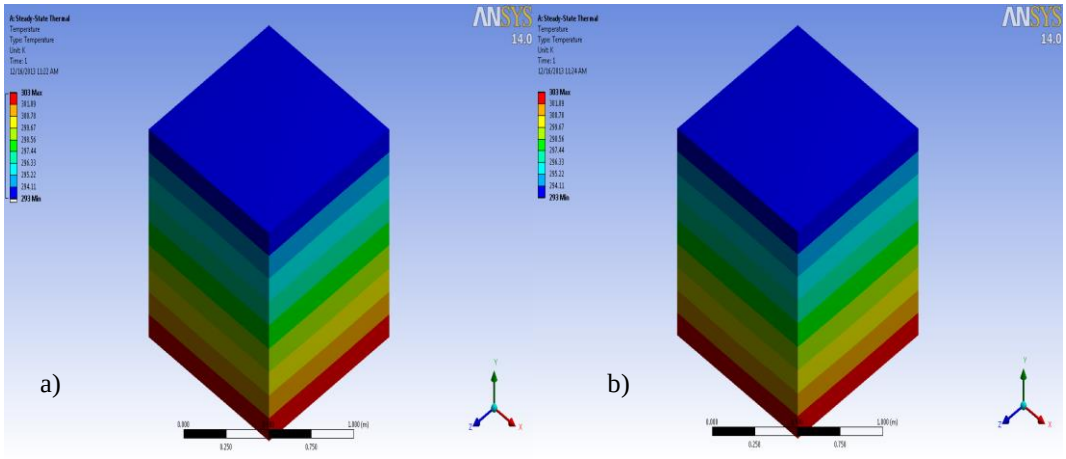

Figure E.1.6. Temperature distribution over 1-piece- a)shpere and b)cube -filler model for Ø=2%

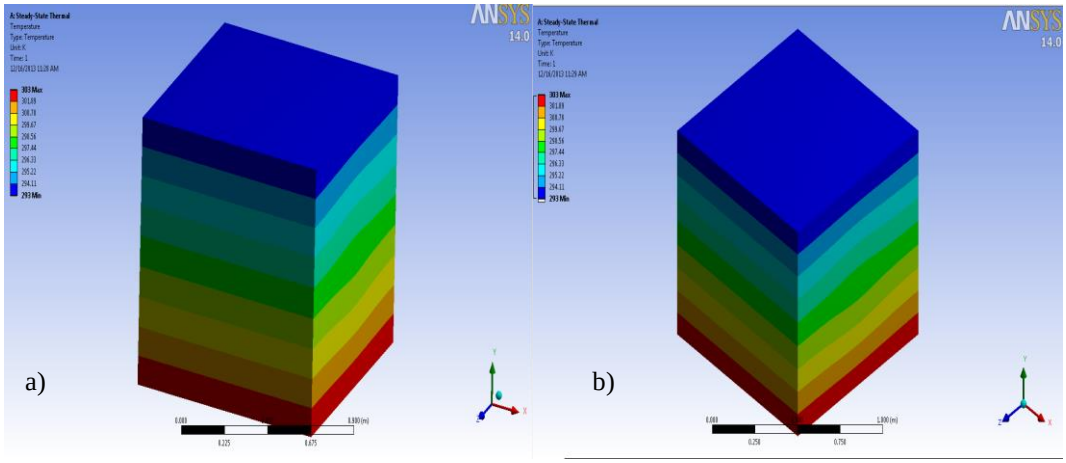

Figure E.1.7. Temperature distribution over 2-piece- a)shpere and b)cube -filler model for Ø=2%

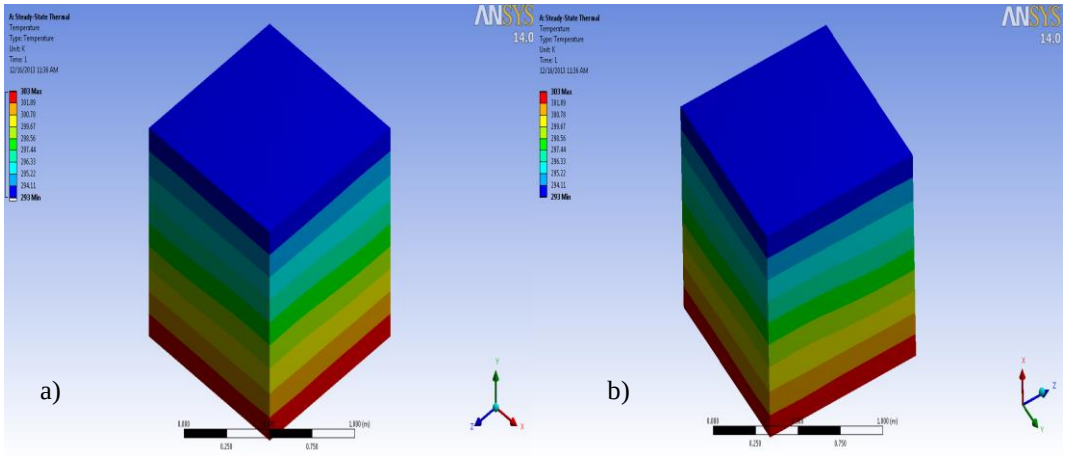

Figure E.1.8. Temperature distribution over 4-piece- a)shpere and b)cube -filler model for Ø=2%

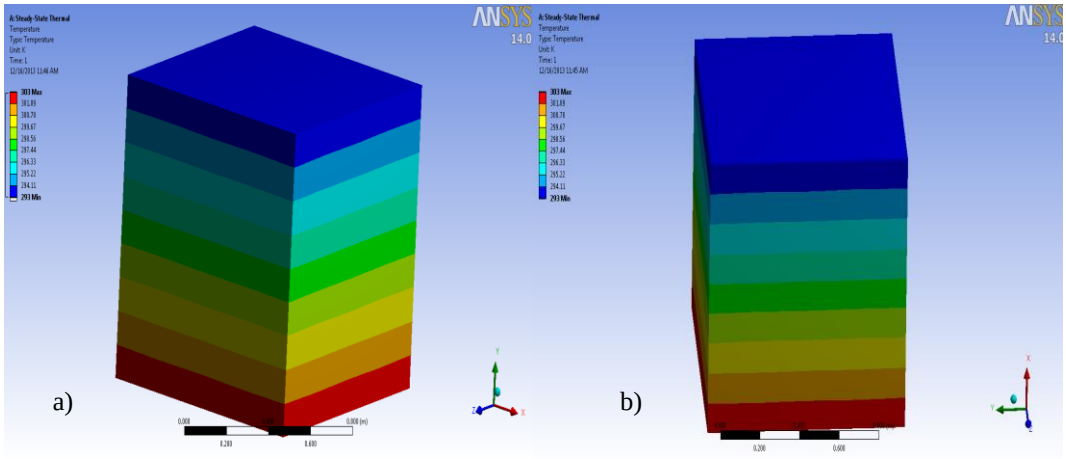

Figure E.1.9. Temperature distribution over 8-piece- a)shpere and b)cube -filler model for Ø=2%

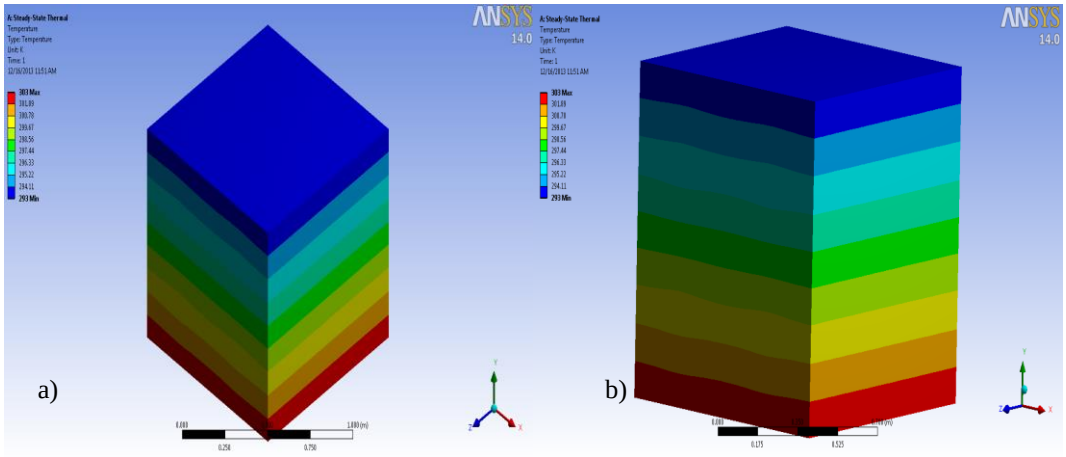

Figure E.1.10. Temperature distribution over 16-piece- a)shpere and b)cube -filler model for Ø=2%

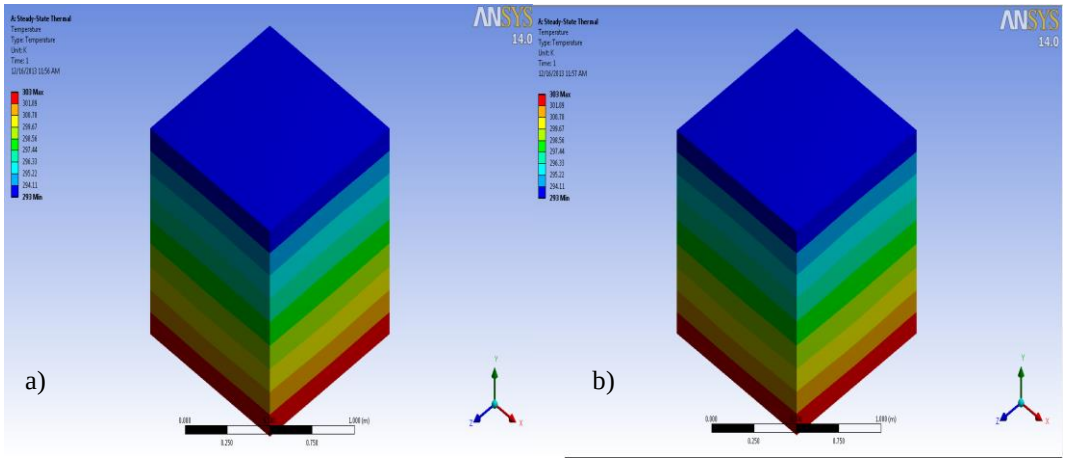

Figure E.1.11. Temperature distribution over 1-piece- a)shpere and b)cube -filler model for Ø=4%

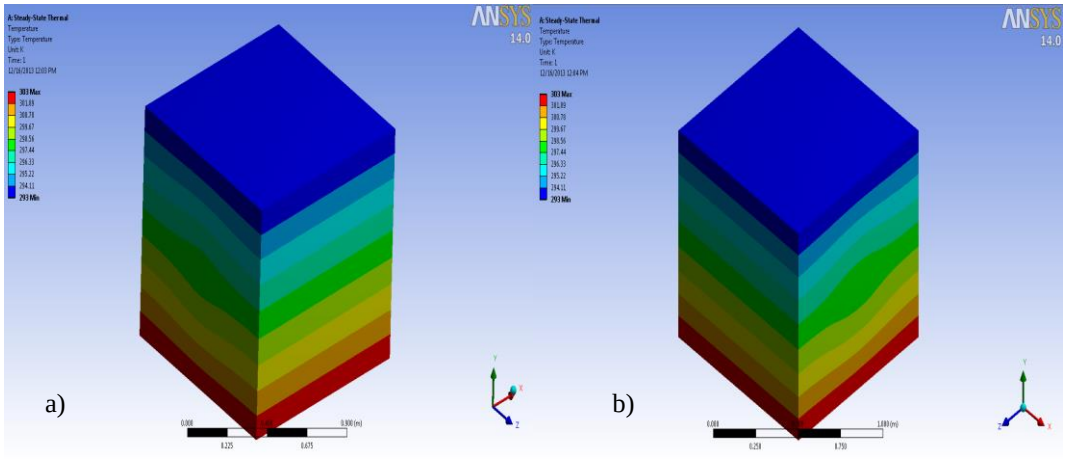

Figure E.1.12. Temperature distribution over 2-piece- a)shpere and b)cube -filler model for Ø=4%

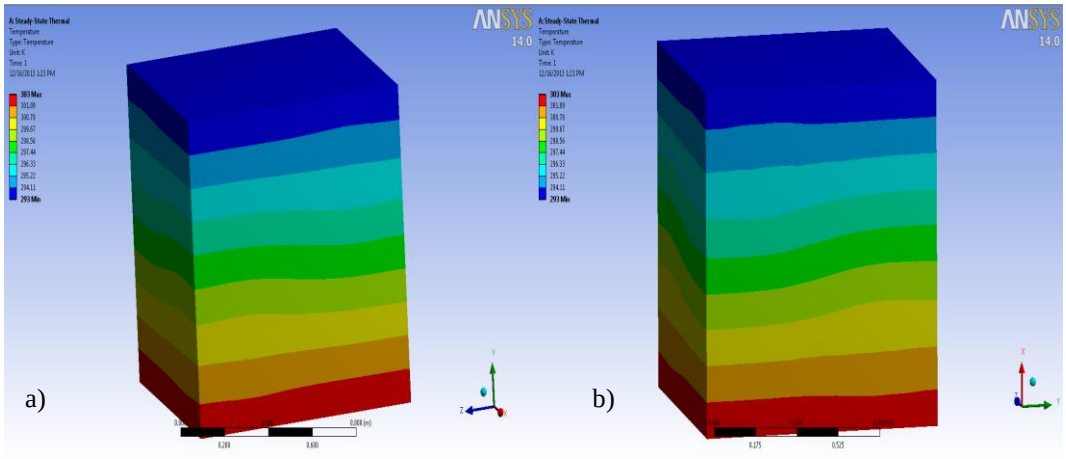

Figure E.1.13. Temperature distribution over 4-piece- a)shpere and b)cube -filler model for Ø=4%

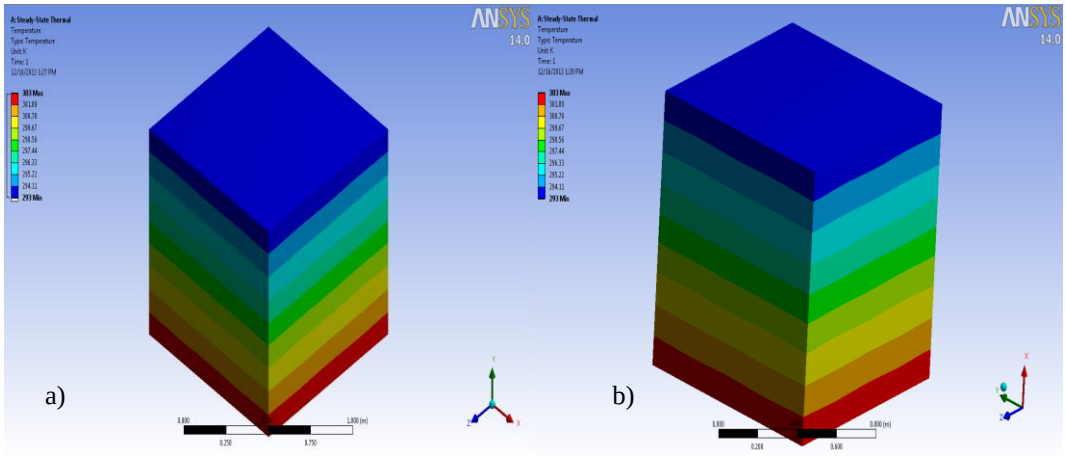

Figure E.1.14. Temperature distribution over 8-piece- a)shpere and b)cube -filler model for Ø=4%

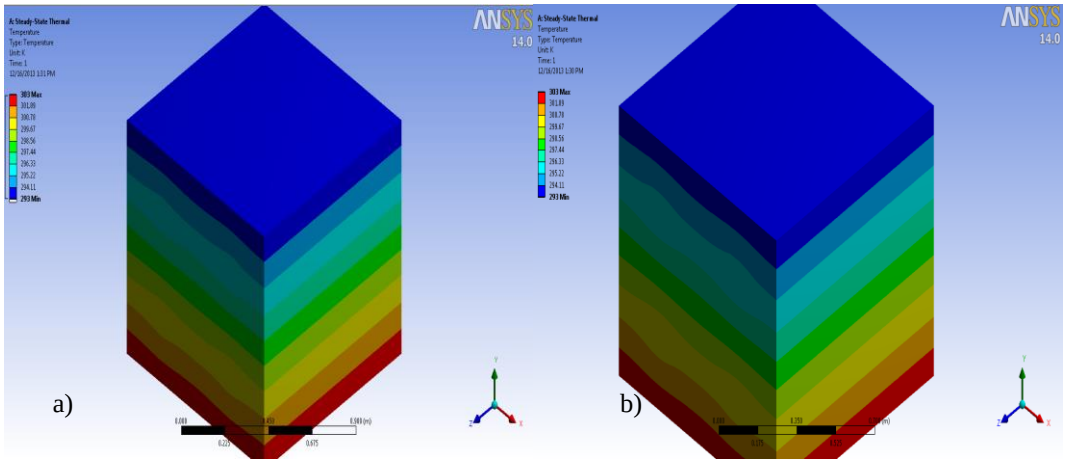

Figure E.1.15. Temperature distribution over 16-piece- a)shpere and b)cube -filler model for Ø=4%

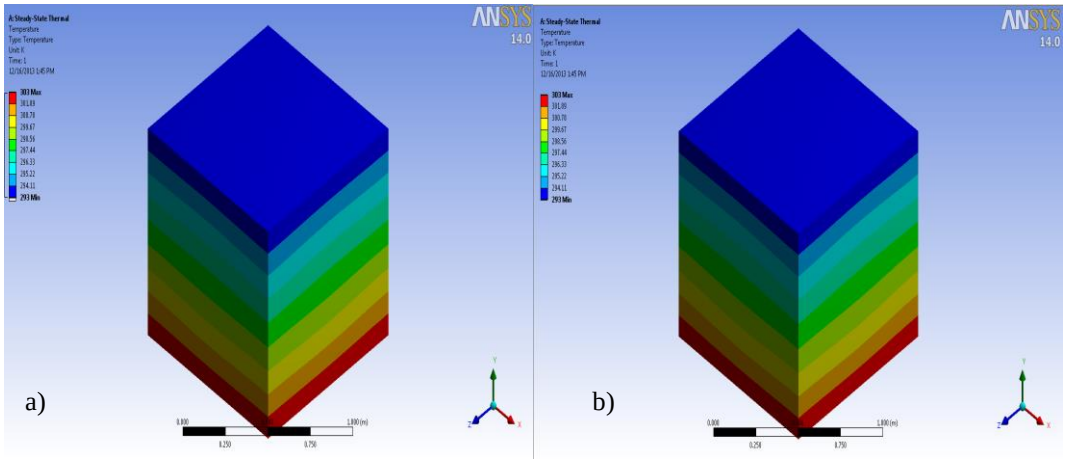

Figure E.1.16. Temperature distribution over 1-piece- a)shpere and b)cube -filler model for Ø=6%

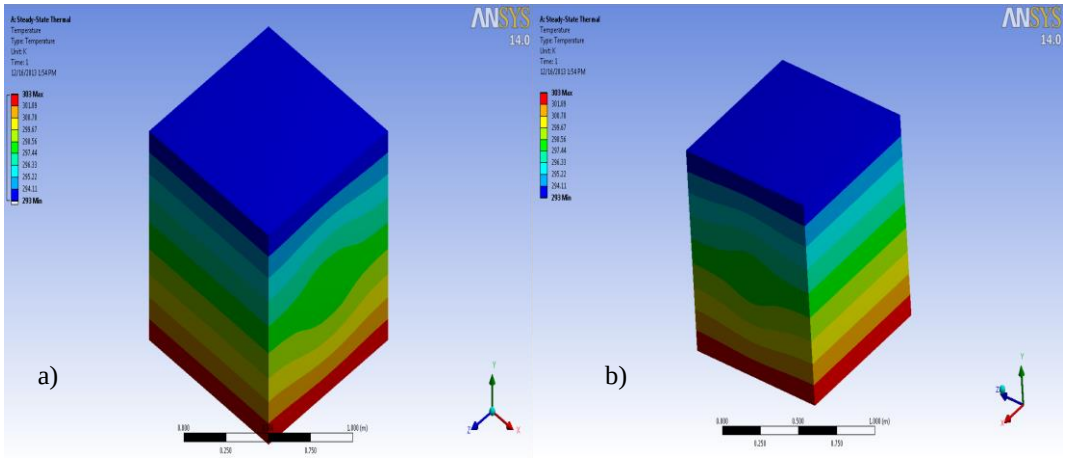

Figure E.1.17. Temperature distribution over 2-piece- a)shpere and b)cube -filler model for Ø=6%

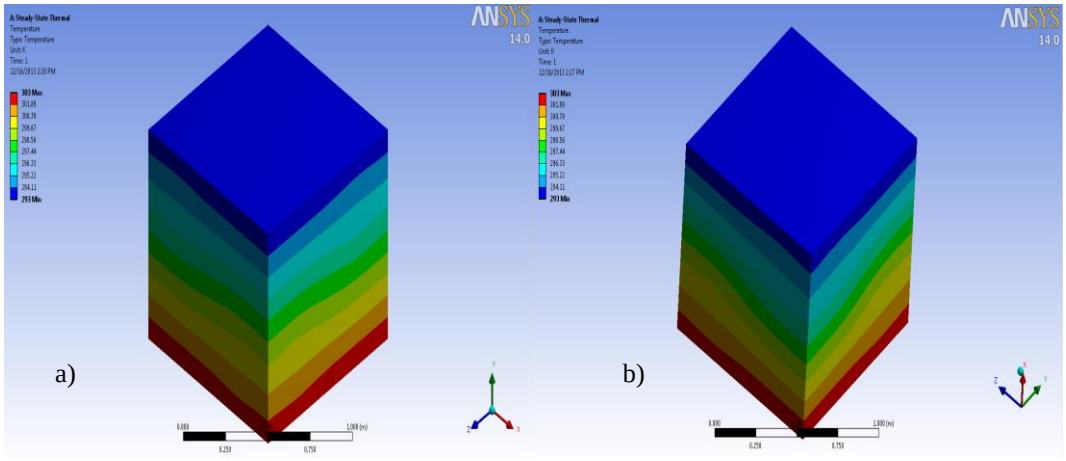

Figure E.1.18. Temperature distribution over 4-piece- a)shpere and b)cube -filler model for Ø=6%

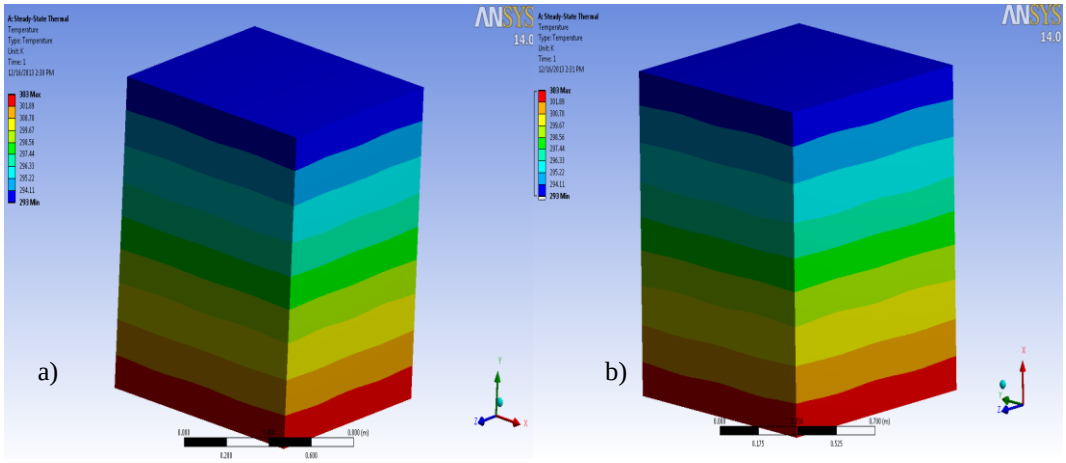

Figure E.1.19. Temperature distribution over 8-piece- a)shpere and b)cube -filler model for Ø=6%

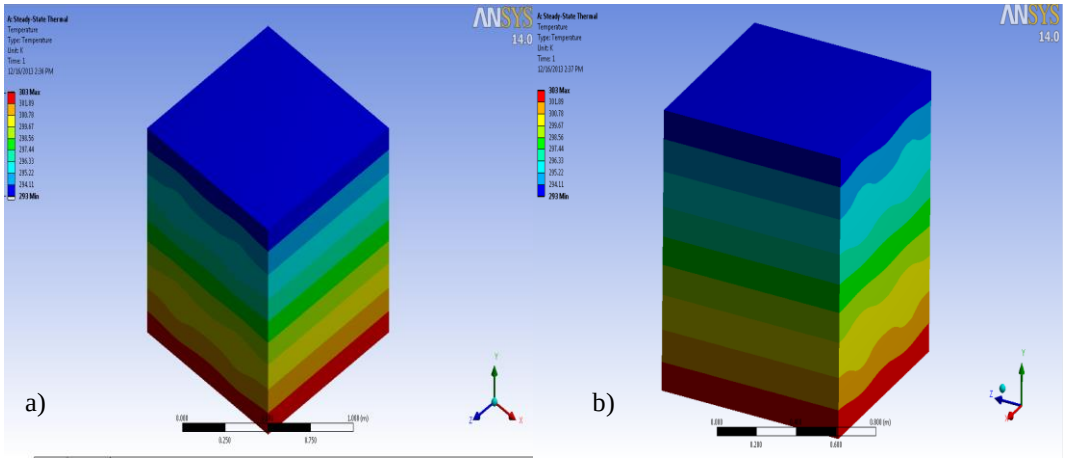

Figure E.1.20. Temperature distribution over 16-piece- a)shpere and b)cube -filler model for Ø=6%

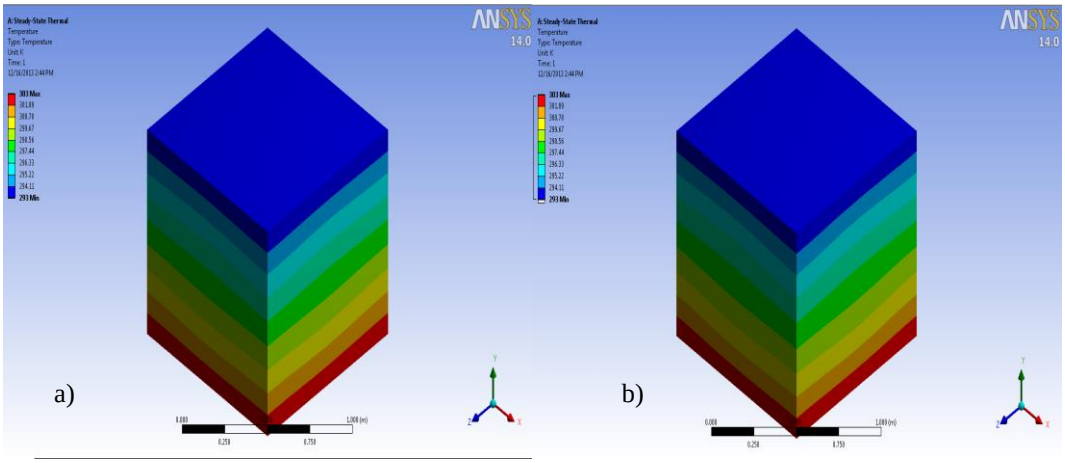

Figure E.1.21. Temperature distribution over 1-piece- a)shpere and b)cube -filler model for Ø=8%

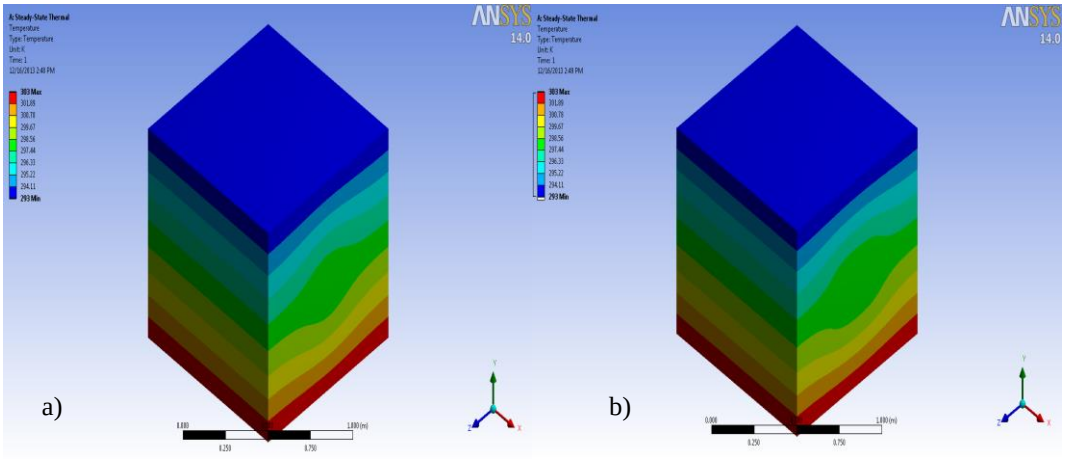

Figure E.1.22. Temperature distribution over 2-piece- a)shpere and b)cube -filler model for Ø=8%

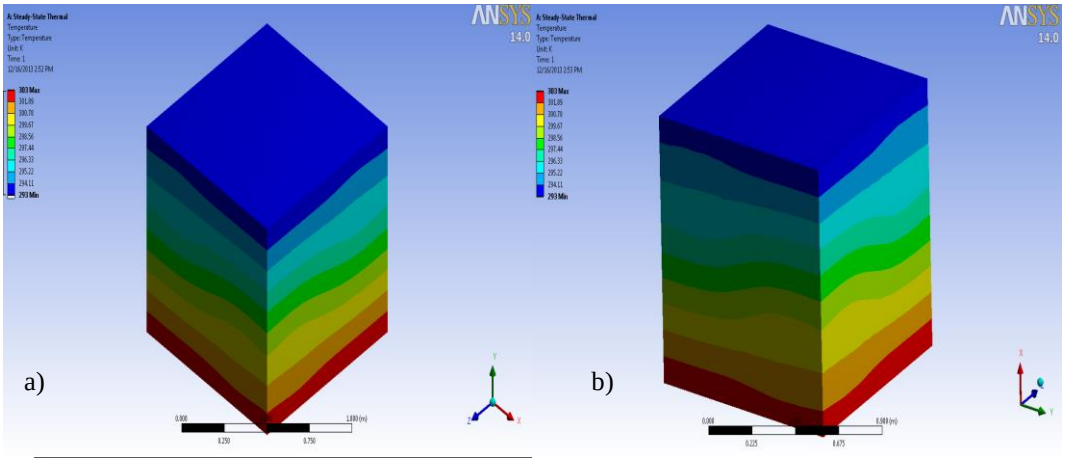

Figure E.1.23. Temperature distribution over 4-piece- a)shpere and b)cube -filler model for Ø=8%

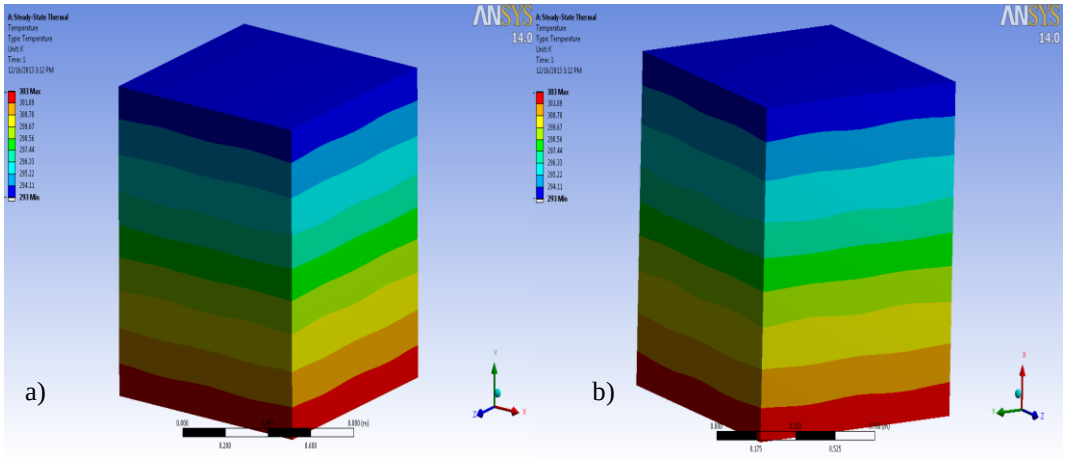

Figure E.1.24. Temperature distribution over8-piece- a)shpere and b)cube -filler model for Ø=8%

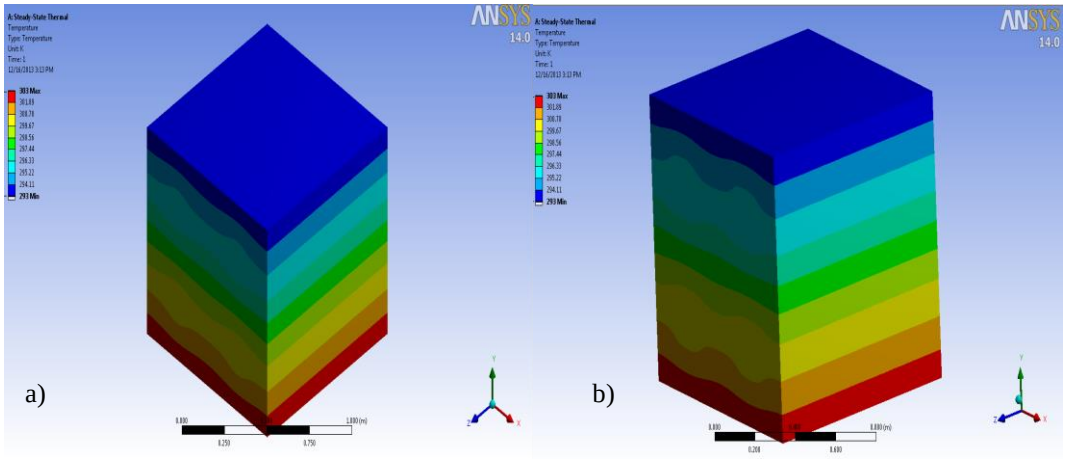

Figure E.1.25. Temperature distribution over 16-piece- a)shpere and b)cube -filler model for Ø=8%

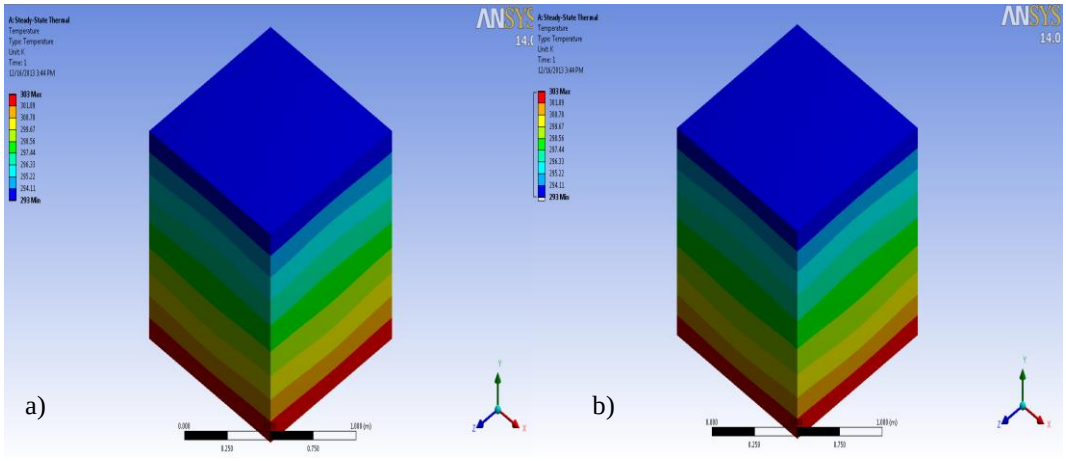

Figure E.1.26. Temperature distribution over 1-piece- a)shpere and b)cube -filler model for Ø=10%

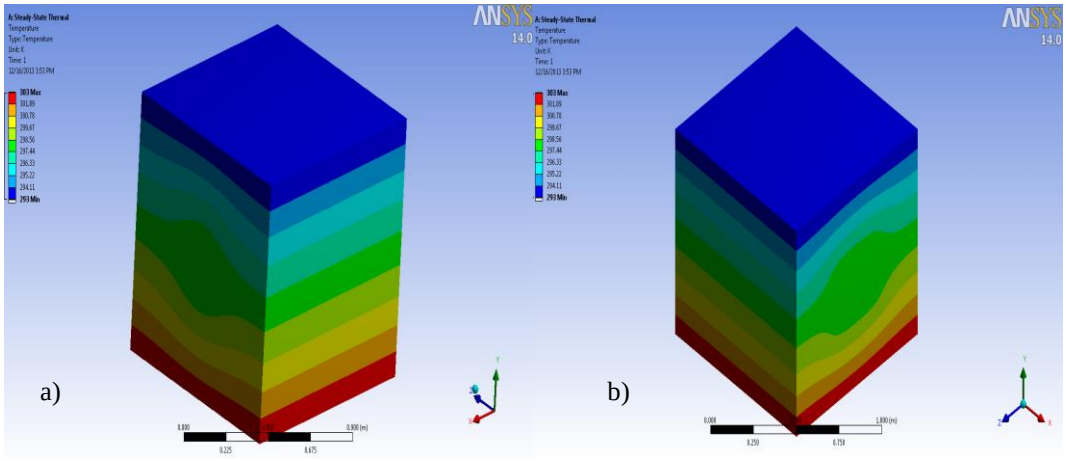

Figure E.1.27. Temperature distribution over 2-piece- a)shpere and b)cube -filler model for Ø=10%

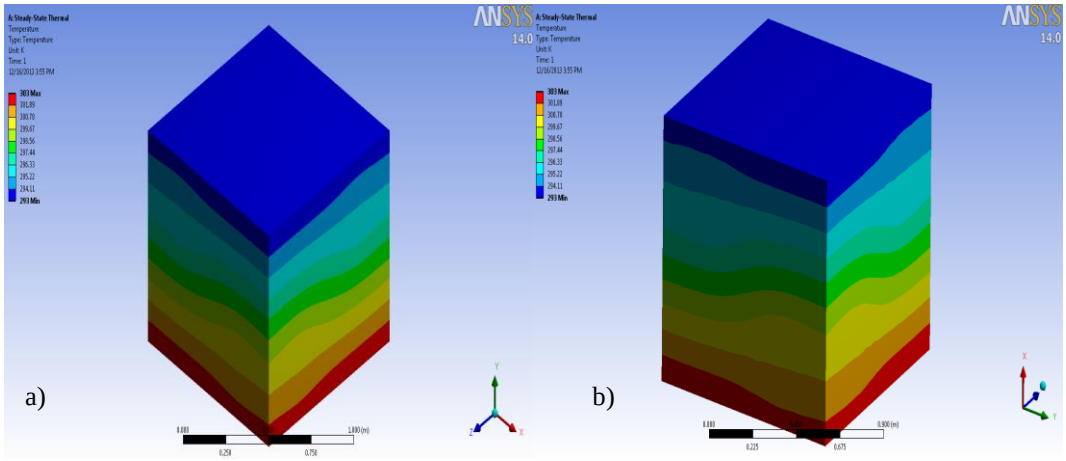

Figure E.1.28. Temperature distribution over 4-piece- a)shpere and b)cube -filler model for Ø=10%

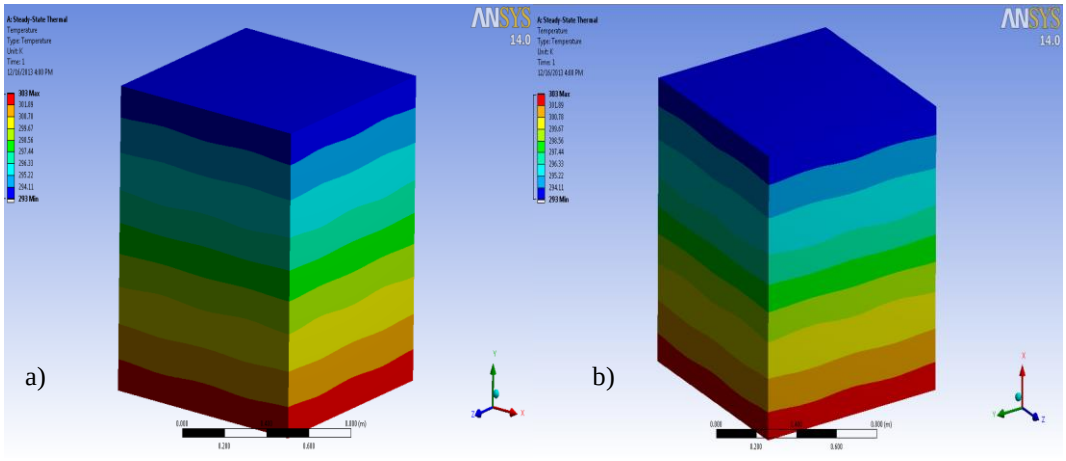

Figure E.1.29. Temperature distribution over 8-piece- a)shpere and b)cube -filler model for Ø=10%

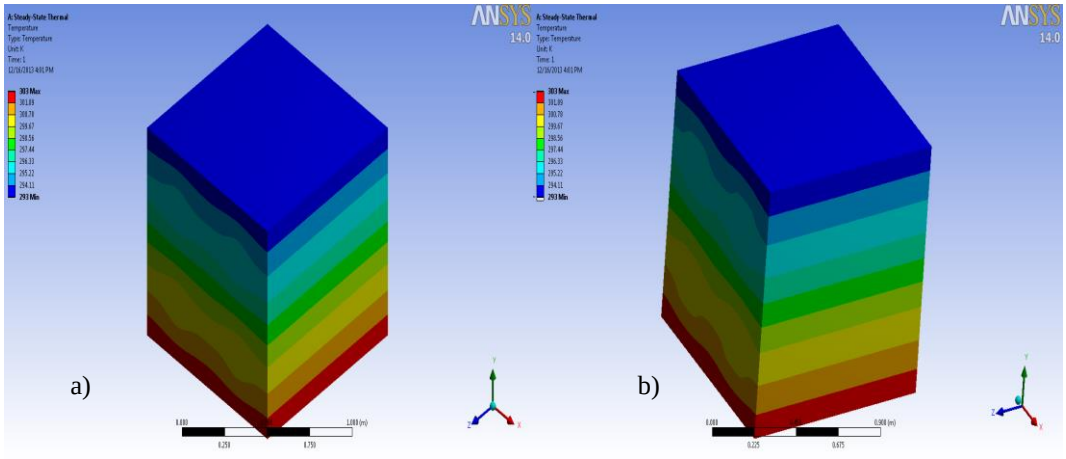

Figure E.1.30. Temperature distribution over 16-piece- a)shpere and b)cube -filler model for Ø=10%

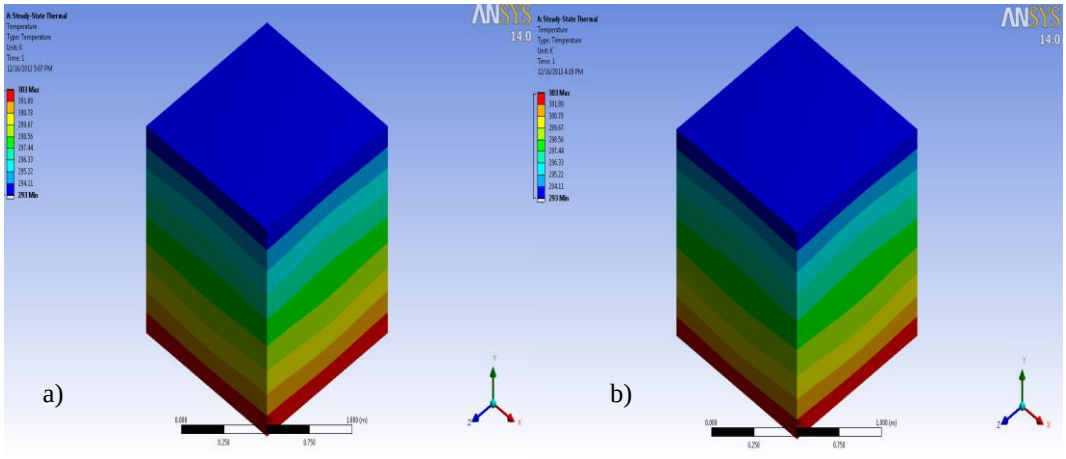

Figure E.1.31. Temperature distribution over 1-piece- a)shpere and b)cube -filler model for Ø=12%

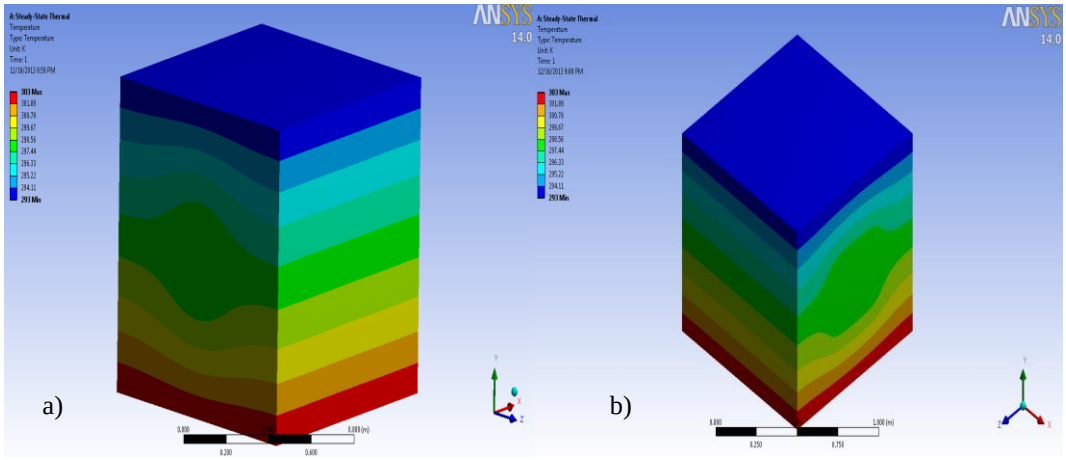

Figure E.1.32. Temperature distribution over 2-piece- a)shpere and b)cube -filler model for Ø=12%

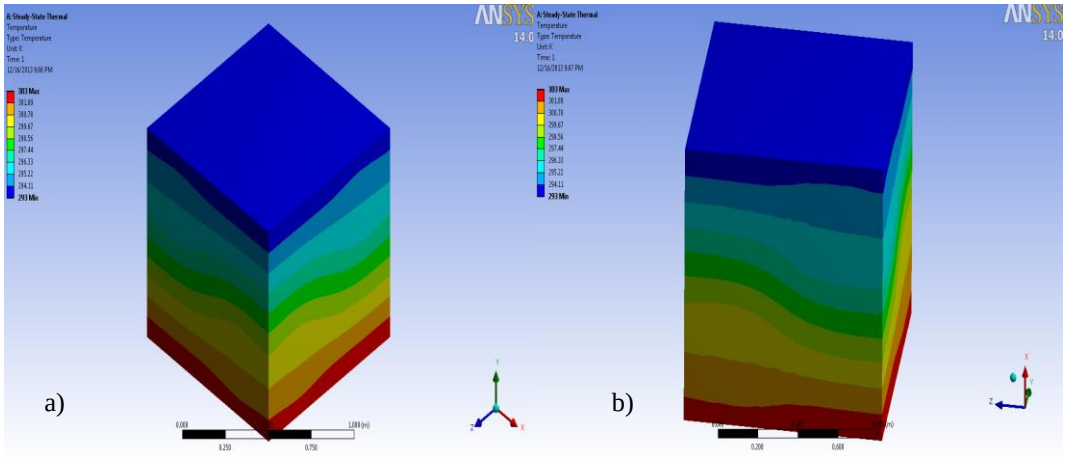

Figure E.1.33. Temperature distribution over 4-piece- a)shpere and b)cube -filler model for Ø=12%

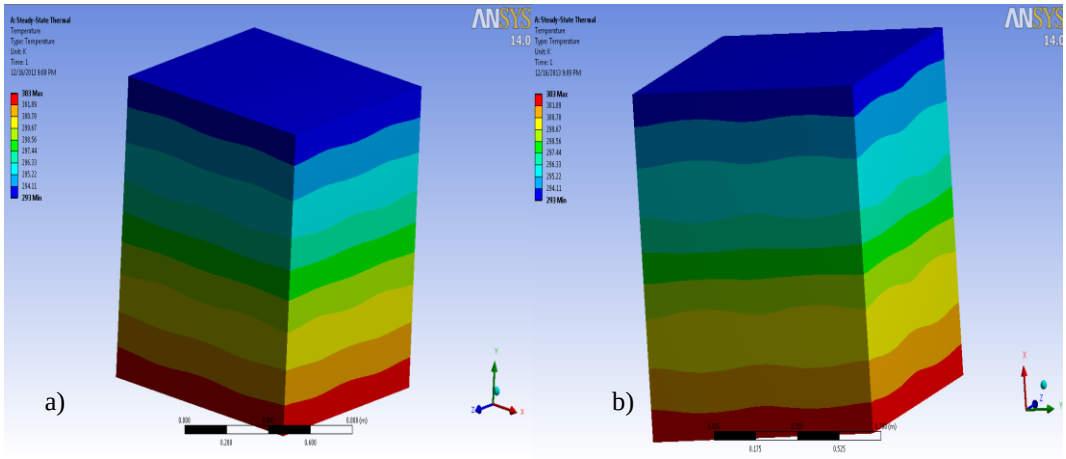

Figure E.1.34. Temperature distribution over 8-piece- a)shpere and b)cube -filler model for Ø=12%

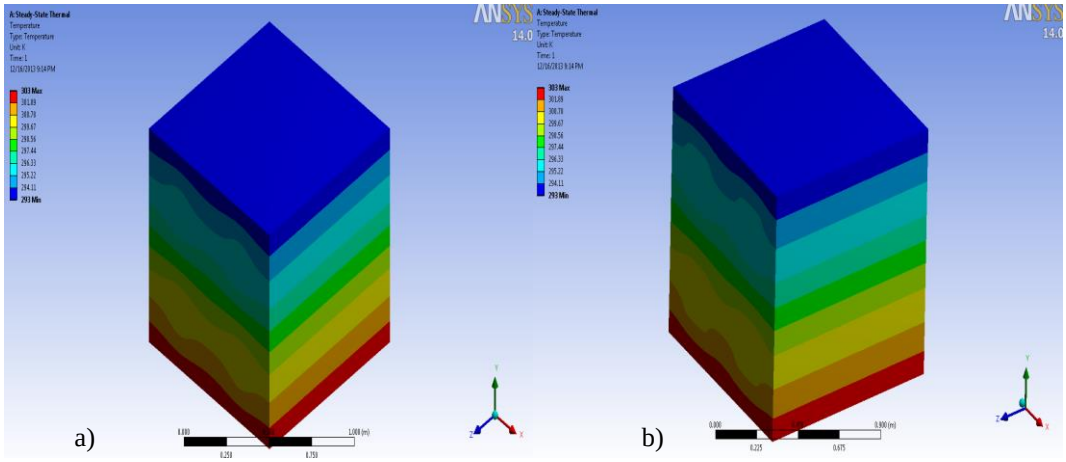

Figure E.1.35. Temperature distribution over 16-piece- a)shpere and b)cube -filler model for Ø=12%

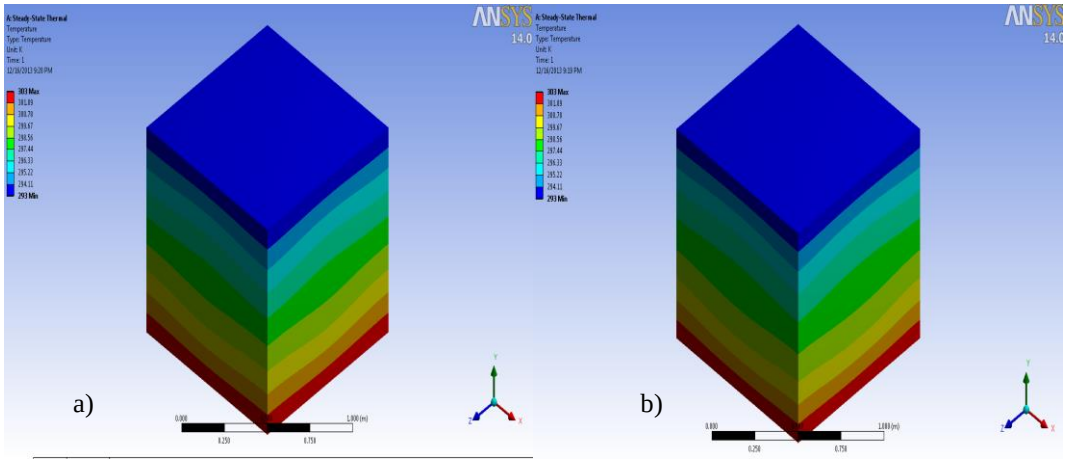

Figure E.1.36. Temperature distribution over 1-piece- a)shpere and b)cube -filler model for Ø=15%

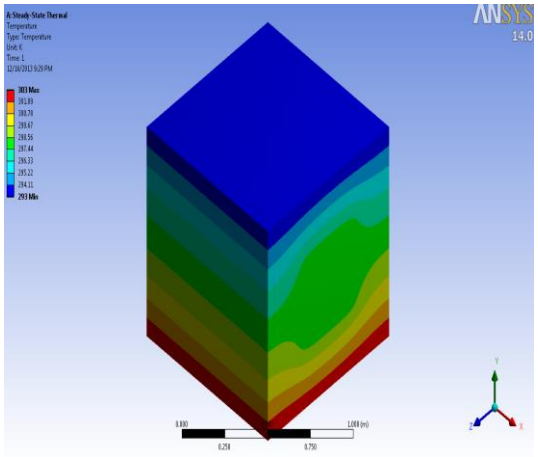

Figure E.1.37. Temperature distribution over 2-piece- cube -filler model for Ø=15%

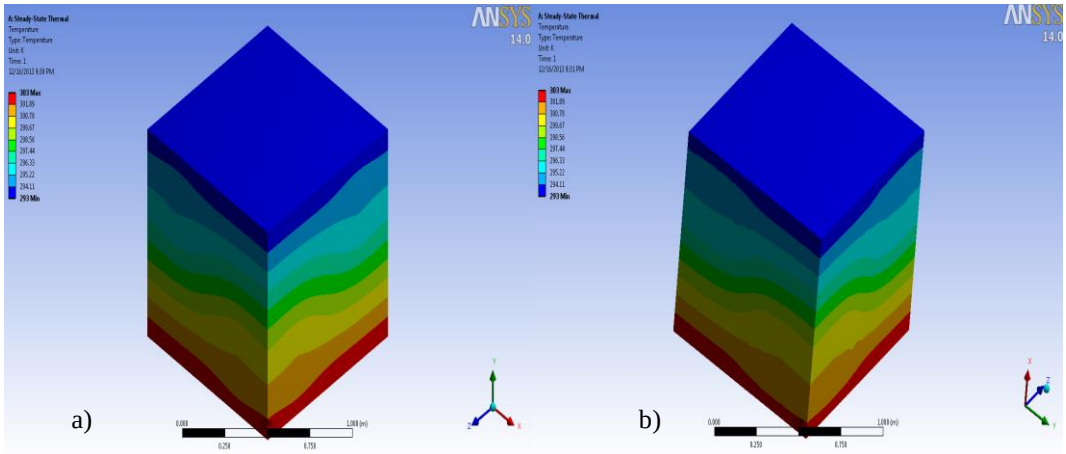

Figure E.1.38 Temperature distribution over 4-piece- a)shpere and b)cube -filler model for Ø=15%

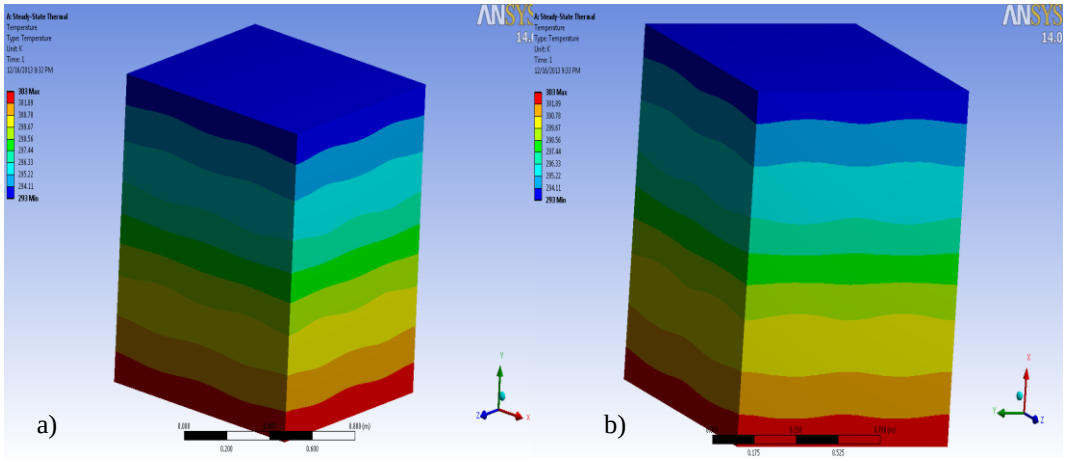

Figure E.1.39. Temperature distribution over 8-piece- a)shpere and b)cube -filler model for Ø=15%

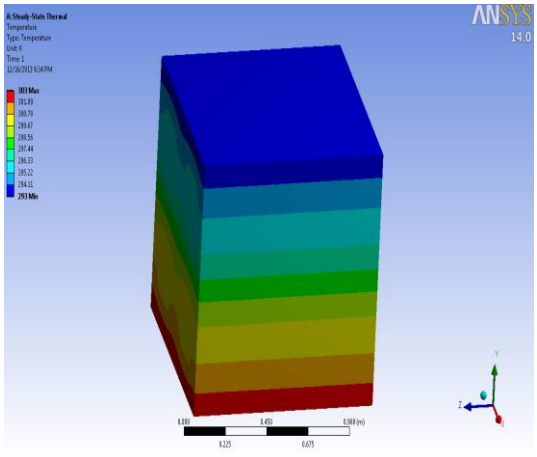

Figure E.1.40. Temperature distribution over 16-piece- cube -filler model for Ø=15%

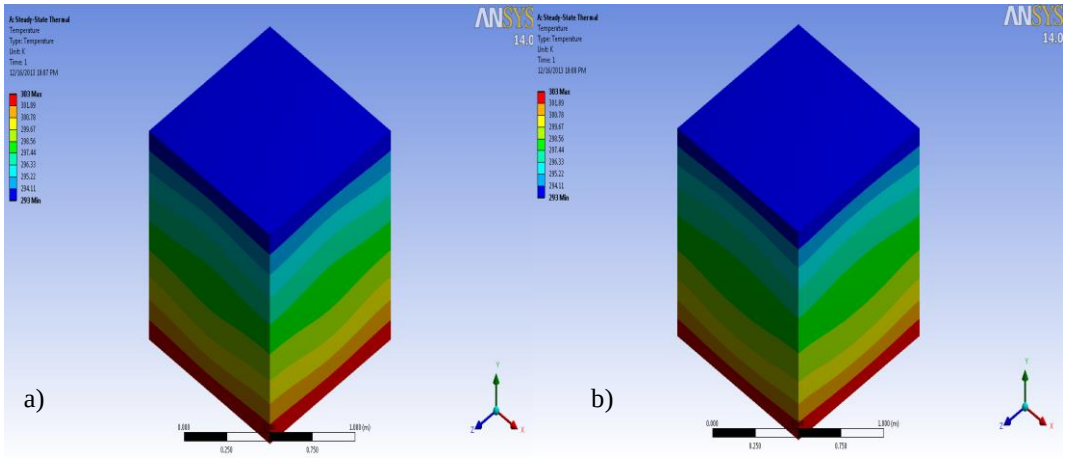

Figure E.1.41. Temperature distribution over 1-piece- a)shpere and b)cube -filler model for Ø=18%

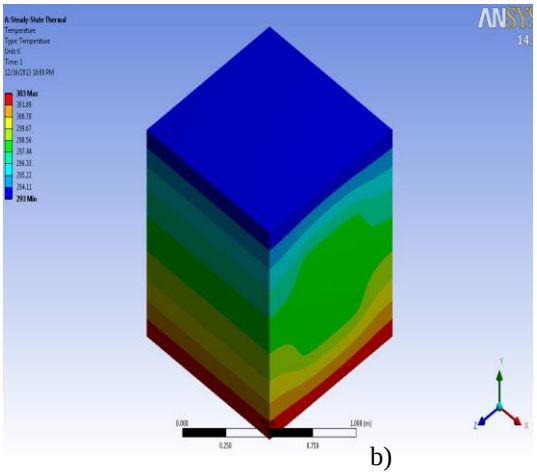

a) b)

Figure E.1.42. Temperature distribution over 2-piece- cube -filler model for Ø=18%

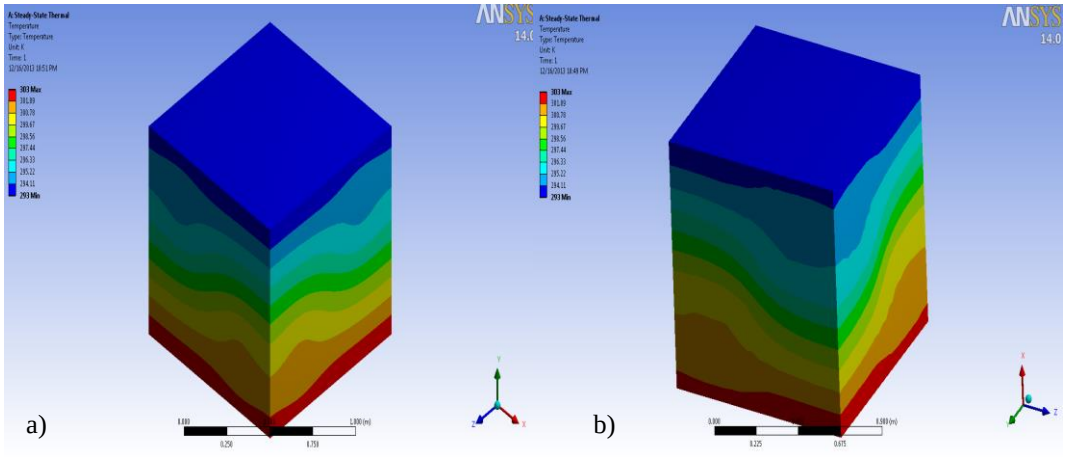

a) b)

Figure E.1.43.Temperature distribution over 4-piece- a)shpere and b)cube -filler model for Ø=18%

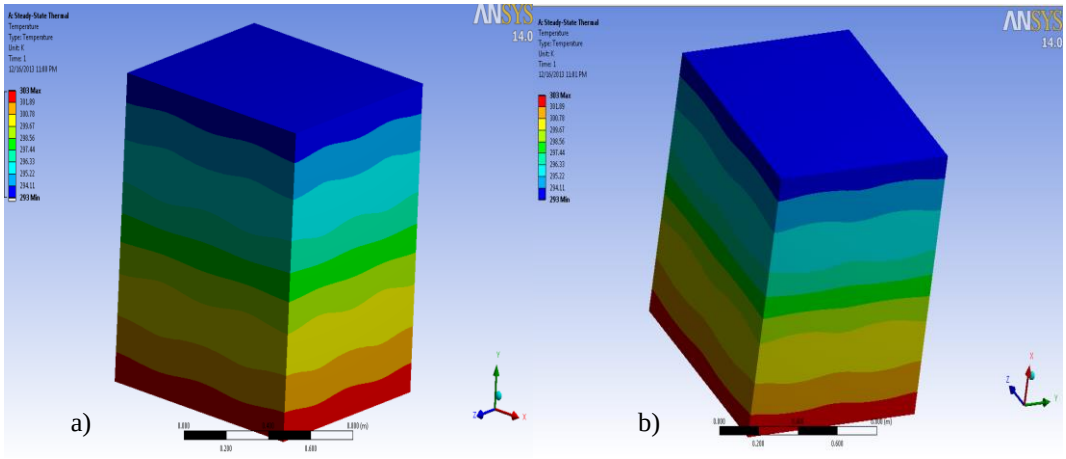

a) b)

Figure E.1.44. Temperature distribution over 8-piece- a)shpere and b)cube -filler model for Ø=18%

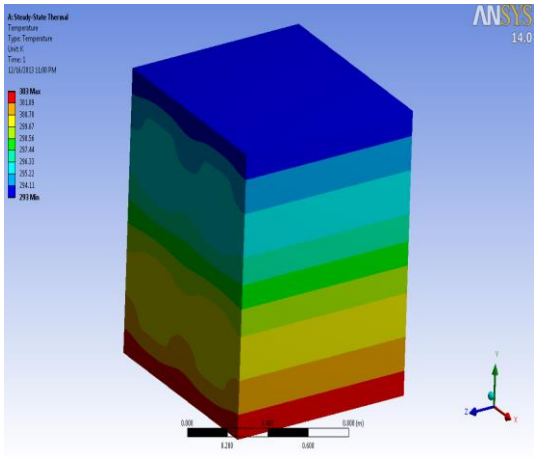

Figure E.1.45. Temperature distribution over 16-piece- cube -filler model for Ø=18%

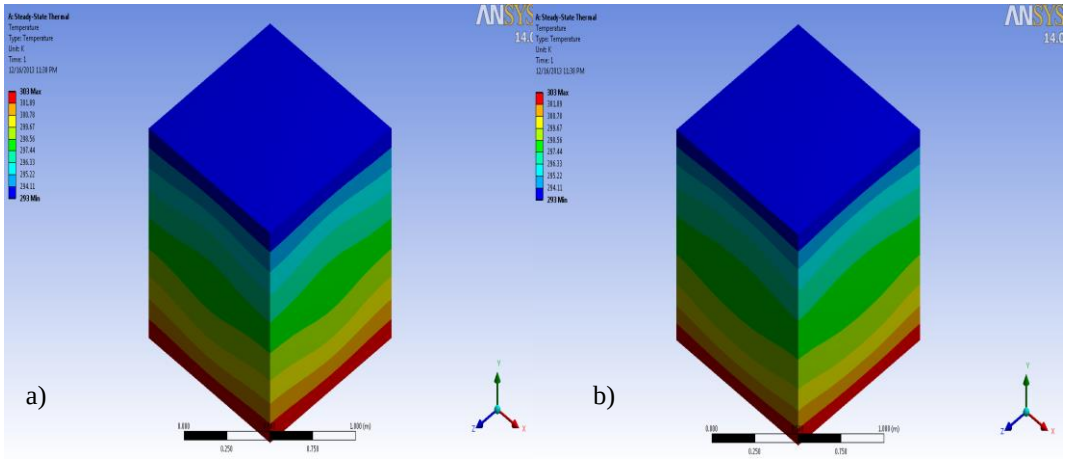

Figure E.1.46. Temperature distribution over 1-piece- a)shpere and b)cube -filler model for Ø=21%

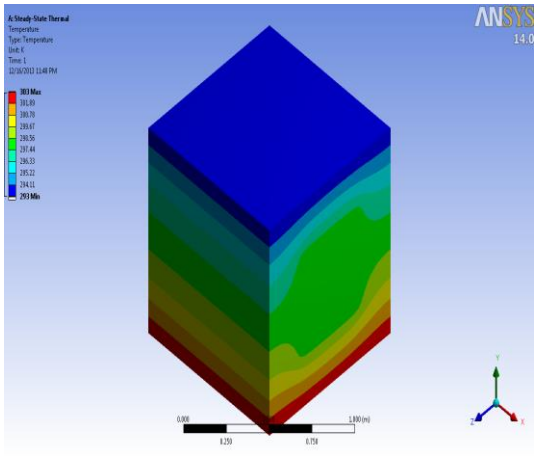

Figure E.1.47. Temperature distribution over 2-piece- cube -filler model for Ø=21%

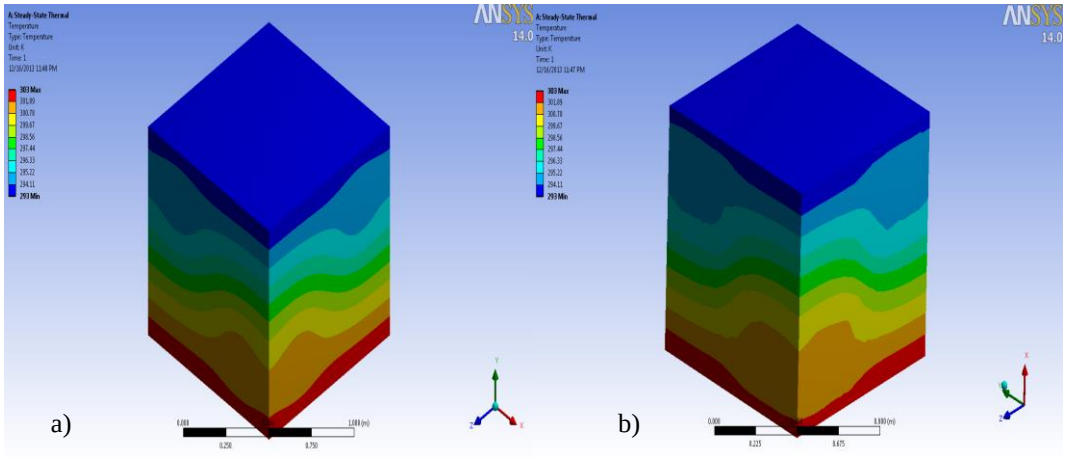

Figure E.1.48. Temperature distribution over 4-piece- a)shpere and b)cube -filler model for Ø=21%

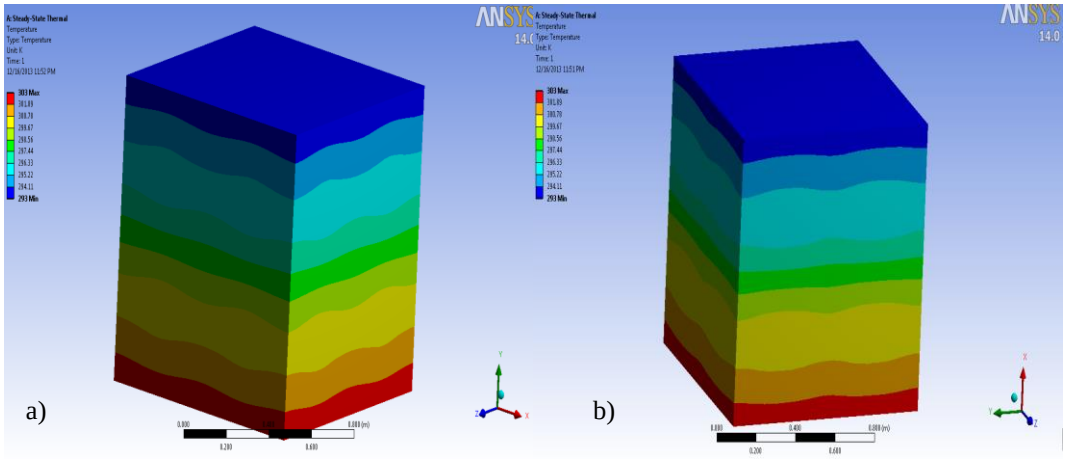

Figure E.1.49. Temperature distribution over 8-piece- a)shpere and b)cube -filler model for Ø=21%

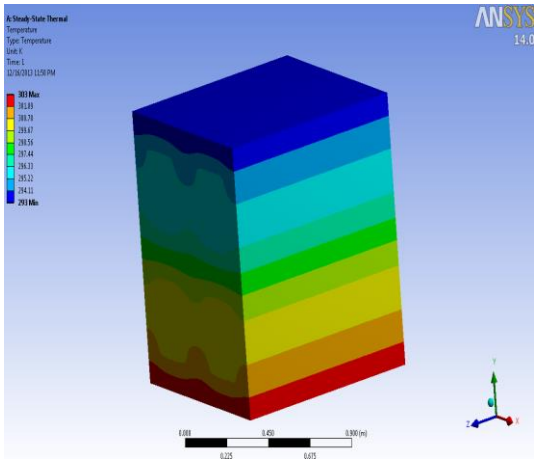

Figure E.1.50. Temperature distribution over 16-piece- cube -filler model for Ø=21%

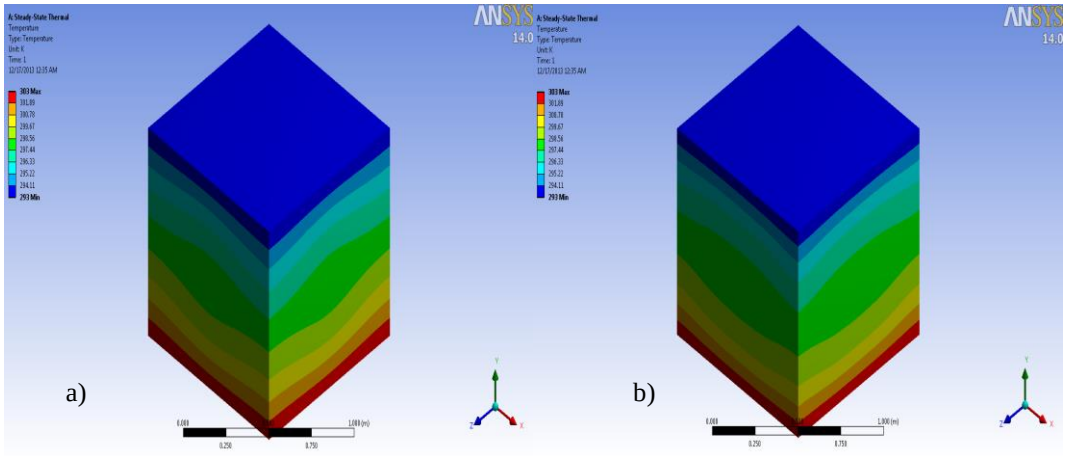

Figure E.1.51. Temperature distribution over 1-piece- a)shpere and b)cube -filler model for Ø=25%

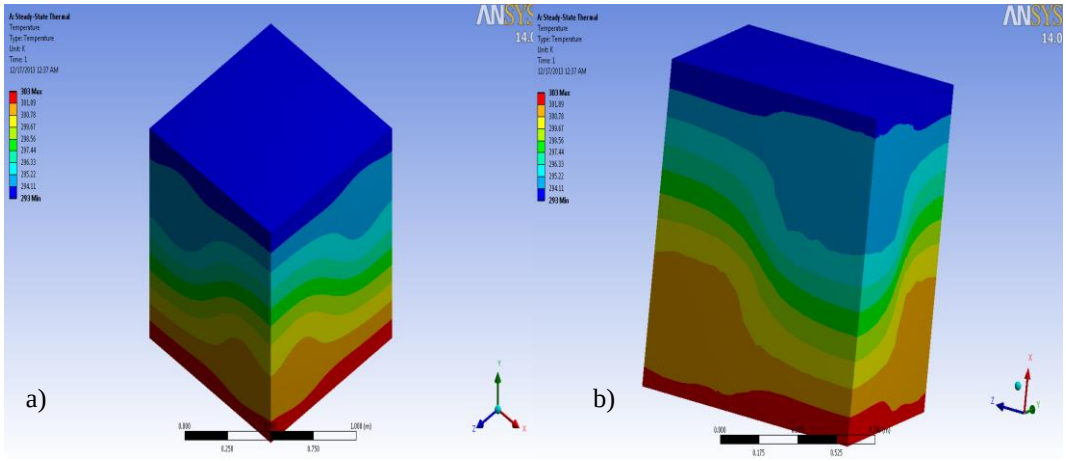

Figure E.1.52. Temperature distribution over 4-piece- a)shpere and b)cube -filler model for Ø=25%

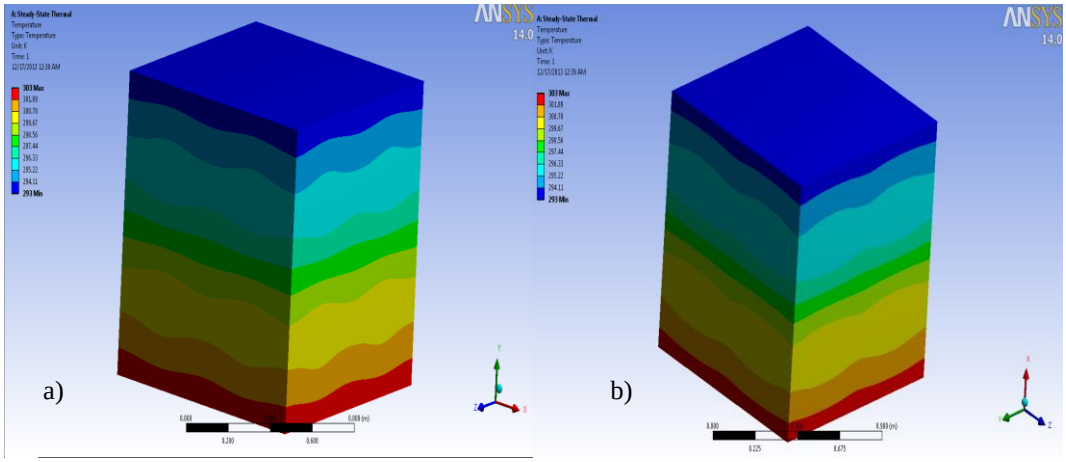

Figure E.1.53. Temperature distribution over 8-piece- a)shpere and b)cube -filler model for Ø=25%

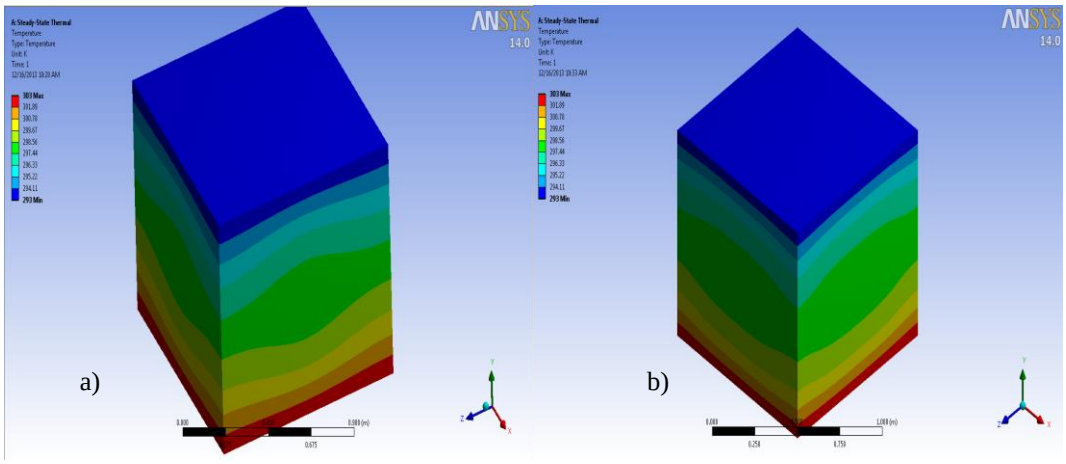

Figure E.1.54. Temperature distribution over 1-piece- a)shpere and b)cube -filler model for Ø=30%

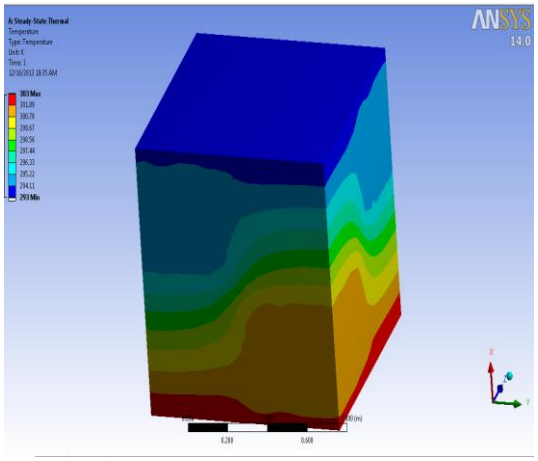

Figure E.1.55. Temperature distribution over 4-piece- cube -filler model for Ø=30%

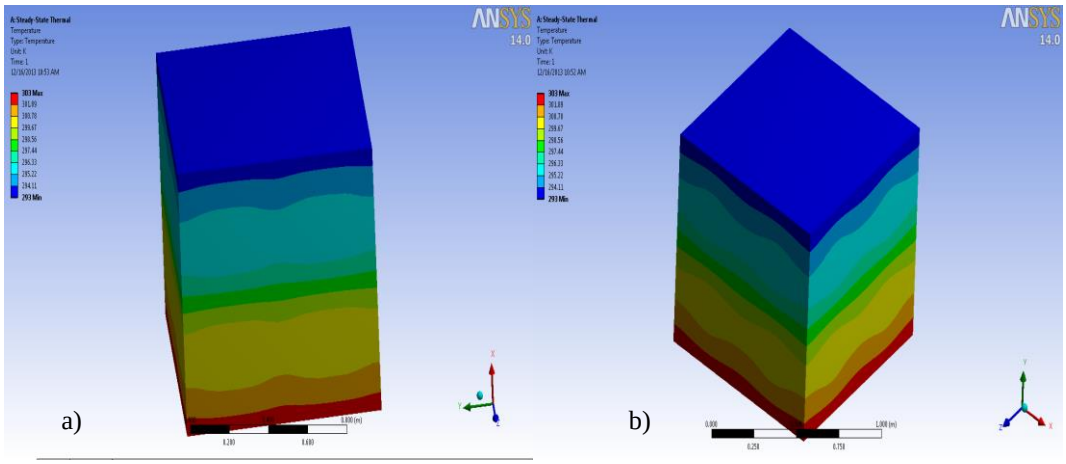

Figure E.1.56. Temperature distribution over 8-piece- cube -filler model for Ø=30%

E.2 Heat Flux Results

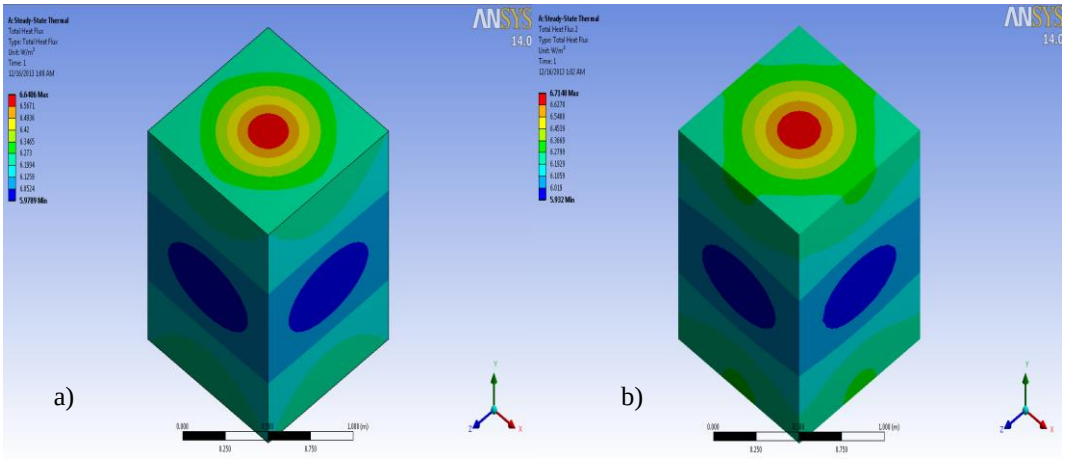

Figure E.2.1. Total heat flux over 1-piece- a)shpere and b) cube -filler model for Ø=1%

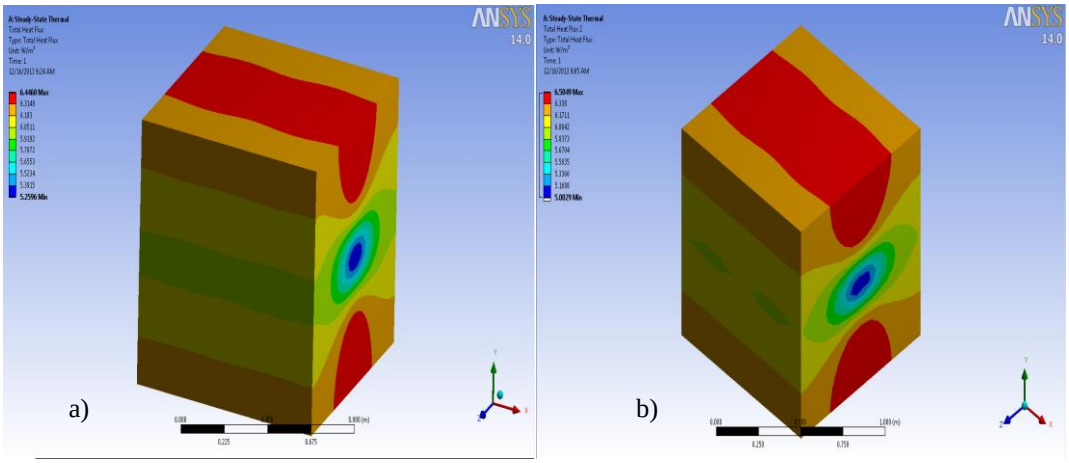

Figure E.2.2. Total heat flux over 2-piece- a)shpere and b) cube -filler model for Ø=1%

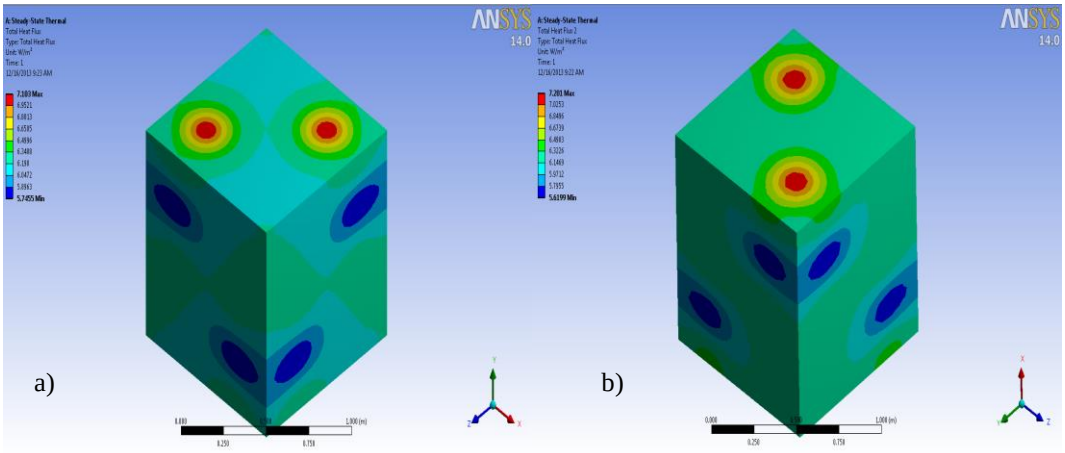

Figure E.2.3. Total heat flux over 4-piece- a)shpere and b) cube -filler model for Ø=1%

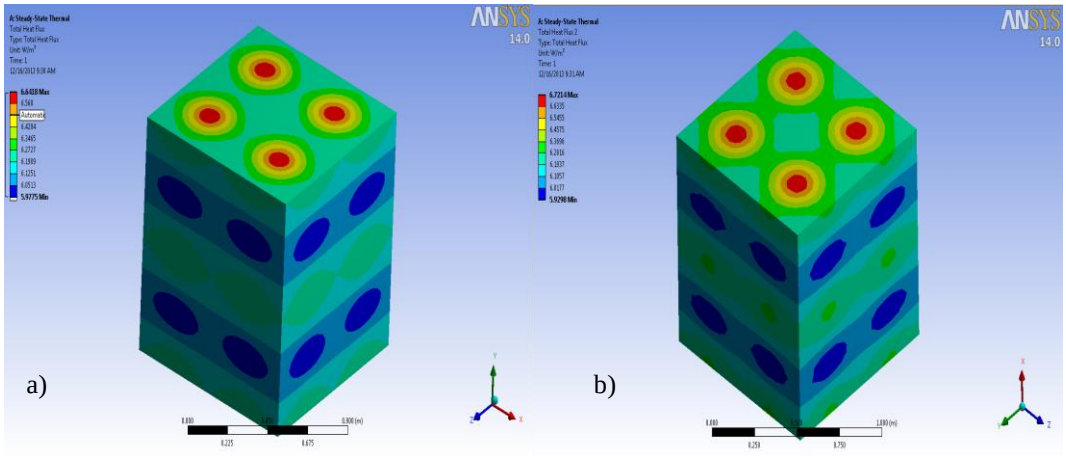

Figure E.2.4. Total heat flux over 8-piece- a)shpere and b) cube -filler model for Ø=1%

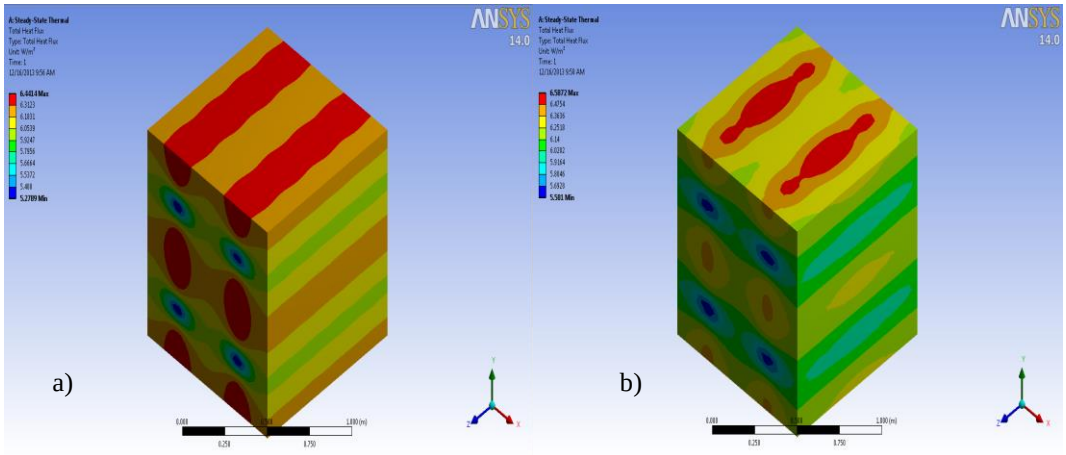

Figure E.2.5. Total heat flux over 16-piece- a)shpere and b) cube -filler model for Ø=1%

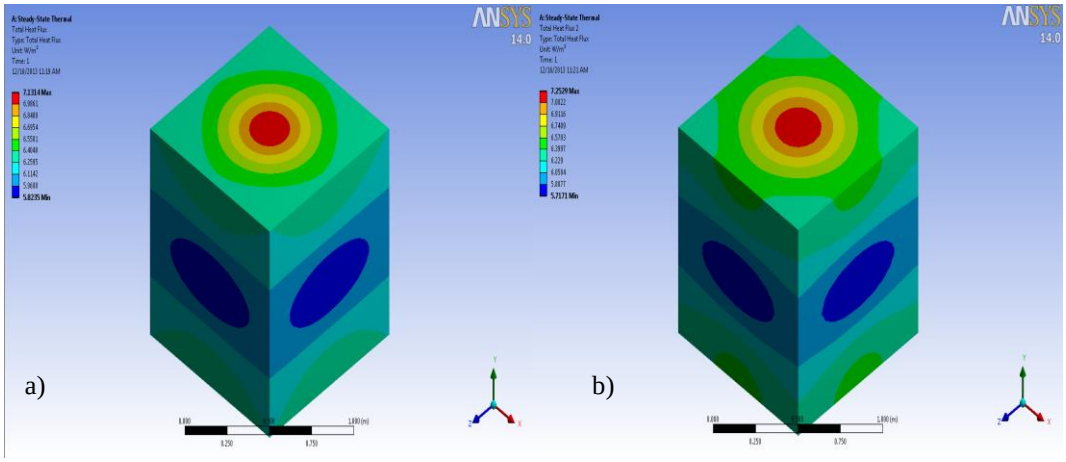

Figure E.2.6. Total heat flux over 1-piece- a)shpere and b) cube -filler model for Ø=2%

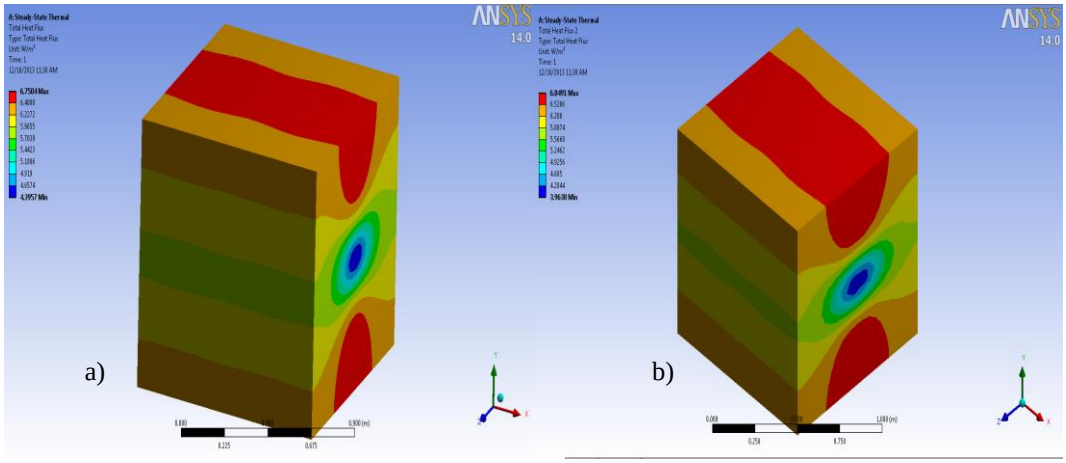

Figure E.2.7. Total heat flux over 2-piece- a)shpere and b) cube -filler model for Ø=2%

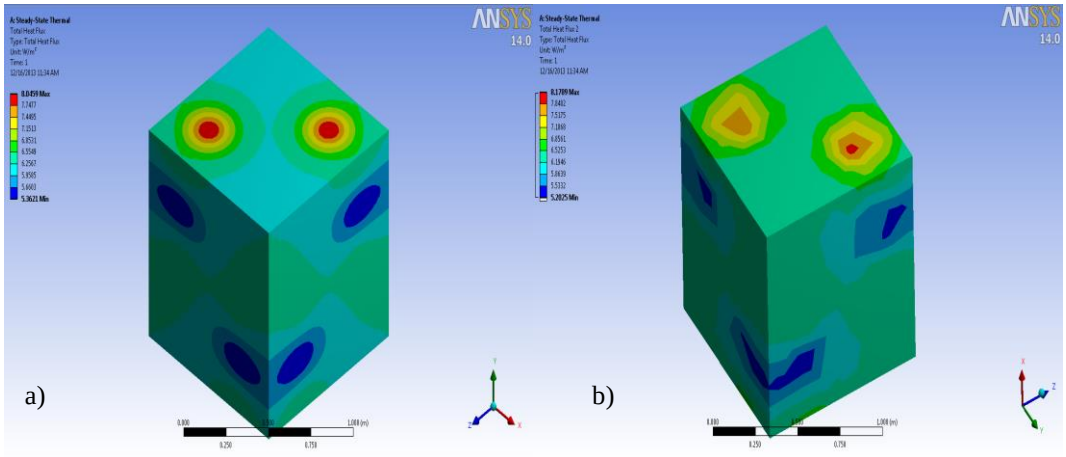

Figure E.2.8. Total heat flux over 4-piece- a)shpere and b) cube -filler model for Ø=2%

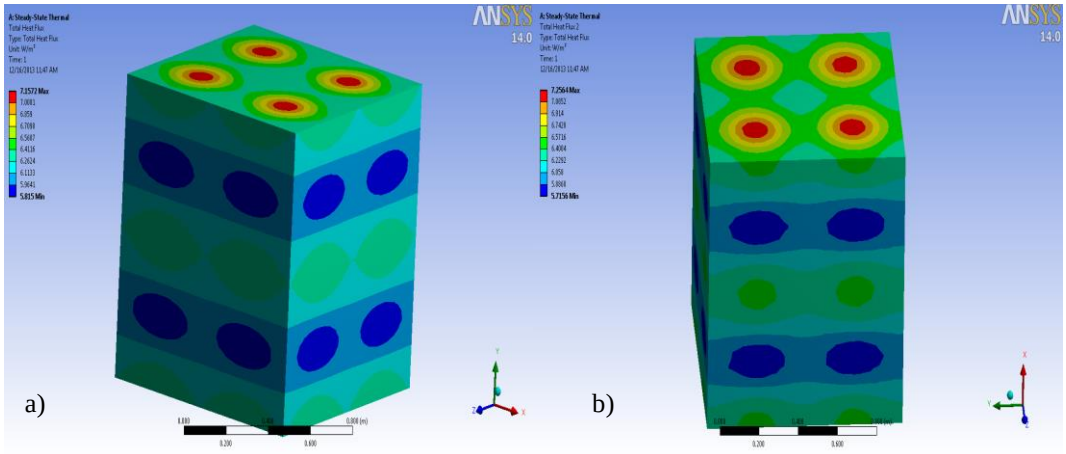

Figure E.2.9. Total heat flux over 8-piece- a)shpere and b) cube -filler model for Ø=2%

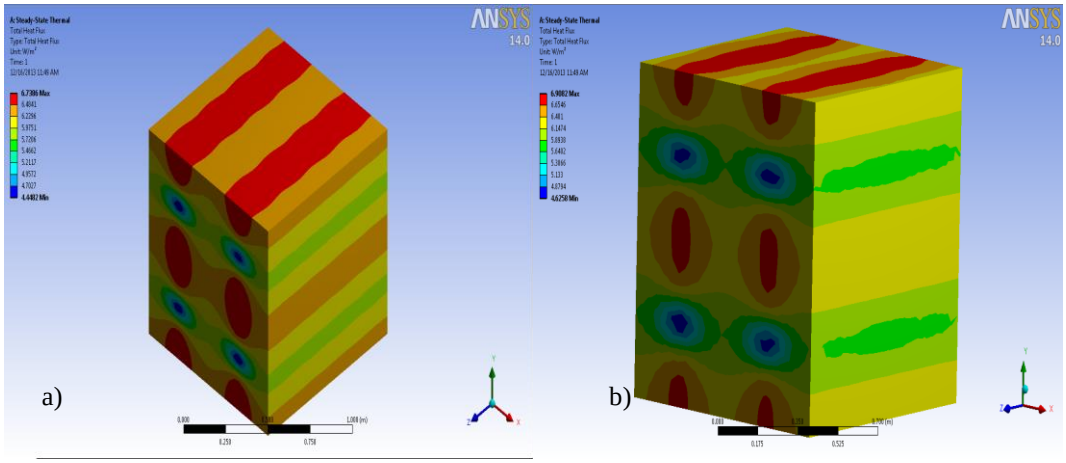

Figure E.2.10. Total heat flux over 16-piece- a)shpere and b) cube -filler model for Ø=2%

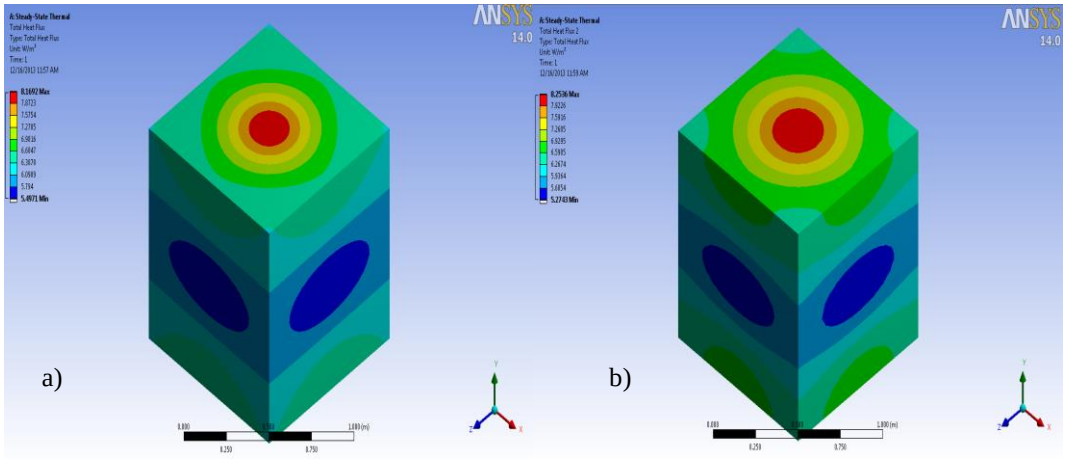

Figure E.2.11. Total heat flux over 1-piece- a)shpere and b) cube -filler model for Ø=4%

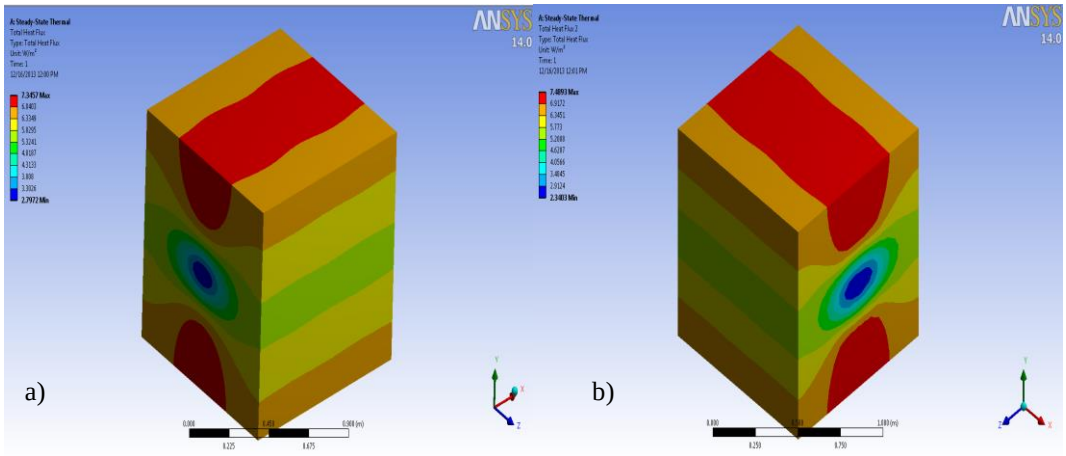

Figure E.2.12. Total heat flux over 2-piece- a)shpere and b) cube -filler model for Ø=4%

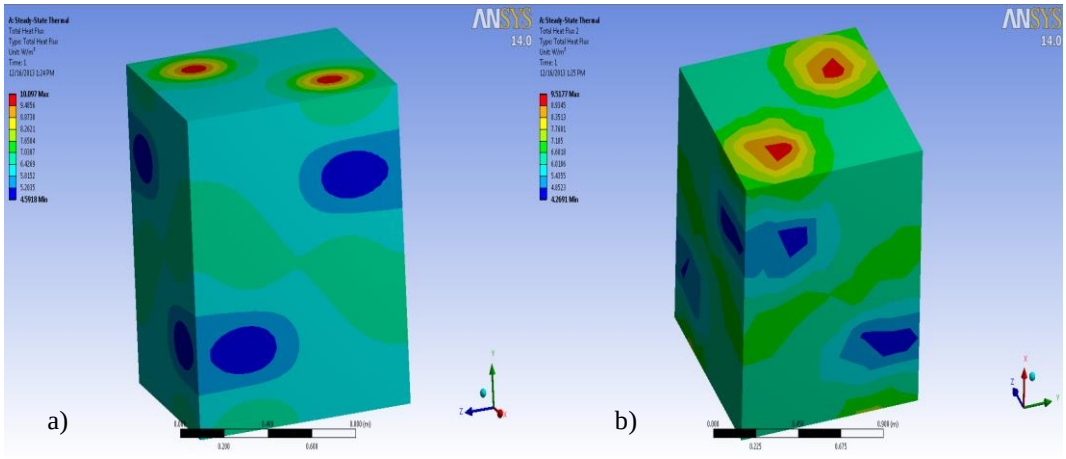

Figure E.2.13. Total heat flux over 4-piece- a)shpere and b) cube -filler model for Ø=4%

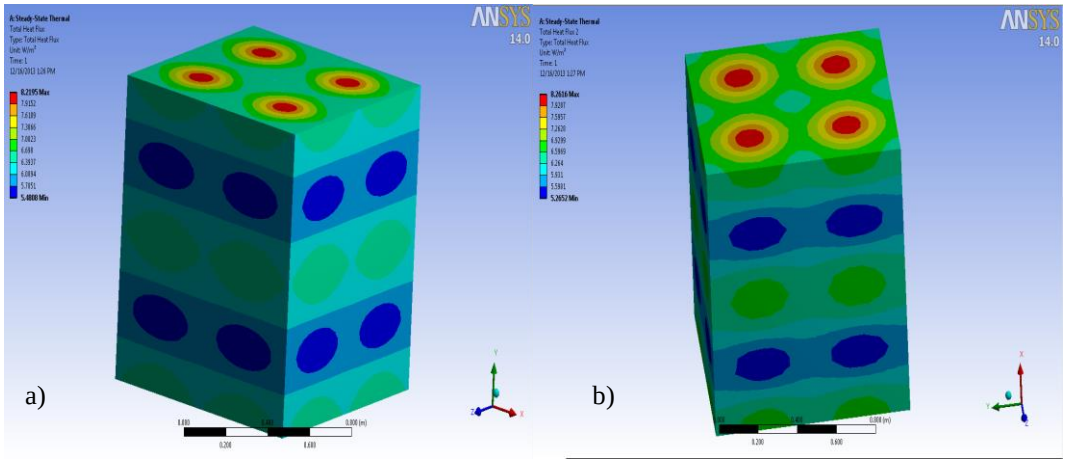

Figure E.2.14. Total heat flux over 8-piece- a)shpere and b) cube -filler model for Ø=4%

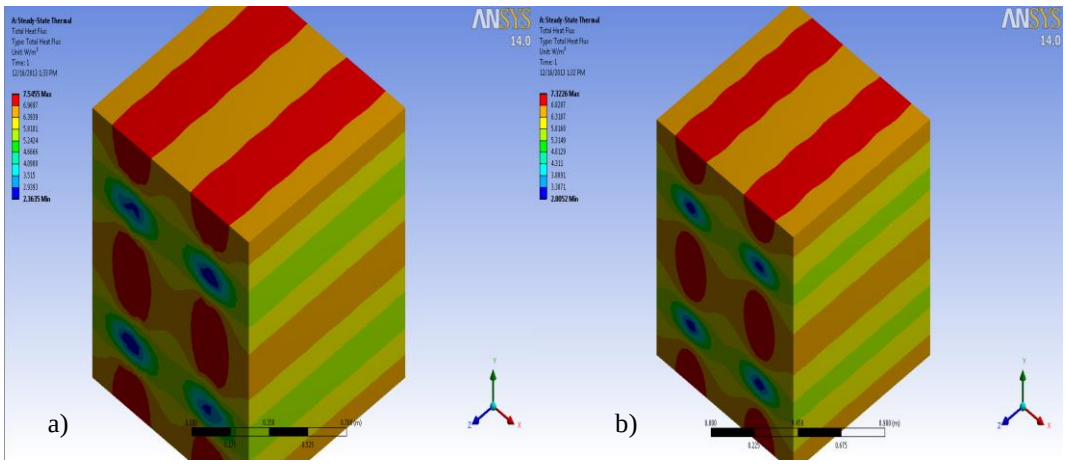

Figure E.2.15. Total heat flux over 16-piece- a)shpere and b) cube -filler model for Ø=4%

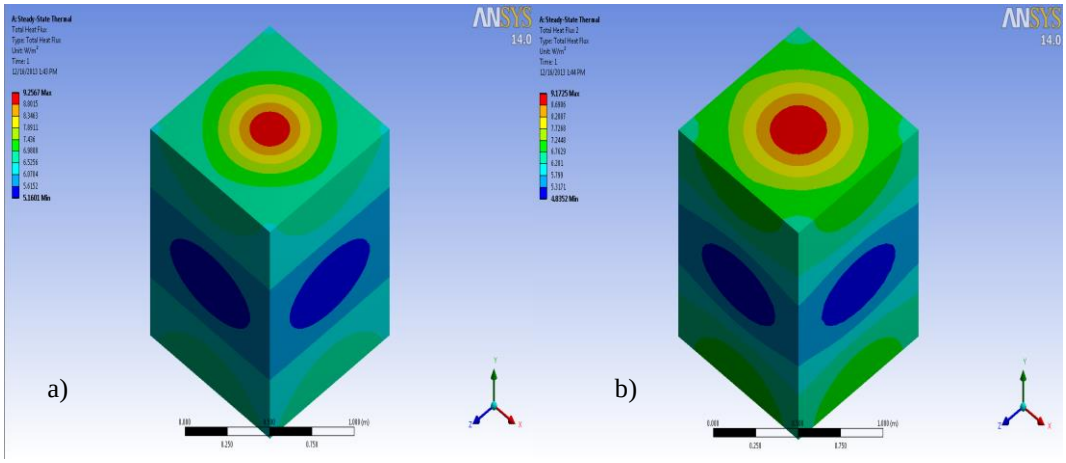

Figure E.2.16. Total heat flux over 1-piece- a)shpere and b) cube -filler model for Ø=6%

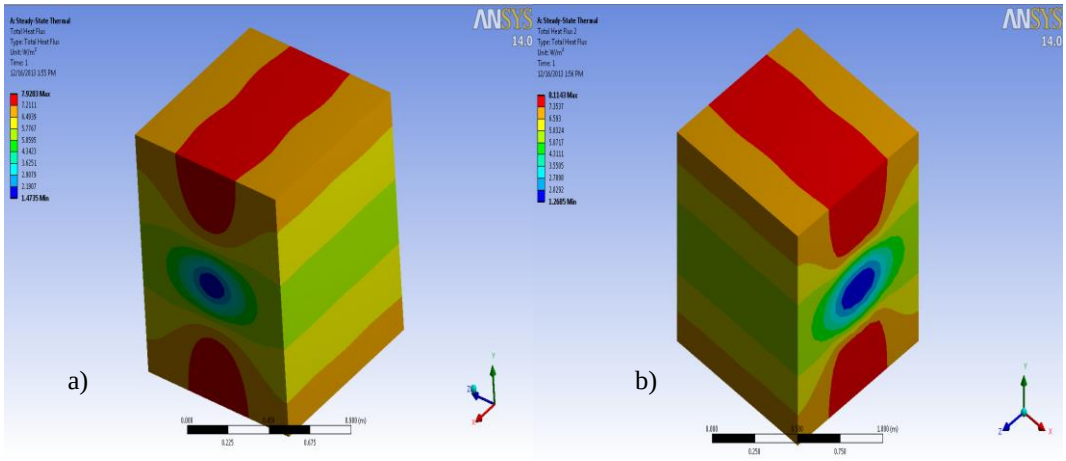

Figure E.2.17. Total heat flux over 2-piece- a)shpere and b) cube -filler model for Ø=6%

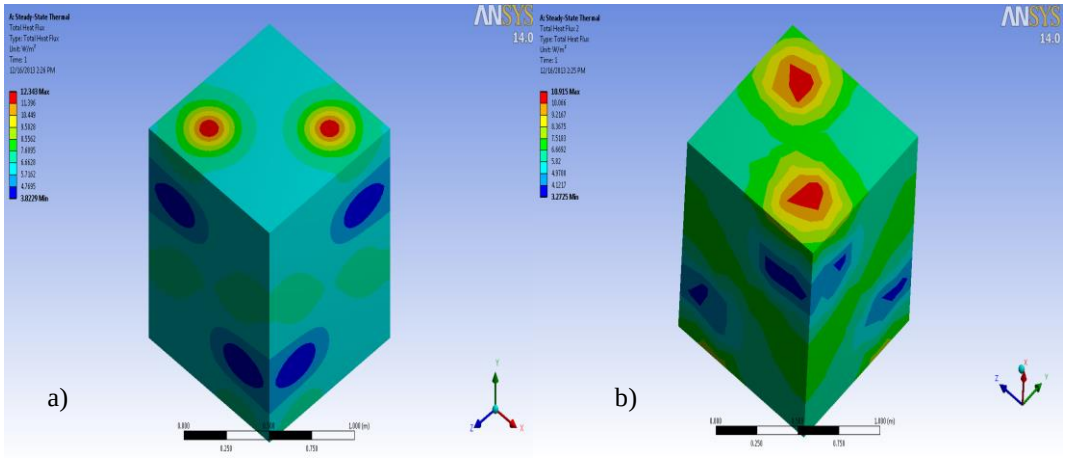

Figure E.2.18. Total heat flux over 4-piece- a)shpere and b) cube -filler model for Ø=6%

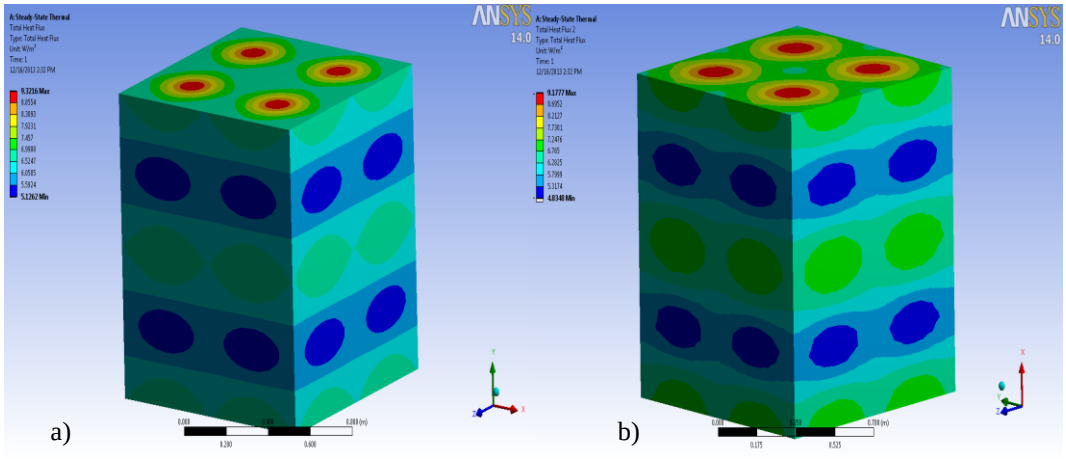

Figure E.2.19. Total heat flux over 8-piece- a)shpere and b) cube -filler model for Ø=6%

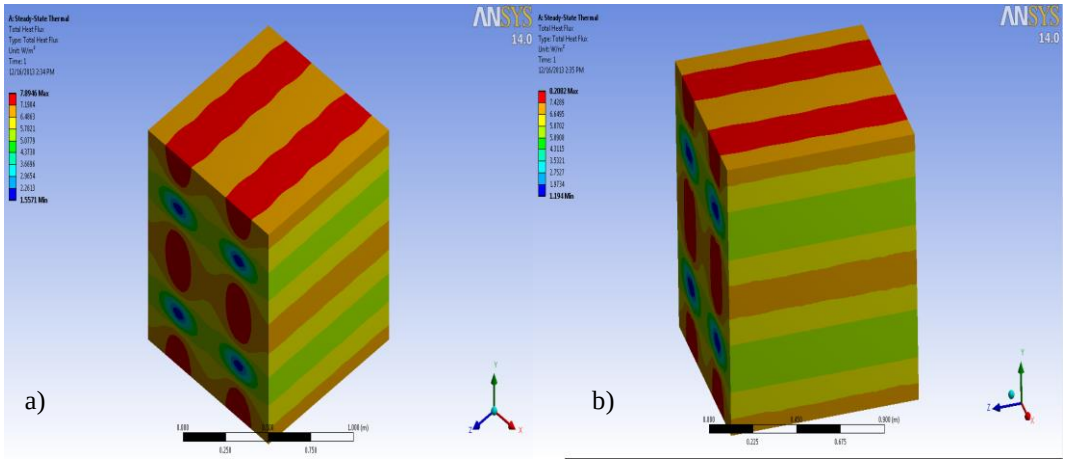

Figure E.2.20. Total heat flux over 16-piece- a)shpere and b) cube -filler model for Ø=6%

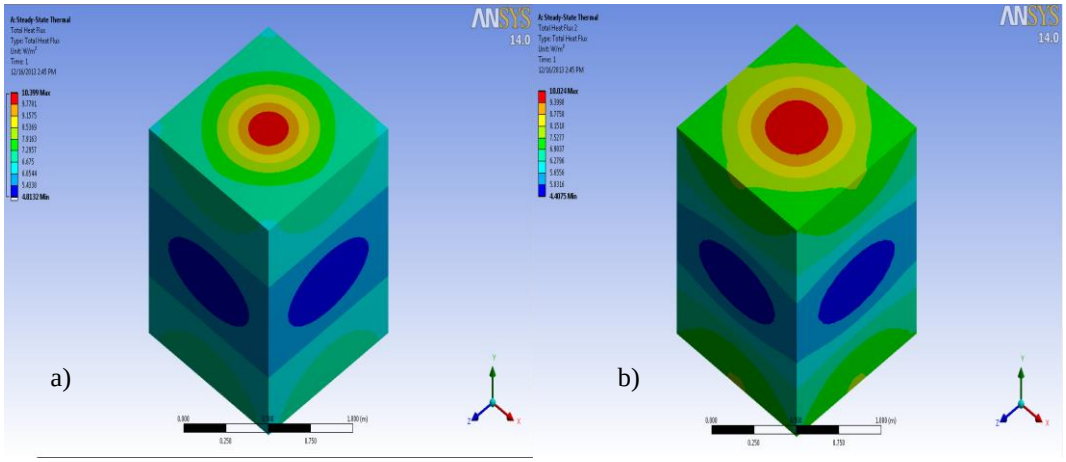

Figure E.2.21. Total heat flux over 1-piece- a)shpere and b) cube -filler model for Ø=8%

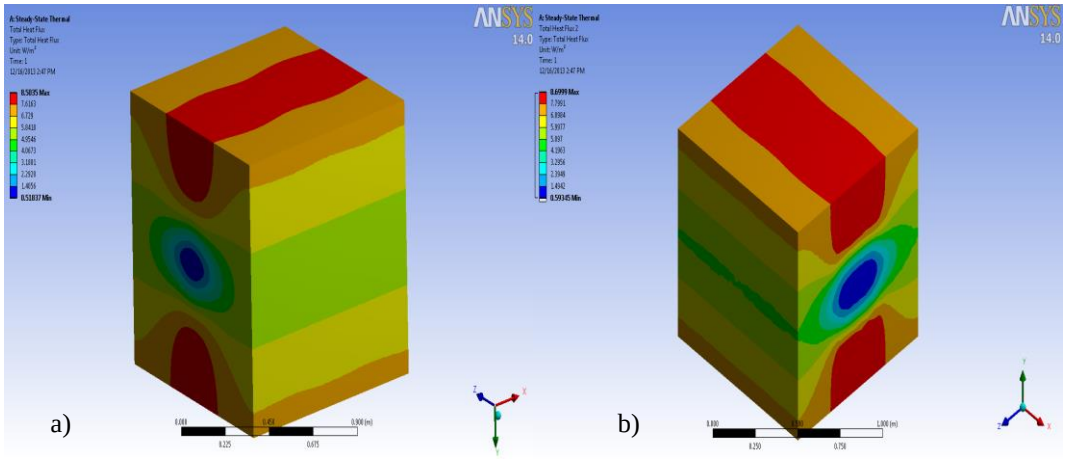

Figure E.2.22. Total heat flux over 2-piece- a)shpere and b) cube -filler model for Ø=8%

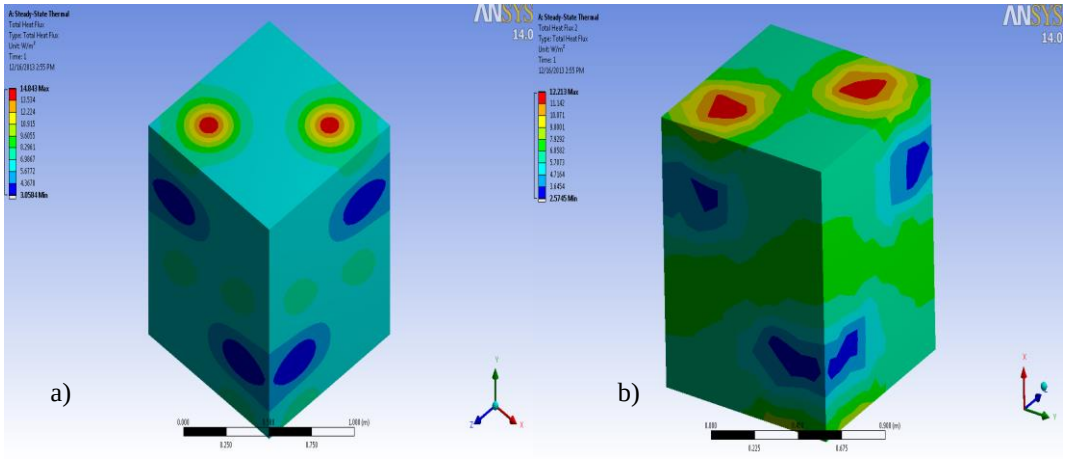

Figure E.2.23. Total heat flux over 4-piece- a)shpere and b) cube -filler model for Ø=8%

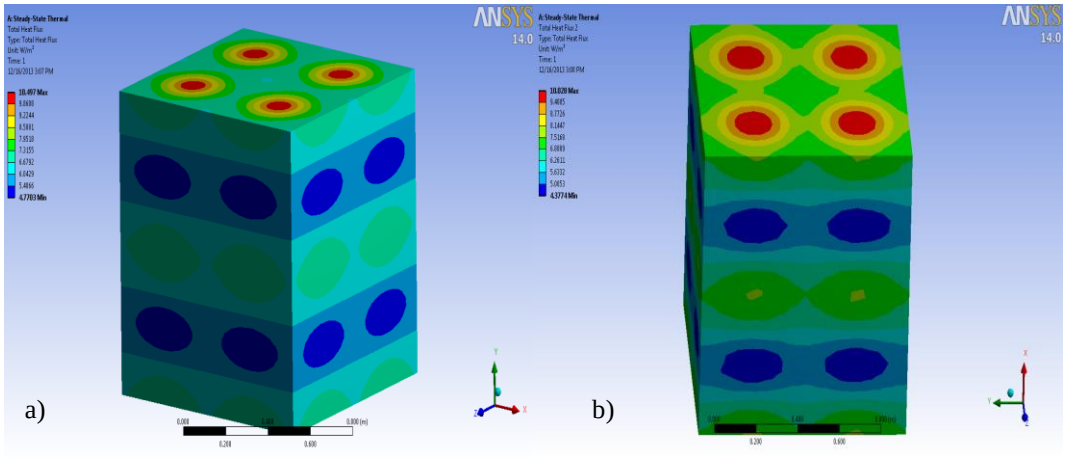

Figure E.2.24. Total heat flux over 8-piece- a)shpere and b) cube -filler model for Ø=8%

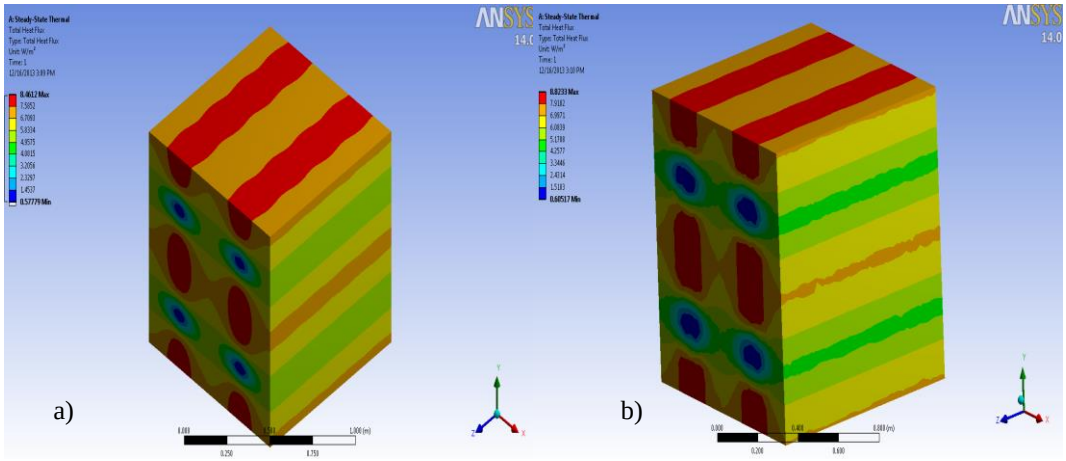

Figure E.2.25. Total heat flux over 16-piece- a)shpere and b) cube -filler model for Ø=8%

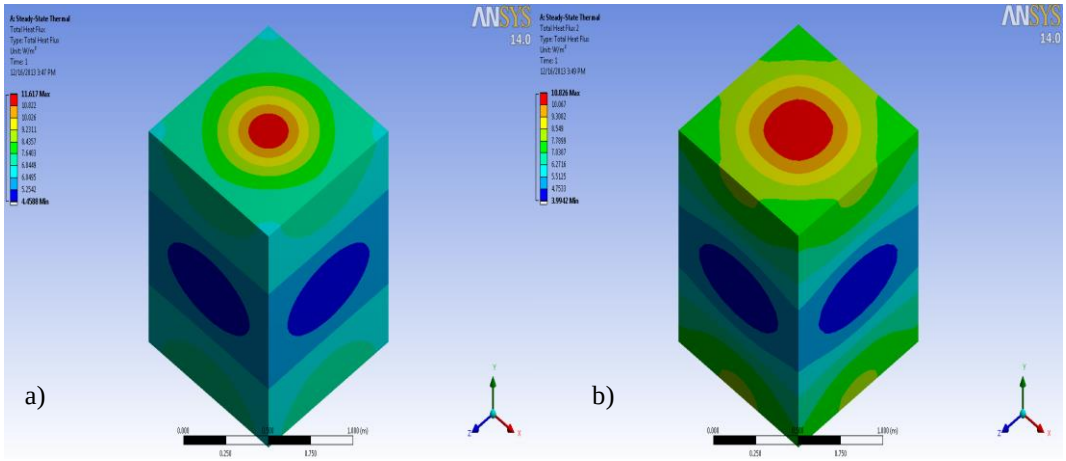

Figure E.2.26. Total heat flux over 1-piece- a)shpere and b) cube -filler model for Ø=10%

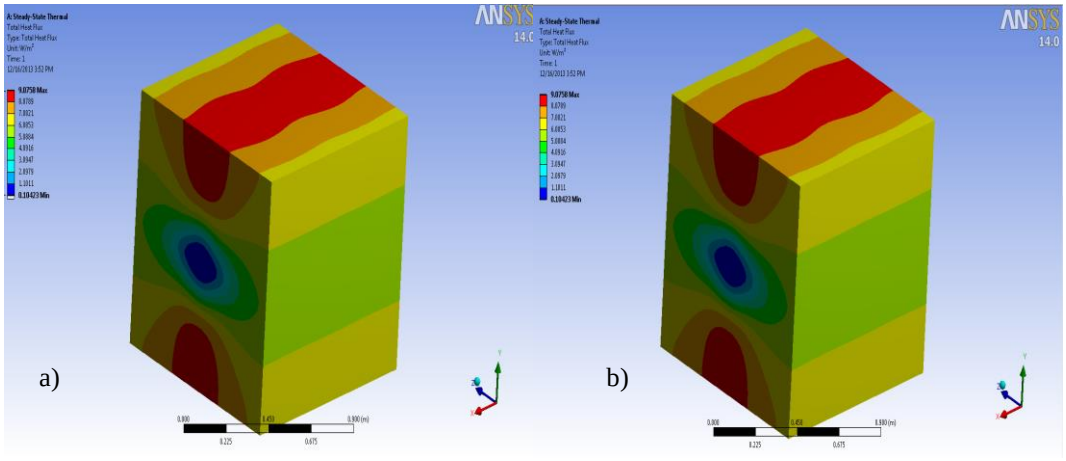

Figure E.2.27. Total heat flux over 2-piece- a)shpere and b) cube -filler model for Ø=10%

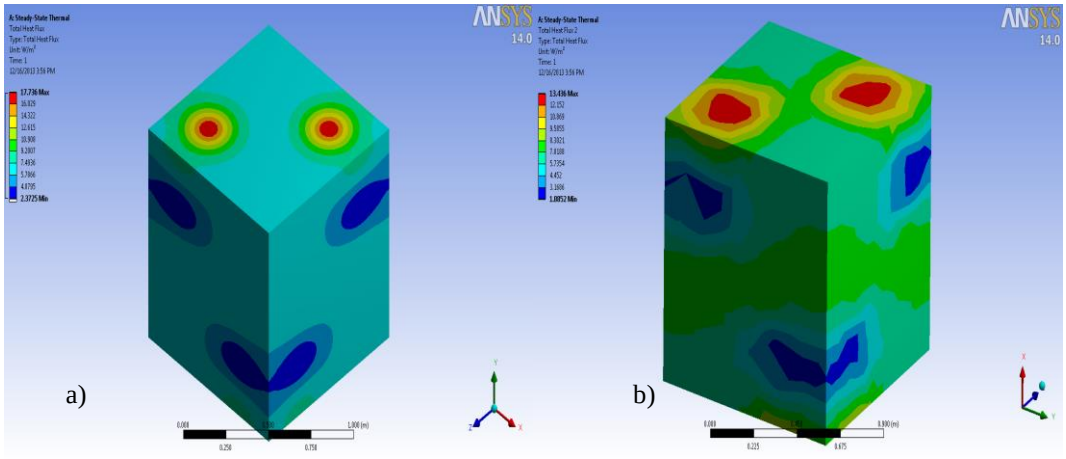

Figure E.2.28. Total heat flux over 4-piece- a)shpere and b) cube -filler model for Ø=10%

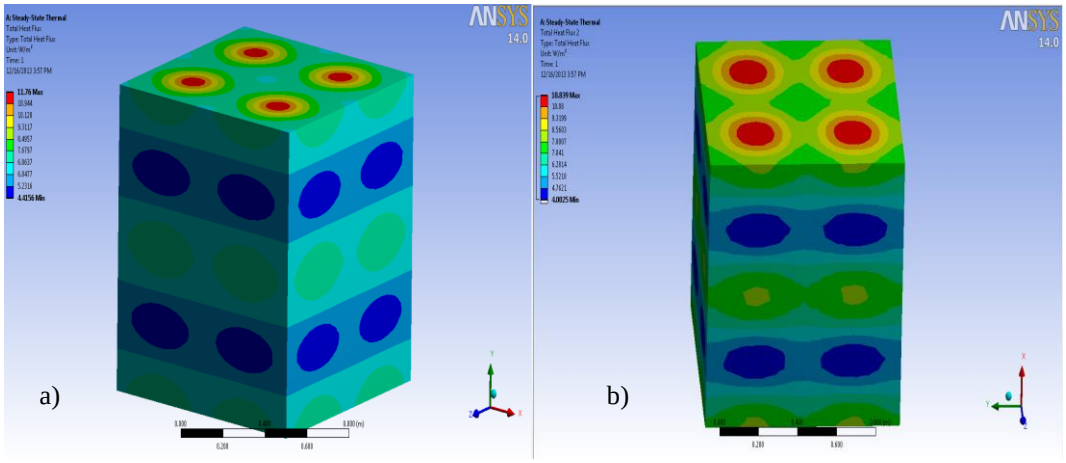

Figure E.2.29. Total heat flux over 8-piece- a)shpere and b) cube -filler model for Ø=10%

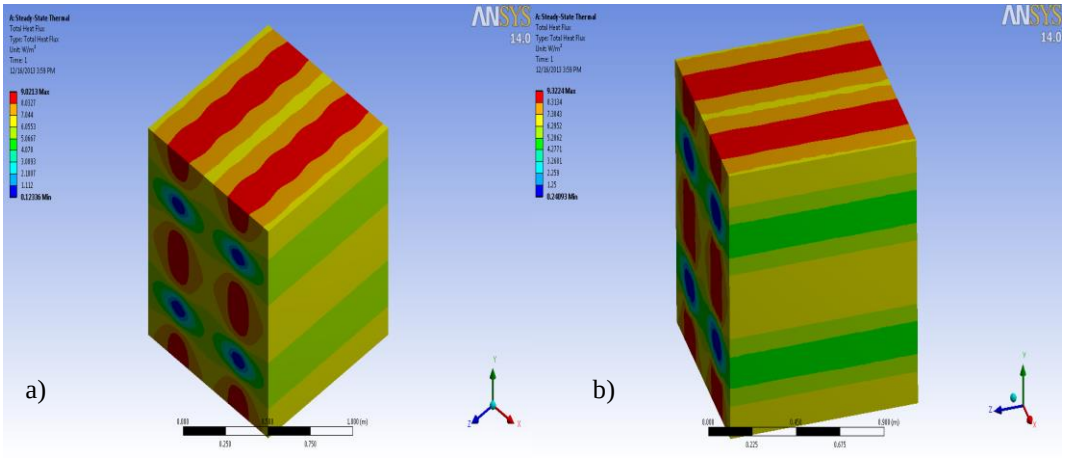

Figure E.2.30. Total heat flux over 16-piece- a)shpere and b) cube -filler model for Ø=10%

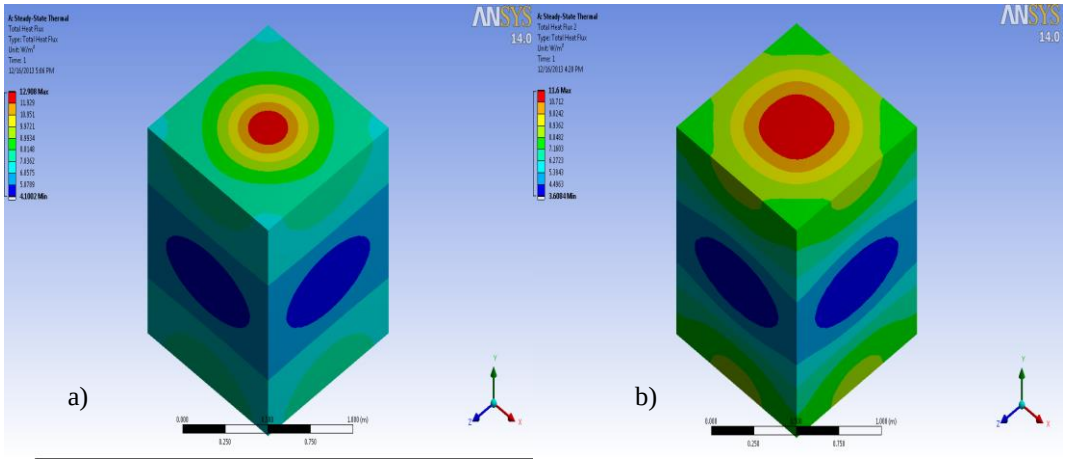

Figure E.2.31. Total heat flux over 1-piece- a)shpere and b) cube -filler model for Ø=12%

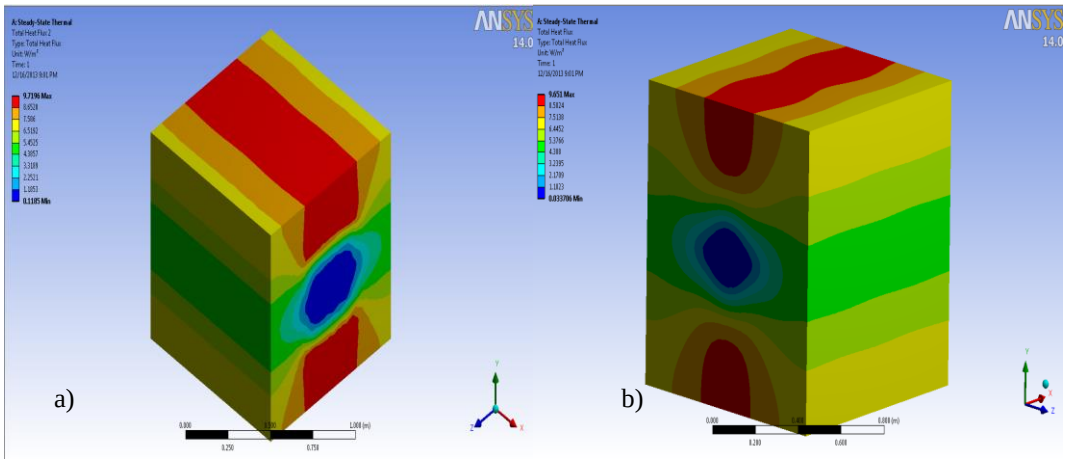

Figure E.2.32. Total heat flux over 2-piece- a)shpere and b) cube -filler model for Ø=12%

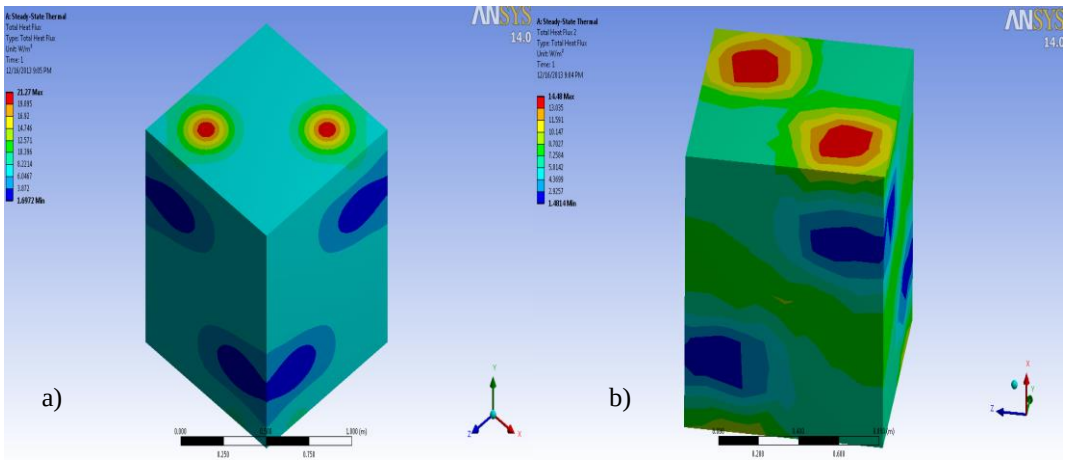

Figure E.2.33. Total heat flux over 4-piece- a)shpere and b) cube -filler model for Ø=12%

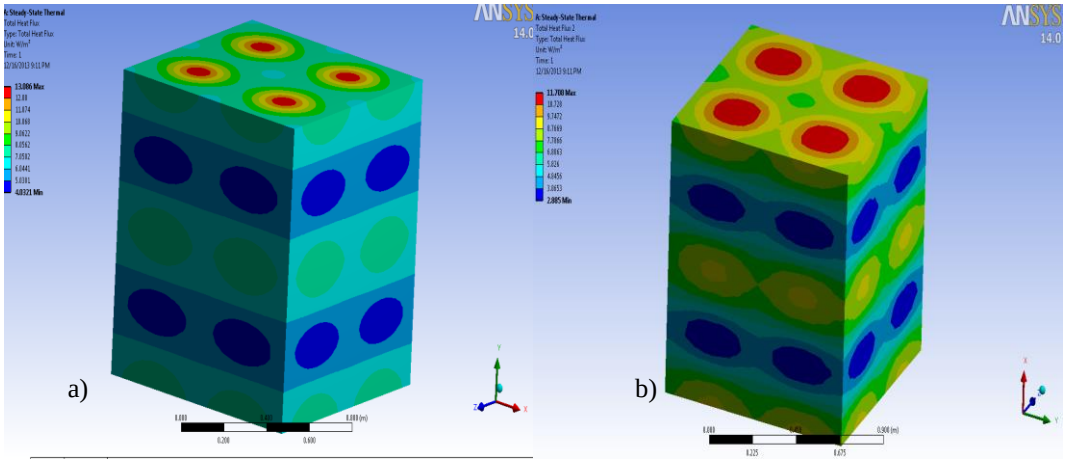

Figure E.2.34. Total heat flux over 8-piece- a)shpere and b) cube -filler model for Ø=12%

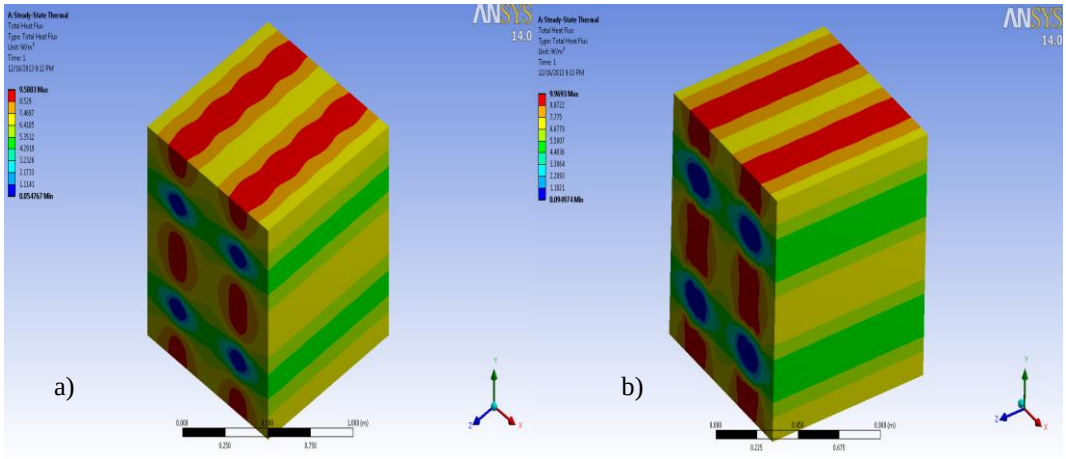

Figure E.2.35. Total heat flux over 16-piece- a)shpere and b) cube -filler model for Ø=12%

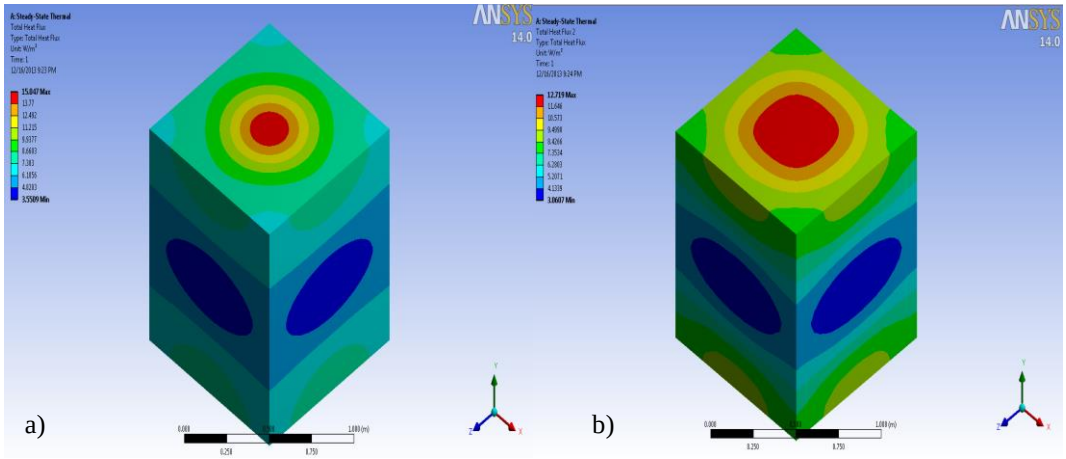

Figure E.2.36. Total heat flux over 1-piece- a)shpere and b) cube -filler model for Ø=15%

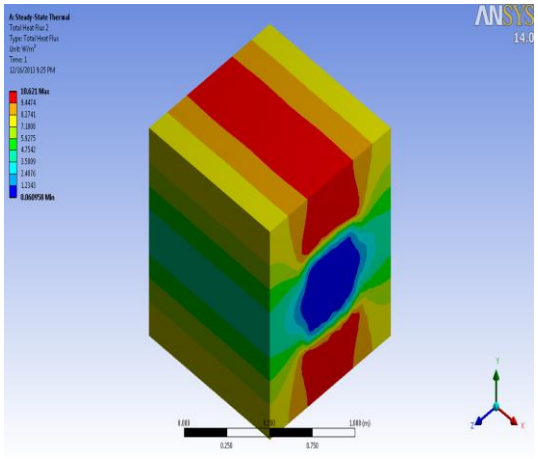

Figure E.2.37. Total heat flux over 2-piece- cube -filler model for Ø=15%

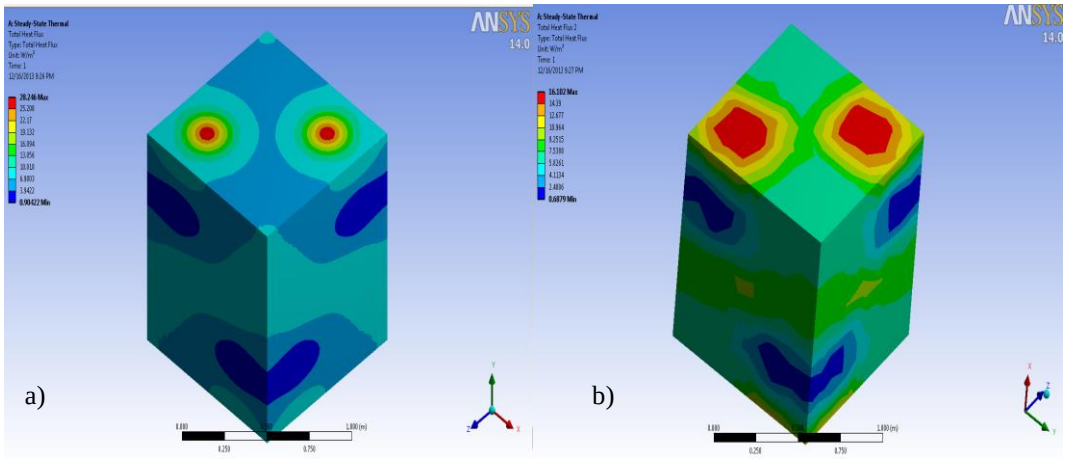

Figure E.2.38. Total heat flux over 4-piece- a)shpere and b) cube -filler model for Ø=15%

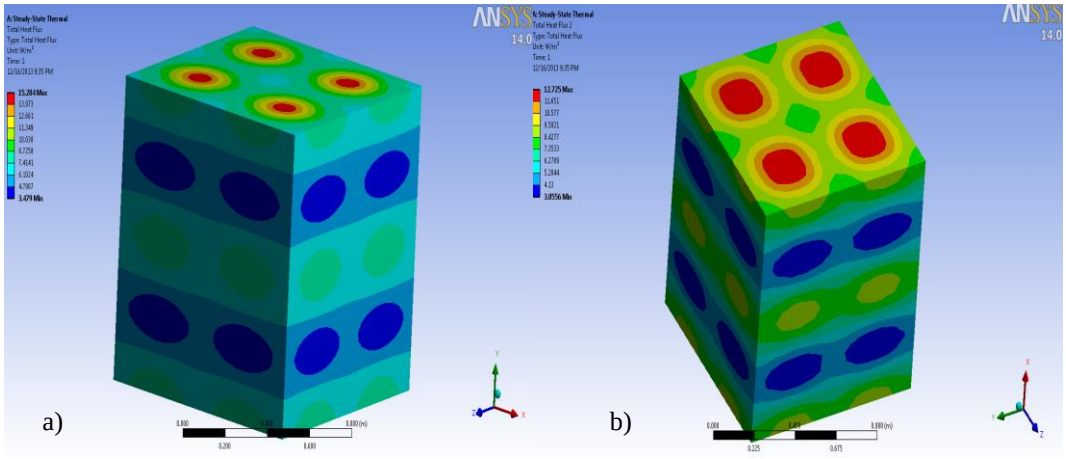

Figure E.2.39. Total heat flux over 8-piece- a)shpere and b) cube -filler model for Ø=15%

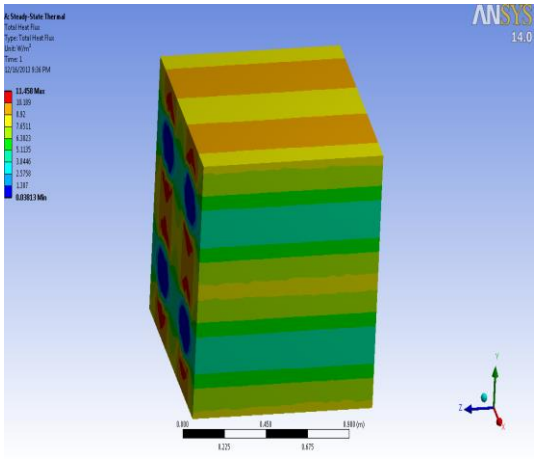

Figure E.2.40. Total heat flux over 16-piece- cube -filler model for Ø=15%

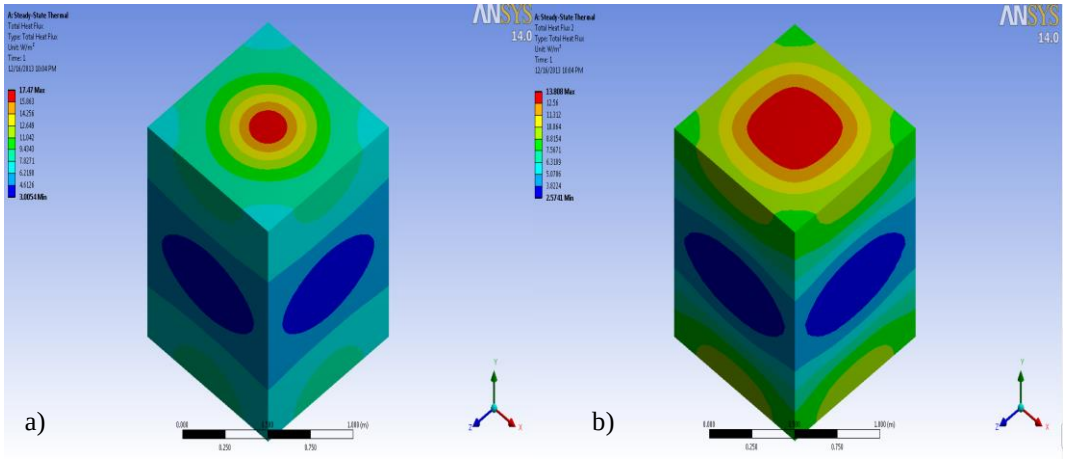

Figure E.2.41. Total heat flux over 1-piece- a)shpere and b) cube -filler model for Ø=18%

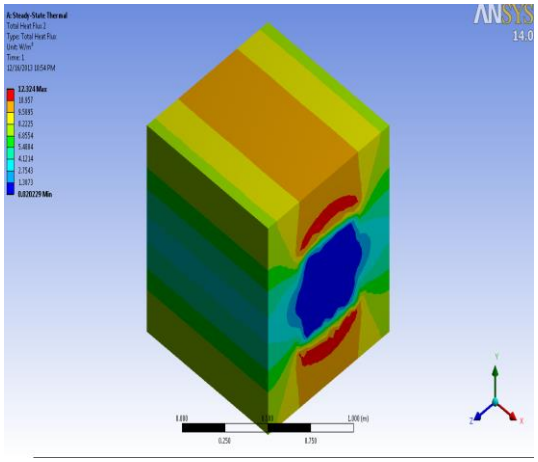

Figure E.2.42. Total heat flux over 2-piece- cube -filler model for Ø=18%

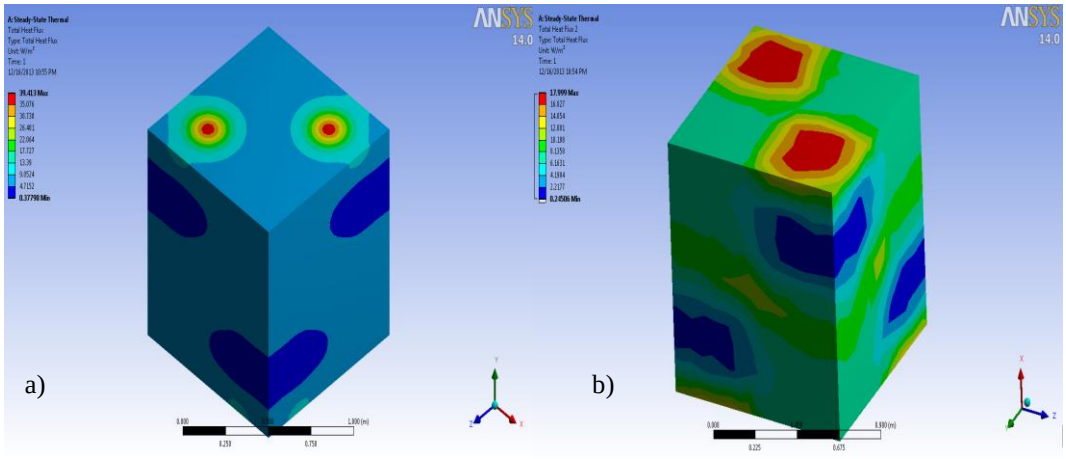

Figure E.2.43. Total heat flux over 4-piece- a)shpere and b) cube -filler model for Ø=18%

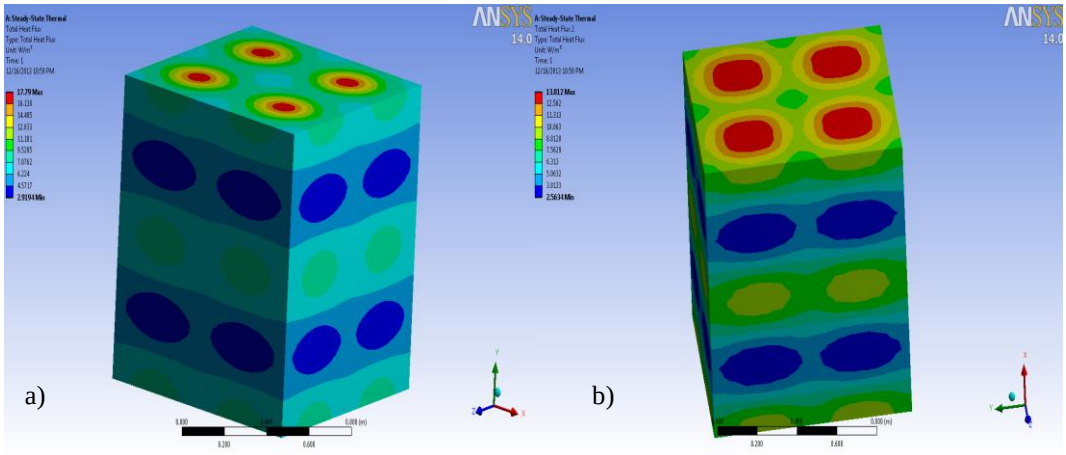

Figure E.2.44. Total heat flux over 8-piece- a)shpere and b) cube -filler model for Ø=18%

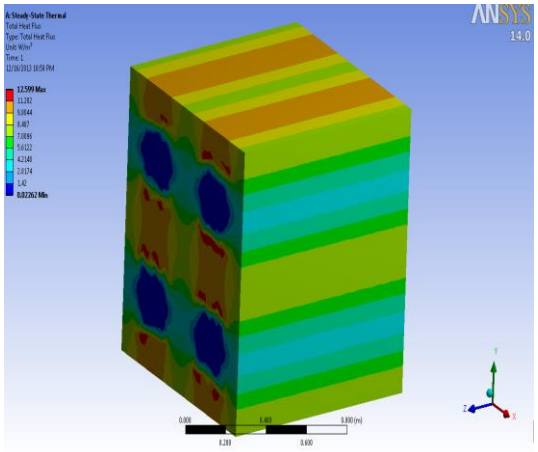

Figure E.2.45. Total heat flux over 16-piece- cube -filler model for Ø=18%

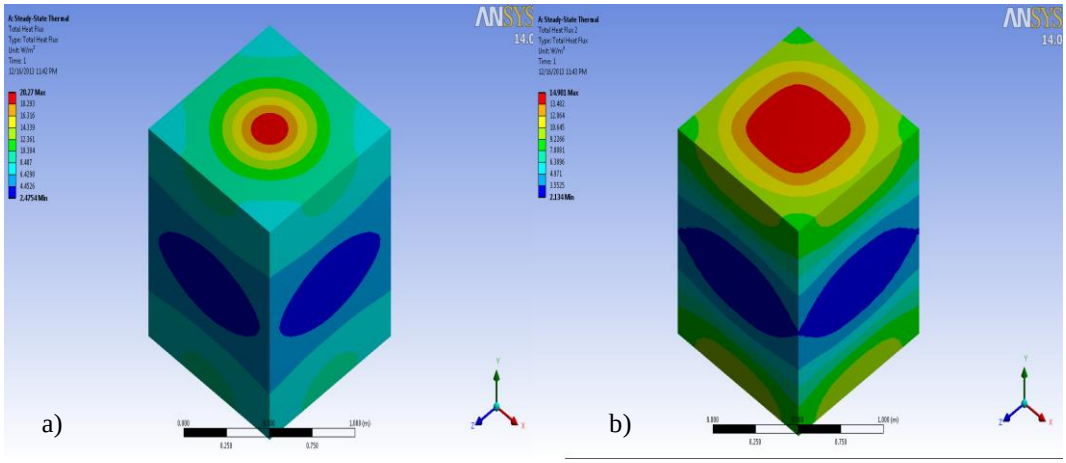

Figure E.2.46. Total heat flux over 1-piece- a)shpere and b) cube -filler model for Ø=21%

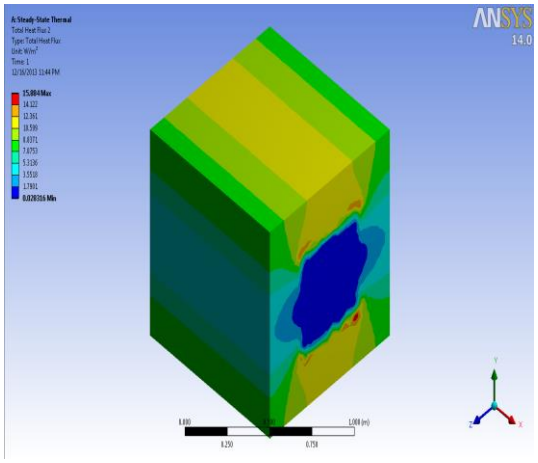

Figure E.2.47. Total heat flux over 2-piece- cube -filler model for Ø=21%

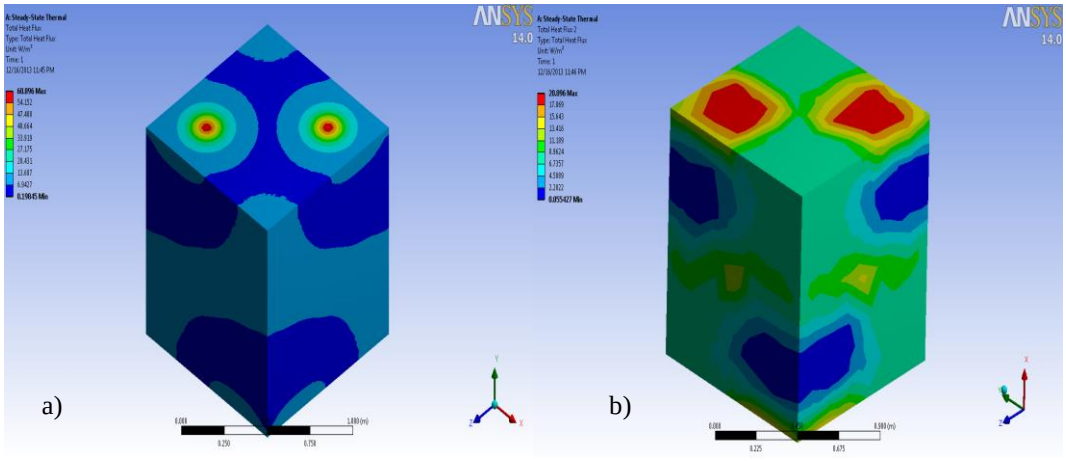

Figure E.2.48. Total heat flux over 4-piece- a)shpere and b) cube -filler model for Ø=21%

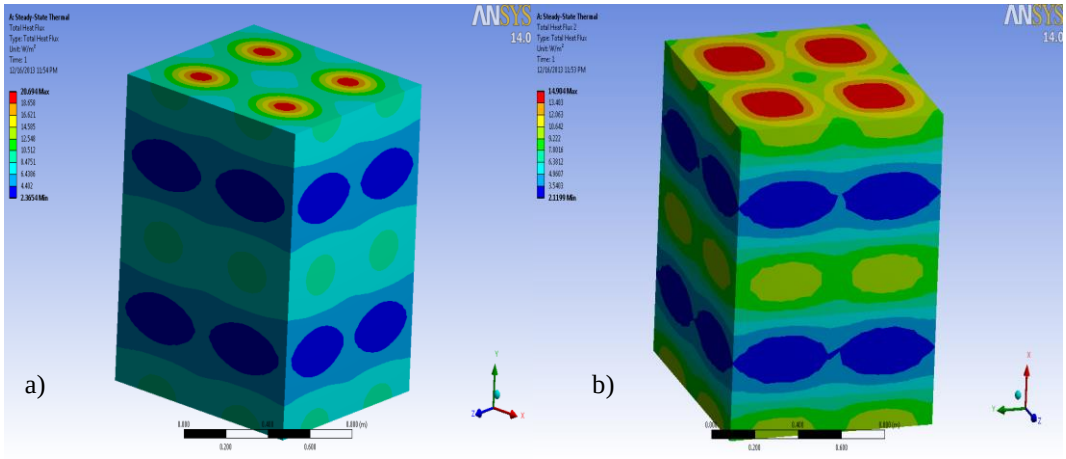

Figure E.2.49. Total heat flux over 8-piece- a)shpere and b) cube -filler model for Ø=21%

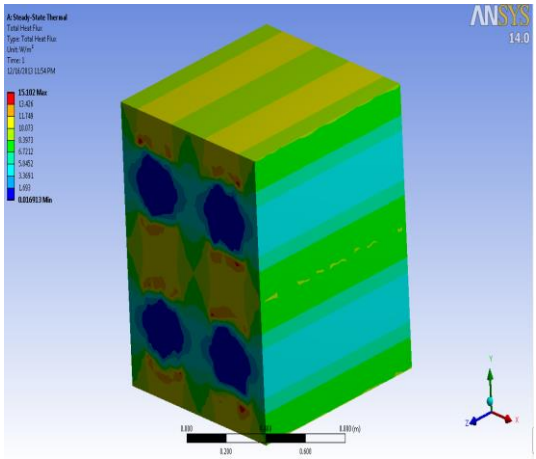

Figure E.2.50. Total heat flux over 16-piece- cube -filler model for Ø=21%

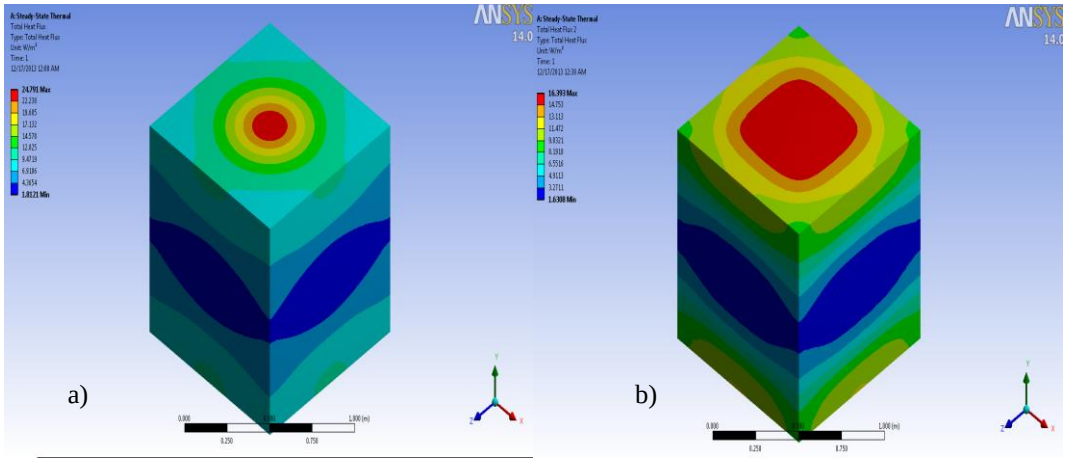

Figure E.2.51. Total heat flux over 1-piece- a)shpere and b) cube -filler model for Ø=25%

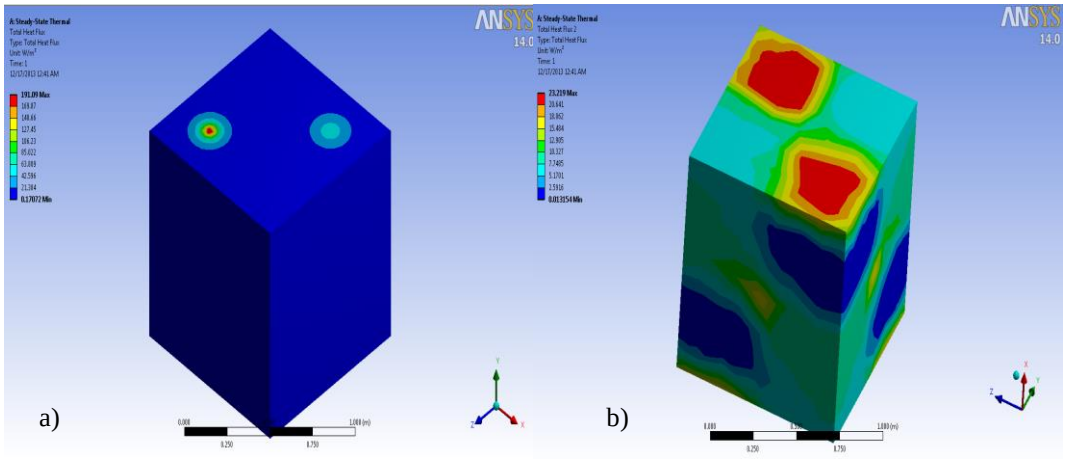

Figure E.2.52. Total heat flux over 4-piece- a)shpere and b) cube -filler model for Ø=25%

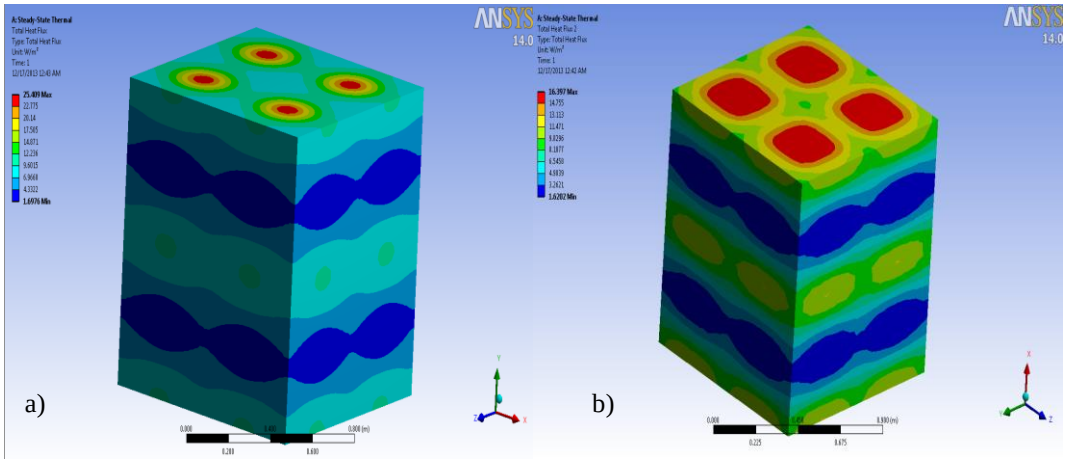

Figure E.2.53. Total heat flux over 8-piece- a)shpere and b) cube -filler model for Ø=25%

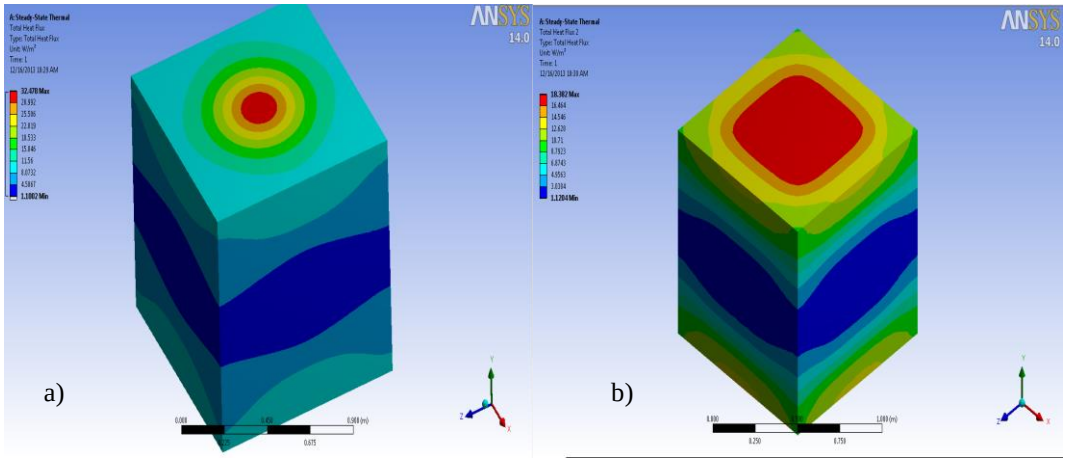

Figure E.2.54. Total heat flux over 1-piece- a)shpere and b) cube -filler model for Ø=30%

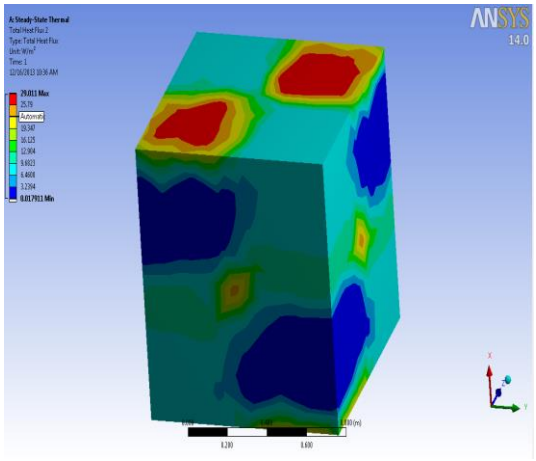

Figure E.2.55. Total heat flux over 4-piece- cube -filler model for Ø=30%

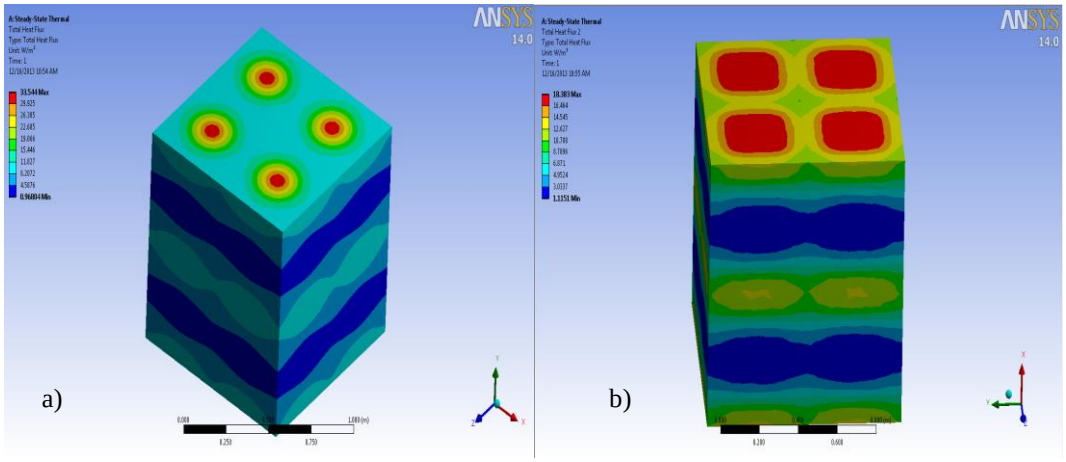

Figure E.2.56. Total heat flux over 8-piece- a)shpere and b) cube -filler model for Ø=30%

Appendix F

NUMERICAL ANALYSIS RESULTS

Table X.Y. Effective thermal conductive of circle filler models values for various arrangement

Volume Fraction	Thermal Conductivity (W/mK)				
	1 piece	2 piece	4 piece	8 piece	16 piece
0.00	0.614	0.614	0.614	0.614	0.614
0.01	0.626	0.626	0.626	0.626	0.626
0.02	0.639	0.638	0.639	0.638	0.639
0.04	0.664	0.663	0.665	0.662	0.665
0.06	0.692	0.687	0.694	0.687	0.692
0.08	0.720	0.711	0.720	0.711	0.711
0.10	0.749	0.735	0.749	0.735	0.749
0.12	0.780	0.759	0.780	0.759	0.780
0.15	0.829	0.795	0.829	0.795	0.829
0.18	0.881	0.830	0.881	0.830	0.881
0.21	0.938	0.866	0.938	0.866	0.938
0.25	1.020	0.914	1.020	0.914	1.020
0.30	1.137	0.976	1.137	0.976	1.137

Table X.Y. Effective thermal conductive of square filler models values for various arrangement

Volume Fraction	Thermal Conductivity (W/mK)				
	1 piece	2 piece	4 piece	8 piece	16 piece
0.00	0.614	0.614	0.614	0.614	0.614
0.01	0.627	0.628	0.627	0.628	0.627
0.02	0.641	0.640	0.641	0.640	0.641
0.04	0.670	0.667	0.670	0.667	0.670
0.06	0.700	0.693	0.699	0.693	0.699
0.08	0.730	0.719	0.731	0.719	0.731
0.10	0.763	0.745	0.763	0.745	0.763
0.12	0.797	0.770	0.797	0.797	0.770
0.15	0.851	0.808	0.851	0.807	0.851
0.18	0.908	0.844	0.908	0.844	0.909
0.21	0.970	0.880	0.970	0.880	0.970
0.25	1.059	0.928	1.059	0.928	1.059
0.30	1.184	0.986	1.184	0.986	1.184

Table X.Y. Effective thermal conductive of cube filler models values for various arrangement

Volume Fraction	Thermal Conductivity (W/mK)				
	1 piece	2 piece	4 piece	8 piece	16 piece
0.00	0.614	0.614	0.614	0.614	0.614
0.01	0.635	0.635	0.636	0.636	0.636
0.02	0.657	0.656	0.659	0.658	0.657
0.04	0.703	0.697	0.704	0.703	0.699
0.06	0.750	0.735	0.755	0.751	0.737
0.08	0.799	0.772	0.803	0.800	0.774
0.10	0.850	0.808	0.859	0.851	0.810
0.12	0.903	0.842	0.911	0.936	0.844
0.15	0.987	0.892	1.001	0.988	0.895
0.18	1.075	0.941	1.093	1.076	0.944
0.21	1.169	0.989	1.197	1.171	0.992
0.25	1.303	NOT APPLICABLE	1.360	1.305	NOT APPLICABLE
0.30	1.491	NOT APPLICABLE	1.621	1.491	NOT APPLICABLE

Table X.Y. Effective thermal conductive of sphere filler models values for various arrangement

Volume Fraction	Thermal Conductivity (W/mK)				
	1 piece	2 piece	4 piece	8 piece	16 piece
0.00	0.614	0.614	0.614	0.614	0.614
0.01	0.631	0.631	0.631	0.631	0.631
0.02	0.649	0.649	0.649	0.649	0.648
0.04	0.685	0.683	0.685	0.686	0.681
0.06	0.722	0.716	0.723	0.725	0.714
0.08	0.762	0.748	0.763	0.765	0.746
0.10	0.803	0.780	0.804	0.807	0.777
0.12	0.846	0.812	0.849	0.851	0.808
0.15	0.914	NOT APPLICABLE	0.921	0.921	NOT APPLICABLE
0.18	0.987	NOT APPLICABLE	1.004	0.997	NOT APPLICABLE
0.21	1.066	NOT APPLICABLE	1.102	1.079	NOT APPLICABLE
0.25	1.184	NOT APPLICABLE	1.132	1.200	NOT APPLICABLE
0.30	1.355	NOT APPLICABLE	NOT APPLICABLE	1.379	NOT APPLICABLE

Appendix G

RESULTS OF THEORETICAL THERMAL CONDUCTIVITY MODELS

Table X.Y. Thermal conductive of therotical models for various volume fraction

	Thermal Conductivity (W/mK)				
Volume Fraction	Series	Parallel	Geometric Mean	Maxwell	Lord Rayleigh
0.00	0.614	0.614	0.614	0.614	0.614
0.01	0.620	2.648	0.651	0.632	0.632
0.02	0.626	4.682	0.689	0.651	0.651
0.04	0.639	8.749	0.774	0.690	0.690
0.06	0.653	12.817	0.870	0.730	0.730
0.08	0.667	16.885	0.977	0.772	0.772
0.10	0.682	20.952	1.097	0.816	0.816
0.12	0.697	25.020	1.232	0.862	0.863
0.15	0.722	31.122	1.467	0.935	0.936
0.18	0.748	37.223	1.746	1.014	1.014
0.21	0.776	43.325	2.078	1.098	1.100
0.25	0.818	51.460	2.621	1.220	1.224
0.30	0.876	61.630	3.504	1.393	1.403

Table X.Y. Thermal conductive of therotical models for various volume fraction(continue)

Volume Fraction	Thermal Conductivity (W/mK)			
	Meredith and Tobias	Hamilton and Crosser	Lewis and Nielsen (A=1.5, Q_m=0.637)	Lewis and Nielsen (A=3, Q_m=0.637)
0	0.614	0.614	0.614	0.614
0.01	0.632	0.632	0.629	0.638
0.02	0.651	0.651	0.645	0.664
0.04	0.690	0.690	0.678	0.716
0.06	0.730	0.730	0.713	0.771
0.08	0.772	0.772	0.751	0.830
0.10	0.817	0.816	0.791	0.892
0.12	0.863	0.862	0.833	0.958
0.15	0.936	0.935	0.903	1.066
0.18	1.016	1.014	0.982	1.186
0.21	1.102	1.098	1.071	1.322
0.25	1.231	1.220	1.210	1.532
0.30	1.420	1.393	1.427	1.858

Table X.Y. Thermal conductive of therotical models for various volume fraction(continue)

Volume Fraction	Thermal Conductivity (W/mK)			
	Russell	Cheng and Vachon	Spinger and Tsai	Baschirow and Selenew
0	0.614	0.614	0.614	0.614
0.01	0.769	0.693	0.621	0.622
0.02	0.830	0.735	0.628	0.630
0.04	0.921	0.804	0.644	0.650
0.06	0.996	0.866	0.662	0.673
0.08	1.066	0.926	0.681	0.698
0.10	1.132	0.987	0.702	0.725
0.12	1.197	1.049	0.725	0.755
0.15	1.294	1.147	0.761	0.805
0.18	1.393	1.252	0.802	0.863
0.21	1.495	1.368	0.847	0.928
0.25	1.638	1.543	0.915	1.029
0.30	1.832	1.809	1.014	1.186

Table X.Y. Thermal conductive of therotical models for various volume fraction(continue)

Volume Fraction	Thermal Conductivity (W/mK)		
	Zehner and Schlünder	Woodside and Messner	Agari and Uno
0	0.614	0.614	0.614
0.01	1.636	-	0.627
0.02	2.664	-	0.644
0.04	4.737	2.667	0.682
0.06	6.832	6.734	0.721
0.08	8.950	10.802	0.763
0.10	11.091	14.870	0.807
0.12	13.257	18.938	0.854
0.15	16.553	25.039	0.929
0.18	19.908	31.141	1.011
0.21	23.326	37.242	1.100
0.25	27.987	45.378	1.231
0.30	33.994	55.547	1.417

Nomenclature

Q	Heat rate (W)
k	Thermal conductivity coefficient (W/m. K)
A	Surface area of the medium (m^2)
L	Length/thickness of the medium (m)
Ø	Concentration ratio (%)
k_e.	Effective thermal conductivity coefficient (W/m. K)
k_m.	Thermal conductivity coefficient of matrix material (Continuous phase) (W/m. K)
k_f.	Thermal conductivity coefficient of filler material (Discontinuous phase) (W/m. K)
X	Shape factor for the discontinuous phase
ϕ_m	Maximum packing fraction
L_x	Length in x direction (m)
L_y	Length in y direction (m)
L_z	Length in z direction (m)
ΔT	Temperature difference (C or K)
q_y	Heat flux in y direction (W/m^2)
x	Distance (m)